1

Hemijska industrija

Vol. 77

Časopis Saveza hemijskih inženjera Srbije

Chemical Industry

Specijalna sveska: Napredak u istraživanju proizvodnje biodizela
Special Issue: Advances in Biodiesel Production Research
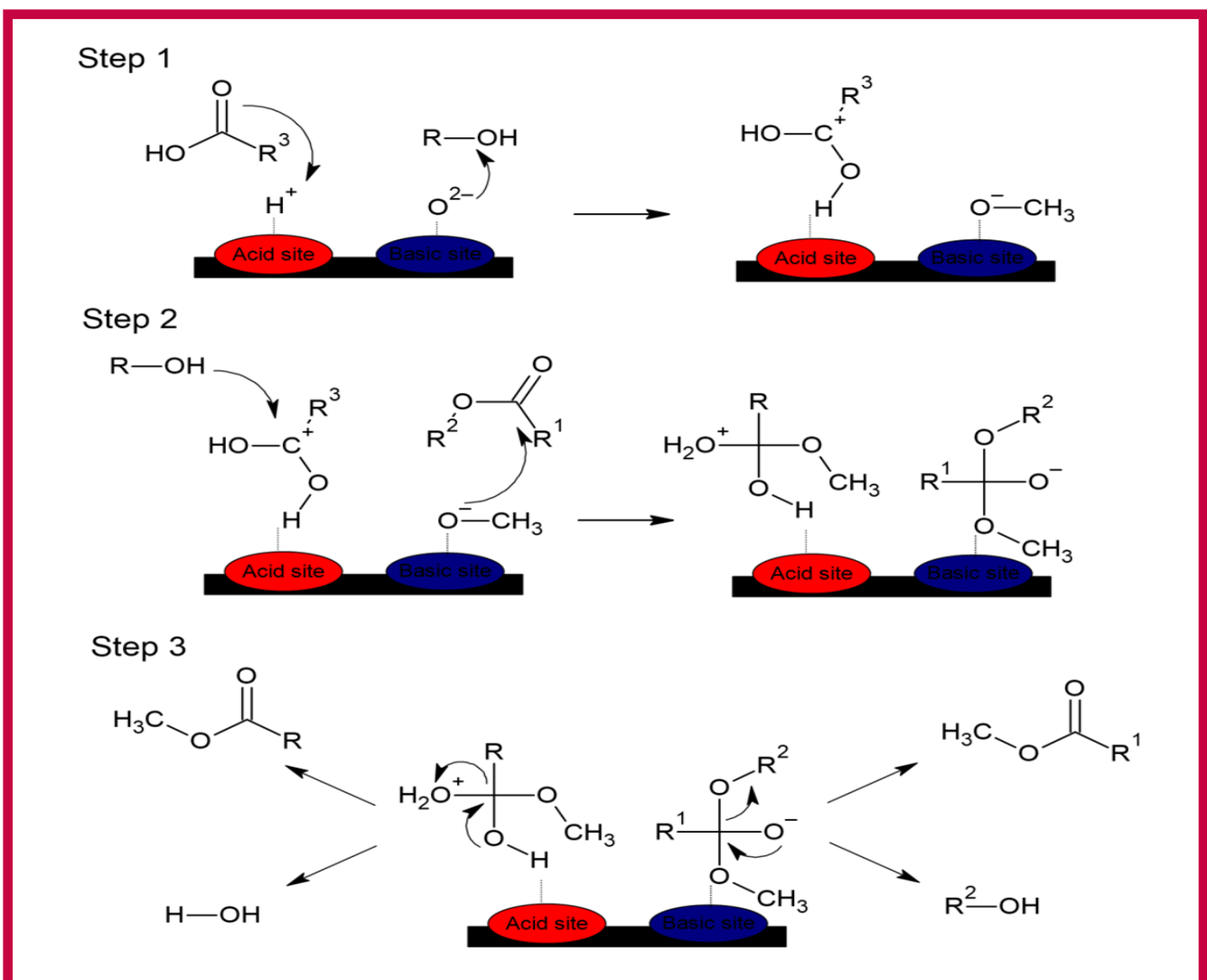
Aktivnosti Saveza hemijskih inženjera Srbije pomažu:

**MINISTARSTVO NAUKE,
TEHNOLOŠKOG RAZVOJA
I INOVACIJA
REPUBLIKE SRBIJE**

Tehnološko-metalurški fakultet
Univerziteta u Beogradu

Prirodno-matematički fakultet
Univerziteta u Novom Sadu

Institut za tehnologiju nuklearnih i
drugih mineralnih sirovina, Beograd

Tehnološki fakultet
Univerziteta u Novom Sadu

Institut za hemiju, tehnologiju i metalurgiju
Univerziteta u Beogradu

Fakultet tehničkih nauka
Univerziteta u Novom Sadu

Tehnološki fakultet
Univerziteta u Nišu, Leskovac

Fakultet tehničkih nauka
Univerziteta u Prištini
Kosovska Mitrovica

Institut IMS, Beograd

DCP HEMIGAL
Leskovac

Elixir Prahovo

Specijalna sveska:
Napredak u istraživanju proizvodnje biodizela
Special Issue:
Advances in biodiesel production research

Gostujuće urednice / Guest Editors
Ivana Banković-Ilić and Marija Miladinović
University of Niš, Faculty of Technology, Leskovac, Serbia

SADRŽAJ/CONTENTS

Advances in biodiesel production research

Ivana Banković-Ilić and Marija Miladinović

University of Niš, Faculty of Technology, Leskovac, Serbia

Keywords: environmental protection; waste materials as catalysts; zeolitic materials; deep eutectic solvents; adsorptive capacity of quicklime; oxidation stability

Available on-line at the Journal web address: http://www.ache.org.rs/HI/

Global energy demand is increasing alongside the growing concern for environmental protection. The energy crisis triggered by the current political and economic situation in the world requires the transition to a more sustainable and secure energy system. Therefore, the focus is on alternative fuels as a solution to replace fossil oil sources in the transport sector. Biofuels stand out as the most promising alternative to fossil fuels providing energy transition without changes in the current infrastructure. Among biofuels, biodiesel is a renewable alternative to fossil diesel obtained from bio-sources such as vegetable oils (edible, nonedible, and waste/used), animal fats, or algae oil. It has many advantages, such as biodegradability, low toxicity, reduced emissions of char, benzene, toluene, sulphur oxides, harmful nitrogen compounds, and other greenhouse gasses due to the closed CO_2 cycle, and improved engine combustion due to the adequate O_2 content. In addition, it can be used without the internal combustion engine modification and mixed in any ratio with ordinary fossil-based diesel fuel, so it can be easily commercialized. Besides the environmental aspect, biodiesel production has a positive impact on the rural economy. Still, there is a need for improvements in the biodiesel production concerning the replacement of edible oils as feedstocks for the manufacturing process, reducing the high synthesis cost, and increasing the quality of the final product. Therefore, this special issue aims to provide recent developments and advances in sustainable biodiesel production regarding feedstocks, catalysts, properties, and technologies.

Significant advances were made in the valorisation of waste materials into biodiesel. Reusing wastes without a practical value and other applications is essential for reducing production costs and, thus, biodiesel prices. In this respect, Marinković and Pavlović [1] provide a comprehensive overview of the utilization of waste-based and natural zeolitic materials as catalysts or catalyst supports in biodiesel production. Synthesis routes of the zeolite-based catalysts are analysed in detail with an emphasis on the economy of the process and then the catalyst stability and reusability in transesterification of oils into biodiesel. Furthermore, the reaction mechanisms are also discussed in detail for reaction conditions optimization. This article can be valuable as a new ideas generator for researchers interested in the further investigation of waste-based zeolites and their applications.

A contribution to the valorisation of waste materials as catalysts was also given by a study by Miladinović *et al.* [2]. The catalytic activity of ashes obtained after combustion of waste plum stones and stone shells for heat generation was tested in transesterification of plum kernel oil into biodiesel. In this way, the complete utilization of waste plum stones in biodiesel production was demonstrated. The study revealed the plum stone shell ash as the most active catalyst compared to waste plum stones ash and plum kernel cake ash, so that it was characterized in detail, and investigated regarding the effect of reaction temperature on methyl esters synthesis. Kinetic analysis was performed to determine the reaction rate constant and activation energy. This study is significant for the development of biodiesel production processes based on utilization of the same low-cost materials as a source for the oily feedstock and for the catalyst because it provides data for predicting the reaction rate and reactor design.

Considering that mass transfer can limit the rate of transesterification catalysed by solid catalysts, the study of Todorović *et al.* [3] proposed co-solvents based on deep eutectic solvents (DES) to improve the rate of ethanolysis of cold-pressed black mustard (*Brassica nigra* L.) seed oil catalysed by either calcined or non-calcined CaO. Several lecithin-

based DES were characterized, and the lecithin : glycerol system was selected as a co-solvent. The use of DES accelerates not only the reaction but enhances separation of the final reaction mixture phases. This paper provides novel knowledge on the use of lecithin for DES preparation and its utilization as co-solvents for biodiesel production.

Although the utilization of waste oily feedstocks for biodiesel production adds value to the wastes, these oils require pretreatment due to the high content of free fatty acids (FFA). In the study of Lukić *et al.* [4], the adsorptive capacity of quicklime, which was already proved as an inexpensive and suitable catalyst in transesterification of oil into biodiesel, was tested for removal of FFA from waste cooking oil. The results have indicated that quicklime has considerable potentials for the FFA removal from the WCO at lower temperatures, being inexpensive, available, and efficient. This study can be of interest to biodiesel producers since both the removal of FFA and the heterogeneously catalysed methanolysis are environmentally and economically acceptable processes.

Quality of biodiesel is important for its commercialization. The biodiesel stability during extended storage depends on its oxidation stability. Therefore, Djurišić-Mladenović *et al.* [5] investigated the oxidation stability of biodiesel obtained from sunflower oil using the RapidOxy method as an alternative technique and compared it with the use of the standard Rancimat method. Improvements in the oxidation stability were achieved by adding a synthetic antioxidant and a mixture of bio-based antioxidant compounds extracted from vinery waste. This study is important and serves as a starting point for further developments of bio-based antioxidants from vinery waste and employing the RapidOxy method for high-throughput analysis with high repeatability for determination of oxidation stability of biodiesel.

We hope that the selected papers will have an impact on the scientific as well as broader community and become a driving force for research and developments in the future leading to sustainable solutions.

The guest editors wish to thank the authors for their effort to contribute to this topic and commitment to improve their manuscripts; the reviewers for willingness to provide careful evaluation and constructive reviews; and the editorial staff for managing the review and publication processes efficiently.

<div align="right">

Guest Editors
Dr. Ivana Banković-Ilić, Full professor
Dr. Marija Miladinović, Assistant Professor

</div>

REFERENCES

[1]   Marinković DM, Pavlović SM. Recent advances in waste-based and natural zeolitic catalytic materials for biodiesel production *Hem Ind.* 2023; 77(1): 5-38. https://doi.org/10.2298/HEMIND220804007M

[2]   Miladinović MR, Pavlović S, Banković-Ilić IB, Kostić MD, Stamenković OS, Veljković VB. Utilization of waste plum stones as a source of oil and catalyst for biodiesel production. *Hem Ind.* 2023; 77(1): 39-52 https://doi.org/10.2298/HEMIND221113009M

[3]   Todorović ZB, Đorđević BS, Troter DZ, Veselinović LjM, Zdujić MV, Veljković VB. Effects of temperature on physicochemical properties of the lecithin-based deep eutectic solvent and their use in the CaO-catalyzed transesterification. *Hem Ind.* 2023; 77(1): 53-67. https://doi.org/10.2298/HEMIND220527016T

[4]   Lukić I, Kesić Ž, Zdujić M, Skala U. Adsorptive pretreatment of waste cooking oil using quicklime for fatty acid methyl esters synthesis. *Hem Ind.* 2023; 77(1): 69-84 https://doi.org/10.2298/HEMIND220628005L

[5]   Đurišić-Mladenović N, Tomić M, Pajin B, Buljovčić M, Lončarević I, Rankov Šicar M. Stability evaluation of biodiesel supplemented with synthetic and bio-based antioxidants by a pressurized accelerated oxidation method. *Hem Ind.* 2023; 77(1): 85-93. https://doi.org/10.2298/HEMIND220808003D

Napredak u istraživanju proizvodnje biodizela

Ivana Banković-Ilić i Marija Miladinović

Univerzitet u Nišu, Tehnološki fakultet, Leskovac, Srbija

Kao rešenje za zamenu izvora fosilnih goriva u sektoru transporta i osiguranja održivog energetskog sistema ističu se biogoriva, a među njima biodizel koji se dobija iz bio-izvora kao što su biljna ulja, životinjske masti ili ulje algi. Potreba je da se proizvodnja biodizela unapredi zamenom jestivih sirovina nejestivim ili već korišćenim, da se smanje visoki operativni troškovi i poveća kvalitet finalnog proizvoda. Stoga, ovo specijalno izdanje časopisa Hemijska industrija ima za cilj da pruži najnovija saznanja u razvoju i napretku održive proizvodnje biodizela u pogledu sirovina, katalizatora, svojstava i tehnologija. U tom pogledu najpre je dat sveobuhvatan pregled primene otpadnih i prirodnih zeolitnih materijala kao katalizatora ili nosača katalizatora, a zatim opisana katalitička aktivnost pepela dobijenog sagorevanjem otpadnih koštica šljive radi primene u reakciji transesterifikacije ulja iz jezgara koštica šljive do biodizela. U cilju poboljšanja brzine reakcije i razdvajanja faza finalne reakcione smeše, predložena je upotreba eutektičkih smeša kao korastvarača. Kako otpadne uljne sirovine često imaju visok sadržaj slobodnih masnih kiselina, to se za njihovo efikasno otklanjanje preporučuje korišćenje negašenog kreča kao adsorbenta. Na kraju, pokazano je da se oksidaciona stabilnost biodizela, kao mera njegovog kvaliteta, može efikasno odrediti korišćenjem RapidOxy metode i poboljšati dodavanjem mešavine antioksidativnih jedinjenja na biološkoj bazi.

Recent advances in waste-based and natural zeolitic catalytic materials for biodiesel production

Dalibor M. Marinković and Stefan M. Pavlović

University of Belgrade, Institute of Chemistry, Technology and Metallurgy, Belgrade, Serbia

Abstract

Considering the current world crisis and definite future energy challenges, biomass-to-fuel transformation is increasingly becoming important both to the policy makers and to the industry. In this perspective, the valorisation of oils and fats *via* transesterification/esterification reaction is an attractive method for producing biodiesel with qualities suitable for diesel engines. The recent interest indicated a significant shift to industrial waste valorisation as another approach for achieving process eco-efficiency. In this respect, the use of zeolite-based catalysts for the production of biofuels is reviewed here, with a special emphasis on the utilization of waste raw materials following the principles of green chemistry and sustainable development. Zeolites are interesting due to their outstanding catalytic properties, including the presence of intrinsic acid sites, simple loading of base sites, shape-selectivity, and high thermal stability. Neat zeolites or modified by the loading of active species are classified into several groups following their origin. For each group, the most relevant recent results reported in the literature are reviewed together with some critical considerations on the catalyst effectiveness, stability, reusability, and economy of synthesis. As an important part required for understanding and optimization of the biodiesel production process, the mechanisms of the reaction were discussed in detail. Finally, key perspective directions for further research studies were carefully identified and elaborated.

Keywords: zeolite; waste raw materials; fly ash; industrial waste; heterogeneous catalysis; transesterification.

Available on-line at the Journal web address: http://www.ache.org.rs/HI/

1. INTRODUCTION

In recent decades, especially in recent years, more and more attention is focused on energy consumption, energy efficiency, fossil fuel emission and depletion, as well as on alternative energy sources and uses [1]. World crises are only intensifying these issues. The world dependence on fossil fuels is still dominant, but some renewable solutions are available, while many are being intensively researched. Biofuels, such as biodiesel, are significant competitors to fossil diesel fuel, due to lower contents of CO_2, SO_2, and hydrocarbons during combustion, as well as biodegradability, high flash point, high lubricant properties, and high octane number [2,3]. Additionally, biodiesel can be used in modern internal combustion engines without modification [4]. Commercial production of biodiesel began in Austria in 1991, and for the next 15 or so years, biodiesel production was booming. It seems that after that first run, interest in biodiesel declined until recently when it became attractive again with the intensification of the world energy crisis. Current chemical technology practices of obtaining biodiesel imply the following concepts: base-catalysed transesterification (homogeneous or heterogeneous) [5-7], acid-catalysed esterification and transesterification [8,9], enzyme-catalysed transesterification [10,11], biodiesel synthesis catalysed by bifunctional heterogeneous solid catalysts [12,13], deoxygenation [14,15], and supercritical methanolysis [16,17]. Process intensification in terms of the reaction mixture treatment by microwave [18,19] and ultrasound [20,21] is also a part of the latest interest of the researchers. The modern approach in biodiesel research, however, synergistically focuses on new catalytic systems based on waste sources, the use of non-edible or waste triacylglycerol (TG) feedstock, and on advanced batch and continuous reactor systems. Such an approach is not only sustainable and environmentally friendly but also economically viable.

Nowadays, homogeneous base and acid catalysts are still used in most industrial plants for biodiesel production, despite their numerous disadvantages (demanding catalyst recovery, soap formation, difficult product purification, high corrosion, and inhibition by water) [3]. The modern concept of sustainable industrial processes strongly supports design of new catalysts based on waste materials, such as biomass fly ash, coal-fired power stations fly ash, industrial waste rich in calcium and other alkali and alkaline earth metals such as mud and slug, agricultural and animal waste, and natural sources [22]. The use of these materials has a double benefit, as economic and environmental problems of disposal and treatment of waste materials are being solved, and, on the other side, very useful and valuable catalytic materials are obtained, further utilized in obtaining biofuels. Particular attention of researchers is focused on the challenge of adaptation of the mentioned catalytic systems to produce biodiesel from waste TG sources, such as non-edible oils, waste cooking oils (WCOs), and oils with high free fatty acid (FFA) contents [23]. Also, attention is paid to the modern biodiesel production process from oils obtained from microalgae [24].

Zeolite is a crystalline aluminosilicate material with various spatial three-dimensional structures that allow the adsorption and diffusion of molecules. It can occur naturally or can be synthesized from pure chemicals, natural minerals, or waste materials. Zeolitic materials have found great interest among researchers and in the industry because of their easily tunable physical and chemical properties. Nowadays, they are successfully investigated and used as catalysts in different processes such as isomerisation, condensation and oligomerization, pyrolysis or liquefaction, hydrolysis, esterification, and transesterification [25]. Unlike many other materials that could be employed as catalysts for TGs conversions, zeolites are highly stable with the potential to resist severe reaction conditions [26]. Their structure is responsible for very high melting points (higher than 1,000 °C), so zeolites can withstand elevated reaction pressures and temperatures and are stable in air and many solvents used in catalysis. Tunable acidity/basicity and suitable structural properties of zeolitic materials account for their wide exploitation as prospective catalysts.

One of the major drawbacks of a heterogeneously catalysed transesterification process is diffusion-limited mass transport in porous materials. Furthermore, the reaction mixture molecules could be massively deposited onto the catalyst surface and cause pore-blocking, leading to a reduction in catalyst activity [27]. These issues can be resolved by using hierarchically structured zeolitic materials with double or triple porosity, *i.e.*, meso- and/or macroporosity [28]. Besides that, along with the principles of sustainable development, zeolitic materials can be obtained from waste that has an adequate ratio of constituent atoms (Al and Si), such as fly and bottom ashes generated in thermal power plants [29].

Several review papers already dealt with the use of zeolite catalysis in biofuel production [25,26,30]. Thus, the present review is focused on waste-based and natural zeolitic materials and their use as catalysts or catalyst supports in biodiesel production as a supplement to previous articles. The synthesis routes of zeolite-based catalyses will be analysed in detail, with an emphasis on the economy of synthesis, as well as on key analytical parameters of the synthesized materials. The quality of biodiesel obtained by using zeolite-based catalysts and mainly non-edible or waste oil feedstocks will be considered, as well as the stability and recyclability of the catalyst. Finally, reaction mechanisms will be discussed in detail as for optimization of the reaction conditions, it is necessary to understand what happens to the reactants and products in the course of the reaction.

2. ZEOLITES, ORIGIN, STRUCTURE

Zeolites are crystalline porous materials structured as a tetrahedral TO_4 (T = Al, Si) in different orders, resulting in 253 unique frameworks, with over 40 naturally occurring frameworks [31]. The term "zeolite" was originally addressed by the Swedish mineralogist Axel Cronstedt in the mid-eighteenth century. He observed that rapid heating of material produces huge amounts of vapour that had been previously adsorbed. Based on this observation, he called the material "zeolite", from the Greek words "zeo" and "lithos", meaning "to boil" and "stone", respectively. [32]. zeolite-specific structure, *i.e.* channel- or cage-like system, acts as a trap for molecules of specific sizes and shapes [33]. In the porous structure of zeolite a wide variety of cations can be accommodated, such as Na^+, K^+, Ca^{2+}, Mg^{2+}, and others. These cations are loosely bonded and can be easily exchanged with other ions present in the contact solution. The relationship between the contents of exchangeable cations and aluminium in the aluminosilicate framework is always (Ca + Mg + Ba + Na_2 + K_2)/Al = 1. Zeolites differ from all the other framework silicates by the presence of water molecules. The general

formula for a zeolite mineral is: (Ca, Na$_2$, K$_2$, Ba, Sr, Mg, Cs$_2$, Li$_2$)$_a$[Al$_2$Si$_{n-a}$O$_{2n}$]×H$_2$O, where atoms in the square brackets represent the framework atoms, and the rest represents the exchangeable ions plus water [34].

Zeolitic materials can occur naturally but can be also produced industrially on a large scale. Natural zeolite groups include: analcime (pollucite and wairakite), chabazite (herschelite and willhendersonile), gismondine (amicite, garronite, and gobbinsite), heulandite (clinoptilolite), natrolite (mesolite and scolecite), harmotome (phillipsite and wellsite), and stilbite (barrerite and stellerite) [34]. An example of the structure of one of the most abundant natural zeolites mordenite, with a mineral formula of (*Ca, Na$_2$, K$_2$*) *Al$_2$Si$_{10}$O$_{24}$·7H$_2$O* is presented in Figure 1.
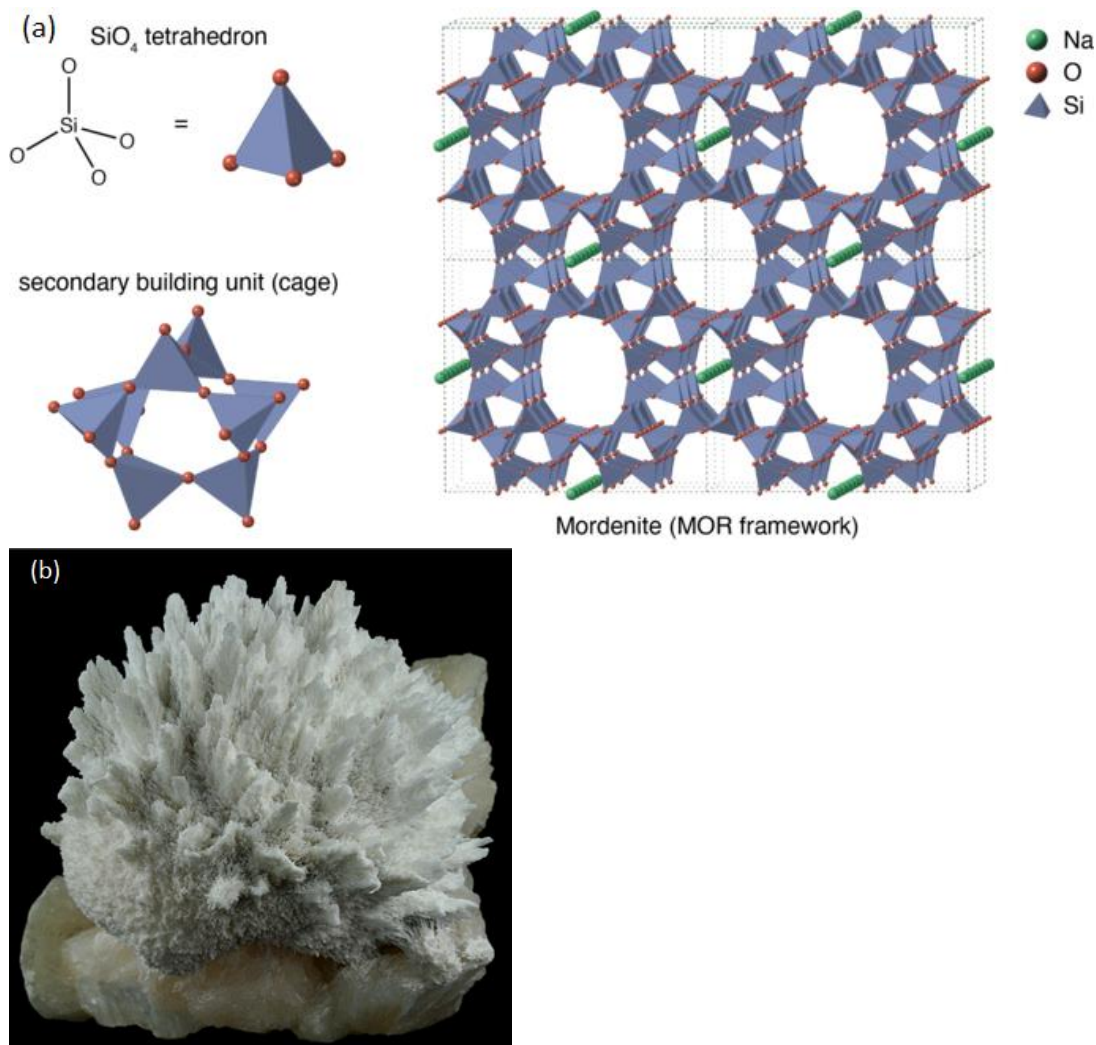
Figure 1. Typical structure (a) and appearance (Indian mine) (b) of mordenite framework [34]

Zeolite materials find application in many industrial processes, the most important being catalysis [35], adsorption [36], and separation [37]. The term „molecular sieve" related to zeolitic materials refers to the particular ability to selectively sort other molecules based on their size, due to a rather regular zeolite framework, that is the pore structure. For industrial applications synthetic zeolites are certainly more important since their structure may be more regular than that of natural ones.

The interest of researchers in biodiesel and the use of zeolitic materials in catalytic biodiesel production is increasing over the 21st century. Figure 2 shows the number of published papers indexed in the Scopus database [38,39], which have as their topic biodiesel and the use of zeolite materials in heterogeneous catalytic production of biodiesel. The number of papers shows that interest in biodiesel is significant, with about a hundred papers published annually from the beginning of the 21st century, up to about as many as 4,000 articles published annually nowadays. The attractiveness

of zeolitic materials as catalysts for biodiesel production also tends to expand. Interest in this topic was almost negligible at the beginning of the 21st century, at least according to published articles, while today there are more than 50 articles published per year (Fig. 2).
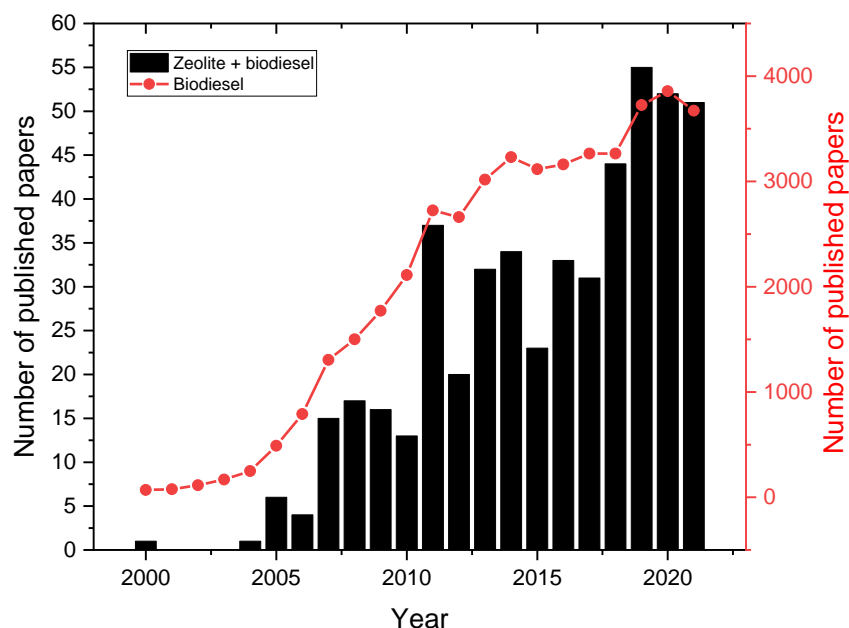
Figure 2. Number of published articles related to the use of zeolite in biodiesel production and the overall number of articles on biodiesel indexed by Scopus in the period 2000-2021 [38,39]

2. 1. Natural zeolites

Natural zeolites are conventionally obtained in open-pit mines, where the overburden is mechanically removed to excavate the ore. Common zeolite groups with similar frameworks and their main and distinctive characteristics are presented in Table 1 [34].

Natural zeolites are formed in Earth's crust in a water-abundant environment under a wide range of temperatures and, often, under low pressure. They are rarely pure and are accompanied by various contents of other minerals, such as quartz, metals, and other zeolite species. Zeolites are formed in the contact of volcanic ash, rocks, and pyroclastic materials with saline, alkaline water, deep sea sediments, shallow marine seas, hot springs, and freshwater lakes. There are several mechanisms of natural zeolite formation, and two distinctive pathways are: low-temperature (4-40 °C) and elevated-temperature origins (40-250 °C). An example of the first is phillipsite, which is formed in deep-sea sediments and needs approximately 150,000 to 10,000,000 years to crystallize. Examples of the second pathway can be the formation of different zeolitic crystals depending on the increase in temperature during the contact metamorphism process, which are as follows [34]:

mordenite-quartz → chabazite-stilbite-heulandite-gmelinite → mesolite-scolecite-natrolite-thompsonite--laumontite-analcime → albite-epidote-prehnite-pumpellyite → granitic intrusion

World reserves of natural zeolites have not been estimated yet. Deposits occur in many countries, but companies and states rarely publish reserves data. The United States, for example, reported combined reserves of 80 million tons in 2021, while the total U.S. reserves are likely substantially larger [41]. In 2021, the world´s annual mine production of natural zeolite was estimated at 944,000 t, which is significantly lower than a few years ago as the production of natural zeolite in 2015 was about 2.78 million tons. Major producers in 2021 (estimation) included Georgia (140,000 t), Indonesia (130,000 t), the Republic of Korea (130,000 t), Slovakia (120,000 t), Unites States (87,000 t), Cuba (53,000 t), China (52,000 t), and Turkey (50,000 t). China has significantly reduced its production, for example in 2015 it produced as much as 2 million tons of natural zeolite [41]

Table 1. Groups of zeolite types sorted by the framework [34]

Group holder	Associated types	Main characteristics
Analcime	Pollucite Wairakite	• Wide variation in chemical composition and disorder-order in the framework • Analcime contains Na • Pollucite contains Cs • Wairakite contains Ca
Chabazite	Horschelite Willhendersonite	• Wide variation in chemical composition and disorder-order in the framework • Chabasite crystals are Ca dominant, although K, Mg, and Na could be present • Chabazite and willhendersonite have the same triclinic framework and can have the same K dominant chemical composition (they differ in the amount of Si and Al)
Gismondine	Amicite Garronite Gobbinsite	• The associated members could be considered disordered gismondine or Na-K-dominant gismondine
Heulandite	Clinoptilolite	• These crystals have been divided into three sets of criteria, a gap in Si/Al mole ratio (Si/Al), a gap in Na-K-Mg-Ca-content, and a gap in the heating characteristics of the framework • Clinoptilolite is often considered as Si dominant heulandite
Natrolite	Mesolite Scolecite Tetranatrolite Gonnardite	• Natrolite, mesolite, and scolecite have a dominantly ordered framework, with different chemical composition • Natrolite, tetranatrolite, and gonnardite differ in the amount of disorder/order of Al and Si in the framework and Na and Ca content • Tetranatrolite is often considered as a Na dominant gonnardite
Harmotome	Phillipsite Wellsite	• These crystals have a single framework with a continuous chemical series ranging from K-Ca-Na-dominant in phillipsite to K-Ca-Ba-dominant in wellasite to Ba-dominant in harmotome
Stilbite	Barrerite Stellerite	• These crystals have identical morphology; the difference is in the ordering of Si/Al in the framework, and the exchangeable Ca and Na ions • Stellerite has Ca as the exchangeable cation and most of the sectors in the framework are orthorhombic • Barrerite has also an orthorhombic structure with present Na, K, and Ca • Stilbite has a wide range of Ca, Na, and K with various amounts of monoclinic, orthorhombic, and triclinic sectors in the same crystal

World reserves of natural zeolites have not been estimated yet. Deposits occur in many countries, but companies and states rarely publish reserves data. The United States, for example, reported combined reserves of 80 million tons in 2021, while the total U.S. reserves are likely substantially larger [41]. In 2021, the world´s annual mine production of natural zeolite was estimated at 944,000 t, which is significantly lower than a few years ago as the production of natural zeolite in 2015 was about 2.78 million tons. Major producers in 2021 (estimation) included Georgia (140,000 t), Indonesia (130,000 t), the Republic of Korea (130,000 t), Slovakia (120,000 t), Unites States (87,000 t), Cuba (53,000 t), China (52,000 t), and Turkey (50,000 t). China has significantly reduced its production, for example in 2015 it produced as much as 2 million tons of natural zeolite [41],

2. 2. Synthetic zeolites

In the mid-1940s, Barrer and Milton opened the story of zeolite synthesis [41] and since then, the interest in various synthesis routes of different zeolitic materials did not stop. Today, the Structure Commission within the International Zeolite Association denotes each synthesized zeolite by a three-letter code. The latest zeolite codes approved since 2020 and their frameworks are presented in Table 2 [31].

Zeolites are commonly synthesized under hydrothermal/solvothermal conditions with alkali metal ions or organic amines/ammonium ions as the structure-directing agents (SDAs) or templates. The reactive reagents usually include tetrahedral atom (Al, Si, P, *etc*.) sources, SDA, mineraliser (OH⁻ or F⁻), solvent, *etc*. Many synthesis parameters are crucial in the zeolite formation such as: source materials, composition, the solvent Si/Al mole ratio, SDA, crystallization temperature, pH value, and ageing/crystallization time. Due to the vast diversity of routes, there is insufficient understanding, so far, of the formation mechanism of zeolite materials. Somewhat harsh conditions of synthesis inspired many researchers to make efforts toward greener synthesis routes [41].

The published studies emphasize the use of renewable or waste feedstock, energy efficiency, safer solvents and auxiliaries, and utilization of less hazardous chemicals and synthesis conditions [28]. However, the traditional zeolite synthesis deviates to a certain extent from the principles of green chemistry.

Table 2. Newest framework types of synthetic zeolites approved by the International Zeolite Association [34]

Framework type	Cell parameters	Accessible volume fraction, %	Framework image
ANO	hexagonal	12.4	
PTO	monoclinic	9.12	
PTT	trigonal	10.38	
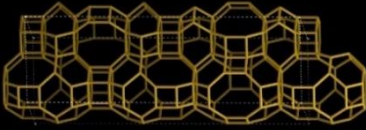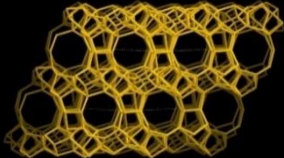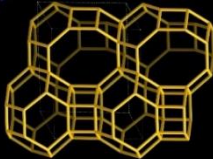
The hydrothermal or solvothermal synthesis methods commonly require high temperatures and pressures, which unequivocally increases energy consumption and raises process risks. Organic solvents are usually expensive and toxic and therefore increase costs and environmental impact. The obtained filtrates contain inorganic/organic molecules that should be recuperated and reused. Finally, the resulting precursors need to be calcined at high temperatures, which is not economically nor environmentally attractive. Researchers have therefore been making huge efforts to develop different routes to guide the process of zeolite synthesis according to the principles of green chemistry, such as: waste reusing [29], environmental and cost impact reduction, increased energy efficiency [29,42], process safety [41], *etc*. Many studies are oriented towards the rational synthesis of zeolitic materials with specific novel framework structures and functions [43].

3. ZEOLITES AS CATALYSTS

Since WWII, the development of zeolite-based catalysts has been one of the most impressive breakthroughs in the catalysis world. In the beginning, it was just the curiosity of researchers to investigate their property of adsorption and desorption of water when heated, so in the period of 1940s researchers at the Union Carbide (Linde division) synthesized zeolites A, B, and X [25]. In the following years, commercialisation of these zeolites started as gas separation adsorbents. Shortly afterwards, researchers at Union Carbide and Mobil discovered the zeolite shape selectivity and how to control it and thus, the golden age of zeolite use as catalysts began.

Different zeolite origins, structures and the resulting physical and chemical characteristics have logically resulted in the classification of zeolite-based catalysts into several groups: natural- zeolite-based catalysts, synthetic zeolite-based catalysts, and waste-based zeolitic catalysts.

3. 1. Natural zeolites as catalysts

Chemically modified natural minerals and rocks were investigated widely in the synthesis of low-cost, easily available, and environmental heterogeneous catalysts for biodiesel production [44]. Natural zeolitic materials are widely available in mines around the world and are considered relatively inexpensive [45]. This type of zeolite material is highly desirable because of the possibility to control the functionalisation of the zeolite surface by acidic or basic groups to achieve high catalytic performance and consequently high biodiesel yields. In addition, natural zeolite-based catalysts have the important advantage of avoiding the zeolite synthesis step compared to synthetic zeolite-based catalysts and waste-based zeolitic catalysts, which significantly shortens the catalyst synthesis time and lowers the energy used.

Conducted studies (Table 3) demonstrated that decoration of zeolite by nanoparticles or modification of zeolite structure by alkali or alkali earth metals/oxides resulted in catalysts of enhanced morphological properties, high surface area with good porosity, and finely dispersed numerous catalytically active sites. These catalytic materials have most often succeeded in achieving high activity and yielding FAME greater than 90 % using mild reaction conditions (Table 4).

Table 3. Review of preparation routes and characteristics of natural zeolitic catalysts

Catalyst designation and origin	Catalyst preparation	Catalyst characteristics	Ref.
KOH/clinoptilolite Clinoptilolite (Semnan, northeast of Iran)	**Impregnation** • Impregnation under constant stirring at 60 °C for 24 h • KOH/clinoptilolite ratio of 1:4 • Drying and calcination at 400 °C for 5 h	Content (XRF), %: (SiO_2) 60.6; (K_2O) 25.5; (Al_2O_3) 6.8; (Na_2O) 1.2; (Fe_2O_3) 1.1; (CaO) 1.0; (MgO) 0.65; (TiO_2) 0.11	[45]
K-/Na-/Ca-/Mg-/clinoptilolite	**Green alkali modification** • Mechanical activation • Alkali modification (nitrate salts of Ca, Mg, K, and Na) under ultrasonic irradiation and magnetic stirring (500 rpm) for 1 h • Green-tea solution reducing agent for 4 h with mixing, ageing for 24 h • Extensive washing, and drying (70 °C for 12 h)	Mg/clinoptilolite Content (EDX), %: (Mg) 8.7, (Si) 20.8, (Al) 5.0, (K) 4.3, (Fe) 3.1, (O) 49.4 2θ / ° (XRD): (clinoptilolite) 24, 28.15; (MgO) 29.8, 43.13 Specific surface: 342.5 $m^2\,g^{-1}$ Total volume: 0.05 $cm^3\,g^{-1}$ Average pore size: 19.6 nm Basicity: 4.34 mmol g^{-1} λ (FTIR) / cm^{-1}: (water) 3412, 1640 3412, 1640; (zeolitic structure) 1041, 466	[48]
KOH/zeolite Bandung (Indonesia) natural zeolite, mordenite type.	**Zeolite activation** • Sieved (230 mesh) • 6 M HCl for 4 h with stirring **KOH modification** • 50 % KOH + zeolite under ultrasonic radiation • Dried for 24 h and calcined at 450 °C for 4 h	Content (XRF), %: (Si) 40.7; (K) 38.7; (Fe) 10.2; (Ca) 8; (Ti) 1; (Sr) 0.5 2θ / °(XRD): (KOH) 31, 34, 38; (zeolite) 13.4, 19.6, 22.2, 25, 26.2, 27.6, 30.8	[46]
NaOH/zeolite Natural clinoptilolite from Lampung, Indonesia	**Pretreatment** • Immersed in 1 % HF for 30 min, washed, and dried for 2 h **Impregnation** • 2 M NaOH + zeolite for 24 h and dried for 2 h	Content (XRF), %: (Na) 20.5	[53]
K/zeolite Mordenite type	**Incipient wetness impregnation** • Natural zeolite was sieved (150-200 mesh) • 0.5 M H_2SO_4 activation at 90 °C for 4 h • Washed & dried • Stirring with KNO_3 for 24 h • Calcination at 400 °C for 4 h	Content (AAS), %: (K) 4.76 Specific surface area (BET): 111.6 $m^2\,g^{-1}$ Average pore size: 8.3 nm 2θ / ° (XRD): (K_2O) 31, 39, 51, 55; (zeolite) 12.4, 19.4, 29.9, 37.1, 45, 56, 60.6; λ (FTIR) / cm^{-1}: (broad peak) 3400-3700, 1080, 550	[47]
KOH/zeolite Natural zeolite Bayah Banten (Indonesia)	**Impregnation** • Natural zeolite was sieved (<50 mesh) • Dried at 110 °C for 24 h • KOH solution impregnated at 60 °C for 26 h • Vacuum separated, dried for 24 h and calcined at 450 °C for 4 h	-	[49]
K_2O/zeolite	**Impregnation** • Natural zeolite was crushed and dried • KOH solution impregnated at room temp, dried for 24 h and calcined at 500 °C for 3 h	Acid number of WCO: 2.92 mg KOH g^{-1} Crystal phase (XRD): no K_2O or KOH peaks are observed	[50]
K_2CO_3/zeolite Natural zeolite from Tapanuli Utara, North Sumatera, Indonesia	• Zeolite was treated with 30 % (v/v) H_2O_2, separated, dried for 24 h, and milled (140 mesh) **Impregnation** • Treated zeolite + (45 g / 60 ml H_2O) K_2CO_3 (w/w=1:4), mixed at 60 °C for 2 h • Dried at 60 °C for 24 h, vacuum filtrated, dried at 110 °C for 24 h, and calcined at 450 °C for 4 h • Milled (140 mesh)	Content (AAS): 11.24 % K_2CO_3	[51]
Zeolite	**Zeolite activation** • Natural zeolite crushed and dipped with H_2SO_4 for 0.5 h, aged for 24 h • Calcined at 450 °C for 2 h	-	[54]

Catalyst designation and origin	Catalyst preparation	Catalyst characteristics	Ref.
Na-zeolite/$Fe_2(SO_4)_3$ Natural zeolite from Kenya Clinoptilolite and kaolinite type	**Zeolite activation** • Natural zeolite crushed, sieved (0.25-0.5 mm), washed and dried for 24 h • Acid treated: 16 % HCl at room temp. for 12 h, washed, dried, and calcined at 300 °C for 4 h **Cation exchange** • H-zeolite: 0.1 M NH_4NO_3 refluxed at 80 °C for 3 h, dried, and calcined at 300°C for 4 h • Na-zeolite: 1 M NaCl refluxed at 90 °C for 72 h, washed, dried for 4 h and calcined at 300°C for 3 h • $Fe_2(SO_4)_3$ was added into reactor (w/w =1/2)	Natural zeolite: Si/Al = 3.98 Content (ICP-AES), %: (SiO_2) 62.2, (Al_2O_3) 13.3, (CaO) 12.0, (Fe_2O_3) 4.8, (Na_2O) 3.1, (MgO) - 1.6 λ (FTIR) / cm^{-1}: bands typical for zeolites at 3000-4000 (broad band), 1640, 500-1100, 400-500	[55]
Zeolite 2 % Ru/zeolite 2 % Ag/zeolite 2 % Pd/zeolite 2 % Pt/zeolite	**Impregnation** • Precursor salts: hexachloroplatinic acid, ruthenium chloride, palladium nitrate, and silver nitrate • Dried for 2 h, calcined in air at 400 °C for 4 h, and before the reaction reduced in 5 % H_2-95 % Ar at 300 °C for 1.5 h	Specific surface area (BET), $m^2 g^{-1}$: 25.95 (Z), 26.37 (Ru/Z), 21.32 (Ag/Z), 21.35 (Pd/Z), and 16.11 (Pt/Z) Average pore radius, nm: 4.09 (Z), 5.84 (Ru/Z), 6.20 (Ag/Z), 6.38 (Pd/Z), and 6.67 (Pt/Z) NH_3-TPD total acidity, $mmol g^{-1}$: 1.0 (Z), 2.3 (Ru/Z), 1.9 (Ag/Z), 1.9 (Pd/Z), and 2.1 (Pt/Z) CO_2-TPD, total basicity, $mmol g^{-1}$: 0.8 (Z), 0.6 (Ru/Z), 0.5 (Ag/Z), 0.5 (Pd/Z), and 0.6 (Pt/Z) Natural zeolite: XPS: Si/Al = 4.42 Identified crystal phase(XRD): mordenite, calcite, clinoptilolite and quartz	[56]

Table 4. Review of the optimal reaction conditions when using natural zeolitic materials as a catalyst/catalyst support

Catalyst designation	Feedstock	Reactor type	Optimal reaction conditions				Yield (conversion), %	Ref.
			T / °C	CC*, wt.%	$t(\tau)$ / min	Alcohol to oil molar (volume) ratio		
Continuous processes								
KOH/clinoptilolite	WCO methanolysis Acid value of 3.12 mg KOH/g	Microreactor	65	8.1	(13.4)	(2.25:1)	(97.4)	[45]
Batch processes								
Mg/clinoptilolite	WCO methanolysis	Stirred batch reactor	70	4	120	16:1	98.7	[48]
70 % KOH/zeolite Mordenite from Bandung, Indinesia	Castor oil methanolysis	Stirred batch reactor	55	17	420	15:1	92.11	[46]
NaOH/zeolite Natural clinoptilolite from Lampung, Indonesia	Microalgal oil (*Chlorella vulgaris*) methanolysis	Stirred batch reactor	60	3	4	(50:1)	36.8	[53]
K/zeolite	Rice bran oil methanolysis	Stirred batch reactor	67.5	5	240	12:1	83.2	[47]
KOH/ zeolite Natural zeolite bayah banten, Indonesia	WCO methanolysis	Stirred batch reactor	60	3	120	7:1	94.8	[49]
K_2O/zeolite	WCO methanolysis (HCl esterification as a pretreatment	Stirred batch reactor	65	2.5	120	8:1	95	[50]
K_2CO_3/zeolite Natural zeolite from Tapanuli Utara, North Sumatera	Rice bran oil methanolysis	Batch stirred reactor (500 rpm)	65	4	180	10:1	98.2	[51]
Zeolite	Palm oil methanolysis	Batch stirred reactor (200 rpm)	65	0.75	120	14:1	85	[54]
Na-zeolite/$Fe_2(SO_4)_3$ Natural zeolite from Kenya	*Jatropha curcas* oil methanolysis	Batch stirred reactor (600 rpm)	65	28.9	330	6:1	57	[55]

Catalyst designation	Feedstock	Reactor type	Optimal reaction conditions				Yield (conversion), %	Ref.
			T / °C	CC*, wt.%	$t(\tau)$ / min	Alcohol to oil molar (volume) ratio		
Zeolite 2 % Ru/zeolite 2 % Ag/zeolite 2 % Pd/zeolite 2 % Pt/zeolite	Rapeseed oil methanolysis	Autoclave	260	-	120	9:1	Zeolite-67.2 Ru/zeolite-71.0 Ag/zeolite-71.6 Pd/zeolite-73.8 Pt/zeolite-94.6	[56]

*Catalyst content

Natural zeolite from Bandung Indonesia modified with KOH was used for castor oil methanolysis [46]. By using demanding castor oil (about 84 % of ricinoleic acid) over the zeolite catalyst loaded with high content of KOH (70 wt.%), the FAME content of 92.1 % was obtained, but at a somewhat longer reaction time of 7 h. Unusual, but a reaction temperature (55 °C) slightly below the boiling point of methanol was shown to provide the best results in this case. Potassium as active species in KNO_3 loaded natural zeolite mordenite type from Indonesia did not show activity as similar catalysts [47]. In the reaction with rice bran oil under mild reaction conditions, but at a slightly higher temperature (67.5 °C), a FAME yield of 83.2 % in 4 h was obtained. On the other side, another potassium-modified natural zeolite catalyst, showed significantly better activity [48]. Also, under mild reaction conditions (catalyst loading of 4 wt.%, methanol to waste cooking oil molar ratio of 16:1, and reaction temperature of 70 °C) the catalyst achieved a biodiesel yield of 93.6 % in 2 h. A similar catalyst in the same study showed even better performance, *i.e.*, magnesium-modified natural zeolite achieved a biodiesel yield of 98.7 % under the same reaction conditions. The authors of this study gave the synthesized materials a green and environmental insignia, because they used a green alkali modification synthesis method based on one step using a green tea-based reducing reagent. In addition, the catalysts showed very good reusability.

Also, good activity results were obtained by another potassium-loaded zeolite catalyst, obtained by impregnation of natural Bayah Banten zeolite from Indonesia by KOH [49]. The FAME yield of 94.8 % was achieved in 2 h of reaction with WCO. A similar short study [50], in terms of the catalytic material and reactor system, showed a great potential of a KOH/natural zeolite catalyst for biodiesel production. In specific, 25 % nominal KOH impregnated on natural zeolite from Indonesia achieved a high biodiesel yield of 95 % in 2 h of reaction with a rather low methanol to oil ratio of 8:1 and catalyst loading of 2.5 wt.%. It should be noted that WCO was pretreated with HCl to esterify FFA. The rice bran oil methanolysis over K_2CO_3 loaded on natural zeolite from North Sumatra, Indonesia, under mild reaction conditions resulted in a biodiesel yield of 98.2 % in 3 h [51]. All these presented studies were conducted in simple batch-stirred reactors, except for one study that was performed under continuous reaction conditions [42]. A KOH/clinoptilolite catalyst (clinoptilolite originating from Semnan, Iran) was used in a microreactor for the methanolysis reaction with WCO [45]. The microreactor consisted of a micromixer and a microtube (5 m long, 0.8 mm in diameter) and was equipped with a peristaltic pump to transport reactants. In this study, the already demonstrated advantage of microreactors as compared to classical batch-stirred reactors were confirmed [52]. This is reflected in the required time to reach the reaction equilibrium of 2 h in a batch-stirred reactor, while it took only 13.4 min in the microreactor in which case a biodiesel yield of 97.4 % was achieved. It should be considered that WCO with an acid value of 3.12 mg KOH g^{-1} was used in the reaction.

Sustainable biodiesel production was investigated in a study combining the use of natural zeolite as a catalyst and microalgal oil (*Nannochloropsis oculate* and *Chlorella vulgaris*) as a feed [53]. Natural clinoptilolite from Lampung in Indonesia was simply activated by NaOH even without the usual thermal activation, which certainly resulted in significant energy savings. In this study, *Chlorella vulgaris* oil showed better potential than *Nannochloropsis oculate* oil as a feedstock resulting in 98 % FAME yield as compared to 83.5 % obtained in the latter case under the same mild reaction conditions with a rather higher lipid to methanol volume ratio of 1:50.

A neat simply acid-activated natural zeolite exhibited, surprisingly, solid performance in the reaction with palm oil and methanol [54]. Under mild reaction conditions and 2 h of reaction time, the FAME yield was 82.5 %.

A catalyst obtained in a relatively complex manner (Table 4), based on cation exchange with Na in natural clinoptilolite from Kenya followed by additional chemical modification with $Fe_2(SO_4)_3$, was used in difficult reaction conditions with very high FFAs level (about 14 %) in Jatropha oil [55]. It was shown that such a demanding oil for the transesterification reaction with the proposed catalyst should have been pretreated by esterification. The highest FAME

yield of only 57 % was achieved in 6 h of reaction, and, based on the FAME profile *vs.* time, the reaction has reached equilibrium. It turned out that the added $Fe_2(SO_4)_3$ in a w/w ratio of 1:2 was unable to catalyse esterification and the overall catalytic activity was primarily in the transesterification reaction.

Noble metals, like Pd, Ru, and Ag, supported by natural zeolite exhibited modest activity in the methanolysis of vegetable oil, bearing in mind that the reaction took place in an autoclave at an elevated temperature (260 °C) and only Pt/zeolite was achieved the FAME yield of 94.6 % in 2 h [56]. Interestingly, the neat natural zeolite achieving a FAME yield of 67.2 % was even more active than the Pd/zeolite catalyst, and it was approximately as active as the other two investigated catalysts, Ru/zeolite and Ag/zeolite. These catalysts exhibited an unusual reaction behaviour in their selectivity, inducing a TG conversion higher than 95.3 %.

3. 2. Synthetic zeolite-based catalysts

Synthetic zeolitic-based materials are a very important group, especially as they have been widely exploited in many large-scale industrial processes [25,57]. Many zeolite framework types exist, but for catalytic purposes currently commercially are employed only a dozen such as Beta, ZSM, FAU, MFI, MOR, *etc.* [25]. The average pore diameter in these zeolites is about 1.0 nm (Table 5), which can be a problem for applications in reactions involving large molecules. TG and FAME molecules are relatively large [58], so preparation or use of mesostructured materials is a necessity in these cases to overcome diffusion limitations. Generally, synthetic zeolite-based catalysts showed very high activity, reaching the reaction equilibrium in only 30 min, but in some cases, the biodiesel yield was insignificant, which largely depended on the reaction conditions, the used reactor system, and the type of oily feedstock (Table 6). These catalysts exhibited a very high specific surface area (Table 5) compared to the other zeolite-based catalysts (Tables 3, 7, and 8) and, correspondingly, a smaller pore diameter. Interestingly, such morphological characteristics did not negatively affect the catalyst activity, because the small pore diameter limiting the access of molecules from the reaction mixture was compensated by the large external surface area of the catalyst, which was one to two orders of magnitude greater than that of, for example, natural zeolite-based catalysts.

Biodiesel production from low-quality fatty substrates, such as waste oils or some inedible oils, is certainly challenging. A relatively new approach was proposed and termed hydro-esterification involving hydrolysis of TG in the first step, and esterification of FFA in the second [59]. The hydrolysis step is insensitive to the moisture content or low pH of the feedstock, so impurities are removed from the oily feed in a robust process.

Table 5. Review of preparation routes and characteristics of synthetic zeolite-based catalysts

Catalyst designation and origin	Catalyst preparation	Catalyst characteristics	Ref.
H-ZSM-5 SiO_2 to Al_2O_3 ratio (SAR) of 15 SAR of 140	Commercial catalyst • Calcined in the air at 550 °C for 5 h with a heating rate of 2 °C min^{-1}	Structural parameters: Surface area, $m^2 g^{-1}$: (SAR 15) 410; (SAR 140) 450 Micropore volume, $cm^3 g^{-1}$: (SAR 15) 0.09; (SAR 140) 0.12 Pore size, nm: (SAR 15) 0.51×0.55; (SAR 140) 0.53×0.56 NH3-TPD, mmol g^{-1}: (SAR 15) Brønsted sites 0.27; (SAR 140) Brønsted sites 0.99	[59]
Gismondine-based: Na-MAP K-MAP CsK-MAP K-A CsK-A FAU-based: Na-X K-X CsNa-X Na-Y K-Y CsNa-Y	Cs- and CsK-containing zeolites: • Na-form of zeolites A, MAP, X, and Y was treated with the solutions of $CsNo_3$ and CsOH (4/1 v/v) at 80 °C for 1 h. • Washed and dried overnight at 80 °C. • Calcination in the air at 450 °C for 2 h with a heating rate of 1 °C min^{-1}. Other zeolites were commercial	TGA: (Na-MAP) ≈20 wt.% H_2O loss (25-350 °C) Content (EDX), Si/Al: (Na-MAP) 1.0; (K-MAP) 1.0; (CsK-MAP) 1.0; (K-A) 1.0; (CsK-A) 1.0; (K-Y) 2.5; (CsNa-Y) 2.5; (K-X) 1.2; (CsNa-X) 1.2 Na/Al: (Na-MAP) 1.0; (K-MAP, CsK-MAP) 0.1; (K-A) 0.55; (CsK-A) 0.5; (K-Y) 0.2; (CsNa-Y) 0.35; (K-X) 0.4; (CsNa-X) 0.6 N_2-physisorption, BET, $m^2 g^{-1}$: (K-A) 15; (K-MAP) 45; (K-X) 615, (K-Y) 670. Total basicity (TPD-CO_2), μmol g^{-1}: (Na-MAP) 235, (Na-X) 275; (Na-Y) 320; (K-Y) 345; (K-X) 390; (K-A) 420, (K-MAP) 430	[62]

Catalyst designation and origin	Catalyst preparation	Catalyst characteristics	Ref.
Mo-NaBeta	**NaBeta zeolite support** • NaOH + NaAlO$_2$ + tetraethylammonium hydroxide (TPAOH) stirred at room temp. for 1 h. • Silica gel is added, stirred (1 h). • A cationic copolymer containing quaternary ammonium groups (RCC) added dropwise [the resulting gel - Al$_2$O$_3$/32SiO$_2$/2Na$_2$O/0.01RCC/2.6TPAOH/296H$_2$O] • Autoclave crystallization at 140 °C for 6 days. • Filtered, dried, and calcined at 550 °C for 6 h. **Mo-NaBeta catalyst** • Incipient wetness impregnation method with ammonium molybdate. • Aged for 24 h, dried, and calcined at 550 °C for 3 h.	2θ / ° (XRD): (NaBeta zeolite) 7.7, 21.4, 22.5, 25.4, 27.1 λ (Raman) / cm^{-1}: (MoO$_3$ phase) 116, 129, 157, 246, 278, 338, 381, 668, 821, 997 Specific surface area (BET): 453 m^2 g^{-1} Average pore diameter: 5.4 nm $V_{mesopore}$: 0.18 cm^3 g^{-1} $V_{micropore}$: 0.13 cm^3 g^{-1} H4 hysteresis	[63]
HPW/ZIF-67 (HPW modified Co-based zeolite imidazole framework)	**ZIF-67 synthesis** • Cobalt nitrate + methanol and 2-methylimidazole + methanol were ultrasound treated for 15 min. • Stirred at ambient temp. for 4 h, centrifuged, washed x3, and dried overnight at 130 °C. **HPW/ZIF-67 synthesis** • HPW + ZIF-67 was ultrasound treated for 30 min. • Stirred at ambient temp. for 24 h, centrifuged, washed x3, dried in vacuum at 200 °C.	Specific surface area (BET): 1137 m^2 g^{-1} (88.7 % micropore) Average pore size: 3.16 nm Ishoterm Type I with H3 hysteresis Basicity: 2.46 mmol g^{-1} (Lewis/Brønsted acid ratio=0.18) λ (FTIR) / cm^{-1}: (HPW) 808, 889, 947, 1043	[67]
CaO/zeolite (ZSM-5; CAS No. 1318-02-1)	• Zeolite activation by calcination in air at 500 °C for 4 h (autoclave). **Impregnation** • Calcium acetate + zeolite solution was aged for 12 h. • Dried and calcined in the air at 700 °C for 3 h.	35 % CaO/zeolite λ (FTIR) / cm^{-1}: (bi-carbonate group) 1640 and 1400; (Ca-O group) 528 TPD-CO$_2$: (Desorption peaks) 87, 336, 634, 695 and 886 °C	[61]
HMCM-36 (MWW zeolite type)	**MCM-22(P)** • Hydrothermal synthesis NaAlO$_2$ + H$_2$O and NaOH + H$_2$O mixed, hexamethylenimine added and stirred for 45 min, Aerosil 200 + H$_2$O was added under vigorous stirring for 2 h. Resulting gel (1 SiO$_2$/0.09 Na$_2$O/0.5 HMI/45 H$_2$O/0.01 Al$_2$O$_3$) Crystallization: stirred (600 rpm) at 135 °C for 8 days, washed, and dried overnight at 75 °C. **MCM-36** • Swelling: MCM-22(P) + CTAB + TPAOH + H$_2$O (w/w; 1/5.61/2.44/21.4) stirred at 40 °C for 48 h; washed and dried at 75 °C. • Pillaring: swollen material + TEOS was stirred at 80 °C for 24 h; filtered, dried at 30 °C for 12 h. Samples + H$_2$O (w/w; 1/10) hydrolysed at 40 °C for 5 h, and dried at 30 °C. • Two-step calcinations: 6 h at 450 °C in N$_2$ (1 °C min^{-1}) and 12 h at 550 °C in the air (2 °C min^{-1}). **HMCM-36** • Ion exchange: 1 M NH$_4$NO$_3$ solution for 8 h (pH 7, NH$_4$OH), filtered, dried and calcined at 500 °C for 5 h	Specific surface area (BET), m^2 g^{-1}: 635, 205 (micropore), 430 (mesopore) Isotherm Type IV DRIFT pyridine ads., µmol g^{-1}: (Brønsted sites) 34.3; (Lewis sites) 10.2 λ (FTIR) / cm^{-1}: 1087, 805, 595, 554	[65]
Lipozyme-TL/FM-8 (Commercial FM-8 zeolite, mordenite type)	**Lipase immobilization** • Zeolite + lipase enzyme (2.5 mg mL^{-1}) + 0.1 M phosphate buffer (pH 7) aged for 18 h at room temp	Chemical composition of zeolite: Na$_{0.17}$[(AlO$_2$)$_{1.10}$(SiO$_2$)$_{0.45}$]1.34H$_2$O	[66]
Ba-Sr/ZSM-5	**Incipient wetness impregnation method** • ZSM-5 zeolite calcined at 600 °C for 6 h • Impregnated with 6 wt.% of Sr(NO$_3$)$_2$ • Impregnated with 4 wt.% of Ba(NO$_3$)$_2$ • dried for 12 h and calcined at 600 °C for 6 h	Specific surface area (BET): 224.2 m^2 g^{-1} Average pore diameter: 1.89 nm Phase (XRD): identified phase - Al$_2$SiO$_8$, BaO, SrO (monoclinic), and Al$_2$O$_3$SiO$_2$ (orthorhombic) λ (FTIR) / cm^{-1}: (H$_2$O) broad band at 3454 & 1636, (Lewis acid sites) ≈1490, (Brønsted acid sites) 1540-1630, (SrO & BaO) 520-600	[60]

Catalyst designation and origin	Catalyst preparation	Catalyst characteristics	Ref.
2D Na/ITQ-2 (Two-dimensional MWW-type structure)	**Rotational hydrothermal synthesis of 2D zeolite** • Hexamethyleneimine (HMI) as an organic structure-direction agent, starting gel was 1.0 Al_2O_3 : 30 SiO_2 : 2.5 Na_2O : 10 HMI : 580 H_2O • NaOH & $NaAlO_2$ were dissolved in H_2O + colloidal silica (40 wt.%) & HMI and stirred for 3 h • Crystallization: stirred autoclave at 140 °C for 4 days • Centrifuged, washed with H_2O & ethanol and dried at 80 °C • A precursor was suspended in aqueous cetyltrimethylammonium hydroxide/tetrapropylammonium hydroxide at 85 °C for 16 h • Delamination: ultrasound bath for 1 h at 50 °C & pH of 12.5 • Washed, dried and calcined at 600 °C for 8 h **Solid-state ion exchange** • Ion exchange with 1 M NH_4NO_3 at 80 °C for 8 h • 1 mmol alkali & alkaline-earth acetate was mixed with zeolite support and grinded (1:1 of molar ratio) • Calcined at 600 °C for 10 h	Content (ICP-OES), 2.1 wt.%: Na, Na/Al = 1.2, Si/Al = 22 Specific surface area (BET): 613 m^2 g^{-1} V_{meso} / cm^3 g^{-1}: 0.77 V_{micro} / cm^3 g^{-1}: 0.08 Type IV isotherm	[64]

Table 6. Review of optimal reaction conditions when using synthetic zeolite-based materials as catalysts/catalyst supports

Catalyst designation	Feedstock	Reactor type	Optimal reaction conditions				Yield (conversion), %	Ref.
			T / °C	CC*, wt.%	t / min	Alcohol to oil molar ratio		
H-ZSM-5	WCO methanolysis	Stirred batch • Two-step reaction • Hydrolysis (H) with water • Esterification I with ethanol	H-100 E-77	H & E=5	240	H (water to oil)-3:1 E-3:1	H-(40) E-(63)	[59]
K-MAP (K-form of synthetic gismondine based on the maximum Al P)	Refined rapeseed oil methanolysis	Pressured stirred batch high power density (Biotege Initiator + single-mode microwave system)	160	5	15	12:1	(96), [TOF, h^{-1} = 202]	[62]
7 % Mo-NaBeta	Rice bran oil methanolysis	Stirred autoclave (300 rpm)	140	1.5	480	13.7:1	(84.6)	[63]
0.25 HPW/ZIF-67	Microalgal oil (*Chlorella vulgaris*) esterification and methanolysis	Autoclave	200	1	90	20:1	(98.5)	[67]
CaO/zeolite	Waste lard methanolysis	Microwave (595 W)	-	8	75	30:1	90.1	[61]
HMCM-36	Palmitic acid esterification	Stirred batch reactor	80		360	30:1	(100)	[65]
Lipozyme-TL/FM-8	WCO methanolysis	Stirred batch (200 rpm)	Room (24)	4	1440	4:1	Insignificant (≈0.65)	[66]
Ba-Sr/ZSM-5 (6 wt.% Sr; 4 wt.% Ba)	Sunflower oil methanolysis	Stirred batch (500 rpm)	60	3	180	9:1	87.7	[60]
2D Na/ITQ-2 (2D MWW-type structure)	Triolein methanolysis	Stirred batch (1000 rpm)	60	15	60	10:1	95	[64]

*Catalyst content

In that manner, this step circumvents soap formation as a major drawback of common and commercialised biodiesel production processes. A commercial H-ZSM-5 catalyst was used for the hydro-esterification of WCO under relatively mild reaction conditions (under 100 °C). Structurally the catalyst had a small pore size (about 0.55 nm) unfavourable for this kind of reaction, and consequently very high surface area, but the displayed activity was surprising. In 4 h of reactions, WCO hydrolysis with 40 % conversion into a fatty acid mixture and 63 % conversion of the synthesized fatty acids in esterification to biodiesel was observed. ZSM-5 zeolite supporting Ba and Sr was used in another study [60] showing solid activity under mild reaction conditions.

Yet, more interesting, the biodiesel yield did not fluctuate much with the change in reaction parameters such as the methanol to oil molar ratio, reaction time, and even the reaction temperature. The highest biodiesel yield (87.7 %) was achieved in 3 h of reaction. The best methanol to oil molar ratio was found to be 9:1, but in the whole interval from 3:1 to 21:1 ratio, the yield was almost constant, even at the theoretical molar ratio of 3:1. Also, the influence of reaction

temperature in the range from 50 °C to 65 °C was negligible. ZSM-5 zeolite impregnated with CaO showed a biodiesel yield of 97.1 % from waste lard under mild reaction conditions in 1.25 h of reaction in a microwave reactor [61]. To achieve such a good activity of the catalyst in a relatively short reaction time, it was necessary to load 35 wt.% CaO on the zeolite surface.

Table 7. Review of preparation routes and characteristics of zeolitic materials obtained from natural or waste sources

Catalyst designation and origin	Catalyst preparation	Catalyst characteristics	Ref.
Co-Ni-Pt-FAU FAU-type zeolite prepared from shale rock (Wexford, Ireland)	**Zeolite** • Shale was crushed, sieved (<90 μm), and calcined in air at 800 °C for 4 h • Deferrization: 5 M HCl at 85 °C for 4 h • Alkali activation: 1:1.5 m/m, 40 wt.% NaOH, heated in air at 850 °C for 3 h, crushed • Fused shale + sodium silicate + water, stirred (3 h), aged at room temp. for 18 h • Hydrothermal treatment: 100 °C for 24 h **NH$_4^+$ zeolite (H-FAU)** • 3x (2 M ammonium chloride+ zeolite stirred at room temp. for 2 h, washed) • Washed, dried, and calcined in air at 500 °C for 4 h **Co-Ni-Pt-FAU** • Incipient wetness method (Co, Ni, and Pt precursors in 0.1 M HCl), loadings of 1 wt.% • Dried and calcined in air at 500 °C for 4 h	Specific surface area (BET), m^{2}g^{-1}: (H-FAU) 571; (CO-Ni-Pt-FAU) 490	[57]
Zeolite Steel furnace slag	• Furnace slag was ground (<90 μm) and calcined at 700 °C for 3 h • 3 M HCl at 100 °C for 2 h • Hydrated silica-gel (90 % of silica) was separated, filtered, rinsed 2×, dried, powdered and dissolved in 6 M NaOH + NaAlO$_2$ • The solution was stirred at room temp. for 1 h and another 1 h at 90 °C **Crystallization** • In autoclave at 100 °C for 6 h, filtered, washed, dried, and calcined at 450 °C for 4 h	2θ/ ° (XRD): (zeolite structure) 24.7, 29.6, 39.2, 57.1 Mass loss temperature (TGA), °C: 100-150, 450, and 800 Specific surface area (BET): 10.3 m^{2}g^{-1}	[72]
HY-kaolin Zeolite prepared from Iraqi kaolin clay, faujasite structure	**NaY zeolite** • Sieved kaolin + 40 wt.% NaOH (w/w=1:1.5) was heated at 850 °C for 3 h; milled • Activated kaolin + Na silicate + H$_2$O was stirred at 50 °C for 1 h (pH=13.3); aged at 50 °C for 24 h and crystallized at 100 °C for 48 h • Washed, dried at 110 °C for 16 h, and calcined in air at 500 °C for 1 h **HY zeolite** • NaY + 1 M NH$_4$NO$_3$ was stirred at 100 °C for 4 h • NH$_4$Y zeolite was washed, dried at 100 °C for 6 h, and stirred with 0.5 N oxalic acid at room temp. for 8 h • Washed, dried, and calcined in air at 550 °C for 5 h	Content (XRF), %: (Al$_2$O$_3$) 15.92; (SiO$_2$) 58.11; (CaO) 4.11; (Fe$_2$O$_3$) 3.19, (MgO) 1.22 2θ/ ° (XRD): 6.3, 15.8, 23.8 Specific surface area (BET): 390 m^{2}g^{-1}65 % of zeolite Y purity	[74]
Zeolite/chitosan/KOH Clinoptilolite zeolite	**Impregnation** • Zeolite/chitosan powder + KOH aqueous solution (w/w=1:4) was stirred at 60 °C for 24 h; dried and calcined at 450 °C for 4 h	2θ/ ° (XRD): (chitosan) 10, 20; (zeolite) 6.6, 9.8, 22.2, 22.4, 25.7, 26.6, 27.6, 28.1, 29.9; (K$_2$O) 31.5, 32.4 λ (FTIR) / cm^{-1}: 2874, 1668, 1348, 1021, 821, 703, 460.8	[68]
LTA-kaolin Linde type A zeolite from kaolin	• Kaolin calcination at for 800 °C for 10 h **Hydrothermal synthesis** • 1.4 wt.% kaolin + H$_2$O + NaOH (kaolin/NaOH=1/2) at 90 °C for 24 h; washed and dried at 110 °C for 24 h • Calcination at 400 °C for 6 h	Specific surface area (BET): 44.9 m^{2}g^{-1} Content (NMR): Si/Al = 1.16 λ (FTIR) / cm^{-1}: 1076, 804, 557, 474	[73]
Na/zeolite-chitosan Clinoptilolite zeolite	**Impregnation** • Chitosan + zeolite + methanol (5 % v/v) mixed for 3 h + methanol (5 %) mixed for another 2 h • 0.5 M NaOH added drop-wise, mixed (100 rpm) for 3 h, dried at room temp.	Content (EDX), wt.%: I 37.2, (Na) 11.7, (Si) 10.3, (Al) 1.9, (O) 37.5 Mass loss (TGA): 5 % at 700 °C Specific surface area (BET): 3.73 m^{2}g^{-1} (8.3 for zeolite) λ (FTIR) / cm^{-1}: 1560, 1021, 643	[69]

Catalyst designation and origin	Catalyst preparation	Catalyst characteristics	Ref.
Na/CAN Cancrinite-type zeolite Natural diatomaceous earth (Vietnam)	**Hydrothermal synthesis** • Sieved with mesh No. 50 • Diatomite + NaOH + Al_2O_3 + H_2O stirred at 800 rpm for 30 min at room temp. and aged for 30 min • Hydrothermal reaction at 220 °C for 12 h • Washed, dried and calcined at 500 °C for 6 h	Phase (XRD): the complete transformation of diatomite to CAN zeolite λ (FTIR) / cm^{-1}: Typical CAN zeolite bands at 1036, 1003 and 966, 760, 683 TGA: evaporation of H_2O bounded in pores at 300-400 °C; dehydroxylation of silanol groups at ≈575 °C and change in aluminium structure on zeolite) at ≈800 °C Specific surface area (BET), $m^2 g^{-1}$: 29.83 (fresh), 30.41 (spent)	[77]
FAU-type zeolite Irish shale rock	**Hydrothermal synthesis** • Clean shale was crushed, sieved (<90 µm) and calcined in air at 800 °C for 4 h • Acid treated: 5 M HCl at 85 °C for 4 h • Alkali fusion: 40 wt.% NaOH (1/1.5 w/w), heated at 850 °C for 3 h, crushed • Hydrothermal treatment: fused shale + Na_2SiO_3 + H_2O stirred at room temp. for 3 h, aged for 18 h, hydrothermally treated at 100 °C for 24 h **NH_4 form** • Prepared zeolite + 2 M NH_4Cl stirred at room temp. for 2 h, the procedure was repeated 3 times • Washed, dried, and calcined at 500 °C for 4 h	Si/Al = 1.98 Specific surface area (BET): 571 $m^2 g^{-1}$ Average particle size: 2 µm	[76]
Ni/zeolite Geothermal solid waste	**Hydrothermal synthesis** • Si/Al molar ratio of 10:1 • Solution of NaOH (heated at 100 °C and stirred at 300 rpm) + $Al(OH)_3$ + geothermal waste was stirred for 2 h at 30 °C • Hydrothermal process: autoclave at 100 °C for 6 h • Washed until pH=7 and calcined at 500 °C for 5 h **Impregnation** • $Ni(NO_3)_2$ solution (5 % w/w) at 60 °C for 4 h • Calcined at 500 °C for 5 h	Geothermal solid waste composition, %: (SiO_2) 75.1; I 23.3; (Na_2O) 0.3; (Cl) 0.2; (Al_2O_3) 0.1 2θ / ° (XRD): (analcime) 15.9, 26.1, 30.1; (NiO) 43.0, 63.0, 75.0, 79.0 EDX: Ni was highly dispersed on the surface Specific surface area (BET): 81.9 $m^2 g^{-1}$ Pore radius: 1.56 nm	[70]
Zeolite Geothermal solid waste (Indonesia)	• Geothermal solid waste was washed, dried, and sieved (40 mesh) **Hydrothermal synthesis** • 3 M NaOH + geothermal waste + $Al(OH)_3$ was mixed (300 rpm) at 100 °C for 2 h • Crystallization in an autoclave at 150 °C for 8 h • Washed (until pH 7-8), dried, and calcined at 550 °C for 5 h	Content (XRF), %: (Fe) 9.3, (K) 8.2, (Cl) 6.7, (Ca) 6.7, (Si) 5.3, (S) 4.9, (P) 3.8, (As) 3.1, (Al) 2.2, (Sb) 2.0, (Zn) 1.9, (Cu) 1.5 Si/Al = 2.39 2θ / ° (XRD): (analcime) 16, 26.1, 30.7 Specific surface area (BET): 224.5 $m^2 g^{-1}$	[71]

Nano-crystalline synthetic gismondine-type MAP zeolite modified *via* cation exchange has been utilised as a highly active and selective catalyst to produce biofuel [62]. K-form of gismondine, based on the maximum aluminium MAP zeolite, exhibited a significant improvement in catalytic performance in the methanolysis of rapeseed oil in comparison with low silica zeolites FAU and LTA. Such behaviour was explained by its nanoparticle morphology and high basicity associated with the high Al content and a high degree of ion exchange. The highest yield of biodiesel (98 %) was obtained in only 30 min, but under microwave irradiation and elevated pressure and temperature of 1,5 MPa (15 bar) and 160 °C, respectively. It should be noted that also a high FAME yield (>95 %) was obtained even after only 15 min of reaction.

NaBeta zeolite was synthesized using a surfactant tetraethylammonium hydroxide in an energetically demanding process since the crystallization lasted for 6 days at 140 °C [63]. Finally, the catalyst was synthesized by impregnation of the zeolite support with molybdenum. The synthesized NaBeta zeolite possessed a very high specific surface area of 650 m^2 g^{-1}, while by loading Mo, that surface area was certainly reduced, but it remained significant, higher than 400 m^2 g^{-1}. The Mo content was optimized indicating the 7 % Mo/NaBeta zeolite catalyst as the most active, but still, its performance was limited yielding the TG conversion of 84.6 % in 8 h of reaction with rice bran oil in the autoclave at the elevated temperature of 140 °C. At a higher temperature a slightly higher conversion was achieved, however, the attempt to lower the temperature to 110 °C resulted in a very low catalytic activity (the TG conversion of about 37 % in 8 h). Optimisation of several parameters were performed in this study showing that smaller catalyst particles (0.15 to

0.55 mm) exhibited uniform and better activity than 0.65 mm and 0.75 mm particles. Agitation (50-500 rpm) of the reaction mixture in the autoclave did not contribute to increasing the catalyst activity, while higher methanol concentrations contributed to better TG conversion, especially to higher reaction rates in the initial stage.

Table 8. Review of preparation routes and characteristics of fly ash-based zeolitic materials

Catalyst designation and origin	Catalyst preparation	Catalyst characteristics	Ref.
Zeolite • Coal fly ash zeolite, sodalite type	**Hydrothermal process** • Alkali treatment: NaOH + H$_2$O + NaAlO$_2$ solution and NaOH + H$_2$O + fly ash solution formed sticky gel structure • Aged for 6 days • Crystallized at 100 °C for 24 h • Washed until pH 9.0 and dried for 24 h	Catalyst 2θ / ° (XRD): (sodalite zeolite) 14.1, 24.5, 31.8, 37.9, 43.2 Specific surface area (BET): 9.7 m^2 g^{-1} Isotherm type-IV Coal fly ash Content (XRF), %: (SiO$_2$) 68.4, (Al$_2$O$_3$) 14.8, (Fe$_2$O$_3$) 7.9, (CaO) 3.8, (K$_2$O) 2.5, (TiO$_2$) 1.2, (SO$_3$) 0.6, (MgO) 0.3, (ZrO$_2$) 0.1 Specific surface area (BET):3.4 m^2 g^{-1}	[79]
FA/K-X • Zeolite from South African class F fly ash	**FA/Na-X** • The conventional hydrothermal synthesis procedure **FA/K-X** • FA/Na-X was dried for 2 h + 1 M solution of K acetate (v/v=1/10), aged for 24 h at 70 °C. • Washed, dried at 120 °C for 2 h, and calcined in air at 500 °C for 2 h.	Fly ash SiO$_2$/Al$_2$O$_3$ = 1.65 Specific surface area (BET):257 m^2 g^{-1}: Phase (XRD), 2θ°: 12, 14, 24 λ (FTIR) / cm^{-1}: 300-430, 500-600, 620, 740, 950 Base strength: 15.0<$H\_$<18.4	[86]
Li/NaY • Zeolite from Chinese coal fly ash	**Alkali activation:** • Sieved fly ash + 0.5 M NaOH stirred at 80 °C for 1 h; washed and dried at 100 °C for 3 h. • Grounded with NaOH and calcined at 850 °C for 2h. **Hydrothermal synthesis:** • Molar ratio of Al$_2$O$_3$:SiO$_2$:Na$_2$O:H$_2$O = 1:8.8:4.3:250; stirring and ageing for 12 h. • Crystallization at 100 °C for 10 h, washed and dried. **Microemulsion-assisted co-precipitation:** • Ultrasound treated for 0.5 h (H$_2$O + isooctane + polyethylene glycol + *n*-propanol + NaY zeolite + Li$_2$CO4) • 1 M Na$_2$CO$_3$ was added in droplets under stirring at 60 °C for 1 h; aged for 12 h at 60 °C. • Washed x3, vacuum dried for 12 h, and calcined at 750 °C for 4 h (3 °C min^{-1})	Li/NaY molar ratio = 1.1 (TG): major weight loss ≈650 °C and ≈775 °C Phase (XRD): NaY and Li$_2$CO$_3$ peaks are not visible, new peaks of LiAlO$_2$, Li$_4$SIO$_4$, Li$_2$SiO$_3$, and Li$_3$NaSiO$_4$ emerged Specific surface area (BET): 105.7 m^{2}g^{-1} Average Pore size: 6.3 nm Basicity: 12.4 mmol g^{-1}; Basic strength: 15<$H\_$<18.4 λ (FTIR) / cm^{-1}: 3574, 3426, 1446, 952, 628, 512 Fresh and catalyst exposed to air for 10 days had very similar FTIR profile	[85]
CaO/ZM$_{FA}$ • Lignite coal fly ash (Serbia) • CaO from eggshell	**Thermo-chemical treatment** • Fly ash was calcined at 850 °C for 2 h • Acidification: 6 M HCl (S/L=1:5) at 80 °C for 6 h, filtrated, washed (pH neutral), and dried **Alkali activation** • 6 M NaOH (S/L=1:5) at 260 °C for 4 h in the rotating miniature autoclave, filtrated, washed (pH 9), and dried **Ultrasound-assisted impregnation** • Raw eggshells, dried, grounded, and calcined at 900 °C for 4 h • Calcined eggshells + 10 wt.% zeolite alcoholic suspension ultrasonically dispersed for 15 min • Dried and calcined at 550 °C for 4 h	2θ / ° (XRD): (lime) 37.5, 43.7, 63.4 Zeolite crystallite size: 47.8 nm; crystallinity degree of 81 % Catalyst crystallite size: 23.4 nm; crystallinity degree of 83 % λ (FTIR) / cm^{-1}: (Zeolitic structure) 961, 684, 626, 557; (CaO) 1436 Porosity, %: (zeolite) 13.3; (catalyst) 86.5 Specific surface area, m^2 g^{-1}: (zeolite) 15.7; (catalyst) 22.6 Av. pore diameter, nm: (zeolite) 13.5; (catalyst) 18.2 H2 hysteresis type; TPD-CO$_2$, µmol g^{-1}: 62.0	[29]
SC-Na • Zeolite from Korean coal fly ash	• Fly ash + (3 M HCl + 4 M H$_2$SO$_4$) (w/w=1/2) mixed at 60 °C for 1.5 h; washed and dried • Precursor + NaOH mixed (w/w=1:3) and calcined at 700 °C for 3 h	Content (XRF), %: (Na$_2$O) 60.2; (SiO$_2$) 27.4; (Al$_2$O$_3$) 3.6; (Fe$_2$O$_3$) 1.4; (TiO$_2$) 1.4; (CaO) 1.3	[84]
Zeolite X • Indian F-type coal fly ash	**Alkaline fusion:** • Calcined at 850 °C for 2 h • 10 % hydrochloric acid at 80 °C for 1.5 h • Fly ash + NaOH (w/w=1/1.5) at 550 °C for 1 h **Hydrothermal treatment:** • Fusion mixture + H$_2$O + 20 wt.% Na aluminate was crystallized at 90 °C for 8 h; washed and dried • Calcined at 500 °C for 2 h	Si/Al molar ratio = 3.16 Specific surface area (BET): 727.7 m^{2}g^{-1} Type II isotherm, H3 hysteresis (XRD): major phase was quartz, crystalline mullite, and less intense hematite and amorphous glassy phase. Average particle diameter: 2-5 µm	[83]

Catalyst designation and origin	Catalyst preparation	Catalyst characteristics	Ref.
AZ-KX • (Acid-treated X zeolite ion-exchanged with K) • Zeolite prepared from Indian coal fly ash	**Zeolite activation** • Calcination at 800 °C for 2 h • Acid treatment: hydrochloric acid (10 %) at 80 °C for 1 h. • Alkaline fusion: fly ash/NaOH=1:1.2; 1 h at 550 °C; 30 wt.% of Na aluminate for Si/Al ratio control • Hydrothermal crystallization: 110 °C for 12 h **Ion exchange** • 1 M Potassium acetate + zeolite (S/L=1:10) heated at 60 °C for 24 h; washed, dried, and calcined at 500 °C for 2 h	Cation exchange capacity: 380.6 meq 100 g^{-1} Specific surface area (BET): 334.7 $m^2 g^{-1}$ Type II isotherm, H3 hysteresis λ (FTIR) / cm^{-1}: 1467, 982, 756, 675 TGA: 9 % at 950 °C	[81]
26Hydroxy sodalite • South African coal fly ash	**Hydrothermal treatment:** • 6 M NaOH + fly ash (1:1.2 w/w) aged (800 rpm, 70 °C, and 1.5 h) • Hydrothermal crystallisation at 140°C for 24 h; washed (until pH 10), and dried	XRD: (crystallinity) 18 %; (crystal size) 21.1 nm Content (EDS), %: (Al) 16.5, (Si) 13.3, (Na) 4.9, (Ca) 2.7, (Fe) 1.1, (Mg) 1.0, (O) 59.4 Si/Al = 0.81	[82]
CaO/FA-ZM • Lignite coal fly ash (Serbia) • CaO from eggshell	**Thermo-chemical treatment** • Fly ash was calcined at 850 °C for 2 h • Acidification: 6 M HCl (S/L=1:5) at 80 °C for 6 h, filtrated, washed (pH neutral), and dried **Alkali activation** • 6 M NaOH (S/L=1:5) at 260 °C for 4 h in the rotating miniature autoclave, filtrated, washed (pH 9), and dried **Hydration-dehydration method** • Raw eggshell was washed, dried, ground, and calcined at 900 °C for 2 h • Hydration: activated eggshells + 10 wt.% zeolite water suspension stirred (700 rpm) at 60 °C for 6 h • Dried and calcined at 650 °C for 4 h	Fly ash was class F Si/Al (zeolite) = 2.28; Si/Al (catalyst) = 1.94 Content (ED XRF), %: (CaO) 50.0, (SiO$_2$) 24.1, (Al$_2$O$_3$) 12.7, (Na$_2$O) 10.1, (Fe$_2$O$_3$) 1.9, (MgO) 1.2 (XRD): lime, gismondine, and ά-dicalcium silicate phases identified λ (FTIR) / cm^{-1}: (Zeolitic structure) 543; (CaO) 1415, 871 Porosity: (zeolite) 82.9 % (catalyst) 87.8 Specific surface area, $m^2 g^{-1}$: (zeolite) 21.1, (catalyst) 18.7 Average particle size, μm: (zeolite) 36.4, (catalyst) 17.7 Basicity, mmol g^{-1}: (zeolite) 0.36, (catalyst) 23.2	[42]
Kaliophilite • Circulating fluidized bed fly ash (Inner Mongolia, China)	**Fly ash-based geopolymer** • Water glass + KOH (S/L=1.5) + fly ash stirred for 5 min, aged at 80 °C for 24 h **Hydrothermal synthesis** • Geopolymer + 6 M KOH at 180 °C for 24 h, washed, dried, and granulated (0.15-0.315 mm)	2θ / ° (XRD): (kaliophilite) 20.85, 26.5, 26.7, 33.3, 40.9 λ (FTIR) / cm^{-1}: (Kaliophilite structure) 985, 698, 607, 561, 480 (Adsorbed water) 3446, 1656 Specific surface area (BET): 3.5 $m^2 g^{-1}$ Average pore size: 20.9 nm Type IV isotherm, H3 hysteresis Basic strength: 9.8<$H\_$<15	[87]

Zeolites, conventionally used in three-dimensional forms generally induced mass transfer limitations, which affects the overall catalytic activity. To overcome this deficiency, a two-dimensional structure was designed with a large external surface area and hierarchical characteristics [64]. In the study, the solid-state ion-exchange method was adopted for Li$^+$, Na$^+$, K$^+$, Ca^{2+}, and Mg^{2+} loading on zeolite with an MWW-type structure. The investigation of the influence of cation type on the catalyst performance showed the following order in activity: Na$^+$ > K$^+$ > Ca^{2+} >Li$^+$ ≈ Mg^{2+}. The influence of the zeolite carrier type on the activity was also investigated indicating the two-dimensional Na/MWW zeolite catalyst as superior compared to the two-dimensional Na/MCM zeolite catalyst and a three-dimensional Na/Y zeolite catalyst. The most successful two-dimensional Na/MWW catalyst was synthesized by expansion, delamination, and subsequent solid-state ion-exchange approach using hexamethylene imine as an organic structure-directing agent under stirred hydrothermal process. The obtained catalyst possessed a very high total surface area of 613 $m^2 g^{-1}$, but the most significant result was that the material had the highest percentage of basic sites on the external surface areas. For only 1 h, the two-dimensional Na/MWW zeolite catalyst reached a biodiesel yield of 95 % under mild reaction conditions, in contrast to the three-dimensional Na/Y zeolite catalyst, which achieved a biodiesel yield of only 6 %. Layered MWW zeolite was also used for the esterification of palmitic acid [65]. The zeolite was modified by pillaring and swelling using cetyltrimethylammonium bromide (CTAB) and silica as swelling and pillaring reagents, respectively. In that manner, a mesoporous material was obtained with a very high surface area of 635 $m^2 g^{-1}$ and the increased number of Brønsted and Lewis acid sites, as compared to the other synthesized catalysts (such as MCM zeolite-based catalysts). Under very mild esterification conditions (70 °C and 30:1 methanol to oil molar ratio) the pillared H MWW zeolite

showed high stability in consecutive cycles and 85.3 % conversion of palmitic acid in 6 h of reaction in the first cycle. For a longer reaction time, the total conversion (100 %) was obtained.

The idea to obtain biodiesel enzymatically turned out to be very demanding [66]. Commercial Lipozyme TL containing lipase was immobilized on FM-8 zeolite mordenite-type with Na^+ as a major cation and used for methanolysis of WCO under very mild reaction conditions, which meant room temperature, alcohol to oil molar ratio of 4:1, lipase content of 4 %, 24 h of reaction and mixing at 200 rpm. However, under these reaction conditions, the immobilized lipase on zeolite did not show any activity. It should be also emphasized that the realized immobilization efficiency was unsatisfactory yielding only 56.1 % (95.8 % was obtained for hydrotalcite as support). The very high level of FFA microalgal lipids (*Chlorella vulgaris*, 34 mg KOH g^{-1} and calculated FFA content of 17 %) were successfully converted to biodiesel using a bifunctional phosphotungstic acid-modified zeolite imidazolate framework catalyst [66]. Activity of the bifunctional catalyst was achieved at higher temperatures due to the requirement for activation of catalytically active centres for esterification and transesterification, so that the conversion of 98.5 % is obtained at 200 °C in 1.5 h of reaction. For example, when performing the reaction at the temperature of 80 °C, conversion of only about 10 % was achieved. The best activity was obtained with the optimum phosphotungstic acid (HPW) content in the catalyst of 0.25 wt.% achieving at the same time impressive textural characteristics, with the BET surface area of 1137 m^2 g^{-1} and external surface area of 129 m^2 g^{-1}. Considering the very unfavourable quality of the used microalgal lipids and the demonstrated good stability and recyclability of the material, this catalyst can be considered very promising to produce biodiesel.

3. 3. Zeolite-based catalysts originating from natural and waste sources

Natural zeolites and zeolites derived from waste sources may not have very large specific surface areas and hierarchical structures as synthetic zeolites, but they support sustainable chemistry, contribute to waste reduction solutions, and exhibit suitable characteristics (Table 7) and catalytic activity (Table 9) due to adequate bonding of catalytically active species and the zeolite support. Many studies [68-72] couple natural- or waste-based zeolite catalysts and WCO as feedstock guided by the principles of green chemistry. These catalysts can be applied in qualitatively unfavourable feed oils achieving respectable biodiesel yields in a one-step process (Table 9).

To conduct the process of WCO transesterification under mild reaction conditions, a heterogeneous catalyst was used based on a zeolite/chitosan/KOH composite [68]. The catalyst was synthesized from natural polysaccharide chitosan and natural zeolite clinoptilolite-type with KOH impregnation. FAME was produced at room temperature by an electrolysis process using a graphite electrode, at a relatively low methanol to oil molar ratio (7:1), 2 wt.% of deionised water, and a co-solvent. It has been shown that in 3 h reaction time, with 10 wt.% acetone as a co-solvent and only 1 wt.% of the catalyst, a biodiesel yield of 93 % was achieved. WCO methanolysis was investigated by a geothermal solid waste-derived Ni/zeolite catalyst [67]. The geothermal solid waste from Indonesia contained mainly SiO_2 (75.1 %) and trace amounts of Al_2O_3 and Na_2O. Generally, the high content of Si led to low acidity of zeolite and, consequently, the basicity of the resulting zeolite is increased. The obtained catalyst had a medium-developed surface area (81.9 m^2 g^{-1}) with an average pore radius of about 5 nm. The satisfactory activity of the catalyst was obtained under mild reaction conditions for 4 h of reaction. The study provided a simple cost analysis of the catalyst production comparing it to common commercial catalysts. A comparison of two basic and one acidic homogeneous commercial catalysts indicated that nowadays the production cost of Ni/zeolite catalyst is five times higher than that of NaOH, about 50 % higher than that of H_2SO_4, and 2.2 times lower than that of KOH. However, the situation is somewhat more favourable regarding the biodiesel yield per mass of the catalyst.

The Ni/zeolite catalyst is superior to KOH and H_2SO_4, but NaOH is still more economical. Yet, the presented economic analysis was very limited in scope not considering that homogeneous catalysts need a complex separation process and cannot be reused like heterogeneous catalysts, which consequently raises costs. Thus, a more comprehensive economic analysis should be performed before conclusive statements about the economic efficiency of different catalysts. WCO transesterification was performed in a common stirred batch reactor by using a neat zeolite catalyst obtained from waste steel furnace slag [72]. The composition of the steel furnace slag comprising mainly silica, calcium and aluminium suggested the common procedure for transformation to a zeolite structure: calcination - acid treatment - hydrothermal synthesis - autoclave crystallisation - calcination.

Table 9. Review of reaction conditions when using zeolitic materials obtained from natural or waste sources as catalysts/catalyst supports

Catalyst designation	Feedstock	Reactor type	Optimal reaction conditions				Yield (conversion), %	Ref.
			T / °C	CC*, wt.%	t (τ) / min	Alcohol to oil molar ratio		
Continuous processes								
Co-Ni-Pt-FAU Shere rock originated	Oleic acid ethanolysis	Fix-bed tubular reactor (10×650 mm)	70	-	(180)	-	93	[57]
Batch processes								
Co-Ni-Pt-FAU Shere rock originated	Oleic acid ethanolysis	Batch stirred reactor	70	-	90	6:1	89	[57]
HY-kaoline Fujasite type zeolite from kaolin	Oleic acid esterification (ethanolysis)	Batch stirred reactor	70	5	60	6:1	(85)	[74]
Zeolite/chitosan/KOH Clinoptilolite zeolite	WCO methanolysis (1 wt.% acetone as cosolvent and 2 wt.% of H_2O)	Electrolysis-assisted (40 V, 2 wt.% H_2O) stirred (400 rpm) batch reactor	-	1	180	7:1	93	[68]
LTA-kaolin Linde type A zeolite from kaolin	Triolein methanolysis	Batch stirred reactor (600 rpm)	62.9	72	146	36.6:1	92.8±4.0	[73]
Na/zeolite-chitosan Clinoptilolite zeolite	WCO methanolysis	Electrolysis assisted (40 V, 2 wt.% H_2O + 10 wt.% acetone) stirred batch reactor (400 rpm)	25	1	30	8:1	96.5	[69]
Na/CAN Natural diatomaceous earth (Vietnam) cancrinite-type zeolite	Soybean oil methanolysis	Batch stirred reactor (600 rpm)	63	20	90	20:1	(98)	[77]
FAU-type zeolite Irish shale rock	Oleic acid esterification (ethanol)	Batch stirred reactor	70	5	90	6:1	(78)	[76]
Ni/zeolite Geothermal solid waste	WCO simultaneous methanolysis and esterification	Batch stirred reactor (400 rpm)	60	3	240	12:1	89.4	[70]
Zeolite Geothermal solid waste (Indonesia)	WCO simultaneous methanolysis and esterification	Autoclave	300	5	60	4:1	98.3	[71]
Zeolite Steel furnace slag	WCO methanolysis	Batch stirred reactor (500 rpm)	62	3	240	12:1	96	[72]

*Catalyst content

The obtained material had a poorly developed surface area (about 10 $m^2 g^{-1}$), but showed respectable activity, probably due to residual Na_2O from the synthesis process (washing step until neutral pH was not applied). Perhaps the active Na_2O loaded in this way can be also the explanation for a gradual decrease in the catalyst activity in 3 repeated cycles, due to probable Na_2O leaching from the catalyst into the reaction mixture. A similar synthesis route was applied for kaolin clay transformation into LTA zeolite, but in this case, there was no need for acid treatment due to the absence of interfering metals in the starting clay (*e.g.*, Ca, Fe, *etc.*) [73]. It should be also added that after the hydrothermal synthesis step, thorough washing of the resulting material was carried out. Although the catalyst with the longest investigated ageing time of 48 h proved to be the most active, since the conversion yield did not change significantly with prolonging the ageing duration over 24 h, this time period was adopted as optimal. Statistical optimisation of reaction parameters by using the Box-Behnken design revealed optimal reaction conditions in methanolysis of triolein that were somewhat harsh (catalyst loading of 72 wt.%, methanol to oil molar ratio of 37:1, and reaction time of 2.4 h). Kaolin clay was also a starting material for the synthesis of zeolite Y, which was used as an HY zeolite catalyst for the esterification of oleic acid [74]. The Si/Al ratio in the prepared catalyst was 3.1, unlike zeolite X with the Si/Al ratio lower than 1.5, indicating the formation of a more catalytically active and stable form of faujasite (zeolite Y) [75]. Interestingly, the synthesized HY zeolite catalyst from kaolin had similar composition and morphological characteristics as a commercial HY zeolite catalyst. In addition, the synthesized HY zeolite catalyst showed better performance under very mild esterification conditions than the commercial HY zeolite (oleic acid conversion was about 84 and 68 % achieved in 45 min, respectively).

FAU-type zeolite was prepared by using Irish shale rock and tested as a catalyst in the esterification of oleic acid [76]. The catalyst was prepared in a common manner combining acid leaching, alkaline fusion, and hydrothermal treatment.

All these steps were experimentally optimized yielding the optimal mixing time of 3 h, ageing time of 18 h, and hydrothermal time of 24 h. Under these optimized synthesis conditions, a well-developed specific surface area was obtained (571 $m^2 g^{-1}$). The catalytic activity was similar to that of a commercial zeolite Y under the same reaction conditions. In the same manner another FAU-type zeolite catalyst was prepared and additionally modified with precious metals (Co, Ni, and Pt) by using the incipient wetness method to enhance the catalyst activity under continuous reaction conditions [57]. Under the same mild reaction conditions of oleic acid esterification with ethanol in a batch process, the Co-Ni-Pt-FAU zeolite catalyst was superior to the H-FAU zeolite catalyst, achieving the maximum obtained conversion of 93 *vs*. 78 %, respectively. The comparison was also made under continuous reaction conditions in a fixed-bed reactor indicating the Co-Ni-Pt-FAU zeolite catalyst superior again, achieving the conversion of 89 *vs*. 75 %, respectively, at the liquid hourly space velocity of 0.5 h^{-1}.

3. 3. 1. Zeolite-based catalysts originating from coal fly ash

Investigation of fly ash is becoming attractive in recent years due to the search for eco-friendly procedures for zeolite synthesis. Coal fly ash is a product of coal combustion that is composed of fine particles that are driven out of coal-fired boilers together with exhaust gases. Therefore, zeolites originated from this source belong to the group of zeolitic materials obtained from waste but are described in a separate subsection in the present review paper due to the high interest of researchers and engineers in this zeolite type in recent years. Attention to fly ash as a feedstock for zeolites synthesis was raised due to its aluminous and siliceous nature. Three key steps are included in the common production procedure of zeolite from fly ash *via* the alkali hydrothermal method [78]. Fly ash is first dissolved to produce Si^{4+} and Al^{4+} species in the solution followed by condensation of these ionic species to form aluminosilicate gel, which is then crystallized in the third step into desired zeolite crystals. Generally, the obtained catalysts showed excellent activity under mild reaction conditions (10) and respectable stability (11). They exhibited similar morphological characteristics as other waste-based catalysts, due to the similar feedstock composition and synthesis routes, meaning a medium or poorly developed specific surface and a mesoporous structure (Table 8).

Table 10. Review of reaction conditions when using zeolitic materials obtained from fly ash as catalysts/catalyst supports

Catalyst designation	Feedstock	Reactor type	Optimal reaction conditions				Yield (con-version), %	Ref.
			$T /$ °C	CC*, wt.%	$t /$ min	Alcohol to oil molar ratio		
Zeolite Coal fly ash zeolite, sodalite type	Soybean oil methanolysis	Batch stirred reactor (300 rpm)	65	4	120	12:1	95.5	[79]
FA/K-X Fujasite zeolite type from South African class F fly ash	Sunflower oil methanolysis	Batch stirred reactor (600 rpm)	65	3	480	6:1	83.5	[86]
Li/NaY Zeolite from Chinese coal fly ash	Castor oil ethanolysis	Batch stirred reactor (400 rpm)	75	3	160	18:1	98.6	[85]
CaO/ZM$_{FA}$ Lignite coal fly ash (Serbia) CaO from eggshell	Sunflower oil methanolysis	Batch stirred reactor (850 rpm)	60	4	120	12:1	(96.5)	[29]
SC-Na Zeolite from Korean coal fly ash	Soybean oil methanolysis	Batch stirred reactor (200 rpm)	50	2	180	5 $cm^3 g^{-1}$ oil	95	[84]
Zeollite X Indian F-type coal fly ash	Soybean oil methanolysis	Batch stirred reactor	65	3	480	6:1	81.2	[83]
AZ-KX zeolite X zeolite from fly ash	Mustard oil methanolysis	Batch stirred reactor	65	5	420	12:1	(84.6)	[81]
Hydroxy sodalite South African coal fly ash	Maggot oil methanolysis	Batch stirred reactor	60	1.5	90	15:1	86	[82]
CaO/FA-ZM Lignite coal fly ash (Serbia) CaO from eggshell	Sunflower oil methanolysis	Batch stirred reactor (850 rpm)	60	6	30	6:1	(97.8)	[42]
Kaliophilite Circulating fluidized bed fly ash (Inner Mongolia, China)	Canola oil methanolysis	Batch stirred reactor	85	5	360	15:1	99.2	[87]

*Catalyst content

Table 11. Review of stability/reusability of zeolite-based catalysts

Catalyst designation	Reactor type	Catalyst stability/reusability	Ref.
Mg/clinoptilolite	Stirred batch reactor	At least 5 cycles	[48]
K-MAP	Pressured stirred batch high power density (microwave system) reactor	At least 3 cycles (catalyst was washed with methanol 3x and calcined at 450 °C for 2 h)	[62]
7 % Mo-NaBeta	Stirred autoclave	Conversion decreases by 18 % after the first cycle, and after that for the next three remains stable.	[63]
0.25 HPW/ZIF-67	Autoclave	6 cycles (conversion of 91.3 %) After washing with n-hexane and methanol efficiency was restored to 94.6 %	[67]
35 % CaO/zeolite	Microwave reactor	After 2nd cycle yield felt to18.3 %.	[61]
HMCM-36	Stirred batch reactor	At least 4 cycles (Only washing with methanol and drying at 70 °C)	[65]
AZ-KX zeolite	Stirred batch reactor	After 3rd cycle yield has significantly dropped (the catalyst was washed with methanol and calcined at 300 °C for 2 h)	[81]
FA/K-X	Stirred batch reactor	After 2rd cycle yield dropped ≈ 12 %	[86]
1:1-Li/NaY	Stirred batch reactor	In 5 cycles yield dropped from 98.6 to 80 % and after calcination restored to 91.6 %	[85]
SC-Na	Stirred batch reactor	At least 3 cycles	[84]
2D Na/ITQ-2	Stirred batch reactor	At least 4 cycles (yield >94 %)	[64]
Ba/CAN	Stirred batch reactor	Yield drops in 2nd cycle from 98 to 46 %. Regeneration is possible with calcination at 500 °C for 6 h.	[77]
K/zeolite	Stirred batch reactor	Yield drops in the 2nd and 3rd cycles from 81.9 to 62.7 % and 52.3 %, respectively.	[47]
K_2O/zeolite	Stirred batch reactor	At least 4 cycles	[50]
Ni/zeolite	Stirred batch reactor	Yield drops from 82.7 to 73.3 %, from the first to the third cycle, respectively	[70]
Zeolite	Autoclave	Yield drops from 98.3 to 58.93 %, from the first to the third cycle, respectively	[71]
CaO/FA-ZM	Stirred batch reactor	There was almost no decline in catalyst activity in 5 cycles (FAME content from 99.2 to 97.9 %) without any pretreatment	[42]

A neat sodalite form of zeolite was synthesized and used for methanolysis of soybean oil [79]. Fly ash from a Brazilian thermal power plant (Rio Grande do Sul state) had a SiO_2 content higher than 60 wt.% suitable for zeolite synthesis by a common route with 24 h crystallisation, washing until pH of 9, and a somewhat longer ageing period of 6 days. The calculated Si/Al ratio was 3, which places the obtained zeolite in the group of medium silica zeolites (Y, Ω, mordenite, *etc.*) [80]. The zeolite proved to be very catalytically active achieving a biodiesel yield of 95.5 % in 2 h under mild reaction conditions. In another study [81] several zeolite X and A catalysts were synthesized and compared in the methanolysis of mustard oil.

The Si/Al ratio was carefully controlled by the addition of adequate amounts of $NaAlO_2$ in order to avoid the formation of another, undesirable, zeolitic phase. So, Si/Al ratios lower than 2 and equalling to 2 were achieved to favour the formation of zeolite A and zeolite X, respectively. A preference was given to the zeolite X series of catalysts due to much higher specific surface areas as compared to zeolite A catalysts (over 160 m^2 g^{-1} *vs.* about 24 m^2 g^{-1}, respectively).

Among zeolite X catalysts, the acid-treated ion-exchanged (K^+) catalyst showed the highest conversion explained by the increase in base strength upon ion-exchange. Still, even at optimal synthesis conditions this catalyst showed limited performance, especially at the introductory phase of the reaction, which lasted a long time (4-5 h) at a slow reaction rate indicating diffusion limitations [81]. This problem was not present to such an extent in the reaction catalysed by hydroxy sodalite zeolite [82]. Perhaps the reason for such performance is the obtained 100 % relative crystallinity in the catalyst. Both studies were conducted under mild reaction conditions, using used mustard oil and maggot oil with a similar acid value, respectively. The maximal obtained biodiesel yields were similar, but in the second case, it was reached much faster *i.e.*, in 1.5 h needed to reach the reaction equilibrium, which was about 4.6-fold faster than in the first study. A hydroxy sodalite zeolite catalyst was obtained from coal fly ash collected from a power plant in South Africa by using the common synthesis procedure with a relatively longer hydrothermal process time of 72 h [83]. A similar maximum biodiesel yield, as in the previous two studies, was obtained (about 80 %) by using neat hydroxy sodalite zeolite [83]. It is interesting that under very mild conditions of hydrothermal crystallization (90 °C and 8 h), zeolite X with a highly developed specific surface area of 727.2 m^2 g^{-1} was obtained [83].

A series of zeolite-like materials were obtained by acidification and subsequent alkali and alkaline earth metal hydroxides activation of coal fly ash from Korea [84]. In general, using such a synthesis route from coal fly ash, materials with a zeolite structure can be obtained, especially for example the form of a cancrinite-sodalite group of zeolite-like material (vishnevite type) [29, 42]. The study showed that the activity of the obtained catalysts decreased in the following order: Na activated > Ca activated > K activated >>> neat acid-treated fly ash, whereas the last one showed negligible activity. These results were probably obtained according to the order of theoretical basicity of the synthesized catalysts, since they all had approximately equal amounts of deposited metal oxides (about 60 wt.%). Interestingly, transesterification at the reaction temperature of 50 °C proved to be as good as at the commonly applied temperature of 60 °C. However, at the higher temperature, the reaction rate was slightly faster in the introductory stage, so eventually the reaction equilibrium was reached for both temperatures in the third hour. Also, the reactor stirring rate was found to be best at 200 rpm in the investigated range of 50-600 rpm. This is certainly related to the diffusion limitations and the surface morphology of the catalyst, which was not investigated so this phenomenon cannot be explained with certainty. Loading of lithium by co-precipitation on hydrothermal and microemulsion-assisted synthesized NaY zeolites was also investigated [85]. The best catalyst (NaY zeolite/Li_2CO_3 molar ratio = 1/1 and calcination temperature of 750 °C) achieved remarkable activity and stability. The yield of 98.6 % of fatty acid ethyl esters (FAEEs) was achieved under mild reaction conditions in 2 h of reaction. Moreover, the catalyst was proved to be very air tolerant, which is one of the main disadvantages of heterogeneous base catalysts, as well as to be recyclable. The activity of three similar catalysts loaded with Li was compared and a decline in activity was found regarding the support in the following order: NaY zeolite, Al_2O_3, and SiO_2. All three catalysts had a very high basic strength of 15<$H\_$<18.4, but the obtained differences in activity lay in differences in BET surface area and basicity, which were consistent with the activity shown. It was found out that the best catalyst was not the one with the highest Li load, nor the one calcined at the highest temperature. The neat NaY zeolite had a highly developed specific surface area (429 m^2 g^{-1}) that, as expected, decreased with the loading of Li. Interestingly, the 3:1 Li/NaY catalyst had a specific surface area of only 1.6 m^2 g^{-1}. The same pattern of the specific surface area decreases from 193 m^2 g^{-1} to 18 m^2 g^{-1}, following the increase in the calcination temperature from 550 °C to 950 °C. The catalyst with the highest Li load had the highest total basicity, as expected, but the catalyst with a more suitable surface morphology was more active although it contained a lower amount of Li. It is necessary to mention that the difference in basicity was not large and that is why the morphology came to the fore.

A faujasite zeolite material synthesized from a South African class F fly ash was ion-exchanged with K to obtain a potent catalyst for sunflower oil methanolysis [86]. The catalyst was prepared according to the conventional hydrothermal synthesis procedure and the alkali metal (K^+) ion exchange. The obtained material had a finely developed surface area of 257 m^2 g^{-1} (starting fly ash had only 2 m^2 g^{-1}) and a considerably high basic strength of 15<$H\_$<18.4. However, under mild reaction conditions, the catalyst did not show exceptional activity, as in 8 h of reaction the biodiesel yield was 83.5 %. Additionally, even after 24 h, the yield was not much higher. The reason for the average performance of the catalyst might be the unavailability of some of the catalytically active centres dispersed in, probably dominant, small-diameter pores for large organic molecules in the reaction mixture.

A lignite coal fly ash-based zeolite was used as a support for loading chicken eggshell calcium oxide using two synthesis routes in order to obtain sustainable and green catalysts [29,42]. The first route involved a hydration-dehydration method as the last step of the synthesis [42], while the second route used ultrasonic dispersion in an alcoholic suspension [29]. Naturally, both synthesis procedures had calcination as a final catalyst activation step. The cancrinite-sodalite zeolite-like material (vishnevite type) was synthesized by the common procedure: calcination - acidification - alkali activation - hydrothermal crystallization. The fly ash obtained from a Serbian thermal power station was converted into a zeolite-like material using, for the first time, a rotating miniature autoclave reactor system [29]. The reactor allowed adequate agitation by rotating the whole reaction mixture, instead of contact mixing by a stirrer. In this way, significant savings in time and energy were achieved along with obtaining a more homogeneous product. For instance, in the autoclave system set-up, the hydrothermal crystallization step lasted only 4 h. The best catalysts prepared by using both routes had similarly developed specific surface areas of about 20 m^2 g^{-1} and relatively high

basicity. The 50 % CaO/zeolite catalyst showed remarkable activity under mild reaction conditions (*e.g.*, methanol to oil molar ratio of 6:1 proved to be most adequate) and in only 0.5 h the equilibrium FAME content was 97.8 %. It was shown once again, as in the study by Li *et al.* [85], that only one parameter of the catalyst does not decisively determine its activity, but the synergy of several key parameters. The 20 % CaO/zeolite catalyst was more active than the neat eggshell-based CaO despite its almost 4.5-fold higher basicity. Adequate surface texture and morphology combined with finely dispersed base centres were key features for determining the catalytic activity. The specific surface area of neat the CaO was 15-fold lower, while its porosity was 55 %, which is significantly lower than 86.5 % determined for the CaO/zeolite catalyst. The spent catalyst had signs of deposition of organic molecules from the reaction mixture, although it was proven not to be significant, as confirmed by the maintenance of high activity in 5 consecutive cycles, without any catalyst pretreatment.

A circulating fluidized bed fly ash from a laboratory was used to synthesize kaliophilite catalyst *via* a facile and low-energy two-step process: fabrication of an amorphous fly ash geopolymer and hydrothermal transformation of the geopolymer into kaliophilite [87]. The kaliophilite catalyst exhibited a poorly developed surface area (3.5 m^2 g^{-1}), but the average pore diameter of 20.9 nm and the majority of mesoporous pores promoted the catalytic activity for the reaction involving relatively large organic molecules so that a high biodiesel yield and short reaction induction period were achieved confirming these favourable morphological characteristics.

4. REACTION MECHANISMS OF TRANSESTERIFICATION CATALYZED BY ZEOLITE CATALYSTS

Common production of biodiesel implies transesterification of TGs from vegetable oils, oily waste, or animal fats with alcohol in presence of a catalyst to produce fatty acid alkyl esters (FAAEs) and glycerol. The reaction is three-staged, but the overall reaction can be represented by Figure 3. Before obtaining three FAAE molecules, the intermediates diacylglycerol and monoacylglycerol are formed and then broken up in successive reactions.
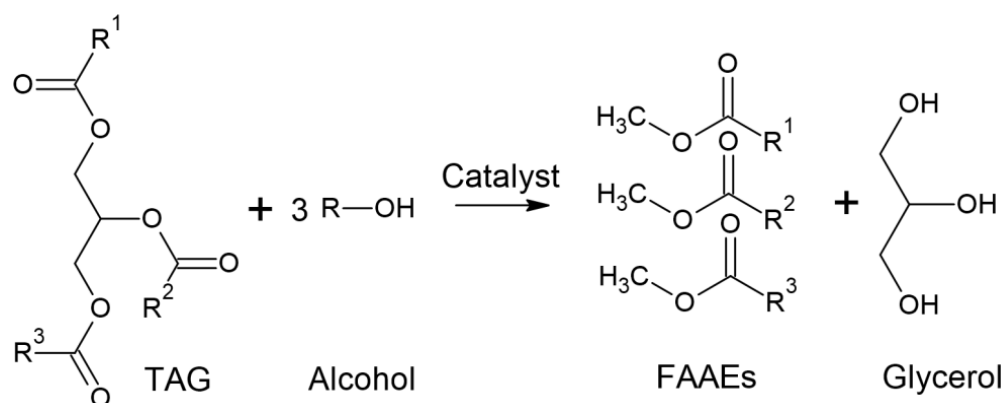
Figure 3. General scheme of transesterification reaction

Heterogeneous catalytic production of biodiesel follows similar principles to those of homogeneous catalysis. In the base-catalysed reaction, the first and main step is to create nucleophilic alkoxides from the present alcohol that attack the electrophilic part of the carbonyl group in TGs, whilst in the acid-catalysed process the carbonyl group in TAGs is protonated and then the present alcohol attacks the protonated carbon to produce a tetrahedral intermediate species [3].

Detailed mechanisms of reactions catalysed by zeolite catalysts have been proposed by several authors [3,63,67,79,88]. Different structural, physical and chemical properties of zeolite catalysts, whether with basic, acid, or bifunctional acid-base active sites, caused somewhat different explanations of the mechanisms.

Figure 4 presents a mechanism proposed for rice bran oil transesterification using a NaBeta zeolite supported-Mo catalyst [63]. First, triglyceride molecules are adsorbed onto the catalyst surface, and intermediate (step 1) species are obtained from the unpaired electron from the oxygen atom of C=O in triglyceride, bond with molybdenum oxide species. Further, carbocation (step 2) is produced due to the transfer of the electron pair from the oxygen atom to the carbon atom within the C=O bond. Next, a nucleophilic reaction takes place where methanol and the intermediate from step 2

form new intermediate species (step 3) in which a new intermediate compound (step 4) is obtained by H^+ transfer. Breaking the C-O bond in C-OH-CH_2 leads to the separation of a diglyceride (DG) molecule. Additionally, C=O group was produced when an electron pair of oxygen atom was transferred into C-O single bond of Mo-C-O whereby a new intermediate compound (step 5) is formed. Finally, heterolysis of the electron pair in the Mo-O bond promotes the formation of a FAME molecule and regeneration of the catalyst, thus finishing one reaction cycle.
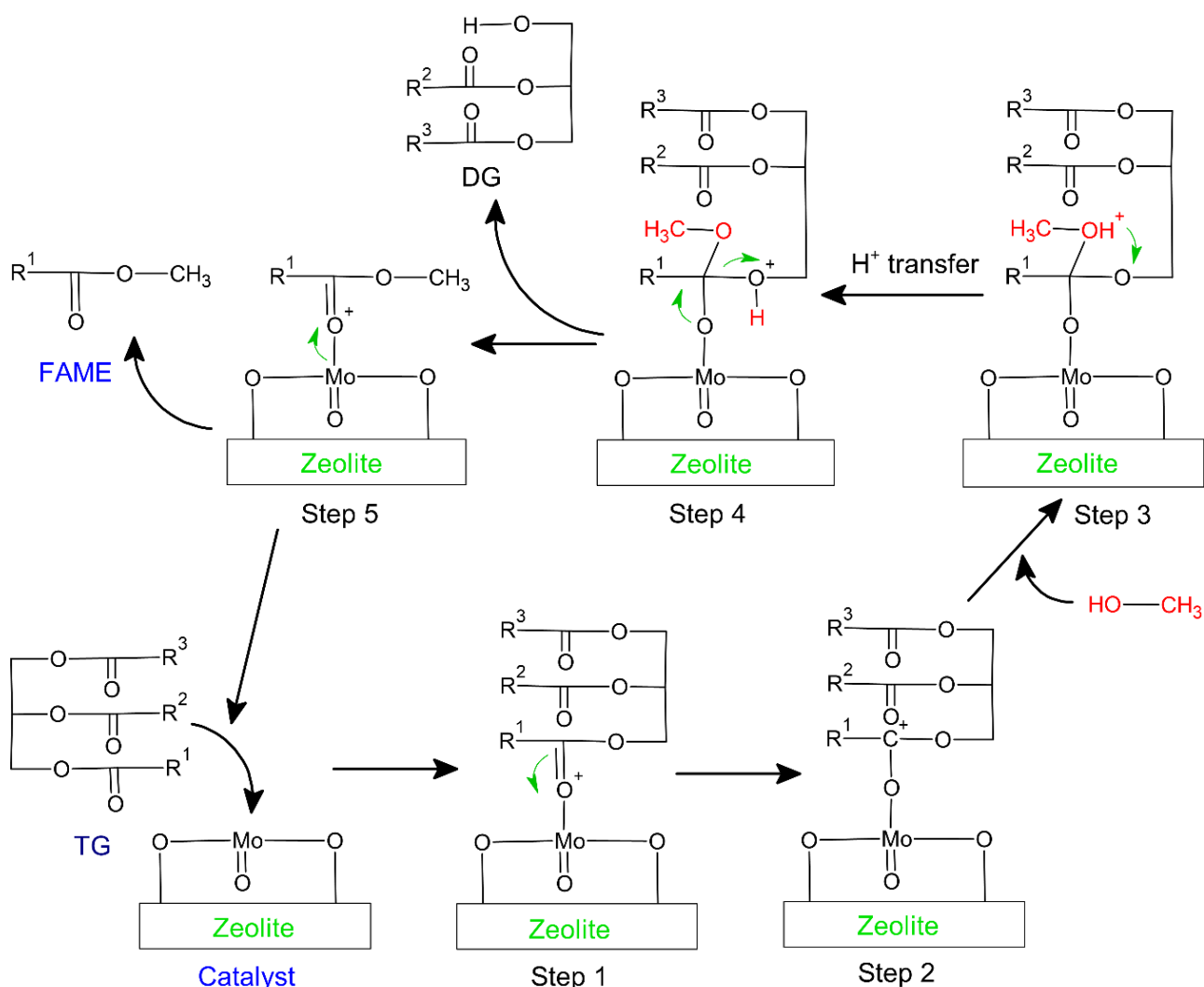
Figure 4. Proposed mechanism of transesterification catalyzed by a Mo/zeolite catalyst [63]

Si-O-Na groups in the structure of a sodalite zeolite catalyst act as active sites for the transesterification reaction [79]. The proposed mechanism (Figure 5) for this zeolite catalyst action follows a similar pathway as for homogeneous base catalysts [3]. In the first step, methanol is adsorbed onto the surface and catalytic active species (methoxide anion) are produced. The second step is the nucleophilic attack of methoxide anion on the carbonyl carbon of triglyceride and the formation of tetrahedral intermediate species. The third stage is unstable intermediate rearrangement forming a FAME molecule. Finally, deprotonation of the catalyst is happening, thus regenerating the catalytically active species. This cycle was repeated two more times to yield glycerol and three molecules of biodiesel.
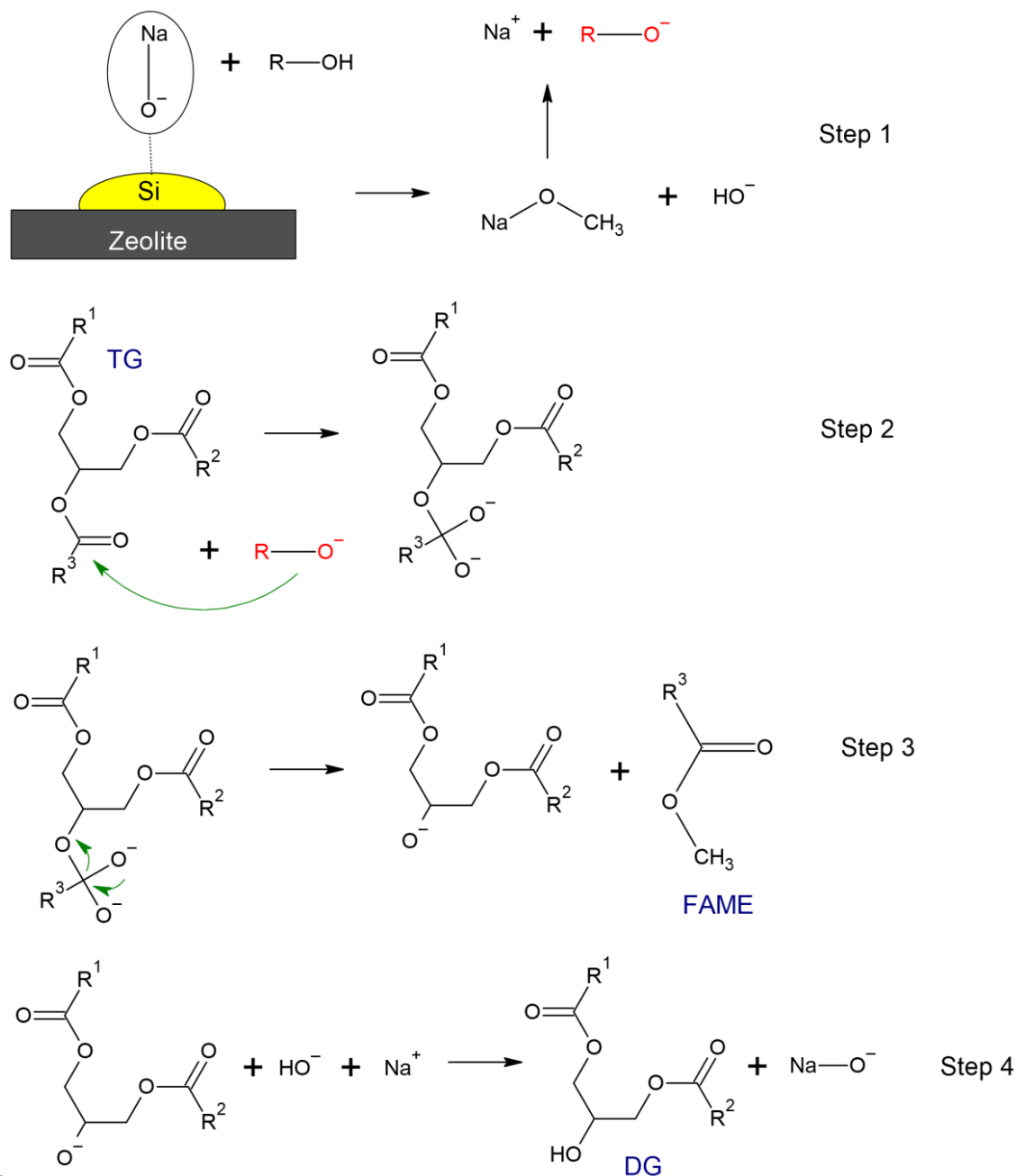
Figure 5. Transesterification reaction mechanism using sodalite zeolite catalyst [79]

Figure 6 presented pathways for the acid-base catalysed biodiesel production using a zeolite-based catalyst. The presence of acid and base catalytic sites allows the catalyst to perform simultaneous esterification and transesterification reactions [88]. In acid-catalysed pathways carbocation is initially formed by adsorption of the carbonyl group of FFA on the acid site on the catalyst surface. In the step 2, a nucleophilic attack by methanol on the carbocation leads to the formation of tetrahedral intermediate species. Breaking the O-H bond and desorption of the hydroxyl group from the catalyst surface in the final 3rd step, produces a FAME molecule. The base-catalysed pathways start with the formation of a methoxide anion as a result of methanol adsorption onto the basic catalyst sites. The resulting methoxide anion as a highly reactive nucleophilic species, attacks the carbonyl carbon in triglycerides to form another tetrahedral intermediate species. The third step involves desorption of alkyl triglycerides from the catalyst surface, *i.e.*, formation of a FAME molecule, after breaking the C-O bond.
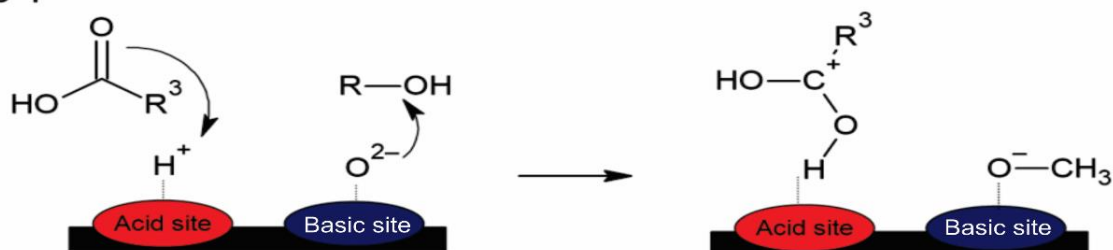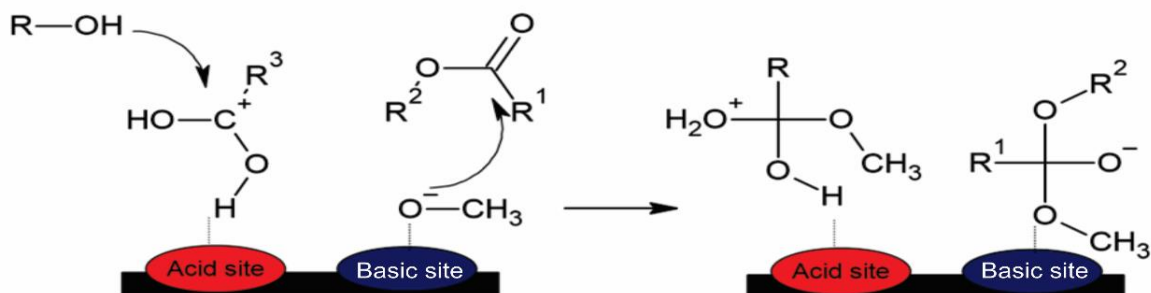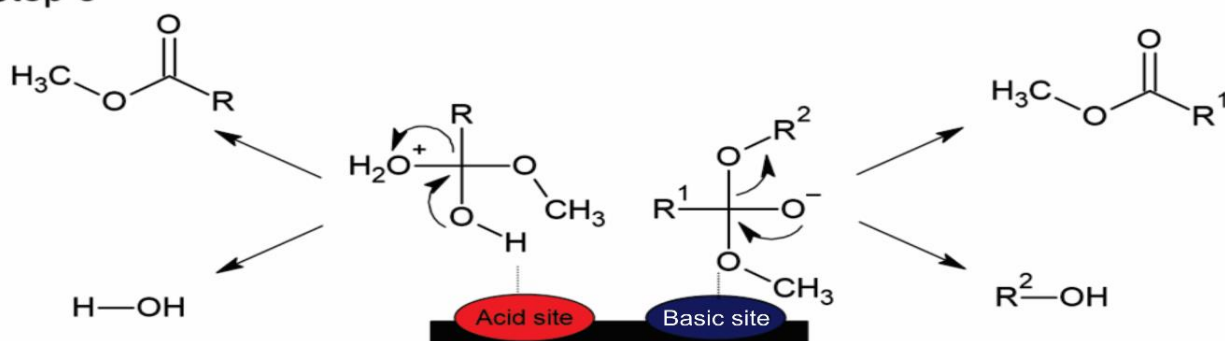
Figure 6. Proposed mechanism of bifunctional acid-base transesterification [88]

Cheng *et al.* [67] suggested a reaction mechanism where a bifunctional HPW/ZIF-65 zeolite-based catalyst exhibited three kinds of catalytically active sites: Brønsted acid sites, and Lewis acid and base sites. Protons of -NH and HPW represented Brønsted acid sites, coordinatively unsaturated cobalt cations represented Lewis acid sites, while N⁻ extremities of imidazole ligands acted as Lewis base sites. As presented in Figure 7, the carbonyl oxygen of the fatty acid is adsorbed on the Lewis acid site (L^+) to form a carbocation as the hypothesis is that these sites mainly catalyse FFAs esterification. Then alcohol starts the nucleophilic attack to the carbocation to produce a tetrahedral intermediate, which is unstable and decomposes to FAME, water molecule, and L^+. The transesterification reaction is catalysed on Lewis base sites (L^-). It starts with the contact of adsorbed alcohol on active sites (N⁻ extremities of imidazolate ligands) and TG to form an oxygen anion. A tetrahedral intermediate is, then, produced in the nucleophilic attack of oxygen anion to TG. The unstable tetrahedral intermediate is in the second step decomposed to FAME and DG. This process is repeated to DG and monoglycerides (MG) to finally form three molecules of FAME. The Brønsted acid sites can act bifunctionally, as they can catalyse FFA esterification and TG transesterification simultaneously. A carbocation is formed in the reaction of the proton from -NH and protonated HPW and the carbonyl group of TG. Then, the nucleophilic attack of alcohol to the carbocation forms a tetrahedral intermediate, which is decomposed to another proton and products.
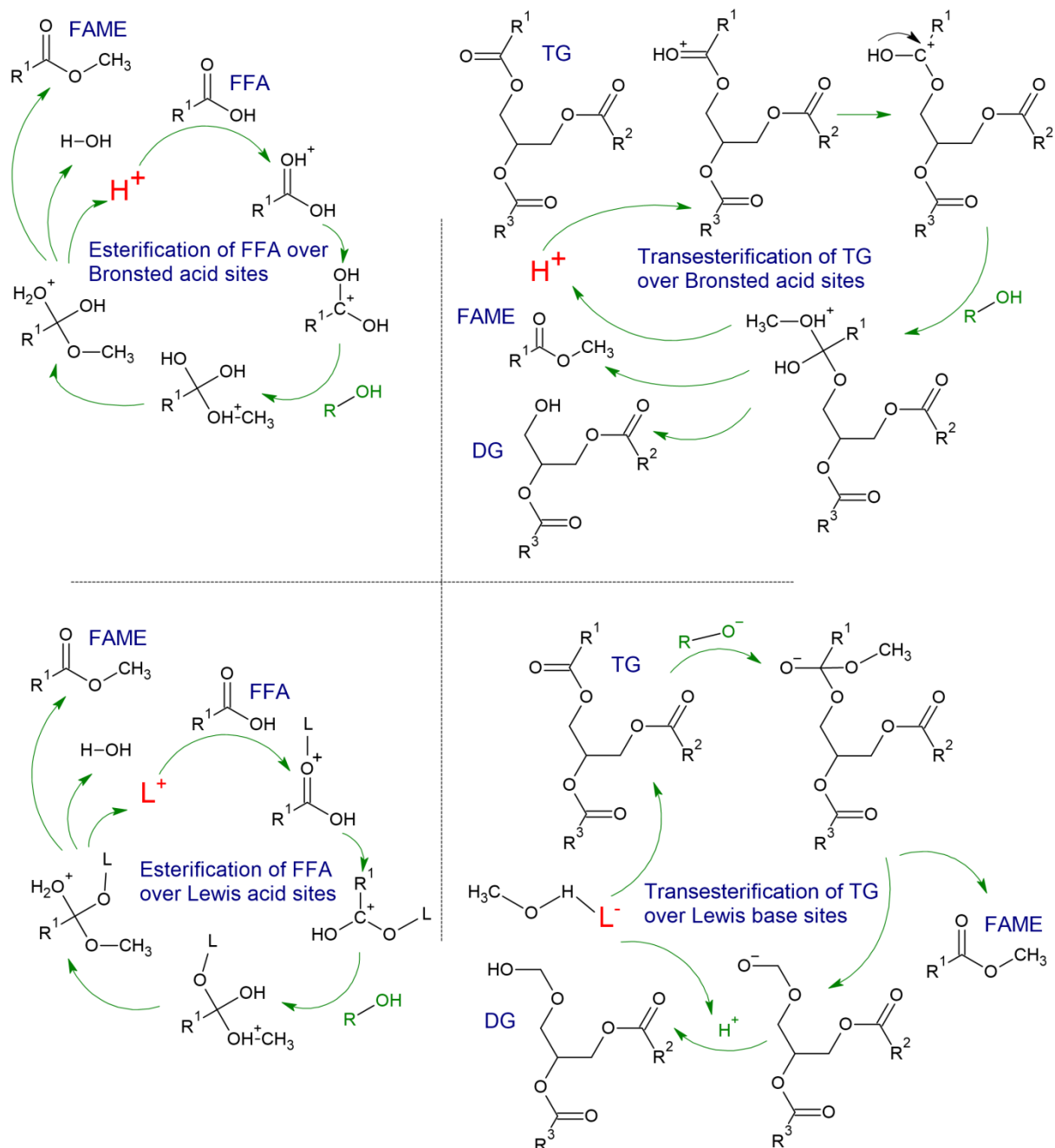
Figure 7. Proposed mechanism of bifunctional zeolite-based catalysis through Lewis acid and base sites and Brønsted base sites [67]

5. STABILITY OF ZEOLITE-BASED CATALYSTS

Most studies of zeolite-based catalysed biodiesel production were performed under batch reaction conditions, so that the catalyst stability can be investigated by determining the catalyst activity in repeated consecutive reaction cycles. The spent catalysts were used in consecutive cycles either without any treatment, subjected to some regeneration procedure, or simply washed in some solvent. Catalyst regeneration was performed in some studies by recalcination [62,81,77,85], while polar (such as methanol) [65,67,81] or non-polar (such as n-hexane) [67] solvents were used for rinsing. A great diversity of zeolite structures in the studied catalysts, as well as different catalytically active species, led to a colourful picture regarding the stability of catalysts. Some materials managed to maintain high activity in six consecutive cycles, while others had a significant decrease in activity already in the second cycle. Furthermore, maintaining high activity in six repeated cycles is the best-achieved performance reported [67] among the reviewed

literature, but this result should be taken with caution as in many studies the maximum stability of the catalyst was not determined, despite the good performance of the material in several cycles [48,50,62,64,65,84].

The stability issue of heterogeneous catalysts exposed to air is one of the most important characteristics for evaluating the catalyst quality. A Li/NaY zeolite catalyst was proved to be very tolerant to air exposure, as after 10 days of exposure the FAEE yield dropped from the initial 98.6 to 92.6 % [85]. In a study of the effects of washing solvents [48] between cycles, methanol showed slightly better results than distilled water as in 5 consecutive cycles the biodiesel yield decreased from 98.7 to 92 % and 94.5 % when using water and methanol for rinsing, respectively. A green catalyst of a lignite fly ash-produced zeolite supporting CaO (from chicken eggshells) showed great reusability in five investigated consecutive cycles without any pretreatment achieving a minor decline in activity (the FAME content decreased from 99.2 to 97.9 %) [42]. It is interesting, that such high activity is preserved despite the rather high leaching of Ca into the FAME phase (range of 1170 mg kg^{-1} to 630 mg kg^{-1}). It should be noted that CaO impregnation on the zeolite support stabilized the catalyst since, under the same reaction conditions, Ca leaching from the neat CaO catalyst was 4-fold higher. In this study as well, the deposition of organic molecules from the reaction mixture on the catalyst surface was observed, but in this case, intriguingly, it seems rather not affecting the catalyst activity. In this case also attention should be paid to the purification of the obtained biodiesel to meet the strict standards (Ca + Mg <5 ppm [89]). A pillared acid HMCM-36 zeolite catalyst proved to be very stable, in four repeated cycles only washed with methanol without a significant decline in activity [65]. A K-form of zeolite MAP was highly active in three repeated cycles (yields from 96 to 94 %) along with a turnover frequency of 202 h^{-1}, with methanol washing and recalcination after each cycle. With the same reactivation procedure, a K/fly ash-originated zeolite X catalyst was also highly active in three cycles, after which the activity significantly dropped. Recalcination was used as a method for reactivation of the spent K$_2$O/zeolite catalyst before each run successfully performing in four consecutive cycles, after which the activity dropped [50]. This finding is explained by morphology changes in the material, such as crystal agglomeration, and a consequent decrease in the catalytic surface area, during the consecutive heating process. The excellent recyclability is displayed by a two-dimensional Na/ITW-2 zeolite catalyst with hardly any changes in activity after four consecutive cycles (the catalyst was washed with ethanol and ethyl acetate) [64].

Without any pretreatment the activity of a Li/NaY zeolite catalyst gradually declined from 98.6 % (FAEE yield) to about 80 %, but after recalcination, the catalyst regained its activity to the FAEE yield of 91.6 % achieved in the sixth cycle [85]. The XRD analysis showed that the reduction of the active component (Li$_4$SiO$_4$ and Li$_3$NaSiO$_4$) in favour of Li$_2$SiO$_3$ was responsible for the activity drop, recovering it by the reverse reaction during recalcination.

A bifunctional phosphotungstic acid-modified zeolite imidazolate framework (ZIF-67) catalyst has shown excellent stability in microalgal lipids esterification and transesterification [67]. The activity dropped by 7.2 % in six repeated cycles (still the conversion was up to 91.3 %) without any pretreatment. The reason for this slight decline in activity was found in the deposition of unrefined microalgal lipids into the pores of the material and the breaking of a small amount of W-O-N bonds resulting in the loss of active HPW. It is significant that after six cycles the activity was completely recovered only by washing with methanol and n-hexane [67].

Significantly lower stability was found in the use of a 35 % CaO/zeolite catalyst, which activity decreased from cycle to cycle, to be negligible in the fourth cycle [61]. In this study, a commercial ZSM-5 zeolite was used as a support, while CaO was loaded by impregnation from an aqueous solution using calcium acetate. Similar CaO/zeolite catalysts were prepared in some other studies [29,42] by hydration-dehydration and ultrasound-assistant alcohol impregnation of CaO on fly ash-based zeolite carrier. The difference in precursors and the synthesis methods probably affected the lower stability and recyclability of the former catalyst [61], especially considering a report that calcium acetate was not shown to be the best precursor for achieving stability of CaO-based catalysts [90]. A high drop in conversion efficiency of soybean oil to biodiesel from 98 % to about 46 % was reported in the second cycle in 1.5 h of reaction catalyzed by a diatomaceous earth cancrinite-type zeolite catalyst [77]. This result is rather surprising considering the presented x-ray diffraction, infrared spectrometry, and electronic microscopy analyses, showing imperceptible differences between the fresh and spent catalyst, except occasional smaller agglomerates evolved on the surface of the spent material. Similarly, a gradual decline in the biodiesel yield from cycle to cycle was reported in a study attempting simple regeneration of a

K/natural zeolite catalyst by washing in n-hexane [47]. The reduction in catalyst activity was explained by the leaching of active species into the reaction medium. The same explanation for the catalyst activity decline was provided in the case of a waste-based zeolite carrier impregnated with Ni [70] and a neat zeolite catalyst obtained from geothermal solid waste [71]. Interesting behaviour was shown by a NaBeta zeolite-supported molybdenum catalyst [63], which showed a relatively good activity in the first cycle, followed by a decline in activity of 18 % in the second cycle and remaining at a constant level in the other three consecutive cycles. This behaviour is explained by the deposition and binding of organic molecules from the reaction mixture to the surface of the catalyst in the first cycle, which did not continue in the subsequent cycles.

In general, it can be concluded that the stability of zeolite-based catalysts has not been comprehensively investigated, changes in the materials occurring during the course of the reaction have not been analytically assessed and discussed in sufficient detail, as well as insufficient attention has been paid to optimization of the catalyst regeneration and exploring the maximal reusability of the catalysts. In particular, it is necessary to conduct research on the stability of these catalysts under industrially more favourable continuous process conditions.

6. QUALITY OF THE OBTAINED BIODIESEL

The use of zeolite-based catalysts produced biodiesel of high quality [48,63] according to the standards (ASTM D-6751 [91] and EN 14214[89]), contrary to some other prominent heterogeneous catalytic materials, such as CaO-based catalysts, in which case the obtained biodiesel has problems meeting the standard due to Ca leaching [3]. For example, methanolysis of high-density (0.959 kg dm^{-3} [92]) castor oil catalysed by a KOH/natural zeolite resulted in biodiesel with a density that exceeds the standard value [46]. Biodiesel produced from WCO by catalysis with a Na-modified clinoptilolite showed a high cetane number of 64.5 and was in accordance with the limiting (Na + K) concentration of 2.4 mg kg^{-1}[48]. Biodiesel with a lower cetane number (57.2) was obtained from castor oil catalysed by a Li/NaY catalyst [85]. Additionally, biodiesel density and viscosity were higher than the values prescribed by the standards due to the higher content of long hydrocarbon chains originating from the demanding feed oil. Other WCO-originated biodiesel obtained over a Ni/zeolite catalyst in a batch reactor [70] as well as over a KOH/clinoptilolite catalyst in a microreactor [45] met the European quality standard for density and kinematic viscosity. Waste lard-originated biodiesel, on the other side, exhibited a desirable FAME profile of 38.3 % saturated and 61.7 % unsaturated fatty acids [61]. Biodiesel obtained from microalgal oil showed a mixed methyl ester profile, where that obtained from the *Nannochloropsis oculata* oil contained a slightly higher amount of unsaturated fatty acids, in contrary to that obtained from the *Chlorela vulgaris* oil [53]. Amount of saturated methyl esters is a significant aspect of biodiesel since it determines its oxidative stability, while higher contents of unsaturated methyl esters make biodiesel suitable for usage in countries in colder regions, therefore, reducing the need for additives [53]. Canola oil-originated biodiesel blends (B10 and B20) satisfied the ASTM standard, moreover, the cetane numbers were high (64.3 and 67.2 for B10 and B20 blends, respectively) [87].

7. FUTURE PERSPECTIVES

Humankind has a real need to reduce GHG emissions into the Earth's atmosphere. Use of carbon-neutral biofuels is still imposed as one of the most immediate and effective approaches to the issue. Several readily available technologies are being developed to produce advanced biofuels. The commercial success of some of these fuels will depend on several issues, such as the production process complexity and consequently economy, availability and quality of the feedstock, and quality of the obtained fuel. Catalysis provides a versatile tool to resolve some of these issues by controlling the process reactions. For example, catalysts can simplify processes, reduce reaction time, and/or improve the resulting fuel quality.

Many studies on zeolite-based catalysts in recent years prove the high potential of these materials for efficient catalysis of biodiesel production reactions in the future. Zeolite-based catalysts show high catalytic activity, whether they possess basic, acid, or bifunctional acid-base active sites. This diversity enables these catalysts to successfully tackle oily feedstocks that have unfavourable characteristics for use in reactions with common heterogeneous, as well as homogeneous, catalysts. This is especially important from the point of view that most raw waste or inedible oils contain

large amounts of FFAs and moisture, which cause problems, particularly for base catalysts. Zeolite-based catalysts provide an additional benefit in the possibility to be obtained from waste raw materials, such as fly ash, a by-product of coal burning in thermal power plants, industrial slags, *etc*. This promotes the sustainability of biodiesel production since waste materials can be used both as oily feedstock in the reaction and as raw material to produce catalysts. Taking all this into account, catalysts based on zeolites, therefore, belong to the group of the most preferred heterogeneous catalysts for the transesterification or esterification reaction of TGs.

There are multiple synthesis methods with relatively simple control of the synthesis parameters providing zeolite-based catalysts with desirable characteristics required for such a reaction involving relatively large organic molecules. Regarding morphological and textural characteristics, these materials show high porosity and regularity of pores without pronounced bottlenecks, and exhibit large specific surface area and external surface area, with most of the pores belonging to the mesoporous region. Regarding the physical and chemical characteristics, they have a high concentration of basic and/or acidic active centres that are finely dispersed. These catalysts show significant stability in repeated reaction cycles as well as at high temperatures and elevated pressures.

Still, from the reviewed literature, It seems that good stability and retention of high long-term activity of zeolite-based catalysts demonstrated in batch processes have not been sufficiently investigated in continuous processes, where these positive properties of the material would be particularly important. Current research lacks implementation studies focusing on the intensification of the reactor operation with the use of these catalysts. Research investigating forced periodic reactor operation by periodic modulation of one or more inputs (*e.g.* reactants concentration, temperature, or flow rate) around a steady state operation shows promising state-of-the-art intensification approach [93,94], as well as the use of reactors in which mass transfer is intensified (microreactors, oscillatory baffled reactors, static mixers, *etc*.), are necessary to exploit the full potential of these catalytic materials.

Still, the main challenges for using zeolite-based catalysts will be the process scale-up, conducting large facility experiments, fine-tuning the materials for commercial applications and finding the synthesis routes that are more eco-friendly and less energy-demanding. Based on the presented encouraging results, it should be expected that more emphasis will be given to these topics in the future. Despite existing issues that remain to be solved, the huge variety of different zeolite-based catalysts, the possibility of obtaining them from waste, and the number of studies that dealt with this subject, confirm the promising potential of these materials as heterogeneous catalysts for biodiesel production in a sustainable manner at the industrial level. In this regard, important developments in the preparation of zeolites with increased acid/base active centres, porosity and external surface accessibility summarized in the present manuscript may pave the way for wider and more efficient use of crystalline-porous waste-based materials in biomass conversion processes.

REFERENCES

[1] Popović Z, Souček I, Marinković D, Jocić O. Viability of newly developed processes for catalytic conversion of bio-glycerin into various "green chemicals" and development opportunities for Serbia. *J Appl Eng Sci.* 2016; 14(3): 409-421 https://doi.org/10.5937/jaes14-9551.

[2] Baláž M, Boldyreva EV, Rybin D, Pavlovic S, Rodríguez-Padrón D, Mudrinic T, Luque R. State-of-the-Art of Eggshell Waste in Materials Science: Recent Advances in Catalysis, Pharmaceutical Applications, and Mechanochemistry. *Front Bioeng Biotechnol.* 2021; 8: 612567 https://doi.org/10.3389/fbioe.2020.612567.

[3] Marinković DM, Stanković MV, Veličković AV, Avramović JM, Miladinović MR, Stamenković OO, Veljković VB, Jovanović DM. Calcium oxide as a promising heterogeneous catalyst for biodiesel production: Current state and perspectives. *Renew Sustain Energy Rev.* 2016; 56: 1387-1408 https://doi.org/10.1016/j.rser.2015.12.007.

[4] Shan R, Lu L, Shi Y, Yuan H, Shi J. Catalysts from renewable resources for biodiesel production. *Energy Convers Manage.* 2018; 178: 277-289 https://doi.org/10.1016/J.ENCONMAN.2018.10.032.

[5] Narasimhan M, Chandrasekaran M, Govindasamy S, Aravamudhan A. Heterogeneous nanocatalysts for sustainable biodiesel production. *J Environ Chem Eng.* 2021; 9(1): 104876 https://doi.org/10.1016/J.JECE.2020.104876.

[6]   Mandari V, Devarai SK. Biodiesel Production Using Homogeneous, Heterogeneous, and Enzyme Catalysts via Transesterification and Esterification Reactions: a Critical Review. *Bioenergy Res.* 2021; 1: 1-27 https://doi.org/10.1007/S12155-021-10333-W.

[7]   Rizwanul Fattah IM, Ong HC, Mahlia TMI, Rahman MM, Silitonga AS, Rahman SMA, Ahmed A. State of the Art of Catalysts for Biodiesel Production. *Front Energy Res.* 2020; 8: 101 https://doi.org/10.3389/fenrg.2020.00101.

[8]   Wang YT, Fang Z, Zhang F. Esterification of oleic acid to biodiesel catalyzed by a highly acidic carbonaceous catalyst. *Catal Today*. 2019; 319: 172-181 https://doi.org/10.1016/J.CATTOD.2018.06.041.

[9]   Gebremariam SN, Marchetti JM. Biodiesel production through sulfuric acid catalyzed transesterification of acidic oil: Techno economic feasibility of different process alternatives. *Energy Convers Manage.* 2018; 174: 639-648 https://doi.org/10.1016/J.ENCONMAN.2018.08.078.

[10] Andrade TA, Martín M, Errico M, Christensen KV. Biodiesel production catalyzed by liquid and immobilized enzymes: Optimization and economic analysis. *Chem Eng Res Des.* 2019; 141: 1-14 https://doi.org/10.1016/J.CHERD.2018.10.026.

[11] Tran NN, Gelonch ME, Liang S, Xiao Z, Sarafraz MM, Tišma M, Federsel H-J, Ley SV, Hessel V. Enzymatic pretreatment of recycled grease trap waste in batch and continuous-flow reactors for biodiesel production. *Chem Eng J.* 2021; 426: 131703 https://doi.org/10.1016/J.CEJ.2021.131703.

[12] Jeon Y, Chi WS, Hwang J, Kim DH, Kim JH, Shul YG. Core-shell nanostructured heteropoly acid-functionalized metal-organic frameworks: Bifunctional heterogeneous catalyst for efficient biodiesel production. *Appl Catal Environ*. 2019; 242: 51-59 https://doi.org/10.1016/J.APCATB.2018.09.071.

[13] Mansir N., Teo SH, Rashid U, Saiman MI, Tan YP, Alsultan GA, Taufiq-Yap YH. Modified waste egg shell derived bifunctional catalyst for biodiesel production from high FFA waste cooking oil. A review. *Renew Sustain Energy Rev.* 2018; 82: 3645-3655 https://doi.org/10.1016/J.RSER.2017.10.098.

[14] Jeon KW, Shim J-O, Cho J-W, Jang W-J, Na H-S, Kim H-M, Lee Y-L, Jeon B-H, Bae JW, Roh H-S. Synthesis and characterization of Pt-, Pd-, and Ru-promoted Ni-Ce$_{0.6}$Zr$_{0.4}$O$_2$ catalysts for efficient biodiesel production by deoxygenation of oleic acid. *Fuel.* 2019; 236: 928-933 https://doi.org/10.1016/J.FUEL.2018.09.078.

[15] Tabandeh M, Cheng CK, Centi G, Show PL, Chen W-H, Ling TC, Ong HC, Ng E-P, Juan JC, Lan SS. Recent advancement in deoxygenation of fatty acids via homogeneous catalysis for biofuel production. *Mol Catal.* 2022; 523: 111207 https://doi.org/10.1016/J.MCAT.2020.111207.

[16] Aboelazayem O, Gadalla M, Saha B. Valorisation of high acid value waste cooking oil into biodiesel using supercritical methanolysis: Experimental assessment and statistical optimisation on typical Egyptian feedstock. *Energy.* 2018; 162: 408-420 https://doi.org/10.1016/J.ENERGY.2018.07.194.

[17] Farobie O, Leow ZYM, Samanmulya T, Matsumura Y. New insights in biodiesel production using supercritical 1-propanol. *Energy Convers Manage.* 2016; 124: 212-218 https://doi.org/10.1016/J.ENCONMAN.2016.07.021.

[18] Khedri B, Mostafaei M, Safieddin Ardebili SM. A review on microwave-assisted biodiesel production. *Energy Sources A.* 2018; 41(19): 2377-2395 https://doi.org/10.1080/15567036.2018.1563246.

[19] Fazril I, Shamsuddin AH, Nomanbhay S, Kusomo F, Hanif M, Ahmad Zamri MFM, Akhiar A, Ismail MF. Microwave-assisted in situ transesterification of wet microalgae for the production of biodiesel: progress review. *IOP Conf Ser: Earth Environ Sci.* 2020; 476(1): 012078 https://doi.org/10.1088/1755-1315/476/1/012078.

[20] Patle DS, Pandey A, Srivastava S, Sawarkar AN, Kumar S. Ultrasound-intensified biodiesel production from algal biomass: a review. *Environ Chem Lett.* 2020; 19(1): 209-229 https://doi.org/10.1007/S10311-020-01080-Z.

[21] Tan SX, Lim S, Ong HC, Pang YL. State of the art review on development of ultrasound-assisted catalytic transesterification process for biodiesel production. *Fuel.* 2019; 235: 886-907 https://doi.org/10.1016/J.FUEL.2018.08.021.

[22] Stankovic M, Pavlovic S, Marinkovi D, Tišma M, Gabrovska M, Nikolova D. *Solid green biodiesel catalysts derived from coal fly ash*, in Mansour Al Qubeissi (Ed.). *Renewable Energy - Resources, Challenges and Applications.* London, UK, IntechOpen. 2020; 1-29 https://doi.org/10.5772/intechopen.91703.

[23] Goh BHH, Chong CT, Ge Y, Ong HC, Ng J-H, Tian B, Ashokkumar V, Lim S, Seljak T, Józsa V. Progress in utilisation of waste cooking oil for sustainable biodiesel and biojet fuel production. *Energy Convers Manage.* 2020; 223: 113296 https://doi.org/10.1016/J.ENCONMAN.2020.113296.

[24] Jacob A, Ashok B, Alagumalai A, Chyuan OH, Le PTK. Critical review on third generation micro algae biodiesel production and its feasibility as future bioenergy for IC engine applications. *Energy Convers Manage.* 2021; 228: 113655 https://doi.org/10.1016/J.ENCONMAN.2020.113655.

[25] Perego C, Bosetti A, Ricci M, Millini R. Zeolite Materials for Biomass Conversion to Biofuel. *Energ Fuel.* 2017; 31(8): 7721-7733 https://doi.org/10.1021/ACS.ENERGYFUELS.7B01057.

[26] Galadima A, Muraza O. Waste materials for production of biodiesel catalysts: Technological status and prospects. *J Clean Prod.* 2020; 263: 121358 https://doi.org/10.1016/J.JCLEPRO.2020.121358.

[27] Marinković DM, Miladinović MR, Avramović JM, Krstić IB, Stanković MV, Stamenković OS, Jovanović DM, Veljković VB. Kinetic modeling and optimization of sunflower oil methanolysis catalyzed by spherically-shaped CaO/γ-Al$_2$O$_3$ catalyst. *Energy Convers Manage.* 2018; 163: 122-133 https://doi.org/10.1016/J.ENCONMAN.2018.02.048.

[28] Maghfirah A, Ilmi MM, Fajar ATN, Kadja GTM. A review on the green synthesis of hierarchically porous zeolite. *Mater Today Chem.* 2020; 17: 100348 https://doi.org/10.1016/J.MTCHEM.2020.100348.

[29]   Pavlović SM, Marinković DM, Kostić MD, Lončarević DR, Mojović LJV, Stanković MV, Veljković VB. The chicken eggshell calcium oxide ultrasonically dispersed over lignite coal fly ash-based cancrinite zeolite support as a catalyst for biodiesel production. *Fuel.* 2021; 289: 119912 https://doi.org/10.1016/J.FUEL.2020.119912.

[30]   Serrano DP, Melero JA, Morales G, Iglesias J, Pizarro P. Progress in the design of zeolite catalysts for biomass conversion into biofuels and bio-based chemicals. *Catal. Rew.* 2018; 60(1): 1-70 https://doi.org/10.1080/01614940.2017.1389109.

[31]   Database of Zeolite Structures. http://www.iza-structure.org/databases/. Accessed Apr. 28, 2022.

[32]   Colella C, Gualtieri AF. Cronstedt's zeolite. *Microporous Mesoporous Mater.* 2007; 105(3): 213-221 https://doi.org/10.1016/J.MICROMESO.2007.04.056.

[33]   Mardiana S, Azhari NJ, Ilmi T, Kadja GTM. Hierarchical zeolite for biomass conversion to biofuel. *Fuel.* 2022; 309: 122119 https://doi.org/10.1016/J.FUEL.2021.122119.

[34]   Tschernich RW. *Zeolites of the World*. Phoenix, Arizona 85032: Geoscience Press, Inc., 1992.

[35]   Yilmaz B, Müller U. Catalytic applications of zeolites in chemical industry. *Top Catal.* 2009; 52(6-7): 888-895 https://doi.org/10.1007/S11244-009-9226-0/FIGURES/10.

[36]   Jiang N, Shang R, Heijman SGJ, Rietveld LC. High-silica zeolites for adsorption of organic micro-pollutants in water treatment. *Water Res.* 2018; 144: 145-161 https://doi.org/10.1016/J.WATRES.2018.07.017.

[37]   Li Y, Yu J. Emerging applications of zeolites in catalysis, separation and host-guest assembly. *Nat Rev Mater.* 2021; 6: 12*:* 1156-1174 https://doi.org/10.1038/s41578-021-00347-3.

[38]   Scopus - Analyze search results for keyword "biodiesel". https://www.scopus.com/term/analyzer.uri?sid=f1b0ecf09e7389b54b3d1c0a408b6c35&origin=resultslist&src=s&s=TITLE-ABS-KEY%28biodiesel%29&sort=plf-f&sdt=b&sot=b&sl=24&count=45946&analyzeResults=Analyze+results&txGid=54ea8ad5e5d75fc82684a63f1fc06138 Accessed Apr. 28, 2022.

[39]   Scopus - Analyze search results for keyword "zeolite + biofuels". https://www.scopus.com/term/analyzer.uri?sid=cc9695bcd8a90aaec9397f592b769798&origin=resultslist&src=s&s=TITLE-ABS-KEY%28zeolite+%2b+biofuels%29&sort=plf-f&sdt=b&sot=b&sl=33&count=875&analyzeResults=Analyze+results&txGid=ffb3d93134573352a7168b2f523ae36a Accessed Apr. 28, 2022.

[40]   Zeolites Statistics and Information | U.S. Geological Survey. https://www.usgs.gov/centers/national-minerals-information-center/zeolites-statistics-and-information. Accessed Apr. 28, 2022.

[41]   Liu J, Yu J. Toward Greener and Designed Synthesis of Zeolite Materials. *Zeolites Zeolite-like Mater.* 2016; 1-32 https://doi.org/10.1016/B978-0-444-63506-8.00001-X.

[42]   Pavlović SM, Marinković DM, Kostić MD, Janković-Častvan IM, Mojović LjV, Stanković MV, Veljković VB*.* A CaO/zeolite-based catalyst obtained from waste chicken eggshell and coal fly ash for biodiesel production. *Fuel.* 2020; 267: 117171 https://doi.org/10.1016/J.FUEL.2020.117171.

[43]   Wang Z, Yu J, Xu R. Needs and trends in rational synthesis of zeolitic materials. *Chem Soc Rev.* 2012; 41(5): 1729-1741 https://doi.org/10.1039/C1CS15150A.

[44]   Rabie AM, Shaban M, Abukhadra MR, Hosny R, Ahmed SA, Negm NA. Diatomite supported by CaO/MgO nanocomposite as heterogeneous catalyst for biodiesel production from waste cooking oil. *J Mol Liq.* 2019; 279: 224-231 https://doi.org/10.1016/J.MOLLIQ.2019.01.096.

[45]   Mohadesi M, Aghel B, Maleki M, Ansari A. The use of KOH/Clinoptilolite catalyst in pilot of microreactor for biodiesel production from waste cooking oil. *Fuel*. 2020; 263: 116659 https://doi.org/10.1016/J.FUEL.2019.116659.

[46]   Amalia S, Khalifah SN, Baroroh H, Muiz A, Rahmatullah A, Aini N, Hs MRA, MN Umam, Isnaini IA, Suryana R. Biodiesel production from castor oil using heterogeneous catalyst KOH/zeolite of natural zeolite Bandung Indonesia. *AIP Conf Proc.* 2019; 2120(1): 080016 https://doi.org/10.1063/1.5115754.

[47]   Hidayat A, Mukti NIF, Handoko B, Sutrisno B. Biodiesel production from rice bran oil over modified natural zeolite catalyst. *Int J Technol.* 2018; 9(2) 400-411 https://doi.org/10.14716/IJTECH.V9I2.1084.

[48]   AbuKhadra MR, Basyouny MG, El-Sherbeeny AM, El-Meligy MA, Abd Elgawad AEE. Transesterification of commercial waste cooking oil into biodiesel over innovative alkali trapped zeolite nanocomposite as green and environmental catalysts. *Sustain Chem Pharm.* 2020; 17: 100289 https://doi.org/10.1016/J.SCP.2020.100289.

[49]   Hartono R, Wijanarko A, Hermansyah H. Synthesis of biodiesel using local natural zeolite as heterogeneous anion exchange catalyst. *IOP Conference Series: Mater. Sci Eng.* 2018; 345(1): 012002 https://doi.org/10.1088/1757-899X/345/1/012002.

[50]   Fitriana N, Husin H, Yanti D, Pontas K, Alam PN, Ridho M, Iskandar. Synthesis of K2O/Zeolite catalysts by KOH impregnation for biodiesel production from waste frying oil. *IOP Conference Series: Mater Sci Eng.* 2018; 334(1): 012011 https://doi.org/10.1088/1757-899X/334/1/012011.

[51]   Taslim, Iriany, Bani O, Parinduri SZDM, Ningsih PRW. Biodiesel production from rice bran oil by transesterification using heterogeneous catalyst natural zeolite modified with K2CO3. *IOP Conference Series: Mater Sci Eng.* 2018; 309(1): 012107 https://doi.org/10.1088/1757-899X/309/1/012107.

[52]   Pavlović S, Šelo G, Marinković D, Planinić M, Tišma M, Stanković M. Transesterification of Sunflower Oil over Waste Chicken Eggshell-Based Catalyst in a Microreactor: An Optimization Study. *Micromachines.* 2021; 12(2): 120 https://doi.org/10.3390/MI12020120.

[53] Dianursanti, Delaamira M, Bismo S, Muharam Y. Effect of Reaction Temperature on Biodiesel Production from Chlorella vulgaris using CuO/Zeolite as Heterogeneous Catalyst. *IOP Conference Series: Earth Environ Sci.* 2017; 55(1): 012033 https://doi.org/10.1088/1755-1315/55/1/012033.

[54] Pasae Y, Melawaty L, Ruswanto, Bulo L, Allo EL. Effectiveness of Heterogenous Catalyst In Biodiesel Production Process: The Use of Zeolite, ZnO and Al_2O_3. *J Phys Conf Ser.* 2021; 1899(1): 012032 https://doi.org/10.1088/1742-6596/1899/1/012032.

[55] Otieno SO, Kowenje CO, Okoyo A, Onyango DM, Amisi KO, Nzioka KM. Optimizing production of biodiesel catalysed by chemically tuned natural zeolites. *Mater Today: Proc.* 2018; 5(4): 10561-10569 https://doi.org/10.1016/J.MATPR.2017.12.388.

[56] Mierczynski P, Mosińska M, Szkudlarek L, Chalupka K, Tatsuzawa M, Al Maskari M, Maniukiewicz W, Wahono SK, Vasilev K, Szynkowska-Jozwik, MI. Biodiesel Production on Monometallic Pt, Pd, Ru, and Ag Catalysts Supported on Natural Zeolite. *Materials.* 2020; 14(1): 48 https://doi.org/10.3390/MA14010048.

[57] Alismaeel ZT, Abbas AS, Albayati TM, Doyle AM. Biodiesel from batch and continuous oleic acid esterification using zeolite catalysts. *Fuel.* 2018; 234: 170-176 https://doi.org/10.1016/J.FUEL.2018.07.025.

[58] Marinković DM, Avramović JM, Stanković MV, Stamenković OS, Jovanović DM, Veljković VB. Synthesis and characterization of spherically-shaped $CaO/\gamma-Al_2O_3$ catalyst and its application in biodiesel production. *Energy Convers Manage.* 2017; 144: 399-413 https://doi.org/10.1016/J.ENCONMAN.2017.04.079.

[59] Mowla O, Kennedy E, Stockenhuber M. In-situ FTIR study on the mechanism of both steps of zeolite-catalysed hydroesterification reaction in the context of biodiesel manufacturing. *Fuel.* 2018; 232: 12-26 https://doi.org/10.1016/J.FUEL.2018.05.096.

[60] Feyzi M, Khajavi G. Investigation of biodiesel production using modified strontium nanocatalysts supported on the ZSM-5 zeolite. *Ind Crops Prod.* 2014; 58: 298-304 https://doi.org/10.1016/J.INDCROP.2014.04.014.

[61] Lawan I, Garba ZN, Zhou W, Zhang M, Yuan Z. Synergies between the microwave reactor and CaO/zeolite catalyst in waste lard biodiesel production. *Renew Energy.* 2020; 145: 2550-2560 https://doi.org/10.1016/J.RENENE.2019.08.008.

[62] Al-Ani A, Mordvinova NE, Lebedev OI, Khodakov AY, Zholobenko V. Ion-exchanged zeolite P as a nanostructured catalyst for biodiesel production. *Energy Rep.* 2019; 5: 357-363 https://doi.org/10.1016/J.EGYR.2019.03.003.

[63] Chen C, Cai L, Zhang L, Fu W, Hong Y, Gao X, Jiang Y, Li L, Yan X, Wu G. Transesterification of rice bran oil to biodiesel using mesoporous NaBeta zeolite-supported molybdenum catalyst: Experimental and kinetic studies. *Chem Eng J.* 2020; 382: 122839 https://doi.org/10.1016/J.CEJ.2019.122839.

[64] Pang H, Yang G, Li L, Yu J. Efficient transesterification over two-dimensional zeolites for sustainable biodiesel production. *Green Energy Environ.* 2020; 5(4): 405-413 https://doi.org/10.1016/J.GEE.2020.10.024.

[65] Purova R, Narasimharao K, Ahmed NSI, Al-Thabaiti S, Al-Shehri A, Mokhtar M, Schwieger W. Pillared HMCM-36 zeolite catalyst for biodiesel production by esterification of palmitic acid. *J Mol Catal A.* 2015; 406: 159-167 https://doi.org/10.1016/J.MOLCATA.2015.06.006.

[66] Yagiz F, Kazan D, Akin AN. Biodiesel production from waste oils by using lipase immobilized on hydrotalcite and zeolites. *Chem Eng J.* 2007; 134(1-3): 262-267 https://doi.org/10.1016/J.CEJ.2007.03.041.

[67] Cheng J, Guo H, Yang X, Mao Y, Qian L, Zhu Y, Yang W. Phosphotungstic acid-modified zeolite imidazolate framework (ZIF-67) as an acid-base bifunctional heterogeneous catalyst for biodiesel production from microalgal lipids, *Energy Convers Manag.* 2021; 232: 113872 https://doi.org/10.1016/J.ENCONMAN.2021.113872.

[68] Fereidooni L, Mehrpooya M. Experimental assessment of electrolysis method in production of biodiesel from waste cooking oil using zeolite/chitosan catalyst with a focus on waste biorefinery. *Energy Convers Manag.* 2017; 147: 145-154 https://doi.org/10.1016/J.ENCONMAN.2017.05.051.

[69] Fereidooni L, Abbaspourrad A, Enayati M. Electrolytic transesterification of waste frying oil using Na^+/zeolite-chitosan biocomposite for biodiesel production. *Waste Managt.* 2021; 127: 48-62 https://doi.org/10.1016/J.WASMAN.2021.04.020.

[70] Satriadi H, Pratiwi IY, Khuriyah M, Widayat, Hadiyanto, Prameswari J. Geothermal solid waste derived Ni/Zeolite catalyst for waste cooking oil processing. *Chemosphere.* 2022; 286: 131618 https://doi.org/10.1016/J.CHEMOSPHERE.2021.131618.

[71] Buchori L, Widayat W, Muraza O, Amali MI, Maulida RW, Prameswari J. Effect of Temperature and Concentration of Zeolite Catalysts from Geothermal Solid Waste in Biodiesel Production from Used Cooking Oil by Esterification-Transesterification Process. *Processes.* 2020; 8(12): 1629 https://doi.org/10.3390/PR8121629.

[72] Mahdavianpour M, Pourakbar M, Alavi N, Masihi N, Mirzaei F, Aghayani E. Biodiesel production from waste frying oils in the presence of zeolite synthesized from steel furnace slag. *Inter J Environ Anal Chem.* 2023; 103(4): 814-827 https://doi.org/10.1080/03067319.2020.1863957.

[73] Đặng TH, Chen BH, Lee DJ. Optimization of biodiesel production from transesterification of triolein using zeolite LTA catalysts synthesized from kaolin clay. *J Taiwan Inst Chem.Eng.* 2017; 79: 14-22 https://doi.org/10.1016/J.JTICE.2017.03.009.

[74] Doyle AM, Albayati TM, Abbas AS, Alismaeel ZT. Biodiesel production by esterification of oleic acid over zeolite Y prepared from kaolin. *Renew Energy.* 2016; 97: 19-23 https://doi.org/10.1016/J.RENENE.2016.05.067.

[75] Weitkamp J. Zeolites and catalysis, *Solid State Ion.* 2000; 131(1-2): 175-188. https://doi.org/10.1016/S0167-2738(00)00632-9.

[76] Doyle AM, Alismaeel ZT, Albayati TM, Abbas AS. High purity FAU-type zeolite catalysts from shale rock for biodiesel production. *Fuel.* 2017; 199: 394-402 https://doi.org/10.1016/J.FUEL.2017.02.098.

[77] Đặng TH, Nguyễn XH, Chou CL, Chen BH. Preparation of cancrinite-type zeolite from diatomaceous earth as transesterification catalysts for biodiesel production. *Renew Energy.* 2021; 174: 347-358 https://doi.org/10.1016/J.RENENE.2021.04.068.

[78] Murayama N, Yamamoto H, Shibata J. Mechanism of zeolite synthesis from coal fly ash by alkali hydrothermal reaction. *Inter J Miner Process.* 2002; 64(1): 1-17 https://doi.org/10.1016/S0301-7516(01)00046-1.

[79] Manique MC, Lacerda LV, Alves AK, Bergmann CP. Biodiesel production using coal fly ash-derived sodalite as a heterogeneous catalyst. *Fuel.* 2017; 190: 268-273 https://doi.org/10.1016/J.FUEL.2016.11.016.

[80] Wang C, Leng S, Guo H, Yu J, Li W, Cao L, Huang J. Quantitative arrangement of Si/Al ratio of natural zeolite using acid treatment. *Appl Surf Sci,* 2019; 498: 143874 https://doi.org/10.1016/J.APSUSC.2019.143874.

[81] Volli V, Purkait MK. Selective preparation of zeolite X and A from fly ash and its use as catalyst for biodiesel production. *J. Hazard Mater.* 2015; 297: 101-111 https://doi.org/10.1016/J.JHAZMAT.2015.04.066.

[82] Shabani JM, Babajide O, Oyekola O, Petrik L. Synthesis of Hydroxy Sodalite from Coal Fly Ash for Biodiesel Production from Waste-Derived Maggot Oil. *Catalysts.* 2019; 9: 12: 1052 https://doi.org/10.3390/CATAL9121052.

[83] Bhandari R, Volli V, Purkait MK. Preparation and characterization of fly ash based mesoporous catalyst for transesterification of soybean oil. *J Environ Cheml Eng.* 2015; 3: 2: 906-914 https://doi.org/10.1016/J.JECE.2015.04.008.

[84] Go YW, Yeom SH. Fabrication of a solid catalyst using coal fly ash and its utilization for producing biodiesel. *Environ Eng Res.* 2019; 24(2): 324-330 https://doi.org/10.4491/EER.2018.029.

[85] Li Z, Ding S, Chen C, Qu S, Du L, Lu J, Ding J. Recyclable Li/NaY zeolite as a heterogeneous alkaline catalyst for biodiesel production: Process optimization and kinetics study. *Energy Convers Manage.* 2019; 192: 335-345 https://doi.org/10.1016/J.ENCONMAN.2019.04.053.

[86] Babajide O, Musyoka N, Petrik L, Ameer F. Novel zeolite Na-X synthesized from fly ash as a heterogeneous catalyst in biodiesel production. *Catal Today.* 2012; 190(1): 54-60 https://doi.org/10.1016/J.CATTOD.2012.04.044.

[87] He PY, Zhang YJ, Chen H, Han ZC, Liu LC. Low-energy synthesis of kaliophilite catalyst from circulating fluidized bed fly ash for biodiesel production. *Fuel.* 2019; 257: 116041 https://doi.org/10.1016/J.FUEL.2019.116041.

[88] Lani NS, Ngadi N. Highly efficient CaO-ZSM-5 zeolite/Fe_3O_4 as a magnetic acid-base catalyst upon biodiesel production from used cooking oil. *Appl Nanosci.* 2022; 12: 3755-3769. https://doi.org/10.1007/S13204-021-02121-X

[89] DIN EN 14214 - European Standards. https://www.en-standard.eu/din-en-14214-liquid-petroleum-products-fatty-acid-methyl-esters-fame-for-use-in-diesel-engines-and-heating-applications-requirements-and-test-methods-includes-amendment-2019/. Accessed Jul. 10, 2022.

[90] Marinković DM, Stanković MV, Veličković AV, Avramović JM, Cakić MD, Veljković VB. The synthesis of CaO loaded onto Al_2O_3 from calcium acetate and its application in transesterification of the sunflower oil. *Advan Technol.* 2015; 4(1): 26-32 https://doi.org/10.5937/SAVTEH1501026M.

[91] Standard Specification for Biodiesel Fuel Blend Stock (B100) for Middle Distillate Fuels. https://www.astm.org/d6751-20a.html. Accessed Jul. 10, 2022.

[92] Patel VR, Dumancas GG, Viswanath LCK, Maples R, Subong BJJ. Castor Oil: Properties, Uses, and Optimization of Processing Parameters in Commercial Production. *Lipid Insights.* 2016; 9: 1-12. https://doi.org/10.4137/LPI.S40233.

[93] Nikolic D, Seidel C, Felischak M, Milicic T, Kienle A, Seidel-Morgenstern A, Petkovska M. Forced periodic operation of a chemical reactor for methanol synthesis - The search for the best scenario based on Nonlinear Frequency Response Method. Part I Single input modulations. *Chem Eng Sci.* 2022; 248: 117134 https://doi.org/10.1016/j.ces.2021.117134.

[94] Nikolic D, Seidel C, Felischak M, Milicic T, Kienle A, Seidel-Morgenstern A, Petkovska M. Forced periodic operation of a chemical reactor for methanol synthesis - The search for the best scenario based on Nonlinear Frequency Response Method. Part II Simultaneous modulations of two inputs. Chem Eng Sci. 2022; 248: 117133 https://doi.org/10.1016/j.ces.2021.1171343.

Najnovija saznanja o upotrebi prirodnih zeolita i zeolitnih katalizatora baziranih na otpadu za proizvodnju biodizela

Dalibor M. Marinković i Stefan M. Pavlović

Univerzitet u Beogradu, Institut za hemiju, tehnologiju i metalurgiju, Institut od nacionalnog značaja za Republiku Srbiju, Beograd, Srbija

(Pregledni rad)

Izvod

Imajući u vidu trenutnu svetsku krizu kao i buduće energetske izazove, transformacija biomase u goriva ponovo dobija veliku pažnju zakonodavaca i industrije. Znajući ovo, valorizacija ulja i masnoća putem reakcija transesterifikacije/esterifikacije postaje atraktivan metod za proizvodnju kvalitetnog biodizela pogodnog za postojeće dizel motore. Veliko interesovanje naučnika ukazuje na značajan pomak ka valorizaciji industrijskog otpada kao još jednom pristupu za razvoj ekološki efikasnih procesa. U tom smislu, ovaj rad predstavlja pregled upotrebe zeolitnih katalizatora za dobijanje biogoriva, sa posebnim akcentom na upotrebu otpadnih sirovina u skladu sa principima zelene hemije i održivog razvoja. Zeolitni materijali su veoma pogodni zbog svojih izvanrednih katalitičkih svojstava, uključujući intrinsičke kisele centre, jednostavno nanošenje baznih centara, strukturnu selektivnost i veliku termičku stabilnost. Čisti zeoliti, ili modifikovani nanošenjem aktivnih centara, klasifikovani su u nekoliko grupa u ovom radu u skladu sa njihovim poreklom. Za svaku od različitih grupa zeolita, najrelevantniji skorašnji literaturni rezultati predstavljeni su zajedno sa kritičkim razmatranjem efikasnosti katalizatora, stabilnosti, mogućnosti ponovne upotrebe i ekonomičnosti njihove sinteze. Kao važan deo neophodan za razumevanje i optimizaciju procesa, detaljno su razmotreni mehanizmi reakcije. Na kraju, pažljivo su identifikovani i obrazloženi ključni perspektivni pravci za dalja istraživanja.

Utilization of waste plum stones as a source of oil and catalyst for biodiesel production

Marija R. Miladinović[1], Stefan Pavlović[2], Ivana B. Banković-Ilić[1], Milan D. Kostić[1], Olivera S. Stamenković[1] and Vlada B. Veljković[1,3]

[1]Faculty of Technology, University of Niš, Bulevar Oslobodjenja 124, 16000 Leskovac, Serbia
[2]University of Belgrade, Institute of Chemistry, Technology, and Metallurgy Center for Catalysis and Chemical Engineering, Njegoševa 12, 11000 Belgrade, Serbia
[3]The Serbian Academy of Sciences and Arts, Knez Mihailova 35, 11000 Belgrade, Serbia

Abstract

Possibilities of using waste plum stones in biodiesel production were investigated. The plum kernels were used as a source to obtain oil by the Soxhlet extraction method, while the whole plum stones, the plum stone shells that remained after the crashing, and the plum kernel cake that remained after the oil extraction, were burned off to obtain ashes. The collected ashes were characterized by elemental composition, porosity, and base strength and tested for catalytic activity in transesterification of esterified plum kernel oil. Dominant elements were potassium, calcium, and magnesium at different contents in the three obtained ashes. The most active catalyst was the plum stone shell ash, so the effect of temperature (40, 50, and 60 °C) on the reaction rate was investigated. The reaction rate constant increased with the reaction temperature with the activation energy value of 58.8 kJ mol^{-1}. In addition, the plum stone shell ash can be reused as a catalyst after recalcination.

Keywords: ash; catalysis; kinetics; methanolysis; transesterification.

Available on-line at the Journal web address: http://www.ache.org.rs/HI/

1. INTRODUCTION

Different waste oily feedstocks, such as used cooking and non-edible oils, have been successfully utilized as suitable raw materials for producing biodiesel [1]. Conversion of these oils into biodiesel is achieved by transesterification with appropriate alcohol (methanol or ethanol) and a suitable homogeneous or heterogeneous acid or base catalyst. Waste biomass ashes occupy a significant place among solid catalytical materials, suitable in terms of environmental parameters, good activity, selectivity, and stability [2]. For example, shells of hazelnuts [3,4] and walnuts [5], produced as waste from the fruit processing industry, were combusted and calcined to ash and then successfully applied as solid base catalysts for sunflower oil methanolysis. In addition, other waste materials, such as salacca and bamboo leave ashes, were used to immobilize ZnO [6] and ZrO$_2$ [7], respectively, to obtain efficient catalysts for biodiesel production. To consider low-cost solid materials as efficient heterogeneous catalysts, they need to have the following characteristics: high catalytic activity, chemical stability, possibility for easy separation, maintained activity, and reusability [8]. Therefore, the catalytic performance of different biomass ash-based catalysts has recently been tested for biodiesel production under various reaction conditions (Table 1).

Similarly, oils extracted from waste kernels and seeds of different fruits remaining after fruit processing might be alternative, cheap sources for biodiesel production. The oils obtained from kernels or seeds of apricot [9], melon [10], almond [11], pumpkin [12], and mandarin orange [13] were used for biodiesel production by base-catalyzed or two-step acid/base-catalyzed processes.

Plum kernels, as a waste product of food processing, can be a source of inexpensive oil suitable for biodiesel production. The total production of plums in the world in 2020 was over 12 million tons, where China is the largest

producer, with over 6 million tons per year, while Serbia produces over half a million tons per year [14]. The oil content in plum kernels is 32-46 wt.% [15], and biodiesel quality depends on its fatty acid profile.

Table 1. Biomass ash-based catalysts for biodiesel production

Type of catalyst	Catalyst characteristics	Oil/Alcohol	Reaction conditions				Content/ Yield / Conversion, %	Reuse	Ref.
			MR[a]	C[b] / wt.%	t[c] / °C	τ[d] / h			
Acai seed ash / calcined	Content, % (EDS): K - 12.7, Mg - 2.7, Ca - 1.4, Si - 3.7, P - 3.6, S - 2.0, O - 31.3 Identified crystal phase (XRD): K_2O, SiO_2, CaO, K_2CO_3, K_2SO_4, $CaCO_3$, $Ca_3(PO_4)_2$, MgO, $CaSiO_3$	Soybean oil / Methanol	18:1	12	100	1	98.5 ± 0.21/-/-	1st, 2nd run (92.5%) 3rd, 4th, 5th, 6th run (>80.0%)	[26]
Palm bunch ash / not calcined	Content, % (XRF): K - 81.1, Si - 7.28, Mo - 3.3, Fe - 2.69, Rb - 2.02, P -1.6 Identified crystal phase (XRD): K_2O, CaO, MgO	Palm oil / Methanol	15:1	18	Room	0.5	98.9/-/-	1st run (97.4%) 2nd run (70.2%)	[27]
Banana peel ash / not calcined	Content, % (XRF): K_2O - 65.11, SiO_2 - 0.864, CaO - 7.787, P_2O_5 - 6.068, SO_3 - 2.857, Cl - 2.07 Content, % (EDS): K - 70.06, Ca - 9.54, P -7.55, Si -4.56, Cl -3.23, Mg - 1.78, Fe - 1.49, O - 1.03, S - 0.75 Surface area: 1.4546 $m^2\,g^{-1}$	Soybean oil / Methanol	6:1	0.7	Room	4	-/-/98.95	1st run (98.95%) 2nd run (81.33%) 3rd run (67.74%) 4th run (52.16%)	[28]
Coconut husk ash / not calcined	Identified crystal phase (XRD): K_2O	*Cerbera manghas* oil	6:1	10	60	3	88.6/-/-	1st, 2nd, 3rd, 4th run (88%)	[29]
Pineapple leaves ash / calcined	Identified elements (XRF): K, Ca Identified crystal phase (XRD): MgO, $Mg_2P_2O_7$, $Na_2Ca_4(PO_4)_2SiO_4$, $Al(SO_4)_3$, $Mn_{0.97}Mg_{0.03}SiO_3$, K_2SO_4	Soybean oil / Methanol	40:1	4	60	0.5	-/-/98	1st run (98.92%) 2nd run (97.6%) 3rd run (94.3%) 4th run (> 85%)	[30]
Biomass fly ash / not calcined	Identified elements (EDX): Ca, Mg, Si, Al, O, K, S, Na, Cl, P Content, % (XRD): $CaCO_3$ - 71.0, $Ca(OH)_2$ - 12.9, KCl - 7.1, CaO - 3.8, SiO_2 - 2.3, other - 3.0 Surface area: 9.028 $m^2\,g^{-1}$	Blends of waste cooking oil and refined palm oil /Methanol	6.7 :1	13.57	55	2	-/73.8/-	1st run (73.5%) 2nd run (76.2%) 3rd run (83.6%)	[31]
Walnut shell ash / calcined	Content, wt.% (EDX): K -23.55, Ca -17.67 Identified crystal phase (XRD): CaO, MgO (periclase), SiO_2 (b-cristobalite), K_2O, Ca_2SiO_4, $KAlO_2$, $Ca(OH)_2$ Surface area: 8.8 $m^2\,g^{-1}$ Base strength: 11 < $H\_$ < 15 Total basicity: 0.352 mmol g^{-1}	Sunflower oil / Methanol	12:1	5	60	0.167	98/-/-	1st, 2nd, 3rd, 4th run (>96%)	[5]

Type of catalyst	Catalyst characteristics	Oil/Alcohol	Reaction conditions				Content/ Yield / Conversion, %	Reuse	Ref.
			MR[a]	C[b] / wt.%	t[c] / °C	τ[d] / h			
Hazelnut shell ash / calcined	Content, wt.% (EDX): K - 26.29, Ca - 11.62, Mg - 6.77, P - 6.10 Identified crystal phase (XRD): KAlO$_2$, K$_4$P$_2$O$_7$, K$_3$FeO$_2$, Ca$_2$SiO$_4$, MgO (periclase), SiO$_2$ (quartz), CaO and K$_2$O Surface area: 4.9 m^2 g^{-1} Base strength: 11 < $H\_$ < 15 Total basicity: 1.03 mmol g^{-1}	Used cooking sunflower oil / Methanol	12:1	5	60	0.167	98/-/-	1st, 2nd, 3rd run (>96%)	[3]
Waste fermented-unfermented kola nut pod / calcined	Identified elements (EDX): Ca, K, Mg SFCKNP Base strength: 175 µmol g^{-1} UCKNP Surface area: 0.8 m^2 g^{-1} Base strength: 140 µmol g^{-1}	Shea butter oil / Methanol	5:1*	2.5	50	0.92	95.30/-/-	1st, 2nd, 3rd run (>95%) 4th run (>90%) 5th run (>85%)	[32]

[a]MR – methanol-to-oil molar ratio; [b]C – catalyst loading; [c]t – reaction temperature; [d]τ – reaction time; *methanol-to-oil volume ratio; UCKNP - unfermented calcined kola nut pod; SFCKNP - solid fermented calcined kola nut pod

Plum oil has rarely been investigated as a feedstock for biodiesel production. One of the first studies referred to biodiesel synthesis via a two-step process consisting of acid-catalyzed esterification (using H$_2$SO$_4$) of free fatty acids followed by base-catalyzed methanolysis (using solid CaO) of the esterified oil, obtained by extraction from plum kernels [16]. Górna *et al.* [17] investigated the potential application of plum kernel oils from twenty-eight varieties of *Prunus domestica* L. and *Prunus cerasifera* Ehrh in the biodiesel industry. The several examined biodiesel properties, such as kinematic viscosity, cetane number, density, and iodine values, satisfied the European biodiesel specification. Almost 70 % of the tested biodiesel samples met the standard for oxidation stability. Composite nano-structured catalysts, obtained by mixing potassium ferricyanide with different low-cost clay support materials such as bentonite, granite, White pocha, Sindh, and Kolten clays, were tested for transesterification of plum kernel oil [15]. Bentonite–potassium ferricyanide composite at a concentration of 0.3 wt.% (reaction conditions: temperature 60 °C, methanol-to-oil molar ratio 10:1) showed a high biodiesel yield, which further increased after calcination of the composite. Also, the obtained biodiesel quality parameters (iodine value, cetane number, acid value, specific gravity, and density) satisfied the standard specifications [15].

Kinetic modeling of homo- or heterogeneously-catalyzed transesterification of different oils has been used for simulation and techno-economic analysis of biodiesel production processes. Kinetic models, such as the second order [18,19], an irreversible pseudo-first-order [20-22], or an irreversible pseudo-second-order [23,24], have been recommended so far. Kostić *et al.* [25] compared kinetic parameters of base-catalyzed methanolysis of different vegetable oils, such as plum kernel, roadside pennycress, olive, melon, grape¬seed, hempseed, and sunflower. Influence of the fatty acid composition of all tested oils on the reaction kinetics was investigated, and the reaction rate constants correlated to the content of unsaturated fatty acids in oils. In addition, the model of the irreversible pseudo-first-order reaction was applied to describe the reaction kinetics. The reaction rate constant increased linearly with increasing the content of unsaturated fatty acids, with the highest value observed for plum oil methanolysis. However, studies about the kinetic modeling of the transesterification reaction of plum oil in the presence of plum stone shell ash as a solid catalyst are lacking.

The present paper is the first attempt to use waste ashes from combustion of the whole plum stone, stone shells, and kernel cake as solid catalysts in methanolysis of plum kernel oil. The possibility of using ash to catalyze methanolysis of oil from the same waste material is advantageous over using other catalysts. Primarily, all catalysts were characterized by determining their elemental and phase composition and textural parameters. Then, the effect of the reaction temperature on the reaction rate and fatty acid methyl esters (FAMEs) content was investigated. Finally, the kinetics of the methanolysis reaction was analyzed to define the appropriate kinetic model.

2. MATERIAL AND METHODS

2. 1. Materials

Plum fruit was purchased at a local market in South Serbia. The plum stones were used for obtaining the oil and catalyst preparation. The chemicals used in transesterification and analytical analysis were methanol (purity of 99.5 %) obtained from Zorka Pharma (Šabac, Serbia), concentrated sulfuric acid (p.a. 96 %) from Lach-Ner Ltd. (Neratovice, Czech Republic), potassium hydroxide standard solution 0.1 N, Titrisol® from Merck (Darmstadt, Germany), methanol, 2-propanol, and *n*-hexane, HPLC purity, from LGC Promochem (Wesel, Germany), phenolphthalein, thymolphthalein, thymol violet, 2,4-dinitroaniline and benzene carboxylic acid (Sigma Aldrich, USA).

2. 2. Oil extraction

Plum kernel oil was obtained by the Soxhlet extraction method [16]. The yield of obtained oil was 332±02 g / kg with a moisture content of 2.7±0.1 wt.% and an acid value of 14.7±0.1 mg KOH/g. Due to its high acid value, the oil was pre-esterified. The presence of free fatty acids (FFA) is not desirable in base-catalyzed transesterification due to the possibility for catalyst consumption. Usually, refined oils with an acid value lower than 2 mg KOH/g are recommended [33]. The esterification of plum kernel oil was carried out at optimal reaction conditions defined by Kostić *et al.* [16] to reduce its acid value to 1.0±0.2 mg KOH/g making it suitable for base-catalyzed transesterification.

2. 3. Catalyst preparation

Three types of catalysts were prepared by burning off the whole plum stones, stone shells, and kernel cake in open air. The obtained chars were calcined in a furnace at 800 °C in the air atmosphere, resulting in 3 wt.% of ash content. Catalytic activity of the calcined ashes obtained from plum stones (PSA), stone shells (PSSA), and kernel cake (PKCA) was tested in transesterification of plum oil with methanol.

2. 4. Catalyst characterization

2. 4. 1. Elemental analysis

Elemental analysis of ashes was determined by using the inductively coupled plasma analytical technique with optical emission spectrometry (ICP-OES). Digestion of samples was carried out in a microwave digester (Ethos 1, Milestone, Italy), in closed Teflon cuvettes, at high pressure (10 MPa) and high temperature (210 ºC) for 20 min. Acids used for the total sample dissolution were H_2SO_4 96 %, H_3PO_4 85 %, HNO_3 65 %, and HF 40 % (Alfa Aesar GmbH & Co KG, Germany). For instrument calibration, standard solutions were prepared from the multi-element standard plasma solution 4, Specpure®, 1000 µg cm^{-3}, and silicon, the standard plasma solution, Specpure®, Si 1000 µg cm^{-3} (Alfa Aesar GmbH & Co KG, Germany). The concentration of elements was measured by using an iCAP 6500 Duo ICP instrument (Thermo Fisher Scientific, Cambridge, UK) with iTEVA operating software.

2. 4. 2. XRD analysis

Identification of phases in PSA, PSSA, and PKCA samples was performed by the X-ray powder diffraction (XRD) technique (Rigaku SmartLab automatic multipurpose X-ray diffractometer) using CuKα radiation (λ = 0.15418 nm) in the 2θ range of 10-90° and step-length of 3º min^{-1}. The crystalline phases were identified by comparing the XRD diffractograms with the diffraction patterns of individual phases provided by the ICDD (International Center for Diffraction Data), the former JCPDS (Joint Committee of Powder Diffraction Standards).

2. 4. 3. Hg porosimetry

Mercury Intrusion Porosimetry measurements were performed in the fully automated conventional apparatus Carlo Erba Porosimeter 2000 (Carlo Erba, Italy; pressure range: 0.1 to 200 MPa; pores with a diameter within 7.5 and 15,000 nm). Acquisition of the analysis data was performed by using the Milestone Software 200 (Milestone Systems, Denmark). Two subsequent intrusion-extrusion runs (Run I and Run II) were conducted. Before the analysis, the samples were evacuated for 2 h in a dilatometer placed in the Macropores Unit 120 (Carlo Erba, Italy).

2. 4. 4. Base strength

Base strength ($H\_$) of catalysts was determined by using Hammett indicators: phenolphthalein ($H\_$ = 9.3), thymolphthalein ($H\_$ = 10.0), thymol violet ($H\_$ = 11.0), and 2,4-dinitroaniline ($H\_$ = 15.0). The procedure included mixing the catalyst (50 mg) with 1 cm^3 of Hammett indicators solution diluted in 2 cm^3 of methanol. The mixture was shaken for 1 h and left to reach color equilibration. The base strength of the catalyst was determined based on the change of color in the solution. The change of colors occurs when the catalyst strength is higher than the weakest indicator, but it remains unchanged when it is lower than the strongest indicator. The catalyst basicity was measured by titration of the Hammett indicator-benzene carboxylic acid (0.02 mol L^{-1} anhydrous ethanol solution).

2. 5. Transesterification

Transesterification of esterified plum kernel oil (20 g) with methanol (8.83 g) using PSA, PSSA, PKCA as a catalyst (catalyst loading of 10 %, based on the oil weight) was carried out in a 250 cm^3 three-neck glass round-bottom flask equipped with a reflux condenser and stirred by a magnetic stirrer. The initial methanol-to-oil molar ratio of 12:1 was kept constant while the reaction temperature varied from 40 to 60 °C. The reaction mixture was intensively agitated at 800 rpm. The samples (0.3 cm^3) were taken at timed intervals (5, 10, 20, 30, 40, 50, 60, 75, 90, and 120 min) and quenched by immersing the vials in ice water and centrifuged (Sigma Laborcentrifugen 2-6E, Germany, 3500 rpm) for 10 min to separate the methyl ester layer. The upper layer aliquot (methyl esters phase) was dissolved in a solution of 2-propanol and *n*-hexane (5/4, v/v) in the ratio of 1:200 and filtered through a 0.45 μm Millipore filter to prepare for HPLC analysis. The HPLC analysis was performed by using HPLC chromatography (Agilent 1100 Series, Agilent Technologies, Germany) according to the method described elsewhere [34]. The test for catalyst reusability was also performed under the same reaction conditions: the catalyst amount of 10 wt.%, the methanol-to-oil molar ratio of 12:1, and the reaction temperature of 60 °C. The catalyst was separated from the reaction mixture at the end of reaction by vacuum filtration and used in the next batch without treatment. Also, the separated catalyst was recalcined (800 °C, 2 h) before the subsequent cycle and then tested for reusability. All experiments were done in duplicate.

3. KINETICS

Kinetics of plum oil methanolysis catalyzed by PSSA was studied under intensive agitation (800 rpm) at various temperatures by monitoring the FAME production. It was assumed that the catalyst, reactants, and products were distributed uniformly in the reaction mixture. As a result, the consumption rates of diacylglycerols (DAGs) and monoacylglycerols (MAGs) were higher than that of triacylglycerols (TAGs), resulting in low concentrations of the two former acylglycerols during the reaction. Hence, the conversion of plum kernel oil into the FAMEs and glycerol, in the presence of ash as a solid catalyst, can be presented by the overall stoichiometric equation instead of presenting separately each of all three reaction steps, equation (1):

A + 3B $\rightleftarrows$ 3R + S   (1)

where A, B, R, and S denote the reactants and products: oil, methanol, FAME, and glycerol, respectively.

The reaction occurred in excess of methanol, so it can be considered irreversible. At lower temperatures, the overall process rate is controlled by the TAG mass transfer rate and the chemical reaction rate in the initial heterogeneous and the later pseudo-homogeneous regime, respectively [35]. On the other hand, only a pseudo-homogeneous regime exists at the highest temperature, where the chemical reaction limits the overall process rate. The pseudo-first-order kinetic model is valid for both heterogeneous and pseudo-homogeneous regimes [35], equation (2):

$$\left(-r_A\right) = -\frac{dc_A}{d\tau} = kc_A$$ (2)

where c_A is the TAG concentration, k is the apparent rate constant, and τ is the reaction time. For the heterogeneous regime, the apparent rate constant corresponds to the TAG mass transfer coefficient. For the pseudo-homogeneous regime, it is the pseudo-first-order reaction rate constant. The TAG concentration is related to the conversion degree x_A as follows, equation (3):

$c_A = c_{A0}(1-x_A)$ (3)

By introducing Eq. (3) into Eq. (2) and by integrating it for the initial condition: $\tau = 0$ and $x_A = 0$, the final equation (4) is obtained:

$-\ln(1-x_A) = k\tau + C$ (4)

where C is the integration constant ($C = 0$ for the heterogeneous regime at 40 and 50 °C and the pseudo-homogeneous regime at 60 °C, because $x_A = 0$ for $\tau = 0$).

4. RESULTS AND DISCUSSION

4. 1. Catalyst characterization

The main elements in the obtained ashes were K, Ca, and Mg (Table 2), at reasonably high contents typical for some ashes, such as *Sesamum indicum* plant ash [36], hazelnut shell ash [3] or *Acai* seed ash [26]. Silicon, a common constituent of ashes from various sources, such as wood, shells, straws, and husks [37], was present in the PSA and PSSA but significantly less in PKCA. The prevalence of K and Ca affects the catalytic activity of ash. A high FAME content was achieved in a shorter reaction time in oil methanolysis catalyzed by ashes containing higher contents of K and Ca than other elements [3,5,26]. Similarly, a higher ash catalytic activity due to the presence of K was demonstrated by comparing the catalytic activities of hazelnut shell ash and quicklime (CaO) under similar reaction conditions [3].

Table 2. Elemental composition of the obtained ashes

Element	Content*, %		
	PSA	PSSA	PKCA
Ca	9.43	11.79	6.55
K	7.82	11.31	12.47
Mg	2.62	2.43	3.08
Si	1.07	2.49	0.05
Fe	0.71	0.68	0.08
Al	0.48	0.58	0
Na	0.32	0.47	0.14

*STD was lower than 0.26

The structure evolution during calcination of raw materials is shown in Fig. 1. The detected crystalline phases in all three samples could be divided into three groups: group I – pure oxide and chloride phases of potassium (sylvite – KCl, PDF#41-1476), calcium (lime – CaO, PDF#37-1497), magnesium (periclase – MgO, PDF#43-1022), and silicon (quartz – SiO_2, PDF#46-1045), group II – calcium silicate phases (rankinite – $Ca_3Si_2O_7$, PDF#22-0539 and laranite – Ca_2SiO_4, PDF#70-0388), group III – complex crystalline phases of potassium, magnesium, calcium, sodium, aluminum, and silicon in the form of sulfate, phosphate, and chloride (hazenite – $KNaMg_2(PO_4)_2 \cdot 14H_2O$, PDF#15-0762, kainite – $KMg(SO_4)Cl \cdot 2.75H_2O$, PDF#35-0812, carnallite - $KMgCl_3 \cdot 6H_2O$, PDF# 24-0869, polyhalite – $K_2Ca_2Mg(SO_4)_4 \cdot 2H_2O$, PDF#5-628, syngenite – $K_2Ca(SO_4)_2 \cdot H_2O$, PDF#74-2159 and flörkeite – $K_3Ca_2Na[Al_8Si_8O_{32}] \cdot 12H_2O$, PDF#34-0137). The phase composition corresponds to the other ashes derived from different biomass sources [38]. Intensities of the primary diffraction line of phases varied according to chemical composition and decreased as the element concentration decreased. However, interactions between elements led to a deviation due to the creation of numerous complex phases. The appearance of group II characteristic phases follows the mechanism of biomass ash formation [38] as a consequence of the interaction between CaO and SiO_2 during the solid-state reaction at the ash fusion temperature. At high temperatures (>700 °C), CaO penetrates the melted glassy phase, whereby a part reacts and forms calcium silicate compounds. The other part of CaO is trapped and inaccessible as an active catalyst center. More significant calcium losses at these temperatures are characteristic for samples with higher silicon contents and for long-term calcination [39]. Besides the simple compounds in the CaO-SiO_2 phase system, creation of more complex crystal forms (group III) takes place, especially in the case of a sample with the low silicon content. The crystalline phases from groups II and III could contribute to the morphological and textural properties of the final catalyst.

The values of textural parameters obtained by Hg porosimetry for the obtained catalysts (*i.e.* calcined ashes) are given in Table 3. Furthermore, the total intruded volume of Hg and the corresponding pore size distribution (PSD) curves for the two subsequent intrusion cycles (I and II) are presented in Fig. 2. In all three samples, a significant reduction in the total intruded mercury can be observed, indicating the existence of interparticle space in the materials [40], which was confirmed by a decrease in porosity amounting to 40 to 65 % in the cycle II. The PSD curve for the PSA sample is bimodal in cycle I with pore diameters centered at 2.48 and 7.53 μm. In cycle II, the PSD curve exhibits a monomodal character with a pore diameter centered at 2.23 μm.
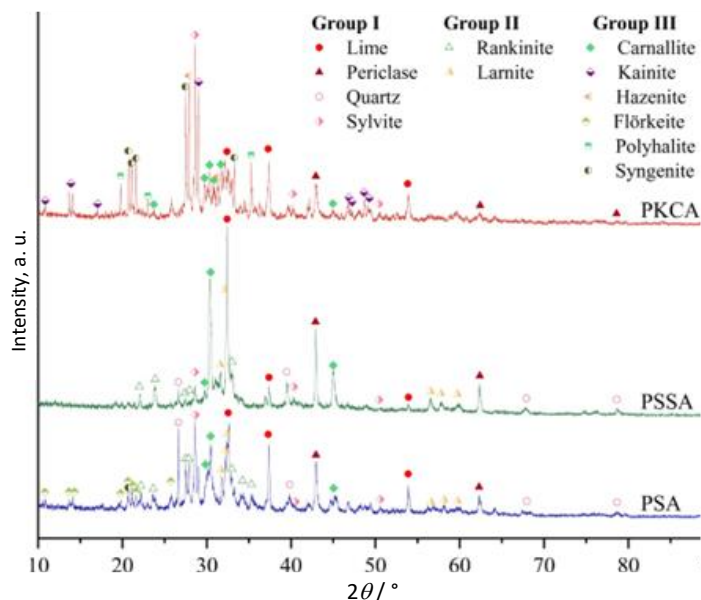
Fig. 1. XRD patterns of calcined PSA, PSSA and PKCA ashes
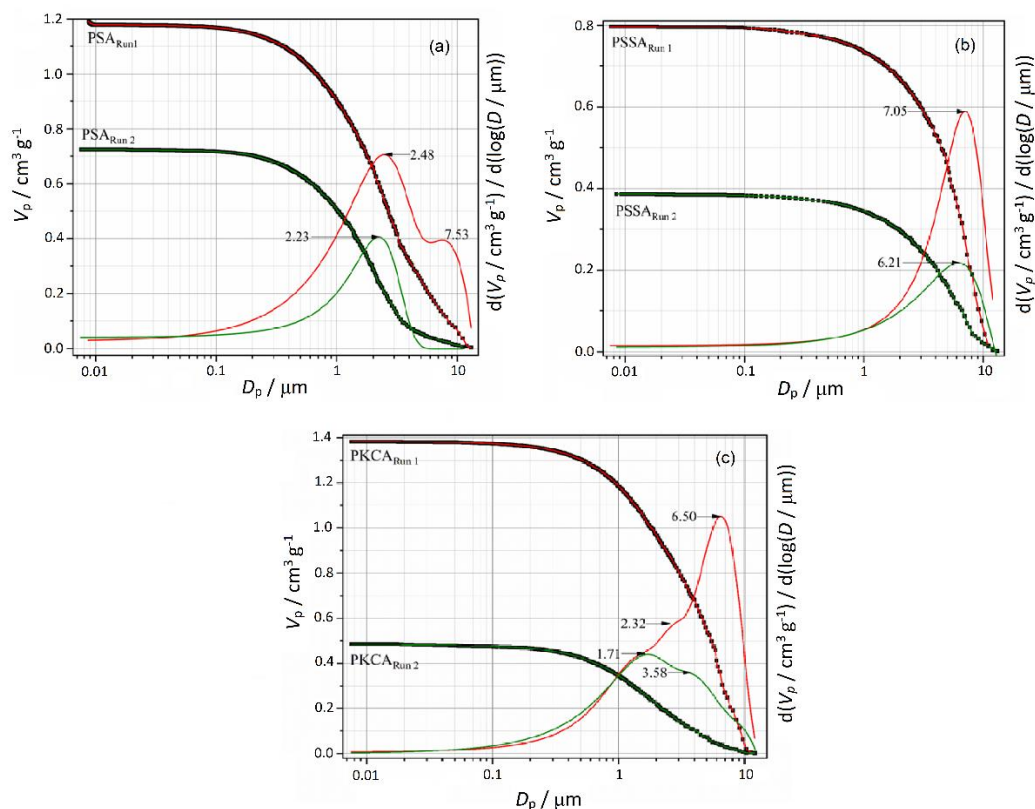
Fig. 2. Pore size distribution curves for (a) PSA, (b) PSSA, and (c) PKCA ashes

On the other hand, the PSD curves for the PSSA sample exhibit monomodal character in both intrusion cycles with a slight change in pore diameter centered at nearly 7.0 µm. Unlike the first two samples, the PSD curves for PKCA are multimodal with pore diameters in a wide range (from 1.71 to 6.50 µm). The multimodal character of the curve was preserved in the cycle II but with a somewhat narrower range of pore diameters, excluding pores of about 7.0 µm. Shifting pore size to a larger diameter leads to a lower surface area [41]. Thus, the pore diameter for all samples is in the macropore region, as confirmed by a low specific surface area. The macroporous pore system is very favorable and suitable for reactions whose reactants are large organic molecules, such as TAGs [3,5,42]. However, for the type of catalyst obtained in the one-way process, such as in this study, the chemical composition plays a more significant role than the textural properties. Although the catalytic activity of solid catalysts is directly related to the surface area, the surface area did not influence the catalytic activity of walnut and hazelnut ashes [3,5]. The PSSA catalyst had the lowest surface area (Table 3) amounting to 1.67 m^2 g^{-1}, which is lower than the value reported for a *Sesamum indicum* plant ash (3.66 m^2 g^{-1}) [36] and close to that of a *Musa acuminata* peel ash (1.45 m^2 g^{-1}) [28].

The base strength ($H\_$) for all catalysts was in the range 9.3<$H\_$<15.0. The PSSA sample exhibited the highest basicity (3.384 mmol g^{-1}), while the basicity of the PKCA and PSA samples was lower (1.293 and 0.924 mmol g^{-1}, respectively).

Table 3. Textural parameters of catalysts

Sample	Intrusion cycle	V_p / cm^3 g^{-1}	S_{Hg} / m^2 g^{-1}	D_p / µm	BD / g cm^{-3}	BD_{Corr} / g cm^{-3}	P / %
PSA	I	1.19	10.35	2.60	0.67	3.31	79.75
	II	0.73	3.83	2.27	0.67	1.30	48.58
PSSA	I	0.80	1.67	7.23	0.93	3.59	74.06
	II	0.39	1.28	5.05	0.93	1.45	35.93
PKCA	I	1.38	4.14	5.81	0.57	2.69	78.83
	II	0.49	3.16	1.67	0.57	0.79	27.65

V_p – Total pore volume; S_{Hg} – Specific surface area; D_p – Average pore diameter; BD – Bulk density; P - Porosity

4. 2. Plum kernel oil methanolysis catalyzed by PSA, PSSA, and PKCA ashes

The catalytic performance of PSA, PSSA, and PKCA was evaluated in methanolysis of the pre-esterified plum oil. Change in FAME contents during the reactions is presented in Fig. 3, where the order of the catalytic performance of the tested ashes was PSSA > PKCA > PSA and it follows their basicity. Significantly higher FAME contents were achieved in the reaction catalyzed by PSSA as compared to those obtained in the reactions catalyzed by PSA and PKCA during the whole reaction period. Furthermore, rapid formation of FAMEs in the initial reaction period contributed to a faster overall reaction catalyzed by PSSA, thus indicating absence of diffusion limitations in the liquid-liquid-solid system at the beginning of the reaction. On the other hand, slow FAME formation at the beginning of the reactions catalyzed by PSA or PKCA was evident.
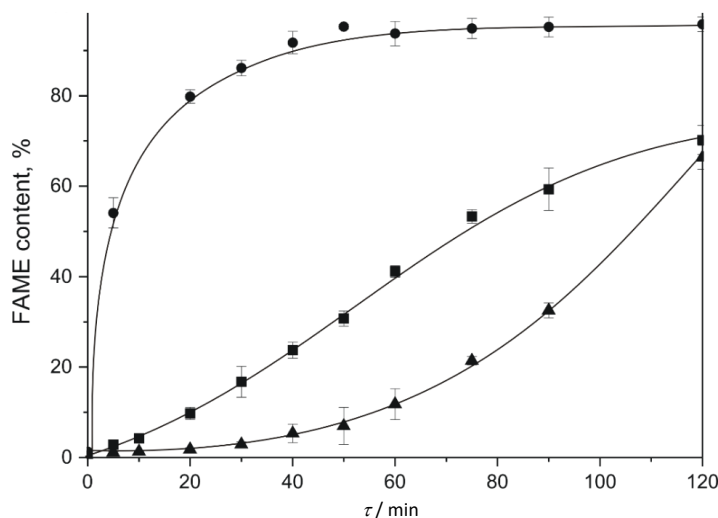
Fig. 3. Methanolysis of plum kernel oil catalyzed by PSSA - ●, PSA - ▲ and PKCA - ■ (reaction temperature 60 °C)

Investigating the catalytic performance of mixed oxides, Fraile *et al.* [43] found that alkaline ions (Na$^+$) were the primary source of the catalyst strong basicity and contributed to the higher catalytic activity. Furthermore, they concluded that solids with a high content of alkaline ions had a low surface area. Therefore, the observed difference in reaction rates could be analyzed from the aspect of elemental composition; the higher content of Ca and K would positively affect the basicity. Buchori *et al.* [44] studied the effect of adding K_2O to CaO-ZnO on the resulting catalyst basicity. The results revealed that a higher molar ratio of CaO and higher content of the added K_2O increased the catalyst basicity. Similarly, Tang *et al.* [45] reported that loading KCl onto CaO can increase the basicity of the catalyst and affect its porosity. Although the pore size diameters of all catalysts investigated in the present study were distributed in the macroporous region (Section 4. 1.) indicating effective diffusion [41], lower reaction rates of the reactions catalyzed by PKCA and PSA were observed.

4. 3. Effect of the reaction temperature on the methanolysis reaction rate and FAME content

Since PSSA showed the best catalytic performance, kinetics of the reaction catalyzed by this catalyst was investigated at three reaction temperatures (40, 50 and 60 °C). Lower FAME contents were achieved when the reaction was performed at lower temperatures (Fig. 4), which was especially pronounced in the initial reaction period. A longer reaction time was required to reach the FAME content over 95 % at 50 °C than at 60 °C. Similarly, Barros *et al.* [30] found that increasing the temperature from 50 to 60 °C significantly increased the FAME content in the reaction catalyzed by calcined pineapple leaves ash. The increase in the reaction temperature increases the reaction rate constant since oil methanolysis is an endothermic reaction. However, by lowering the reaction temperature, diffusion limitations in the liquid-liquid-solid system could also occur, causing a slow initial reaction period. A temperature increases from 40 to 80 °C at a methanol-to-oil molar ratio of 12:1 and a catalyst loading of 7 wt.% positively affected oil conversion over calcined tucumã peel ash, containing mainly K, P, Ca, and Mg [46]. The PSSA-catalyzed methanolysis was performed at a lower temperature (60 °C) than other methanolysis reactions catalyzed by different ashes reported in literature [35,46-48]. Likewise, the high FAME contents were achieved at the same reaction temperature in oil methanolysis using the walnut shell [5] and hazelnut shell [3] ashes as catalysts.
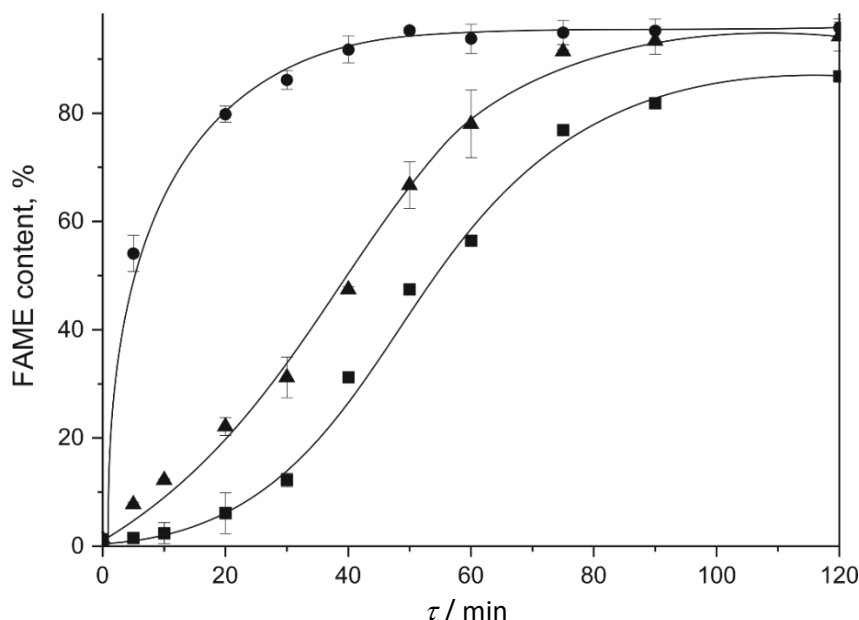
Fig. 4. Changes in the FAME content over the reaction time at different reaction temperatures: 60 °C - ●, 50 °C - ▲ and 40 °C - ■

A simple empirical pseudo-first-order reaction model (Eq. 4) was employed for the kinetic study of plum oil methanolysis catalyzed by PSSA. The dependence -ln (1-x_A) *vs.* time is shown in Fig. 5. The reaction performed at 60 °C was successfully described by the model as a linear dependence -ln (1-x_A) *vs.* time was observed. However, for the reactions at 40 and 50 °C, two straight lines with different slopes in the initial and the final reaction periods were observed. Therefore,

Eq. (4) was applied to calculate only the apparent reaction rate constants for the pseudo-homogeneous regime at different temperatures. The apparent reaction rate constant increased with the temperature (Fig. 6). The activation energy for the plum oil methanolysis catalyzed by PSSA was calculated by applying the Arrhenius equation (5):

$$k = Ae^{\left(-\frac{E_a}{RT}\right)}$$

(5)

where A / min^{-1} is the pre-exponential factor, E_a / J·mol^{-1} is the activation energy, R is the gas constant (8.314 J·mol^{-1}·K^{-1}), and T / K is the reaction temperature.
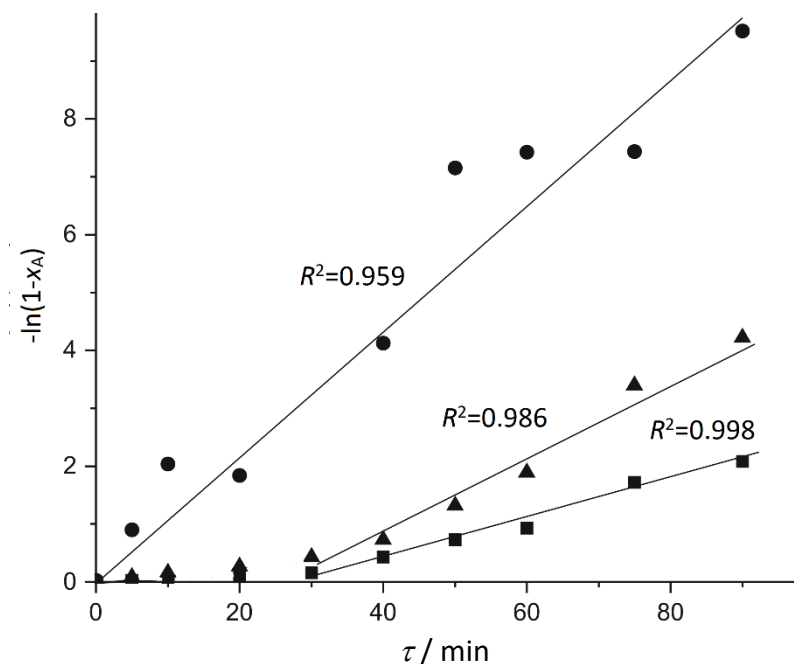
Fig. 5. Application of the irreversible pseudo-first-order kinetic model (lines) for plum kernel oil methanolysis at different reaction temperatures (experimental data: 60 °C - ●, 50 °C - ▲, and 40 °C - ■)
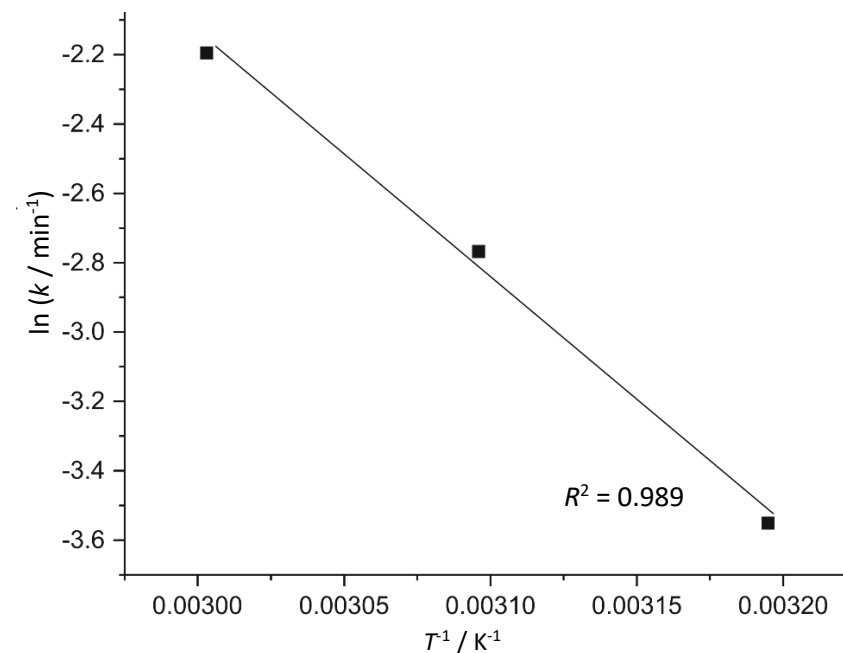
Fig. 6. Dependence of ln k on the 1/T (Arrhenius plot)

The values of ln *k* were linearly dependent on 1/*T*, as shown in Fig. 6 and the activation energy was calculated from the slope of the linear dependence. Hence, the activation energy and pre-exponential factor of plum oil methanolysis catalyzed by PSSA were determined to be 58.8 kJ mol^{-1} and 19.3·10^5 min^{-1}. The activation energy value was in the range of other values reported in literature, presented in Table 4. It is lower than the values for methanolysis of soybean oil catalyzed by pineapple leaves ash [30] and *Tucumã* peel ash [46] but higher than those reported for methanolysis of *J. curcas* oil and soybean oil catalyzed by *L. perpusilla* Torrey ash [49] and waste *Brassica nigra* plant ash [52], respectively.

Table 4. Summary of activation energy values reported for oil methanolysis catalyzed by various solid base catalysts

Catalyst type	Type of oil feedstock	Kinetic model	E_a / kJ mol^{-1}	Ref.
L. perpusilla Torrey ash	*Jatropha curcas* L. oil	Based on TGA analysis	29.49	[49]
Palm oil mill fly ash supported calcium oxide	Crude palm oil	Pseudo-first order	42.56	[50]
Rice husk-derived sodium silicate	Palm oil	Pseudo-first order	48.30	[51]
Tucumã peel ash	Soybean oil	Pseudo-first order	61.23	[46]
Waste *Brassica nigra* plant ash	Soybean oil	Pseudo-first order	27.87	[52]
Pineapple leaves ash	Soybean oil	n.r.	86.84	[30]
Citrus sinensis peel ash (CSPA)@Fe$_3$O$_4$	Waste cooking oil	Pseudo-first order	34.41	[53]
Plum stone shell ash	Plum oil	Pseudo-first order	58.8	This work

n.r. – not reported

4. 4. Reuse of the PSSA catalyst

The PSSA catalyst was tested for reuse as it exhibited the highest catalytic activity. After the reaction completion the catalyst was separated from the reaction mixture and reused in the next batch without treatment. In the repeated reaction a low FAME content (30 %) was obtained at 60 min, indicating the catalytic activity loss. Therefore, the separated catalyst was recalcined (800 °C, 2 h) before the subsequent cycle. In this case, a high FAME content of 93.54 % was achieved in 90 min of reaction (Fig. 7), which was still lower than that achieved in the first batch. Similarly, a lower FAME content at the beginning of the reaction was observed with recalcined walnut and hazelnut shell ashes [3,5]. Therefore, PSSA could be recommended as an effective catalyst for the transesterification of plum kernel oil with the possibility of being reused after recalcination. However, a further detailed investigation of reused catalysts in respect of basicity and elemental and phase composition should be performed to provide information on the effect of the reuse and recalcination on the catalytic activity.
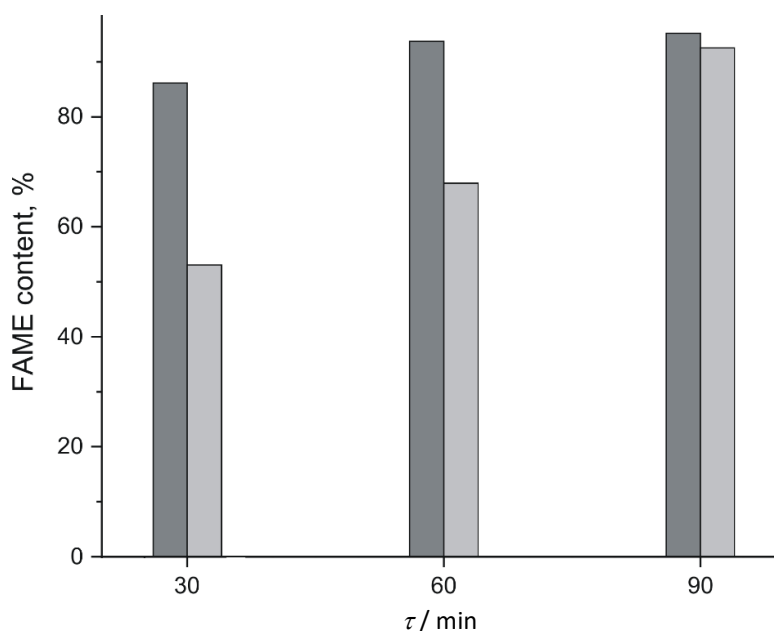
Fig. 7. Comparison of FAME contents obtained by using the fresh PSSA (dark grey) and recalcined PSSA (light grey) as catalysts at different reaction times (temperature of 60 °C, methanol-to-oil molar ratio of 12:1, and catalyst amount of 10 %)

5. CONCLUSION

Waste plum stones can be a significant raw material for biodiesel production as they can be used as a source of oil (kernels) and catalyst (stone shell ash). However, using plum oil in transesterification required its pre-esterification because of its high acid value and basic properties of the catalyst. The plum stone shell ash predominantly contains K, Ca, and Mg compounds. The catalytic test revealed that PSSA at 60 °C was the most active catalyst as compared to PSA and PKCA. The determined activation energy value (58.8 kJ mol^{-1}) was in the range of the values reported for ash-based catalysts. Overall, PSSA can be recommended as a catalyst for biodiesel production from plum kernel oil because of its efficiency and reusability after recalcination.

REFERENCES

[1] Banković-Ilić IB, Stamenković OS, Veljković VB. Biodiesel production from non-edible plant oils. *Renew Sust Energ Rev* 2012; 16(6): 3621-3647. https://doi.org/10.1016/j.rser.2012.03.002

[2] Chen K, Wang J, Dai Y, Wang P, Liou C, Nien C, Wu J, Chen C. Rice husk ash as a catalyst precursor for biodiesel production. *J Taiwan Inst Chem Eng*. 2013; 44(4): 622-629. http://dx.doi.org/10.1016/j.jtice.2013.01.006

[3] Miladinović, MR, Krstić JB, Zdujić MV, Veselinović LjM, Veljović DjN, Banković-Ilić IB, Stamenković OS, Veljković VB. Transesterification of used cooking sunflower oil catalyzed by hazelnut shell ash. *Renew Energy*. 2022; (183): 103-113. https://doi.org/10.1016/j.renene.2021.10.071

[4] Petković M, Miladinović M, Banković-Ilić I, Stamenković O, Veljković V. Optimization of the used sunflower oil methanolysis catalyzed by hazelnut shell ash. *Adv Technol*. 2021; 10(2): 32-39. https://doi.org/10.5937/savteh2102032P

[5] Miladinović MR, Krstić JB, Ivana B. Banković-Ilić, Vlada B. Veljković, Stamenković OS. Valorization of walnut shell ash as a catalyst for biodiesel production. *Renew Energy*. 2020; 147: 1033-1043. https://doi.org/10.1016/j.renene.2019.09.056

[6] Fatimah I, Purwiandono G, Sahroni I, Sagadevan S, Chun-Oh W, Ghazali SAISM, Doong R. Recyclable catalyst of ZnO/SiO$_2$ prepared from *Salacca* leaves ash for sustainable biodiesel conversion. *South African J Chem Eng.* 2022; 40: 134–143. https://doi.org/10.1016/j.sajce.2022.02.008

[7] Fatimah I, Taushiyah A, Najah FB, Azmi U. ZrO$_2$/bamboo leaves ash (BLA) catalyst in biodiesel conversion of rice bran oil. *Mater Sci Eng.* 2018; 349: 012027. https://doi.org/10.1088/1757-899X/349/1/012027

[8] Fatimah I, Yanti I, Totok E. Suharto TE, Sagadevan S. ZrO$_2$-based catalysts for biodiesel production: A review. *Inorg Chem Commun.* 2022; 143: 109808. https://doi.org/10.1016/j.inoche.2022.109808

[9] Wang L, Yu H. Biodiesel from Siberian apricot (*Prunus sibirica* L.) seed kernel oil. *Biores Technol* 2012; 112: 355-358, https://doi.org/10.1016/j.biortech.2012.02.120

[10] Rashid U, Rehman H A., Hussain I, Yusup S. Production and characterization of biodiesel produced from musk melon (*Cucumis melo*) seed oil. In: BIT's 1st Annual World Congress of Bioenergy (WCBE 2011), 25-30 April 2011, Dalian, China.

[11] Chu J, Xu X, Zhang Y. Production and properties of biodiesel produced from *Amygdalus pedunculata* Pall. *Biores Technol*. 2013; 134: 374-376. https://doi.org/10.1016/j.biortech.2012.12.089

[12] Schinas P, Karavalakis G, Davaris C, Anastopoulos G, Karonis D, Zannikos F, Stournas S, Lois E. Pumpkin (*Cucurbita pepo* L.) seed oil as an alternative feedstock for the production of biodiesel in Greece. *Biomass Bioenerg*. 2009; 33(1): 44-49, https://doi.org/10.1016/j.biombioe.2008.04.008

[13] Rashid U, Ibrahim M, Yasin S, Yunus R, Taufiq-Yap Y-H, Knothe G. Biodiesel from *Citrus reticulata* (mandarin orange) seed oil, a potential non-food feedstock. *Ind Crops Prod.* 2013; 45: 355-359, https://doi.org/10.1016/j.indcrop.2012.12.039

[14] *Crops and livestock products*, Food and Agriculture Organization of the United Nations, https://www.fao.org/faostat/en/#data/QCL accessed November 3, 2022

[15] Saeed A, Hanif MA, Haq Nawaz RWKQ. The production of biodiesel from plum waste oil using nano-structured catalyst loaded into supports. *Sci Rep*. 2021; 11: 24120. https://doi.org/10.1038/s41598-021-03633-w

[16] Kostić MD, Veličković AV, Joković NM, Stamenkovic OS, Veljkovic VB. Optimization and kinetic modeling of esterification of the oil obtained from waste plum stones as a pretreatment step in biodiesel production. *Waste Manag*. 2016; 48: 619-629. https://doi.org/10.1016/j.wasman.2015.11.052

[17] Górna P, Rudzi M, Soliven A. Industrial by-products of plum *Prunus domestica* L . and *Prunus cerasifera* Ehrh. as potential biodiesel feedstock: Impact of variety. *Ind Crops Prod*. 2017; 100: 77-84. https://doi.org/10.1016/j.indcrop.2017.02.014

[18] Vicente G, Martinez M, Aracil J, Esteban A. Kinetics of sunflower oil methanolysis. *Ind Eng Chem Res.* 2005; 44: 5447-5454. https://doi.org/10.1021/ie040208j

[19] Vicente G, Martinez M, Aracil J. Kinetics of *Brassica carinata* oil methanolysis. *Energ Fuels* 2006; 20: 1722-1726. https://doi.org/10.1021/ef060047r

[20] Georgogianni KG, Kontominas MG, Pomonis PJ, Avlonitis D, Gergis V. Alkaline conventional and in situ transesterification of cottonseed oil for the production of biodiesel. *Energ Fuels.* 2008; 22: 2110-2115. https://doi.org/10.1021/ef700784j

[21] Jamil AZ, Muslim A. Performance of KOH as a catalyst for transesterification of *Jatropha curcas* oil. *Int J Eng Res Appl*. 2012; 2: 635-639. ISSN: 2248-9622

[22] Rabu RA, Janajreh I, Honnery D. Transesterification of waste cooking oil: Process optimization and conversion rate evaluation. *Energ Conv Manag*. 2013; 65: 764-769. https://doi.org/10.1016/j.enconman.2012.02.031

[23] Kostić MD, Joković NM, Stamenković OS, Veljković VB. Biodiesel production from seed oil of cotton thistle (*Onopordum acanthium* L.). *Adv Technol*. 2014; 3: 35-45. UDK 62.756.3:66.061.34:582.998.1 (In Serbian)

[24] Stamenković OS, Kostić MD, Joković NM, Veljković VB. The kinetics of base-catalyzed methanolysis of waste cooking oil. *Adv Technol*. 2015; 4(1): 33-41. https://doi.org/10.5937/savteh1501033S

[25] Kostić MD, Stamenković OS, Veljković VB. The influence of fatty acid composition on the kinetics of the vegetable oil methanolysis reaction. *Adv Technol*. 2021; 10(2): 24-31. https://doi.org/10.5937/savteh2102024K

[26] Mares EKL, Matheus A, Teresa P, Rafael L. Acai seed ash as a novel basic heterogeneous catalyst for biodiesel synthesis: Optimization of the biodiesel production process. *Fuel*. 2021; 299: 120887. https://doi.org/10.1016/j.fuel.2021.120887

[27] Sitepu EK, Sembiring Y, Supeno M, Tarigan K, Ginting J, Karo-karo JA, Tarigan JB. Homogenizer-intensified room temperature biodiesel production using heterogeneous palm bunch ash catalyst. *South African J Chem Eng*. 2022; 40: 240–245. https://doi.org/10.1016/j.sajce.2022.03.007

[28] Pathak G, Das D, Rajkumari K, Rokhum L. Exploiting waste: Towards a sustainable production of biodiesel using: *Musa acuminata* peel ash as a heterogeneous catalyst. *Green Chem*. 2018; 20(10): 2365-2373. https://doi.org/10.1039/C8GC00071A

[29] Husin H, Abubakar A, Ramadhani S, Sijabat CFB, Hasfita F. Coconut husk ash as heterogenous catalyst for biodiesel production from *Cerbera manghas* seed oil. MATEC Web of Conferences, The 3rd Annual Applied Science and Engineering Conference. Bundung, Indonesia, 2018, vol. 197, p. 09008. https://doi.org/10.1051/matecconf/201819709008

[30] de Barros S, Pessoa Junior WAG, Sá ISC, Takeno ML, Nobre FX, Pinheiro W, Manzato L, Iglauer S, de Freitas FA. Pineapple (*Ananás comosus*) leaves ash as a solid base catalyst for biodiesel synthesis. *Bioresour Technol*. 2020; 312: 123569. https://doi.org/10.1016/j.biortech.2020.123569

[31] Vargas EM, Ospina L, Neves MC, Tarelho LAC, Nunes MI. Optimization of FAME production from blends of waste cooking oil and refined palm oil using biomass fly ash as a catalyst. *Renew Energ*. 2021; 163: 1637-1647. https://doi.org/10.1016/j.biortech.2020.123569

[32] Adepojua TF, Ibeha MA, Babatunde EO, Asuquo AJ, Abegunde GS. Appraisal of CaO derived from waste fermented-unfermented kola nut pod for fatty acid methylester (FAME) synthesis from *Butyrospermum parkii* (Shea butter) oil. *South African J Chem Eng* 2020; 33: 160–171. https://doi.org/10.1016/j.sajce.2020.07.008

[33] Hsiao M-C, Liao P-H, Lan NV, Hou S-S. Enhancement of biodiesel production from high-acid-value waste cooking oil via a microwave reactor using. *Energies*. 2021; 14: 437. https://doi.org/10.3390/en14020437

[34] Miladinović MR, Stamenković OS, Veljković VB, Skala DU. Continuous sunflower oil methanolysis over quicklime in a packed-bed tubular reactor. *Fuel*. 2015; 154: 301-307. https://doi.org/10.1016/j.fuel.2015.03.057

[35] Veljković VB, Stamenković OS, Todorović ZB, Lazić ML, Skala DU. Kinetics of sunflower oil methanolysis catalyzed by calcium oxide. *Fuel*. 2009; 88: 1554–1562. https://doi:10.1016/j.fuel.2009.02.013

[36] Nath B, Kalita P, Das B, Basumatary S. Highly efficient renewable heterogeneous base catalyst derived from waste Sesamum indicum plant for synthesis of biodiesel. *Renew Energy*. 2020; 151: 295-310. https://doi.org/10.1016/j.renene.2019.11.029

[37] Vassilev S V., Vassileva CG, Song YC, Li WY, Feng J. Ash contents and ash-forming elements of biomass and their significance for solid biofuel combustion. *Fuel*. 2017; 208: 377-409. https://doi.org/10.1016/j.fuel.2017.07.036

[38] Vassilev S V, Baxter D, Vassileva CG. An overview of the behaviour of biomass during combustion : Part II. Ash fusion and ash formation mechanisms of biomass types. *Fuel*. 2014; 117: 152-183. https://doi.org/10.1016/j.fuel.2013.09.024

[39] Zdujić M, Lukić I, Kesić Ž, Janković-Častvan I, Marković S, Jovalekić Č, Skala D. Synthesis of CaOSiO$_2$ compounds and their testing as heterogeneous catalysts for transesterification of sunflower oil. *Adv Powder Technol*. 2019; 30: 1141-1150. https://doi.org/10.1016/j.apt.2019.03.009

[40] Emeruwa E, Jarrige J, Mexmain J, Bernardin M. Application of mercury porosimetry to powder (UO$_2$) analysis. *J Nucl Mater*. 1991; 184(1): 53-58. https://doi.org/10.1016/0022-3115(91)90532-C

[41] Lukić I, Krstić J, Jovanović D, Skala D. Alumina/silica supported K$_2$CO$_3$ as a catalyst for biodiesel synthesis from sunflower oil. *Bioresour Technol*. 2009; 100: 4690-4696. https://doi.org/10.1016/j.biortech.2009.04.057

[42] Yang P, Zhou S, Du Y, Li J, Lei J. Self-assembled meso / macroporous phosphotungstic acid/TiO$_2$ as an efficient catalyst for oxidative desulfurization of fuels. *J Porous Mater*. 2017; 24: 531-539. https://doi.org/10.1007/s10934-016-0288-7

[43] Fraile JM, García N, Mayoral JA, Pires E, Roldán L. The basicity of mixed oxides and the influence of alkaline metals: The case of transesterification reactions. *Appl Catal A: General*. 2010; 387: 67-74. https://doi.org/10.1016/j.apcata.2010.08.002

[44] Buchori L, Istadi I, Purwanto P, Marpaung LC, Safitri RL. Roles of K$_2$O on the CaO-ZnO catalyst and its influence on catalyst basicity for biodiesel production. *E3S Web Conf ICENIS 2017*. 2018; 31(3): 02009. https://doi.org/10.1051/e3sconf/20183102009

[45] Tang Y, Liu H, Ren H, Cheng Q, Cui Y, Zhang J. Development KCl/CaO as a catalyst for biodiesel production by tri-component coupling transesterification. *Sust Energ*. 38(2); 2018: 647-653. https://doi.org/10.1002/ep.12977

[46] Mendonça IM, Paes OARL, Maia PJS, Souza MP, Almeida RA, Silva CC, Duvoisin S, de Freitas FA. New heterogeneous catalyst for biodiesel production from waste tucumã peels (*Astrocaryum aculeatum* Meyer): Parameters optimization study. *Renew Energy*. 2019; 130: 103-110. https://doi.org/10.1016/j.renene.2018.06.059

[47] Betiku E, Mistura A, Victor T. Banana peels as a biobase catalyst for fatty acid methyl esters production using Napoleon's plume (*Bauhinia monandra*) seed oil: A process parameters optimization study. *Energy.* 2016; 103: 797-806. https://doi.org/10.1016/j.energy.2016.02.138

[48] Luque R, Pineda A, Colmenares JC, Campelo JM, Romero AA, Serrano-Riz JC, Cabeza LF, Cot-Gores J. Carbonaceous residues from biomass gasification as catalysts for biodiesel production. *J Nat Gas Chem*. 2012; 21(3): 246-250. https://doi.org/10.1016/S1003-9953(11)60360-5

[49] Chouhan APS, Sarma AK. Biodiesel production from *Jatropha curcas* L. oil using *Lemna perpusilla* Torrey ash as heterogeneous catalyst. *Biomass Bioenerg*. 2013; 55: 386-389. https://doi.org/10.1016/j.biombioe.2013.02.009

[50] Ho WWS, Kiat H, Gan S, Huey S. Evaluation of palm oil mill fly ash supported calcium oxide as a heterogeneous base catalyst in biodiesel synthesis from crude palm oil. *Energ Conv Manag*. 2014; 88: 1167-1178. http://dx.doi.org/10.1016/j.enconman.2014.03.061

[51] Roschat W, Siritanon T, Yoosuk B, Promarak V. Rice husk-derived sodium silicate as a highly efficient and low-cost basic heterogeneous catalyst for biodiesel production. *Ener Conv Manag*. 2016; 119: 453-462. https://doi.org/10.1016/j.enconman.2016.04.071

[52] Nath B, Das B, Kalita P, Basumatary S. Waste to value addition: Utilization of waste Brassica nigra plant derived novel green heterogeneous base catalyst for effective synthesis of biodiesel. *J Clean Prod*. 2019; 239: 118112. https://doi.org/10.1016/j.jclepro.2019.118112

[53] Changmai B, Rano R, Vanlalveni C, Rokhum L. A novel *Citrus sinensis* peel ash coated magnetic nanoparticles as an easily recoverable solid catalyst for biodiesel production. *Fuel*. 2021; 286: 119447. https://doi.org/10.1016/j.fuel.2020.119447

Korišćenje otpadnih koštica šljive kao izvora ulja i katalizatora za proizvodnju biodizela

Marija R. Miladinović[1], Stefan Pavlović[2], Ivana B. Banković-Ilić[1], Milan D. Kostić[1], Olivera S. Stamenković[1] i Vlada B. Veljković[1,3]

[1]Tehnološki fakultet, Univerzitet u Nišu, Bulevar Oslobodjenja 124, 16000 Leskovac, Srbija
[2]Univerzitet u Beogradu, Institut za hemiju, tehnologiju i metalurgiju, Centar za katalizu i hemijsko inženjerstvo, Njegoševa 12, 11000 Beograd, Srbija
[3]Srpska akademija nauka i umetnosti, Knez Mihailova 35, 11000 Beograd, Srbija

(Naučni rad)

Izvod

U ovom radu istraživana je mogućnost korišćenja otpadnih koštica šljive u proizvodnji biodizela. Jezgra šljive su iskorišćena kao sirovina za dobijanje ulja primenom Soxhlet-ove metode ekstrakcije. Cele koštice, ljuske koštica šljive i pogača dobijena nakon ekstrakcije ulja iz jezgra šljive spaljeni su da bi se dobio pepeo, koji je korišćen kao katalizator. Dobijene tri vrste sakupljenog pepela su najpre okarakterisane u pogledu hemijskog sastava, poroznosti i baznosti, a zatim je testirana katalitička aktivnost u transesterifikaciji esterifikovanog ulja koštica šljive. Dominantni elementi u pepelu, kao što su kalijum, kalcijum i magnezijum, imali su različit sadržaj u sve tri vrste pepela. Najveću katalitičku aktivnost pokazao je pepeo koštica šljive, zbog čega je dalje istraživan uticaj temperature (40, 50 i 60 °C) na brzinu reakcije katalizovane ovim pepelom. Konstanta brzine reakcije povećavala se sa porastom temperature reakcije, a vrednost energije aktivacije je 58,8 kJ mol⁻¹. Pored toga, pepeo koštica šljive može se ponovo koristiti kao katalizator nakon rekalcinacije.

Ključne reči: pepeo; kataliza; kinetika; metanoliza; transesterifikacija

Effects of temperature on physicochemical properties of the lecithin-based deep eutectic solvents and their use in the CaO-catalyzed transesterification

Zoran B. Todorović[1], Biljana S. Đorđević[1], Dragan Z. Troter[1], Ljiljana M. Veselinović[2], Miodrag V. Zdujić[2] and Vlada B. Veljković[1,3]

[1]*University of Niš, Faculty of Technology, Bulevar Oslobođenja 124, 16000 Leskovac, Serbia*
[2]*Institute of Technical Sciences of the Serbian Academy of Sciences and Arts, Knez Mihailova 35, 11000 Belgrade, Serbia*
[3]*Serbian Academy of Sciences and Arts, Knez Mihailova 35, 11000 Belgrade, Serbia*

Abstract
Deep eutectic solvents (DESs) are called 'designer solvents' due to various structural variations and the benefit of tailoring their physicochemical properties. For industrial applications of DESs it is crucial to know their physical and thermodynamic properties such as density, viscosity, and refractive index. These properties were measured for three lecithin (LEC)-based DESs with glycerol (G), triethanolamine (TEOA), and oleic acid (OLA) as functions of temperature. The viscosity was fitted by both Arrhenius-type and Vogel-Tamman-Fulcher equations. The density, viscosity, and refractive index of tested DESs decreased with the increase in temperature. The LEC:G DES exhibited the lowest density at all tested temperatures. This DES was selected as a cosolvent in the ethanolysis of cold-pressed black mustard (*Brassica nigra* L.) seed oil catalyzed by either calcined or non-calcined CaO. The reaction was carried out in a batch stirred reactor under the following conditions: the temperature of 70 °C, the ethanol-to-oil molar ratio of 12:1, and the amount of DES and CaO of 20 and 10 wt.% (to oil), respectively. The presence of DES accelerated the reaction, while the separation of the final reaction mixture phases was faster.

Keywords: Brassica nigra L.; black mustard; ethanolysis; fatty acid ethyl esters; deep eutectic solvent.

Available on-line at the Journal web address: http://www.ache.org.rs/HI/

1. INTRODUCTION

Tendency to eliminate or reduce the use of organic solvents in various technological processes has led to the increased interest in developing different 'green' solvents, such as deep eutectic solvents (DESs). DESs are defined as mixtures of two or more components, hydrogen bond acceptors (usually choline chloride (ChCl)) and hydrogen bond donors (like alcohols, amides, carboxylic acids, esters, ethers, etc.), which are interconnected by hydrogen bonds. This newly formed mixture has a melting point lower than the individual components. These solvents are desirable and acceptable due to the possibility of adjusting their properties by selecting the appropriate components (often natural, cheap, safe, and available) that enable the formation of hydrogen bonds. Appropriate DESs possess several advantages: low cost, easy preparation, biodegradability, nontoxicity, wide liquid range, non-volatility, thermal stability, and non-reactivity with water [1]. However, for applying any DES, for instance, in biodiesel production combined with non-edible vegetable oils, it is essential to determine their physical and thermodynamic properties.

In recent years, the application of DESs as efficient cosolvents or catalysts in biodiesel synthesis has been raising attention [2,3]. ChCl:glycerol (ChCl:G) DES has been successfully applied for transesterification of different oils, such as palm oil [3], expired sunflower oil [4], cooking waste oil [5], rapeseed oil [6], and *Xanthoceras sorbifolia* Bunge seed oil [7]. The

application of DESs for biodiesel production from black mustard (*Brassica nigra* L., Brassicaceae) seed oil (BMSO) has not been reported in the literature.

Black mustard is one of the few oilseeds adapted to colder regions, with a minimum amount of pesticides and other agricultural inputs [8]. BMSO contains a large proportion of erucic acid (up to 50 %) that can harm the cardiovascular system, so its application in the diet must be cautious [9]. However, due to containing single double-bond, branched, and long-chain fatty acids, this oil has lower pour and cloud points than the oils with a higher content of saturated fatty acids, making it suitable for diesel engines as an alternative fuel [10,11]. Biodiesel produced from BMSO demonstrates excellent potential as a lubricant additive with lower cloud and pour points (3.5 and -15 ºC, respectively), making it suitable for regions with cold climates [8]. Shahzadi et al. [12] performed the KOH-catalyzed methanolysis of a previously esterified BMSO, while Aslan and Eryilmaz [10] reported the KOH-catalyzed ethanolysis of BMSO.

Since lecithin (LEC) has the same choline group in its structure as ChCl, it seems to be a possible replacement for ChCl, a well-known substance used for preparing various DESs. It represents a mixture of naturally occurring lipids, from which more than 50 % are phospholipids [13]. As a surfactant with a hydrophilic head and two hydrophobic tails, LEC forms organogels [14,15], which are used for preparation of cosmetic and pharmaceutical formulations [13], drug delivery [16], lubrication, food processing [17], and extraction [14,18]. The amphiphilic molecular structure of LEC also allows its application as a natural emulsifier in food products [17,19,20]. However, the use of LEC to prepare DESs is not reported in the literature.

In this paper, three novel DESs were prepared by combining LEC with G, triethanolamine (TEOA), or oleic acid (OLA) in a molar ratio of 1:2. Density, viscosity, and refractive index of these DESs were measured at atmospheric pressure in the temperature range of 293.15-363.15 K relevant for the practical use. Several thermodynamic properties were calculated, such as molar volume, lattice energy, heat capacity, as well as molar Gibbs energy, enthalpy, and entropy of activation of viscous flow. Finally, the possibility of using the LEC:G DES as a suitable replacement for the ChCl:G DES as a cosolvent in the heterogeneously-catalyzed ethanolysis of cold-pressed BMSO was tested in which either calcined or non-calcined CaO was used as catalysts. Moreover, the catalytic activities of non-calcined and calcined CaO without or with LEC:G or ChCl:G DESs were compared. To the best of the authors' knowledge, this is the first study of the physical and thermodynamic properties of the DESs mentioned above and the application of the LEC-based DES in transesterification reactions.

2. EXPERIMENTAL

2. 1. Materials

For the preparation of the DESs, soybean LEC (from TCI, Germany), G (Ph Eur grade, MeiLab, Belgrade, Serbia), OLA (99 %, Sigma-Aldrich, St. Louis, USA), and TEOA (99.%, Centrohem, Stara Pazova, Serbia) were used. CaO (extra pure) and ChCl (≥ 98.0 %) were obtained from Sigma Aldrich (St. Louis, USA). Absolute ethanol (99.5 %) was purchased from Sani-Hem (Novi Bečej, Serbia). HPLC grade methanol, 2-propanol, and *n*-hexane were provided from Lab-Scan (Dublin, Ireland). Ethyl acetate (99.5 %, Merck-Millipore, Darmstadt, Germany) and glacial acetic acid (Zorka, Šabac, Serbia) were employed as solvents. Hydrochloric acid (36.0 %) was purchased from Centrohem (Stara Pazova, Serbia). The standards of triolein, diolein, and monoolein and the standards containing ethyl esters of palmitic, stearic, oleic, linolenic, and linoleic acids (20.0 % of each ester), were provided from Sigma-Aldrich (St. Louis, USA).

2. 2. Cold pressing of black mustard seeds

Black mustard seeds were provided from the Institute of Field and Vegetable Crops, Novi Sad, Serbia. The moisture content of the seeds (4.2 ± 0.2 wt.%) was determined by drying seeds at 105 °C until constant weight. The BMSO was obtained by cold pressing (oil press Komet, Germany) and filtered first under vacuum through a sterile gauze and filter paper to remove all impurities. The physicochemical properties of the oil were as follows: the density of 985.1 kg m^{-3} at 20 °C, the viscosity of 123.3 mPa·s at 25 °C, the acid value of 2.08 mg KOH/g, the saponification value of 169.4 mg KOH / g, and the iodine value of 99.2 g I$_2$ / 100 g [9].

2. 3. Preparation of LEC-based DESs

LEC was mixed with the desired compound (G, TEOA, or OLA) at the molar ratio of 1:2 in a round-bottom flask. The flask was placed on a rotary evaporator at 348.15 K until a homogeneous viscous liquid was obtained, as described elsewhere [21]. The prepared DESs were stored in glass bottles placed in a desiccator with $CaCl_2$ until use.

2. 4. Measurements of the physical properties of LEC-based DESs

Density, viscosity, and refractive index were measured by using a densitometer (DMA 4500 Anton Paar, Austria), rotational viscometer (Visco Basic Plus, ver. 0.8, Fungilab S.A., Barcelona, Spain), and an automatic refractometer (Atago A100, Japan), respectively, at atmospheric pressure in the temperature range between 293.15 and 363.15 K. Two replicates were carried out for each measurement.

2. 5. Fourier transform infrared spectroscopy (FTIR) analysis of LEC-based DESs

FTIR spectra of the solid compounds were recorded at 25 °C by a spectrophotometer (Michaelson Bomen MB-series, Canada) using the KBr pastille (1.5 mg/150 mg) technique (4000-400 cm^{-1} range and 2 cm^{-1} resolution). The solid compound and KBr were mixed, vacuumed, and pressed (200 MPa) to form a thin, permeable pastille. The FTIR spectra of the liquid compounds were recorded by the same spectrophotometer with using the special discs.

2. 6. BMSO ethanolysis: equipment and experimental procedure

The reaction of BMSO ethanolysis was performed at 70 ± 0.5 °C under reflux in a magnetically stirred (600 rpm) two-neck round-bottom flask (250 cm^3) placed in a glass chamber. Water temperature in the chamber was kept constant by circulating water from a water bath by a pump. Two series of experiments were performed using calcined and non-calcined CaO. For the first series of experiments, commercial CaO was activated by calcination at 550 °C for 2 h [22], cooled, and kept in well-closed glass bottles in a desiccator with $CaCl_2$ and KOH pellets. The same, not calcined CaO, was used in the second experimental series. For all experiments, ethanol (22.5 g), the catalyst (4 g), and the cosolvent (8 g) were added to the reaction flask. After stirring the suspension for 30 min, BMSO (40 g), previously preheated at the reaction temperature, was poured into the reaction flask, the magnetic stirrer was switched on, and the reaction was timed. The reaction samples (1 cm^3) were taken from the mixture during the reaction at different time intervals, cooled in an ice bath, and centrifuged (Sigma 2-6E, Sigma Laborzentrifugen GmbH, Germany; 3500 rpm, 10 min). The upper ester/oil layer was withdrawn and dissolved in the 2-propanol/*n*-hexane (5:4 v/v) mixture in a 1:10 or 1:200 ratio for qualitative thin layer (TLC) or quantitative liquid chromatography (HPLC) analysis (HPLC chromatograph details: Agilent 1100 Series, Agilent Technologies, Germany), respectively, followed by filtration through a 0.45 µm Millipore filter (Merck KGaA, Germany). After completing the reaction, the reaction mixture was poured into a separation funnel, and the separation of the phases was timed. All experiments were performed twice. For the X-ray powder diffraction (XRD), the precipitated CaO catalyst was removed from the reaction mixture, washed with ethanol, filtered, and dried in an oven at 110 °C for 2 h.

2. 7. Separation of fatty acid ethyl esters (FAEEs)

During the separation of the final reaction mixture, three layers were formed. The upper layer consisted of FAEEs and insignificant amounts of triacylglycerols (TAG), diacylglycerols (DAG), and monoacylglycerols (MAG). The middle layer contained excess ethanol, glycerol, and cosolvent. CaO was precipitated in the bottom layer.

2. 8. Analytical methods

Chemical composition of the reaction mixture samples was analyzed qualitatively and quantitatively by the TLC and HPLC methods, respectively [23,24]. The contents of FAEEs and acylglycerols were calculated from the corresponding peak areas by using the calibration curves obtained by using the standard mixtures. The XRD measurements were performed by using a Philips PW 1050 X-ray powder diffractometer (Philips, The Netherlands) with Ni-filtered Cu $K\alpha_{1,2}$

(λ = 0.154178 nm) radiation and the Bragg–Brentano focusing geometry. Measurements were performed over a 2θ range of 7 to 70° at room temperature. The scanning step was 0.05° the counting time was 3 s per step.

3. RESULTS AND DISCUSSIONS

3. 1. The effect of temperature on the physical properties of LEC-based DESs

3. 1. 1. Density

Figure 1 represents temperature dependences of density of the studied DESs, while the experimental density values are given in Tables A1-A3 in the Supplementary material. The density of the tested LEC-based DESs decreased slightly and linearly with the increase in temperature due to the increased mobility of the molecules and decreased molecular interactions, which agrees with the previous reports [25–27]. For the investigated temperature range, the density of the tested DESs lies within the range of 1285.8 - 1397.6 kg·m^{-3} with the LEC:G DES having the lowest density values. At 313.15 K, all LEC-based DESs are liquid, and their densities follow the following order: LEC:G < LEC:TEOA < LEC:OLA.
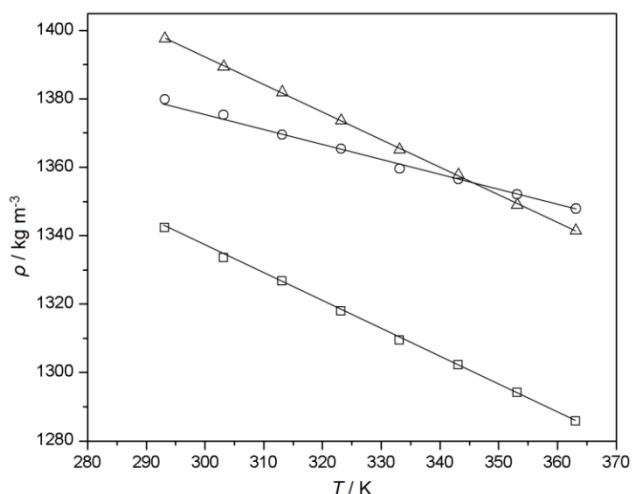
Figure 1. Densities (ρ) of the LEC-based DESs as functions of temperature: LEC:G – □ (STD ≤ 3.5 %), LEC:TEOA – ○(STD ≤ 2.8 %), and LEC:OLA – △(STD ≤ 3.9 %).

Due to the lack of literature data for the tested LEC-based DESs, their density values were compared with those reported for the DESs with the same hydrogen bond donors. Formation of hydrogen bonds between constitutional components of DESs strongly affects the density of all DESs. The LEC:TEOA and LEC:OLA DESs have higher density values than the LEC:G DES due to the highest number of -OH groups in TEOA and the largest molecular size of OLA, providing a stronger intermolecular H-bonds' network as compared to that of the LEC:G DES [28].

The LEC:G DES has a significantly higher density than the DESs with G, such as the *N,N*-diethylethanolammonium chloride:G (1:2) [29], tetrapropylammonium bromide:G (1:3) [30], ChCl:G (1:2) DESs [27,31,32] because LEC has the larger molecular mass than the other hydrogen bond acceptors [28]. For the same reason, the density values for the LEC:TEOA DES are higher than those reported for the ChCl:TEOA (1:2) [33] and ChCl:TEOA (1:1) DESs [25].

For the design of technological processes, it is very important to know the effect of temperature on the density of DESs. In addition, density values can be used to calculate values of thermal expansion or compressibility coefficients that are valuable liquid structure and interactions data. When a DES system is heated, the molecules move faster, increasing the molar volume and, thus, decreasing the density [34]. Although high density of a DES is a problem for handling or mixing in chemical processes, it may be desirable in extraction processes since a relatively large difference in density between the raffinate and extract phases is required to guarantee more efficient phase separation [26].

The density values were correlated to the temperature by the following linear equation (1):

$$\rho = a + bT \tag{1}$$

The parameters *a* (the density at 0 K) and *b* (the coefficient of volume expansion) were obtained from the intercept and slope of the best linear fits, respectively (Table 1). The obtained low mean relative percent deviations (MRPD), and coefficients of determination (R^2) close to unity (> 0.996) indicate excellent agreement of the linear density-temperature dependences with experimental data.

Table 1. Parameters obtained by the best linear fits of ρ as a function of temperature in the range 293.15-363.15 K (Eq. 1) for LEC-based DESs

DES	Density range / kg·m^{-3}	a / kg·m^{-3}	b / kg·m^{-3}·K^{-1}	MRPD, %	R^2
LEC:G	1285.8-1342.3	1577.5	-0.803	0.03	0.999
LEC:TEAO	1347.9-1379.9	1513.6	-0.4581	0.04	0.996
LEC:OLA	1341.4-1397.6	1634	-0.8054	0.02	0.999

According to the values of the coefficient of volume expansion it could be deduced that thermal sensitivities of the LEC-based DESs are in the following order: LEC:OLA > LEC:G > LEC:TEAO.

Expansion of DESs with temperature is best quantified by the thermal expansion coefficient (α), which is obtained as a slope of the ln ρ-*T* linear fit of Eq. (2) [25]:

$$\ln \rho = c - \alpha T \tag{2}$$

where *c* is an empirical constant. Thermal expansion coefficient values were determined in the range between $3\cdot10^{-4}$ K^{-1} and $6\cdot10^{-4}$ K^{-1} (Table 2), indicating that the investigated DESs do not expand appreciably in the covered temperature range.

Table 2. Parameters obtained by the best linear fit of experimental data by Eq. (2) for LEC-based DESs in the temperature range 293.15-363.15 K.

DES	c / kg·m^{-3}·K^{-1}	$\alpha\cdot10^{-4}$/ K^{-1}	MRPD, %	R^2
LEC:G	7.38	6	0.05	0.999
LEC:TEAO	7.33	3	0.16	0.996
LEC:OLA	7.42	6	0.05	0.999

Molar volumes (V_m), lattice energies (U_{pot}), and heat capacities (C_p) for the LEC-based DESs at 313.15 K were calculated using the well-known equations [25,35] and presented in Table 3. The molecular size of OLA induced the highest value of the molar volume of the LEC:OLA DES, which also resulted in its highest heat capacity among all prepared DESs. The liquid state of DESs at lower temperatures can be explained by the lattice energy values similar to those reported for molten salts [36].

Table 3. Calculated values of V_m, U_{pot}, and C_p for the LEC-based DESs at 313.15 K

DES	V_m / nm^3	U_{pot} / kJ·mol^{-1}	C_p / J·mol^{-1}K^{-1}
LEC:G	0.390	1178	450
LEC:TEAO	0.424	1141	485
LEC:OLA	0.528	1048	593

3. 1. 2. Refractive index

The refractive index is correlated with temperature as shown in Figure 2, while the experimental refractive index values are given in Tables A1-A3 in the Supplementary material. The refractive indices of the tested LEC-based DESs linearly decreased with temperature due to the reduction in density. This decrease strongly depends on the structure and nature of the constitutional components combined with LEC. The refractive index values for the investigated temperature range lie within 1.4305–1.4853, with the LEC:OLA DES having the lowest refractive index. At 313.15 K, these values are in the following order: LEC:OLA < LEC:G < LEC:TEOA and are higher than those reported for *N,N*-di-ethylethanolammonium chloride:G [29], and ChCl:G (1:2) [32] DESs. At the same time, they are close to those reported for tetrapropylammonium bromide:G (1:2) [30] and ChCl:G (1:2) [27] DESs.
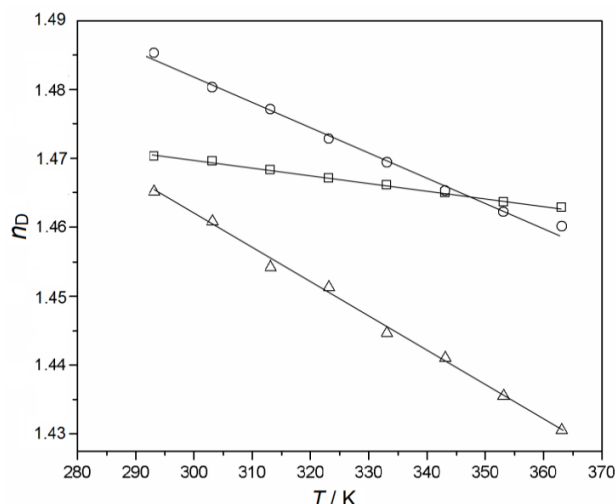
Figure 2. Refractive indices (n_D) of the LEC-based DESs as functions of temperature: LEC:G – □ (STD ≤ 0.05 %), LEC:TEOA – ○ (STD ≤ 0.07 %), and LEC:OLA – △ (STD ≤ 0.11 %).

Refractive index is a property beneficial for many applications, such as identification of individual substances and determination of their concentrations in mixtures, verification of the substance purity, *etc.* [37]. The determined parameters of linear dependences, refractive index ranges, MRPD, and R^2 are listed in Table 4.

Table 4. Parameters obtained by the best linear fits of n_D as a function of temperature in the range 293.15-363.15 K for the LEC-based DESs

DES	n_D range	Intercept	Slope	MRPD, %	R^2
LEC:G	1.4628-1.4703	1.5031	-0.0001	1.98	0.997
LEC:TEAO	1.4601-1.4853	1.591	-0.0004	0.80	0.993
LEC:OLA	1.4305-1.4651	1.61	-0.0005	0.13	0.997

Values of the phase velocity (v), molar refractivity (A), and the free volume (f_m), calculated using the well-known equations, are listed in Table 5 [38,39]. The lowest LEC:OLA DES refraction index values are explained by the lowest phase velocity values. The molar refractivity is mainly affected by the molar mass, while it is only weakly affected by temperature [39]. Also, the influence of density and refraction index is only minor [39]. Heating causes an increase in the free volume of DESs [39]. The highest free volume values determined for the LEC:OLA DES can be explained by the longest alkyl chain of OLA [39].

Table 5. The v, A, and f_m ranges determined for the LEC-based DESs in the temperature range 293.15-363.15 K.

DES	v / 10^7 m·s^{-1}	A / 10^{-6} m^3·mol^{-1}	f_m / 10^{-6} m^3·mol^{-1}
LEC:G	20.40-20.51	64.86-66.78	167.48-175.77
LEC:TEAO	20.20-20.55	84.76-86.94	180.97-188.60
LEC:OLA	20.48-20.97	71.16-72.76	227.48-242.88

3. 1. 3. Viscosity

Knowing viscosity of solvents is of great importance for their further applications in technological processes. High viscosity of DESs poses a significant problem due to reduction of the mass transfer rate, which can be overcome by heating or modifying molar ratios of the DES components [26]. The viscosity values obtained in the present work were correlated with temperature by both the Arrhenius (Eq. 3) [25] and Vogel-Tamman-Fulcher (VTF) (Eq. 4) [40] equations (Fig. 3). The experimental viscosity values are presented in Tables D1–D3 of the Supplementary material. Evidently, the viscosity decreases with the temperature increase, probably due to breaking the hydrogen bonds in DESs. For the investigated temperature range, the viscosity values of the tested DESs lie within the range of 0.588-22.369 Pa·s. At temperatures up to 283.15 K, the LEC:G DES is solid. The viscosity values of the LEC-based DESs at 313.15 K are in the following order: LEC:OLE < LEC:TEOA < LEC:G.
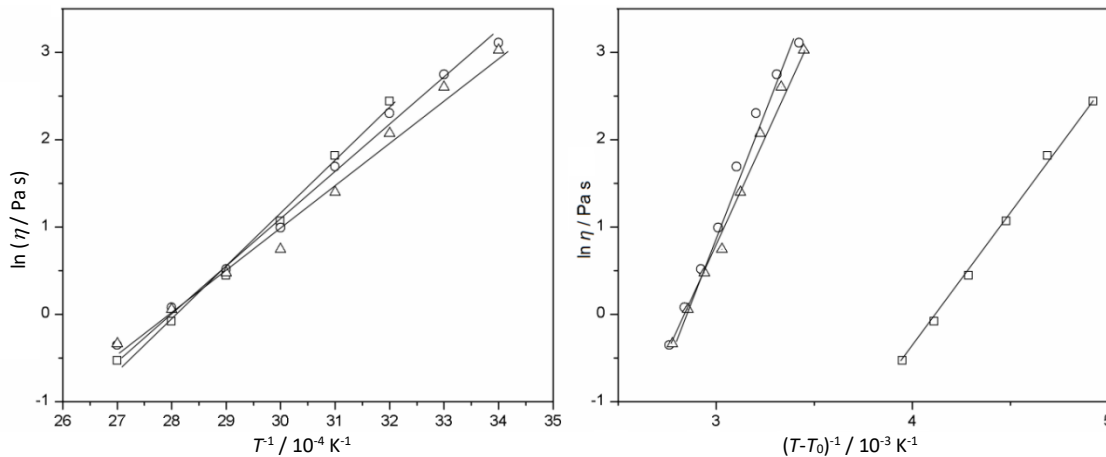
Figure 3. Logarithmic dependences of viscosity (η) of the LEC-based DESs on temperature and application of: a) Arrhenius equation; b) VTF equation (LEC:G – □ (STD ≤ 0.03), LEC:TEOA – ○ (STD ≤ 0.02) and LEC:OLA – △(STD ≤ 0.03))

As expected, the LEC-based DESs are highly viscous at lower temperatures. Due to heating, the constituents move faster, thus reducing the viscosity value [26]. To eliminate the negative viscosity effect on the technological process, these DESs should be used at temperatures higher than 313.15 K. The LEC:G DES exhibits higher viscosity than the *N,N*-diethylethano-lammonium chloride:G (1:2) [29], tetrapropylammonium bromide:G (1:3) [30] and ChCl:G (1:2) [27,31,32] DESs.

In the Arrhenius equation (3):

$$\ln \eta = \ln A_\eta + (E_\eta/RT) \tag{3}$$

η, T, E_η, A_η, and R represent the viscosity, the absolute temperature, the activation energy for the viscous flow, the pre-exponential constant, and the universal gas constant, respectively; values of these parameters are shown in Table 6.

Table 6. Parameters of the Arrhenius-type equation for the LEC-based DESs in the temperature range 293.15-363.15 K.

DES	Viscosity range, Pa·s	Arrhenius equation (η / Pa·s; T / K)	A_η / μPa s	E_η / J·mol^{-1}	MRPD, %	R^2
LEC:G	0.588-11.457	$\ln \eta = 6891.8T^{-1}-19.5$	0.180	57298	10.32	0.997
LEC:TEAO	0.702-22.369	$\ln \eta = 5523.1T^{-1}-15.5$	0.004	45919	11.22	0.990
LEC:OLA	0.711-20.610	$\ln \eta = 5308.0T^{-1}-15.0$	0.305	44131	12.71	0.993

The VTF equation (4) is expressed as:

$$\eta = \eta_0 \exp \frac{B_\eta}{T-T_0} \tag{4}$$

The values of T_0 (so-called ideal glass-transition temperature), η_0 (adjustable parameter), and B_η (factor related to the activation energy) are listed in Table 7.

Table 7. Parameters of the VTF equation for the LEC-based DESs in the temperature range 293.15-363.15 K.

DES	VTF equation (η / Pa·s; T / K)	η_0 / Pa s	B_η / K	T_0 / K	MRPD, %	R^2
LEC:G	$\ln \eta = 3118.4(T-T_0)^{-1}-12.88$	$2.528 \cdot 10^{-6}$	3118	110	8.01	0.998
LEC:TEAO	$\ln \eta = 5489(T-T_0)^{-1}-15.47$	$1.899 \cdot 10^{-7}$	5489	1	11.35	0.990
LEC:OLA	$\ln \eta = 5210.4(T-T_0)^{-1}-14.85$	$3.543 \cdot 10^{-7}$	5210	3	12.67	0.993

To get more information about DESs viscous flow, the equation (5) is used [25]:

$$\ln \frac{\eta V}{h N_A} = \frac{\Delta H^*}{RT} - \frac{\Delta S^*}{R} \tag{5}$$

where V - the molar volume of DES (the ratio of average M_{DES} and density of the DES at desired temperature), N_A - the Avogadro's number; h - the Planck's constant; ΔH^* -viscous flow activation enthalpy; R - universal gas constant; ΔS^* - activation entropy of viscous flow. The plots of ln ($\eta V/h N_A$) *vs.* the inverse temperature are shown in Figure 4, while the values of R^2, ΔH^*, $T\Delta S^*$, and ΔG^* for the LEC-based DESs at 313.15 K are listed in Table 8. The DESs values of the viscous

flow activation enthalpy were greater than the *TΔS** values. These facts indicate that the energetic contribution due to the viscous flow activation enthalpy is more significant than the entropic input to the activation Gibbs energy.

Figure 4. The plot of ln (ηV/hN$_A$) vs. inverse temperature for LEC-based DESs: experimental data (LEC:G – □ (STD ≤ 0.3), LEC:TEOA – ○ (STD ≤ 0.5) and LEC:OLA – △ (STD ≤ 0.9)) and the best linear fits (lines)

Table 8. Values of R^2, $ΔH*$, $TΔS*$, and $ΔG*$ determined for the LEC-based DESs at 313.15 K

DES	Eyring's equation (T / K)	R^2	$ΔH*$ / kJ·mol^{-1}	$TΔS*$ / kJ·mol^{-1}	$ΔG*$ / kJ·mol^{-1}
LEC:G	ln ($ηV_m/hN_A$) = 6821.4T^{-1} - 4.9	0.997	56.7	-12.9	43.8
LEC:TEAO	ln ($ηV_m/hN_A$) = 5487.2T^{-1} - 0.9	0.990	45.6	-2.4	43.2
LEC:OLA	ln ($ηV_m/hN_A$) = 5245.4T^{-1} - 0.2	0.993	43.6	-0.5	43.1

3. 1. 4. FTIR spectra

The FTIR spectra of LEC and the investigated DESs are shown in Figure 5.

Figure 5. FTIR spectra of the LEC and the investigated LEC-based DESs (25 ºC, 400-4000 cm^{-1})

The spectra of the DESs show an intensive broadband at 3200-3500 cm^{-1} due to stretching v(OH) vibrations. The shape and position suggest the existence of hydrogen bonds. This band is intensive in the spectra of all starting components of DESs except for the OLE spectrum since the long carbon chain does not allow the formation of intramolecular hydrogen bonds. The amine vibrations present in the spectrum of TEOA are covered by the stretching vibrations of hydroxyl groups [41]. The FTIR spectra of the DESs and their constituents [41] show stretching v(C-H) vibrations at 2800-3000 cm^{-1}. The intensive band at 1712 to 1773 cm^{-1} in the spectra of all DESs originates from the stretching v(C=O) vibrations characteristic for the spectrum of LEC. The bending δ(OH) vibrations at 1660-1647 cm^{-1} in the spectra of the LEC:G and LEC:TEOA DESs overlap the bending δ(NH$_3^+$) vibration at 1660 cm^{-1} in the spectrum of TEOA. Bending δ(C-H) vibrations at 1376 to 1474 cm^{-1} are present in all spectra. Bands originating from the stretching v(C-O) vibrations are present in all spectra at 1170 to 1287 cm^{-1}. The bands arising from the POC and PO$_2$ groups in LEC overlap in the spectrum of LEC and are visible in all spectra of the DESs at 1060 to 1099 cm^{-1}. The FTIR analysis shows the presence of characteristic functional groups of LEC-based DESs constituents, proving that the preparation of DESs does not lead to their chemical changes. Also, the FTIR analysis shows the presence of hydrogen bonds created in the investigated DESs.

3. 2. CaO-catalyzed ethanolysis of BMSO

Figure 6 presents FAEE contents during the CaO-catalyzed BMSO ethanolysis in the presence of DESs or each component, compared to the control reaction in the absence of any cosolvent. BMSO and ethanol did not react in the absence of CaO catalyst, indicating that the tested DESs did not exhibit catalytic activity. The CaO-catalyzed ethanolysis of BMSO without any cosolvents provides a three-phase system, so the sigmoidal dependence of the FAEE content with time is typical due to the mass transfer limitations and the slow TAG conversion at the start of the reaction [4,42,43].
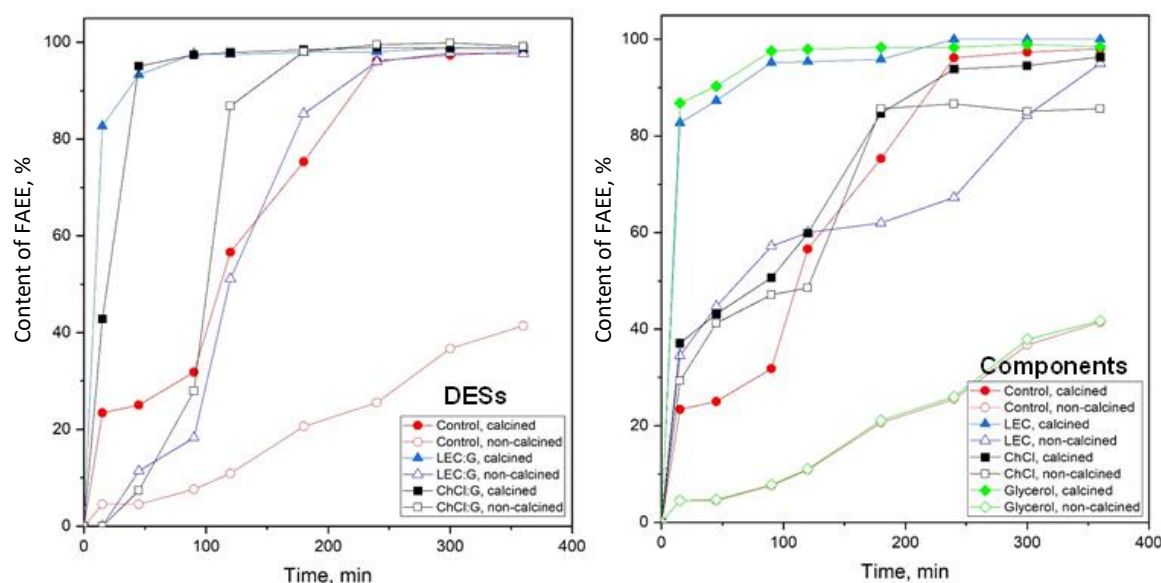
Figure 6. Effects of the LEC- and ChCl-based DESs or their constituents on the FAEE content during the ethanolysis of BMSO catalyzed by non-calcined (open symbols) or calcined (filled symbols) CaO (reaction conditions: temperature 70 °C, ethanol-to-oil molar ratio 12:1, the amounts of DES and CaO to BMSO: 20 and 10 wt.%; average STD ≤ 1.56 (left) and 1.41 (right))

Calcined CaO has shown a more intensive catalytic activity as compared to the non-calcined CaO due to the removal of CO$_2$ and H$_2$O from the catalyst particles in the former case by calcination as these components are considered poisonous to the catalyst active sites. As a result, the FAEE content in the presence of calcined CaO rose to 96.2±1.2 % within 4 h; further prolongation of the reaction resulted in a negligible increase in the FAEE content. On the contrary, in the presence of non-calcined CaO, high FAEE content was not achieved even after 6 h of the reaction.

The LEC:G and ChCl:G DESs accelerated the BMSO ethanolysis over both catalysts. A more positive influence of the hydrophobic LEC:G DES on the calcined CaO-catalyzed reaction was observed after only 15 min reaching the FAEE

content of 82.7±1.8 %, as compared to that reported for the hydrophilic ChCl:G DES (42.8±4.5 %) [4]. However, the efficiency of these DESs was similar after 45 min, with FAEE contents of 93.3±0.9 and 95.1±2.5 % for the system containing the LEC:G and ChCl:G DES, respectively. Maximal FAEE contents of 97.6±0.6 and 97.4±1.2 % for the LEC:G and ChCl:G DES, respectively, were achieved after 90 min. Further prolongation of the reaction resulted in a negligible increase in the FAEE content (97.9±1.5 and 98.1±0.7 %, respectively, after 3 h).

In the reaction catalyzed by non-calcined CaO, the presence of the LEC:G and ChCl:G DESs as cosolvents provided FAEE contents of 96.0±1.1 and 98.1 % after 3 h, respectively. On the other hand, LEC, ChCl, and G were less efficient cosolvents used with the same catalyst, resulting in FAEE contents of 84.32±1.7, 81.09±0.8, and 26.0±3.1 %, respectively, for the same duration of the transesterification.

Positive effects of the ChCl:G DES as a cosolvent in CaO-catalyzed transesterification of vegetable oils have already been reported [4,44]. The results obtained in the present study indicate that the LEC:G DES can successfully activate CaO, providing a more cost-effective procedure than thermal activation.

3. 3. Separation of FAEEs

Addition of the LEC- or ChCl-based DESs in the BMSO ethanolysis accelerated the phase separation of the final reaction mixture (30 min) as compared to the control reaction in the absence of any cosolvent (more than 12 h). Also, the presence of these DESs in reaction systems may cause the reduction of soap formation, as noticed for the ethanolysis of other oily feedstocks [4,45,46]. However, the systems containing CaO without and with LEC, ChCl, or G remained very viscous and separated much slower.

3. 4. XRD of the used CaO catalyst

Figures 7-9 show XRD spectra of the initial and used non-calcined and calcined CaO samples separated from the final reaction mixtures of the BMSO ethanolysis conducted in the presence of the LEC:G and ChCl:G DESs or their constituents (LEC, ChCl, and G).
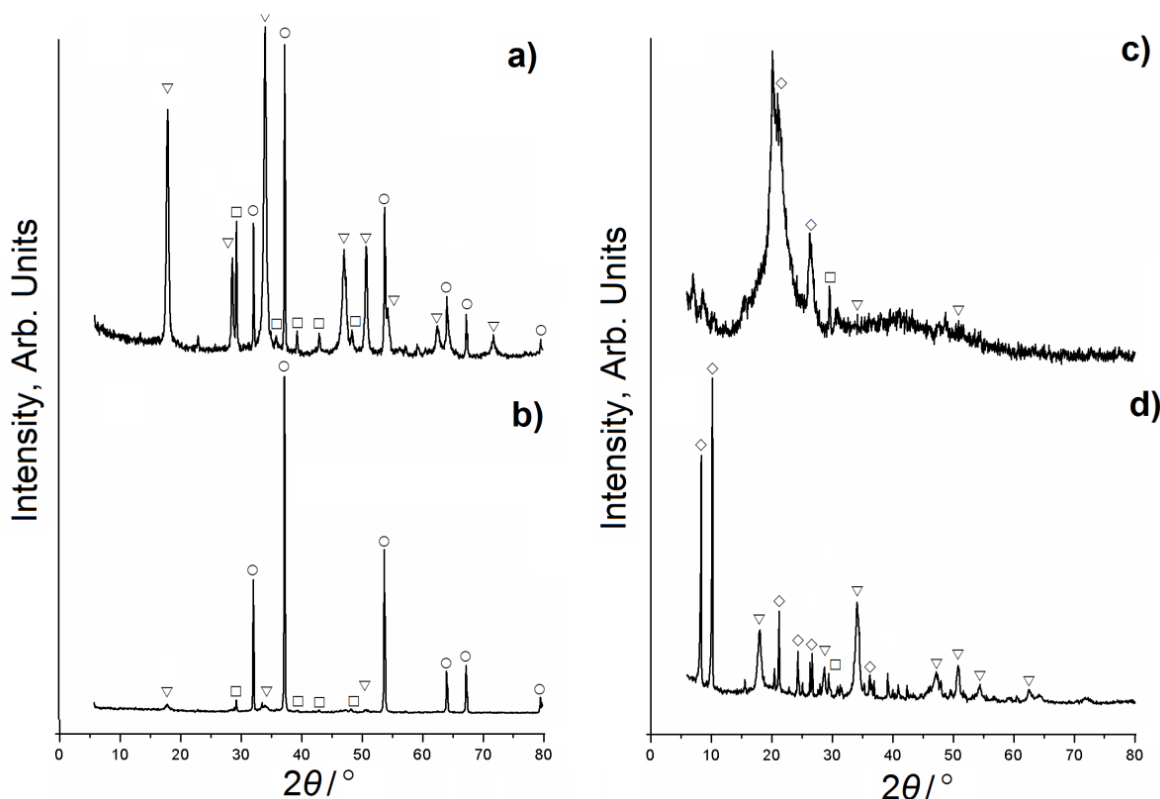
Figure 7. XRD patters of the fresh non-calcined (a) and calcined (b) CaO samples and the used non-calcined (c) and calcined (d) CaO pastes recovered from the reaction mixture after 6 h (○ - CaO, ▽ - Ca(OH)₂, □ - CaCO₃, ◇ - CaDG (calcium diglyceroxide)).
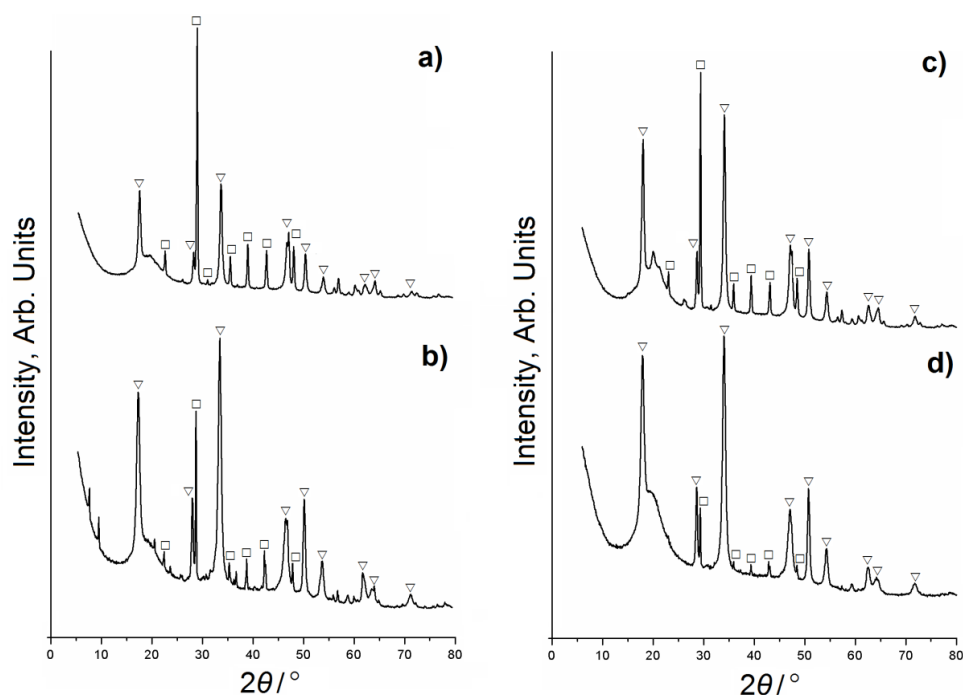
Figure 8. XRD patters of the used non-calcined (a,c) and calcined (b,d) CaO samples taken after 6 h from the ethanolysis reaction carried out in the presence of LEC:G (a,b) and ChCl:G (c,d) DESs (○ - CaO, ▽ - Ca(OH)₂, □ - CaCO₃)
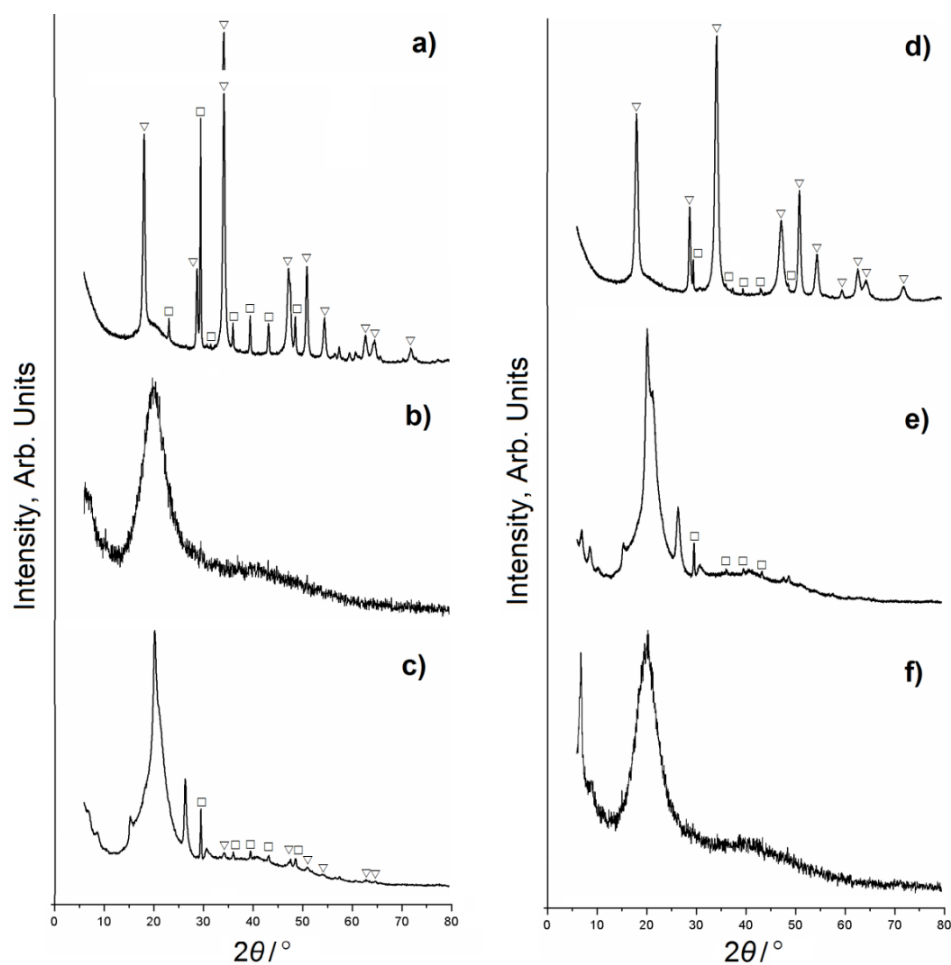
Figure 9. XRD patterns of the used non-calcined (a,c,e) and calcined (b,d,f) CaO samples taken after 6 h from the ethanolysis reaction carried out in the presence of LEC (a,b), ChCl (c,d) or G (e,f) (○ - CaO, ▽ - Ca(OH)₂, □ - CaCO₃)

The XRD analysis of the non-calcined CaO sample revealed the peaks attributed to the CaO phase (2θ = 32.22 (32.4), 37.36 (37.55), 53.86 (54.05), 64.16 (64.35), and 67.38 (67.55)°, JCPDS Card 43-1001), $Ca(OH)_2$ phase (2θ = 18.15 (17.98), 34.25 (34.1), 47.3 (47.18), 51, 62.75 and 64.35°, JCPDS Card 84-1263), and $CaCO_3$ phase (2θ = 29.5 and 43.14°, JCPDS Card 81-2027). The presence of the $CaCO_3$ and $Ca(OH)_2$ peaks was attributed to the sensitivity of CaO towards atmospheric moisture and CO_2.

The fresh calcined CaO sample appeared as an almost single well-crystallized CaO phase with minor peaks characteristic for the $Ca(OH)_2$ phase (2θ = 18.15 (17.98), 34.25 (34.1), 47.3 (47.18), 51, 62.75 and 64.35°), and $CaCO_3$ phase (2θ = 29.5 and 43.14°), confirming the CaO activation by calcination.

There were apparent changes in the XRD patterns of calcined and non-calcined CaO used in the BMSO ethanolysis without or with cosolvents. However, a major difference was due to the absence of the CaO phase, which was converted into $Ca(OH)_2$ and $CaCO_3$ during the hydration and carbonation processes during the collection step [4, 47].

The calcined CaO sample collected from the reactions carried out in the absence of any cosolvent revealed the presence of calcium diglyceroxide (2θ = 8.5 (8.2), 10.4 (10.2), 21.3 (21.2), 24.4, 26.6, 34.4, and 36.2°, PDF#21-1544) along with $Ca(OH)_2$ (2θ = 17.94 (17.98), 28.7 (28.72), 34.08 (34.12), 47.16 (47.18), 50.8 (50.84), 54.54, 59.4, and 62.62 (62.64)°), and $CaCO_3$ (2θ = 29.4 (28.8)°). The XRD spectrum indicated transformation of the majority of the CaO catalyst into calcium diglyceroxide with the by-produced G in the successful CaO-catalyzed transesterification, CaO particles are transformed into $Ca(OH)_2$ in the initial stage. In contrast, in the last stage, these particles become calcium-diglyceroxide [48,49].

Although these phases are also seen in the XRD spectra of the used non-calcined CaO catalyst, the presence of the amorphous phase (a broad peak with a maximum at about 2θ = 20°) was also observed. This peak could originate from calcium ethoxide (produced in the catalyst preparation step when the calcined CaO/ethanol mixture was stirred at 70 °C for 30 min) or be attributed to the deposition of organic molecules on the surface of the used CaO catalyst [47].

In the XRD spectra of non-calcined and calcined CaO used in the reaction with the addition of different DESs or their constituents, the presence of $Ca(OH)_2$ and $CaCO_3$ phases was evident, while calcium diglyceroxide was not identified. Furthermore, the peak at about 2θ = 20.5° was more pronounced in the catalytic systems with the constituents of the DESs, suggesting that the synthesized amount of calcium diglyceroxide was quite low and insufficient for detection by the XRD apparatus.

It should be noted that the absence of peaks characteristic for calcium diglyceroxide could be explained by its low amount (*i.e.*, insufficient to surpass the XRD apparatus limit detection), easy dissolution [50], and instability, causing calcium leaching into the reaction medium [49]. Solubilization of calcium diglyceroxide in alcohol might also produce a soluble precursor, which could be later transformed into the final solid base catalyst [51]. Moreover, amorphization of calcium ethoxide during the catalyst drying [52] would result in the presence of only $Ca(OH)_2$ and $CaCO_3$ phases in the XRD spectra. Amorphisation was also reported after the reactions in which other calcium-based catalysts prepared by calcination of animal waste were used [53].

4. CONCLUSION

Three novel DESs were prepared by combining LEC with G, TEOA, or OLE in 1:2 molar ratio. Densities, viscosities, and refractive indices of the tested DESs decreased with the increase in temperature applied in the range 293.15-363.15 K at the atmospheric pressure relevant for practical applications. All tested LEC-based DESs are liquid at 313.15 K. The FTIR spectra of LEC and investigated LEC-based DESs indicated absence of chemical reactions during the DES preparation. The LEC:G and ChCl:G DESs were further used for ethanolysis of cold-pressed BMSO catalyzed by non-calcined or calcined CaO. Both DESs were shown to successfully activate the non-calcined CaO catalyst providing the FAEE contents of over 96.5 % after 3 h. However, in the presence of these DESs in the reaction catalyzed by calcined CaO, the FAEE contents above 96.5 % were obtained after 90 min. The hydrophobic LEC:G DES proved to be a more successful cosolvent than the hydrophilic ChCl:G prepared in the same molar ratio (1:2) at the beginning of the reaction, while after 45 min of the reaction, their efficiencies were similar. Both DESs accelerated separation of the esters from the final reaction mixture. This study proved that DESs composed of natural, safe, cheap, available, biodegradable and environmental-friendly compounds may serve as efficient cosolvents and/or activators of heterogeneous alkaline

catalyst for transesterification reaction. Thus, further investigation should be focused on improving the reaction by using other non-edible or waste oils and fats, additionally reducing the cost of the process and enabling successful industrialization of biodiesel production.

REFERENCES

[1] Bergua F, Delso I, Muñoz-Embid J, Lafuente C, Artal M. Structure and properties of two glucose-based deep eutectic systems. *Food Chem.* 2021; 336: 127717. https://doi.org/10.1016/j.foodchem.2020.127717

[2] Balaraman HB, Rathnasamy SK. Kinetics and microwave-assisted extractive transesterification studies of high octane methyl esters (HOME) from karanja and chicken lard oil using protic deep eutectic solvent. *Fuel*. 2020; 268: 117299. https://doi.org/10.1016/j.fuel.2020.117299

[3] Manurung R, Taslim T, Siregar AGA. Deep eutectic solvents based choline chloride for enzymatic biodiesel production from degumming palm oil. *Asian J. Chem.* 2020; 3: 733–738. https://doi.org/10.14233/ajchem.2020.22193

[4] Troter DZ, Todorović ZB, Đokić-Stojanović DR, Veselinović LjM, Zdujić MV, Veljković VB. Choline chloride-based deep eutectic solvents in CaO-catalyzed ethanolysis of expired sunflower oil. *J Mol Liq.* 2018; 266: 557–567. https://doi.org/10.1016/j.molliq.2018.06.106

[5] Merza F, Fawzy A, AlNashef I, Al-Zuhair S., Taher H. Effectiveness of using deep eutectic solvents as an alternative to conventional solvents in enzymatic biodiesel production from waste oils. *Energy Rep.* 2018; 4: 77–83. https://doi.org/10.1016/j.egyr.2018.01.005

[6] Gu L, Huang W, Tang S, Tian S, Zhang X. A novel deep eutectic solvent for biodiesel preparation using a homogeneous base catalyst. *Chem Eng Sci.* 2015; 259: 647–652. https://doi.org/10.1016/j.cej.2014.08.026

[7] Zhang Y, Xia X, Duan M, Han Y, Liu J, Luo M, Zhao C, Zu Y, Fu Y. Green deep eutectic solvent assisted enzymatic preparation of biodiesel from yellow horn seed oil with microwave irradiation. *J Mol Catal B Enzym.* 2016; 123: 35–40. https://doi.org/10.1016/j.molcatb.2015.10.013

[8] Alam MM, Rahman KA. Biodiesel from mustard oil: a sustainable engine fuel substitute for Bangladesh. *Int J Renew Energy Dev.* 2013; 2: 141–149. https://doi.org/10.14710/ijred.2.3

[9] Đorđević BS, Troter DZ, Todorović ZB, Đalović IG, Stanojević LjP, Mitrović PM, Veljković VB. The effect of the triethanolamine: glycerol deep eutectic solvent on the yield, fatty acid composition, antioxidant activity, and physicochemical properties of black mustard (*Brassica nigra* L.) seed oil. *J Food Meas Charact.* 2020; 14: 2570–2577. https://doi.org/10.1007/s11694-020-00503-3

[10] Aslan V, Eryilmaz T. Polynomial regression method for optimization of biodiesel production from black mustard (*Brassica nigra* L.) seed oil using methanol, ethanol, NaOH, and KOH, *Energy.* 2020; 209: 118386. https://doi.org/10.1016/j.energy.2020.118386

[11] Knothe G. Dependence of biodiesel fuel properties on the structure of fatty acid alkyl esters. *Fuel Process Technol.* 2005; 86: 1059–70. https://doi.org/10.1016/j.fuproc.2004.11.002

[12] Shahzadi I, Sadaf S, Iqbal J, Ullah I, Bhatti HN. Evaluation of mustard oil for the synthesis of biodiesel: Pretreatment and optimization study. *Environ Prog Sustain Energy.* 2018; 37: 1829–1835. https://doi.org/10.1002/ep.12833

[13] Robert C, Couëdelo L, Vaysse C, Michalski M-C. Vegetable lecithins: a review of their compositional diversity, impact on lipid metabolism and potential in cardiometabolic disease prevention. *Biochimie*. 2020; 169: 121–132. https://doi.org/10.1016/j.biochi.2019.11.017

[14] Jung Y-G, Lee C-R, Kim H-J, Kim Min-G, Jin KS, Lee H-Y. Effect of hydrocarbon chain length of aliphatic solvents on the reverse self-assembly of lecithin and monovalent ion mixtures. *Colloids Surf A Physicochem Eng Asp.* 2020; 607: 125441. https://doi.org/10.1016/j.colsurfa.2020.125441

[15] Tung SH, Huang YE, Raghavan SR. A new reverse wormlike micellar system: mixtures of bile salt and lecithin in organic liquids. *J Am Chem Soc.* 2006; 128: 5751–5756. https://doi.org/10.1021/ja0583766

[16] Kumar R, Katare OP. Lecithin organogels as a potential phospholipid-structured system for topical drug delivery: a review. *AAPS PharmSciTech*. 2005; 6: 298–310. https://doi.org/10.1208/pt060240

[17] Zou H, Zhao N, Li S, Sun S, Dong X, Yu C. Physicochemical and emulsifying properties of mussel water-soluble proteins as affected by lecithin concentration. *Int J Biol. Macromol.* 2020; 163: 180–189. https://doi.org/10.1016/j.ijbiomac.2020.06.225

[18] Amiri-Rigi A., Abbasi S. Extraction of lycopene using a lecithin-based olive oil microemulsion. *Food Chem.* 2018; 272: 568–573. https://doi.org/10.1016/j.foodchem.2018.08.080

[19] Shen Y, Chang C, Shi M, Su Y, Gu L, Li J, Yang Y. Interactions between lecithin and yolk granule and their influence on the emulsifying properties. *Food Hydrocoll.* 2019; 101: 105510. https://doi.org/10.1016/j.foodhyd.2019.105510

[20] Xue J, Zhong Q. Thyme oil nanoemulsions coemulsified by sodium caseinate and lecithin. *J Agric Food Chem.* 2014; 62: 9900–9907. https://doi.org/10.1021/jf5034366

[21] Đorđević BS., Todorović ZB, Troter DZ, Stanojević LjP, Veljković VB. Extraction of quercetin from waste onion (*Allium cepa* L.) tunic by the aqueous solutions of different deep eutectic solvents. *Adv Technol.* 2018; 7: 5–10. https://doi.org/10.5937/SavTeh1802005d

[22] Veljković VB, Stamenković OS, Todorović ZB, Lazić ML, Skala DU. Kinetics of sunflower oil methanolysis catalyzed by calcium oxide. *Fuel.* 2009; 88: 1554–1562. https://doi.org/10.1016/j.fuel.2009.02.013

[23] Stamenkoviæ OS, Rajkoviæ K, Velièkoviæ AV, Miliæ PS, Veljkoviæ VB. Optimization of base-catalyzed ethanolysis of sunflower oil by regression and artificial neural network models. *Fuel Process Technol.* 2013; 114: 101–108. https://doi.org/10.1016/j.fuproc.2013.03.038

[24] Veličković AV, Stamenković OS, Todorović ZB, Veljković VB. Application of the full factorial design to optimization of base–catalyzed sunflower oil ethanolysis. *Fuel.* 2013; 104: 433–442. https://doi.org/10.1016/j.fuel.2012.08.015

[25] Constantin V, Adya AK, Popescu A-M. Density, transport properties and electrochemical potential windows for the 2-hydroxy-*N,N,N*-trimethylethanaminium chlorides based ionic liquids at several temperatures. *Fluid Phase Equilib.* 2015; 395: 58–66. https://doi.org/10.1016/j.fluid.2015.03.025

[26] Mitar A, Panić M, Prlić Kardum J, Halambek J, Sander A, Zagajski Kučan K, Radojčić Redovniković I, Radošević K. Physicochemical properties, cytotoxicity, and antioxidative activity of natural deep eutectic solvents containing organic acid. *Chem Biochem Eng Q.* 2019; 33: 1–18. https://doi.org/10.15255/CABEQ.2018.1454

[27] Troter DZ, Todorović ZB, Đokić–Stojanović DR, Đorđević BS, Todorović VM, Konstantinović SS, Veljković VB. The physicochemical and thermodynamic properties of the choline chloride-based deep eutectic solvents. *J Serbian Chem Soc.* 2017; 82: 1039–1052. https://doi.org/10.2298/jsc170225065t

[28] *Ramón DJ, Guillena G. Deep Eutectic Solvents: Synthesis, Properties, and Applications,* John Wiley & Sons; *2020;* 1–21.

[29] Siongco KR, Leron RB, Li M-H. Densities, refractive indices, and viscosities of *N,N*-diethylethanol ammonium chloride-glycerol or -ethylene glycol deep eutectic solvents and their aqueous solutions. *J Chem Thermodyn.* 2013; 65: 65–72. https://doi.org/10.1016/j.jct.2013.05.041

[30] Jibril B, Mjalli F, Naser J, Gano Z. New tetrapropylammonium bromide–based deep eutectic solvents: Synthesis and characterizations. *J Mol Liq.* 2014; 199: 462–469. https://doi.org/10.1016/j.molliq.2014.08.004

[31] AlOmar MK, Hayyan M, Alsaadi MA, Akib S, Hayyan A, Hashim MA. Glycerol–based deep eutectic solvents: Physical properties. *J Mol Liq.* 2016; 215: 98–103. https://doi.org/10.1016/j.molliq.2015.11.032

[32] Lapeña D, Lomba L, Artal M, Lafuente C, Giner B. The NADES glyceline as a potential green Solvent: A comprehensive study of its thermophysical properties and effect of water inclusion. *J Chem Thermodyn.* 2019; 128: 164–172. https://doi.org/10.1016/j.jct.2018.07.031

[33] Bahadori L, Chakrabarti MH, Mjalli FS, AlNashef IM, Manan NSA, Hashim MA. Physicochemical properties of ammonium–based deep eutectic solvents and their electrochemical evaluation using organometallic reference redox systems. *Electrochim Acta,* 2013; 113: 205–211. https://doi.org/10.1016/j.electacta.2013.09.102

[34] Troter DZ, Zlatković MZ, Đokić-Stojanović DR, Konstantinović SS, Todorović ZB. Citric acid-based deep eutectic solvents: Physical properties and their use as cosolvents in sulphuric acid-catalysed ethanolysis of oleic acid. *Adv Technol.* 2016; 5: 53–65. https://doi.org/10.5937/savteh1601053t

[35] Glasser L. Thermodynamic estimation: Ionic materials. *J Solid State Chem*. 2013; 206: 139–144. https://doi.org/10.15744/2348-9812.1.e105

[36] Haynes WM. CRC Handbook of chemistry and physics, A ready reference book of chemical and physical data, 94th ed., CRC Press, Taylor & Francis Group, Boca Raton, FL; 2013; pp. 12–21.

[37] Hayyan A, Mjalli FS, AlNashef IM, Al-Wahaibi YM, Al-Wahaibi T, Hashim MA. Glucose-based deep eutectic solvents: Physical properties. *J Mol Liq.* 2013; 178: 137. https://doi.org/10.1016/j.molliq.2012.11.025

[38] Born M, Wolf E. Principles of optics: electromagnetic theory of propagation, interference and diffraction of light, 7th Expanded Edition, Cambridge University Press, United Kingdom; 1999; pp. 11–14.

[39] Ghaedi H, Ayoub M, Sufian S, Shariff AM, Lal B, Wilfred CD. Density and refractive index measurements of transition-temperature mixture (deep eutectic analogues) based on potassium carbonate with dual hydrogen bond donors for CO_2 capture. *J Chem Thermodyn.* 2018; 118: 147. https://doi.org/10.1016/j.jct.2017.11.008

[40] Wu TY, Su S-G, Lin YC, Wang HP, Lin MW, Gung ST, Sun IW. Electrochemical and physicochemical properties of cyclic amine-based Brønsted acidic ionic liquids. *Electrochim Acta.* 2010; 56: 853–862. https://doi.org/10.1016/j.electacta.2010.09.084

[41] Đorđević BS, Troter DZ, Veljković VB, Kijevčanin MLj, Radović IR, Todorović ZB. The physicochemical properties of the deep eutectic solvents with triethanolamine as a major component. *J Serb Chem Soc.* 2020; 85: 1303–1315. https://doi.org/10.2298/JSC200425050D

[42] Esipovich A, Danov S, Belousov A, Rogozhin A. Improving methods of CaO transesterification activity. *J Mol Catal A Chem.* 2014; 395: 225–233. https://doi.org/10.1016/j.molcata.2014.08.011

[43] Veličković AV, Avramović JM, Stamenković OS, Veljković VB. Kinetics of the sunflower oil ethanolysis using CaO as catalyst. *Chem Ind Chem Eng Q.* 2016; 22: 409–418. https://doi.org/10.2298/ciceq160106003v

[44] Huang W, Tang S., Zhao H, Tian S. Activation of commercial CaO for biodiesel production from rapeseed oil using a novel deep eutectic solvent. *Ind Eng Chem Res.* 2013; 52: 11943–11947. https://doi.org/10.1021/ie401292w

[45] Manurung R, Ramadhani DA, Maisarah S. One step transesterification process of sludge palm oil (SPO) by using deep eutectic solvent (DES) in biodiesel production. *AIP Conf. Proc.* 2017; 1855: 070004. https://doi.org/10.1063/1.4985531

[46] Manurung R, Winarta A, Taslim Indra L. Biodiesel production from ethanolysis of palm oil using deep eutectic solvent (DES) as cosolvent, *IOP Conf. Ser.: Mater. Sci. Eng.* 2017; 206: 012023. https://doi.org/10.1088/1757-899X/206/1/012023

[47] di Bitonto L, Reynel-Avila HE, Mendoza-Castillo DI, Bonilla-Petriciolet A, Duran-Valle CJ, Pastore C. Synthesis and characterization of nanostructured calcium oxides supported onto biochar and their application as catalysts for biodiesel production. *Renew Energy.* 2020; 160: 52–66. https://doi.org/10.1016/j.renene.2020.06.045

[48] Chen X, Li Z, Chun Y, Yang F, Xu H, Wu X. Effect of the formation of diglycerides/monoglycerides on the kinetic curve in oil transesterification with methanol catalyzed by calcium oxide. *ACS Omega*. 2020; 5: 4646–4656. https://doi.org/10.1021/acsomega.9b04431

[49] Ramos M, Dias A PS, Teodoro F. Soybean oil ethanolysis over Ca based catalyst. Statistical optimization of reaction conditions. *React Kinet Mech Catal.* 2020; 130: 433–445. https://doi.org/10.1007/s11144-020-01791-y

[50] Sánchez-Cantú M, Reyes–Cruz FM, Rubio–Rosas E, Pérez–Díaz LM, Ramírez E, Valente JS. Direct synthesis of calcium diglyceroxide from hydrated lime and glycerol and its evaluation in the transesterification reaction. *Fuel*. 2014; 138: 126–133. https://doi.org/10.1016/j.fuel.2014.08.006

[51] Kouzu M, Hidaka J, Wakabayashi K, Tsunomori M. Solid base catalysis of calcium glyceroxide for a reaction to convert vegetable oil into its methyl esters. *Appl Catal A: Gen.* 2010; 390: 11–18. https://doi.org/10.1016/j.apcata.2010.09.029

[52] Rodriguez–Navarro C, Vettori I, Ruiz–Agudo E. Kinetics and mechanism of calcium hydroxide conversion into calcium alkoxides: implications in heritage conservation using nanolimes. *Langmuir*. 2016; 32: 5183–5194. https://doi.org/10.1021/acs.langmuir.6b01065

[53] Soares Dias AP, Ramos M, Catarino M, Puna J, Gomes J. Solvent assisted biodiesel production by co-processing beef tallow and soybean oil over calcium catalysts. *Waste Biomass Valorization*. 2019; 11: 6249–6259. https://doi.org/10.1007/s12649-019-00903-7

Uticaj temperature na fizičkohemijska svojstva eutektičkih rastvarača sa lecitinom i njihova upotreba u transesterifikaciji katalizovanoj CaO

Zoran B. Todorović[1], Biljana S. Đorđević[1], Dragan Z. Troter[1], Ljiljana M. Veselinović[2], Miodrag V. Zdujić[2] i Vlada B. Veljković[1,3]

[1]*Tehnološki fakultet, Univerzitet u Nišu, Bulevar Oslobođenja 124, 16000 Leskovac, Srbija*
[2]*Institut tehničkih nauka Srpske akademije nauke i umetnosti, Knez Mihajlova 35, 11000 Beograd, Srbija*
[3]*Srpska akademija nauka i umetnosti, Knez Mihajlova 35, 11000 Beograd, Srbija*

(Naučni rad)

Izvod

Zbog različitih strukturnih varijacija i mogućnosti prilagođavanja njihovih fizičkohemijskih svojstava, eutektički rastvarači se nazivaju ,,dizajnerski rastvarači". Za industrijsku primenu eutektičkih rastvarača, važno je poznavati njihova fizička i termodinamička svojstva poput gustine, viskoziteta i indeksa prelamanja. Ova svojstva su merena u funkciji temperature za tri eutektička rastvarača lecitina sa glicerolom, trietanolaminom i oleinskom kiselinom. Za opisivanje viskoziteta primenjene su Arenijusova i jednačina Vogela, Tamana i Fulčera (Vogel-Tamman-Fulcher). Gustina, viskozitet i indeks prelamanja testiranih eutektičkih rastvarača opadali su sa porastom temperature. Eutektički rastvarač lecitin:glicerol (LEC:G) je imao najmanju gustinu na svim testiranim temperaturama. Na kraju, eutektički rastvarač LEC:G je izabran kao kosolvent u etanolizi hladno ceđenog ulja semena crne slačice (*Brassica nigra* L.) katalizovanoj žarenim ili nežarenim CaO. Reakcija je izvedena u šaržnom reaktoru uz stalno mešanje i pri sledećim reakcionim uslovima: temperatura 70 °C, molski odnos etanol-ulje 12:1, koncentracija eutektičkog rastvarača 20 mas. % (u odnosu na masu ulja) i koncentracija CaO 10 mas. % (u odnosu na masu ulja). Prisustvo eutektičkog rastvarača ubrzalo je reakciju i separaciju faza finalne reakcione smeše..

Ključne reči: Brassica nigra L.; crna slačica; etanoliza; etil-estri masnih kiselina; eutektički rastvarači

Adsorptive pretreatment of waste cooking oil using quicklime for fatty acid methyl esters synthesis

Ivana Lukić[1], Željka Kesić[1], Miodrag Zdujić[2] and Dejan Skala[1]

[1]University of Belgrade, Faculty of Technology and Metallurgy, Karnegijeva 4, 11000 Belgrade, Serbia
[2]Institute of Technical Sciences of the Serbian Academy of Sciences and Arts, Knez Mihailova 35, 11000 Belgrade, Serbia

Abstract

Synthesis of biodiesel from various plant oils is realized by the transesterification of triglycerides with methanol or by a reaction usually defined as methanolysis. The usage of low-quality oils, such as waste cooking oil (WCO), is followed by undesirable side reactions as a result of the increased content of free fatty acids (FFA), and water. The presence of FFA in WCO usually requires a pretreatment stage before subjecting it to methanolysis. In the present work, heterogeneously catalyzed methanolysis of WCO with and without pretreatment was investigated. Removal of FFA from WCO was conducted by using only quicklime or with the addition of a small amount of methanol (FFA to methanol = 1:3 molar ratio). The obtained results showed that pretreatment of WCO with quicklime at 30 °C after 1 h reduces the FFA content by 72 %, while the adsorption capacity was determined to be 910 mg g^{-1}. The adsorptive pretreatment, as a simple operation, using low-cost quicklime under mild conditions, had a positive effect on the transesterification rate with CaO·ZnO as a catalyst, enabling the achievement of over 96 % of biodiesel yield in only 15 min, compared to 1 h without the pretreatment. Furthermore, pretreated WCO allows an increase in repeated catalyst use and overall savings in the necessary amount of catalyst. The present study showed that quicklime is an economic, environmental-friendly, and sustainable material for FFA removal from WCO.

Keywords: biodiesel; adsorption; CaO·ZnO; methanolysis.

Available on-line at the Journal web address: http://www.ache.org.rs/HI/

1. INTRODUCTION

Biodiesel, a mixture of fatty acid methyl esters (FAME), has gained significant attention over the past couple of decades due to its environmental benefits, such as nontoxicity and biodegradability, and the fact that it is made from renewable resources. The current commercial use of refined vegetable oils for biodiesel production receives harsh criticism, primarily due to the use of oils, which are human nutrition sources. Besides, the high cost of biodiesel is the major limiting factor against large-scale biodiesel production and its commercialization, while the raw material cost typically contributes about 70−80 % of the total cost of biodiesel production [1,2].

Therefore, researchers have focused on other alternative sources of triglycerides (TG), such as non-edible oils or waste cooking oils (WCO), as feedstock for biodiesel production. Although the use of non-edible crops resolves the fuel *vs.* food debate, it is being discouraged because economic yields of non-edible crops can be only achieved by using arable land and appropriate agricultural practices. The mentioned shortcomings highlight waste resources as the most promising feedstock for biodiesel production. Besides, using WCO as a feedstock also resolves the issue of waste oil disposal, which is otherwise often inappropriate and could cause severe environmental challenges. However, the synthesis of biodiesel from these low-quality oils is challenging due to undesirable side reactions because of the presence of free fatty acids (FFA), water, and solid particles. Solid particles and other impurities could be removed by filtration, centrifugation, or washed away with hot water [2]. To remove water from the oil, it can be heated to above 100 °C [3] or dried with silica gel, magnesium sulphate, or calcium chloride [2,4]. The presence of high FFA contents in

the oil can cause undesirable soap formation when homogeneous base catalysts are used for transesterification, which reduces the FAME yield, causes catalyst loss, and complicates phase separation. Acid catalysts are insensitive to FFA, but the process is much slower compared to the alkali-catalyzed transesterification.

To solve this problem, a two-step transesterification method was proposed. In the first step, pretreatment of WCO is performed to reduce the FFA content, while in the second, WCO is subjected to the transesterification process. Different methods for WCO pretreatment were proposed, including esterification, neutralization, adsorption, and distillation. Esterification of FFA with methanol produces FAME and usually is performed in the presence of an acid catalyst such as H_2SO_4 [5] or a solid acid catalyst [6,7]. The lack of this process is the catalyst removal in both stages – esterification and later transesterification. FFA can be removed by neutralization using alkali (KOH or NaOH) as soaps, which can be separated by decantation [8]. Distillation as a method for FFA removal requires more severe conditions, such as higher temperature and pressure, and consumes a large amount of energy [8].

Among all techniques, the adsorption process appears to be the best choice, as a simple, efficient, environmentally friendly, and low-energy method for the removal of FFA from waste vegetable oil [2]. Furthermore, the adsorption process reduces WCO losses and soap formation, enabling also, simple separation of solid phase and treated WCO by filtration [9]. Different materials have been used as adsorbents for the FFA removal, such as clays (montmorillonite, kaolinite and bentonite) [10-13], ion-exchange resins [14-16], zeolite [17], $Ca(OH)_2$ nanoplates supported on activated carbon [18], K_2O/dolomite [19], charcoal from *Pongamia Pinnata* shells [20], Fe_3O_4 [21], Mg- and Na-silicate from rice hull ash and rice husk [22-26], nanoTiO$_2$/chitosan nanocomposite fibers [27] or nickel ferrite [28].

Many of these studies relate to the FFA removal from virgin oils or isooctane to which pure acids have been added as model compounds [11-17]. WCO is a more complex mixture, since it is formed during the usage of virgin vegetable oils for high-temperature cooking, which leads also to the formation of other unwanted compounds that can affect the FFA removal by their interaction with the adsorbent. Some of the applied adsorbents were obtained by complicated and/or expensive procedures [18,27,28], while others showed relatively low capacity, from 18 to 650 mg g^{-1} [10–12,14–17,20,23]. Pereira et al. reported high values of adsorption capacity (2750–7000 mg g^{-1}) for $Ca(OH)_2$ nanoplates supported on activated carbon as adsorbents [18]. However, synthesis of this adsorbent was energy and time-consuming, including pyrolysis of palm endocarp at 700 °C and subsequent activation in a CO_2 atmosphere at 825 °C to obtain activated carbon, followed by impregnation with $Ca(OH)_2$ nanoparticles prepared from calcium chloride dihydrate and ethylene glycol [18]. On the other hand, quicklime used in the present study is a cheap, natural and easily available material. It can be used as an adsorbent, as received, without any preparation, including thermal activation, and thus it is economic, environmental-friendly, and sustainable material for FFA removal.

In this study, two different routes of FAME synthesis from WCO were proposed, investigated, and compared. The first route was simple one-step WCO methanolysis at 60 °C using CaO·ZnO as a solid catalyst [29,30]. The effect of catalyst amount, stirring speed, and methanol to oil molar ratio on the rate of methanolysis was analyzed. The second route was based on a two-step scheme where the first step involved the pretreatment of WCO in order to remove FFA by adsorption onto quicklime or by esterification in the presence of a small amount of methanol catalyzed by quicklime. The first step was analyzed with the goal to define the optimal adsorption temperature, adsorbent particle size, and calcination procedure, as well as the necessary amount of quicklime to be used. The efficiency of quicklime in the FFA removal from the WCO was also determined. It should be noted, that application of quicklime as an adsorbent for FFA removal from WCO was not yet described in literature. In this study, the best WCO pretreatment conditions were determined, and then, the pretreated WCO was used in the second step of FAME synthesis using CaO·ZnO as a heterogeneous catalyst. The possibility to reuse the catalyst in methanolysis of WCO with and without pretreatment was also investigated. To the best of our knowledge, a two-step process of FAME synthesis using adsorption with quicklime as an adsorbent in the first step and followed by heterogeneously catalyzed methanolysis in the second has not been published in the literature so far.

2. EXPERIMENTAL

2. 1. Materials

Quicklime, obtained from the local market in the southern part of Serbia, was a donation by colleagues from Leskovac [31]. CaO·ZnO catalyst was obtained by mechanochemical treatment of CaO (obtained by calcination of quicklime) and ZnO (Kemika, Zagreb, Croatia) in the molar ratio of 1:2 with stoichiometrically required addition of water in the planetary ball mill Fritsch Pulverisette 5 (Fritsch, Germany), as previously described [29,30]. The mechanochemically prepared precursor was calcined at 700 °C for 3 h in air atmosphere in the furnace Instrumentaria LP-07 (Zagreb, Croatia). The WCO was collected from restaurants in Belgrade, Serbia and methanol (99.5 % purity) was purchased from Fluka, Switzerland. The physical and chemical properties of WCO [29] are listed in Table 1.

Table 1. Physical and chemical properties of WCO [29]

Property	Content, wt.%
Water	0.07
FFA	1.27
Monoglycerides	2.00
Diglycerides	0.10
Myristic, C 14:0	0.98
Palmitic, C 16:0	26.84
Stearic, C 18:0	4.58
Oleic, C 18:1	16.54
Linoleic, C 18:2	43.22
Acid value, mg KOH g^{-1}	2.54
Density, kg m^{-3}	922.2
Viscosity, mPa s	90.33

2. 2. Methanolysis reaction

Methanolysis of the WCO was performed at 60 °C in a 250 cm^3 three-necked thermostated glass flask with a condenser and magnetic stirrer and the effects of mixing intensity (300 and 1000 rpm), the mass percentage of catalyst (2 and 1 wt.%) or the molar ratio of reactants (6:1 and 10:1) on the rate of methanolysis were analyzed. The samples were taken out from the reactor at different reaction times at intervals of 15 min for 6 h. The beginning of methanolysis (*t* = 0) was defined as the time point when the reaction temperature was reached. The samples were analyzed after filtration by gas chromatography (Varian 3400, Varian, Ireland) with a FID detector, on-column injector and a MET-Biodiesel capillary GC column (14 m × 0.53 mm, film thickness 0.16 μm) [29,30,32]. The schematic diagram of the one and two-step transesterification routes is presented in Figure 1.
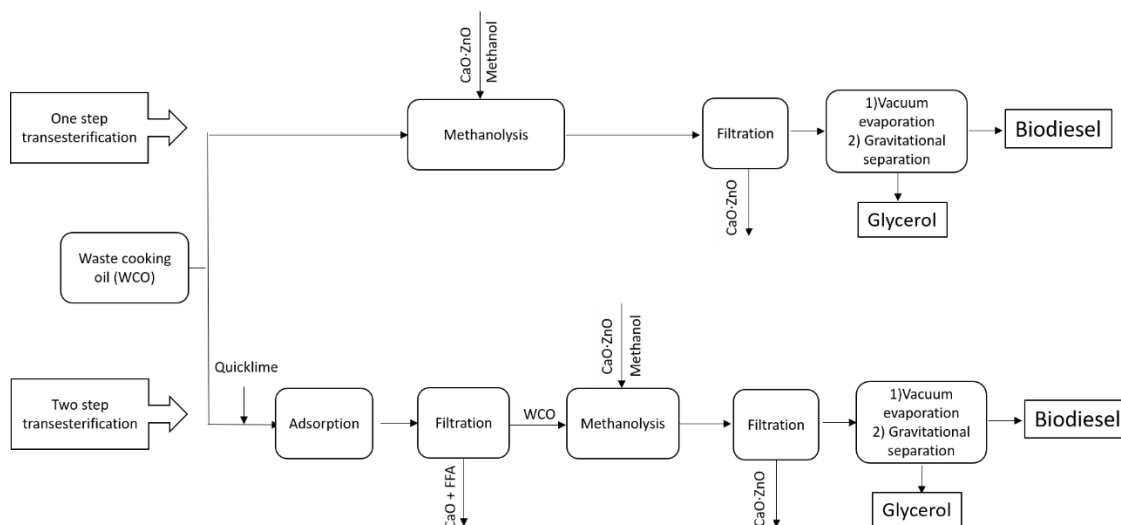
Figure 1. Process diagram of one and two-step transesterification processes applied in the study

2. 3. Pretreatment of WCO

The pretreatment of WCO was performed in a thermostated three-necked glass flask with a magnetic stirrer. When quicklime as an adsorbent was used to remove FFA, the WCO and a defined amount of quicklime were placed in the flask and mixed for 1 h at the preset temperature. The influence of quicklime calcination, amount, particle size, and pretreatment temperature on the efficiency of FFA removal was tested. In order to remove FFA by esterification, quicklime and a small amount of methanol (FFA to methanol = 1 : 3 molar ratio) and WCO were placed in the flask and mixed for 1 h at the desired temperature. Analysis of adsorption kinetics was performed under the condition determined as optimal (uncalcined quicklime, 30 °C, $d < 0.2$ mm, 1 wt.%). The samples were taken out from the flask at different times, and after filtration, analyzed by volumetric titration to determine FFA content.

2. 4. Acid number determination

Volumetric titration was applied to determine the acid value of oil [16]. The sample of WCO was dissolved in a mixture of toluene (≥99.7 % purity, VWR Chemicals, Austria) and isopropanol (≥99.8 % purity, Sigma-Aldrich, Germany). and phenolphthalein was added as an indicator. The prepared solution of WCO sample was titrated with potassium hydroxide solution and acid value was expressed as mg KOH g^{-1} of sample, required to titrate the sample to a specified endpoint. The acid value was calculated by using the following equation:

$$AN = \left(A - B\right) C \frac{56.1}{W}$$
(1)

where: AN is the acid number, A is the volume of KOH used to reach the endpoint (cm^3); B is the volume of KOH used for titration of the mixture without WCO or the so-called blank test (cm^3); C is the concentration of KOH (mol dm^3), and W is the mass of WCO sample (g). All the experiments and titrations were repeated three times and mean values were used. The experimental errors were less than ±2 %.

The FFA removal efficiency (X_{FFA}) was defined as the fraction of the FFA removed and determined from the acid value ratio:

$$X_{FFA} = \left[\frac{AN_0 - AN_t}{AN_0}\right] 100$$
(2)

where AN_0 is the acid value of the WCO at the beginning and AN_t is the acid value of the oil at the end of treatment (after 1 h).

2. 5. Adsorption kinetics

Among a number of kinetic models that have been proposed for the adsorption process, pseudo-first and second-order models are the most widely used because they are simple to describe the adsorption kinetics and the adsorbent-adsorbate interactions [14,29-31]. In the present study, these two models were used to describe the FFA adsorption on quicklime as the adsorbent. The correlated kinetic parameters were also obtained by the least square fitting method of the adsorption model with experimental adsorption data.

2. 5. 1. Pseudo-first order model

The pseudo-first order model [14,33,34] is proposed based on the assumption that the adsorption rate is proportional to the number of vacant adsorption sites. The adsorption rate can be expressed as:

$$\frac{dq}{dt} = k_1 \left(q_e - q_t\right)$$
(3)

where, q_e and q_t are the adsorption capacities at equilibrium and a given time, respectively, k_1 is the pseudo-first order kinetic constant.

The linear form of the Lagergren pseudo- first order equation can be written as [14]:

$$\log\left(q_e - q_t\right) = \log q_e - \frac{k_1 t}{2.303}$$
(4)

The q_e and k_1 were determined from the intercept and slope of the best linear fit of the plot log (q_e-q_t) *vs.* time. The pseudo-first order model represents the reversible interaction between the adsorbent and adsorbate, which is suitable to predict the adsorption behavior of physical adsorbents [34].

2. 5. 2. Pseudo-second order model

The pseudo-second order model is based on the assumption that the adsorption rate is proportional to the square of the number of vacant adsorption sites [34]. This model can be written as follows:

$$\frac{dq}{dt} = k_2 \left(q_e - q_t \right)^2 \tag{5}$$

where k_2 is the pseudo-second order rate constant. The linear form of second order equation is:

$$\frac{t}{q_t} = \frac{1}{k_2 q_e^2} + \frac{t}{q_e} \tag{6}$$

The parameters q_e and k_2 were determined from the intercept and slope of the least square linear fit of the plot t/q_e *vs.* time. The pseudo-second order model assumes that the interaction between the adsorbent and adsorbate is caused by the strong binding of adsorbate to the adsorbent surface, which is suitable to predict adsorption behavior which involves chemical interactions [35].

The significance of both kinetic models was statistically evaluated using the mean relative percent deviation (MRPD) between the experimentally determined and predicted values of q_e:

$$\text{MRPD} = \frac{100}{n} \sum_1^n \left| \frac{q_{e,\text{mod}} - q_{e,\text{exp}}}{q_{e,\text{exp}}} \right| \tag{7}$$

where $q_{e,\text{mod}}$ and $q_{e,\text{exp}}$ are predicted and experimental values, of q_e, respectively, and n is the number of experimental points.

2. 5. 3. Adsorption capacity

Experimental adsorption capacity of quicklime, q, was calculated by using equation [20]:

$$q = \frac{\left(C_0 - C_t \right) V}{m_{\text{ads}}} \tag{8}$$

where m_{ads} is the mass of the adsorbent, V is the volume of the solution, and C_0 and C_t are the initial and the adsorbate concentration in the solution at time t, respectively.

2. 6. FTIR analysis

Fourier-transform infrared (FTIR) spectra were recorded by using a BOMEM (Hartmann & Braun, Australia) spectrometer. Measurements were conducted in the wave number range of 4000–400 cm^{-1}, with 4 cm^{-1} resolution.

2. 7. XRD analysis

The phase composition was determined by the X-ray diffraction analysis (Cu Kα radiation, λ = 0.15418 nm, in the range of 2θ = 10–80°, step-length: 2θ = 0.01° scan time: 5 s) by using D/MAX–RB powder X-ray diffractometer (Rigaku Corporation, Japan).

2. 8. ICP analysis

The content of calcium leached in the oil during the pretreatment with CaO, and in biodiesel during the methanolysis with the CaO·ZnO catalyst was determined by inductively coupled plasma optical emission spectrometry, ICP-OES (iCAP 6500 Duo ICP, Thermo Fisher Scientific, Cambridge, United Kingdom). For this analysis, the samples were prepared by microwave digestion in an Advanced Microwave Digestion System (Ethos 1, Milestone, Italy) using a HPR-1000/10S high-pressure segmented rotor. The external calibration solutions were made from the certified plasma standard solution:

Multi-Element Plasma Standard Solution 4, Specpure®, 1000 µg cm^{-3} (Alfa Aesar GmbH & Co KG, Germany). Quantification of calcium was done at the emission wavelength: Ca II 315.887 nm. Calcium concentration in the samples was expressed as mg kg^{-3} (ppm).

3. RESULTS AND DISCUSSION

3.1 One-step transesterification of WCO using the CaO·ZnO catalyst: influence of different reaction conditions

Since the mechanochemically synthesized CaO·ZnO catalyst has shown good activity in the methanolysis of sunflower and used vegetable oils [29], the influence of different reaction conditions on the rate of methanolysis was further studied.

The agitation speed has a significant influence on the rate of the process since its increase causes a reduction in the dispersed phase (methanol) drop size and an increase in the specific interfacial area between the two immiscible phases (WCO and methanol). This effect enables faster TG mass transfer and the period of usually slow period of transesterification is significantly shorter [29,32]. When agitation speed in methanolysis of WCO was 300 rpm, the initial period lasted 45 min, while for 1000 rpm it was practically eliminated, indicating that the mass transfer resistance at the beginning of methanolysis of WCO is less pronounced (Fig 2a). It can be concluded that more intensive mixing, *i.e.* higher agitation speeds, increased the methanolysis rate as a result of reduced mass transfer resistance and better suspension of the catalyst in the reaction mixture.
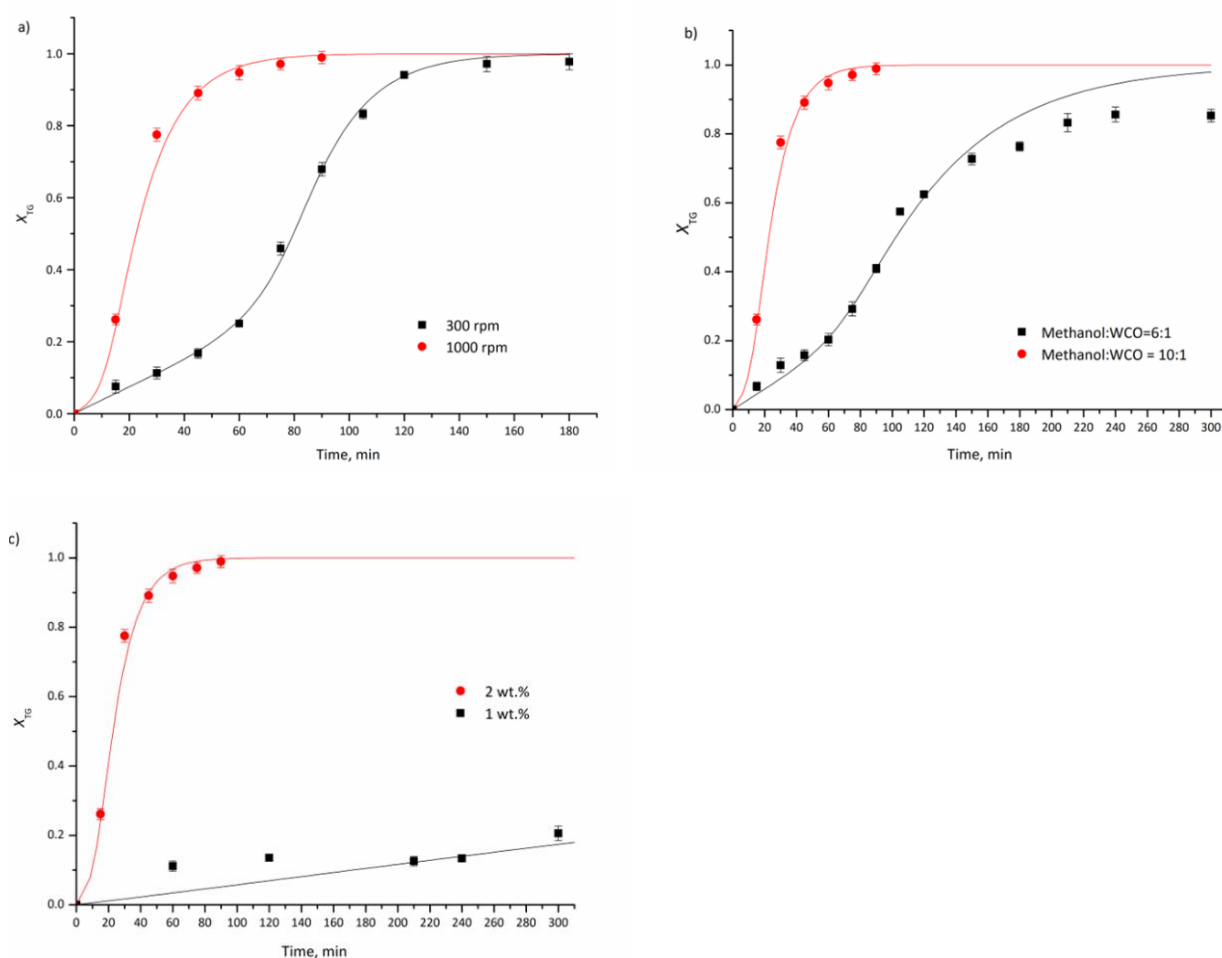
Figure 2. Triglyceride conversion versus time for WCO methanolysis at 60 °C as a function of a) agitation speed (methanol to oil molar ratio = 10:1, 2 wt.% of catalyst); b) methanol to oil molar ratio (agitation speed 1000 rpm, 2 wt.% catalyst); c) catalyst amount (methanol to oil molar ratio =10:1; agitation speed 1000 rpm)

Fig. 2b) shows the influence of the molar ratio of methanol to oil on the methanolysis rate. At the lower ratio, the fraction of dispersed phase (methanol) in the reaction mixture is decreased, and also the specific interfacial area between methanol and oil, which is directly proportional to the fraction of dispersed phase. Because of that, the molar ratio of methanol to oil mostly affects the TG mass transfer, but the initial period is not so pronounced as in the case of methanolysis of sunflower oil at a lower agitation speed [32]. The rate of the chemical reaction on the catalyst surface was lower at a lower molar ratio, and also the maximum obtained yield of FAME which did not exceed 85 %. The lower molar ratio affects the slow and final period of transesterification, which is characterized by approaching the equilibrium composition between FAME and glycerol. A smaller concentration of TG and an increased concentration of glycerol close to the surface of a solid catalyst, with the very low methanol concentration, improve the rate of the reversible reaction between FAME and glycerol, which could be the main reason for the achieved lower FAME yield.

TG conversion *vs*. time is shown in Fig. 2c) for different initial amounts of catalyst. When the reaction mixture contained 1 wt.% of catalyst, even after 5 h of reaction, TG conversion reached only 23 %. WCO contains a certain amount of FFA (Table 1) and other compounds formed during the use of fresh vegetable oil at high temperature for food preparation (thermal processing of food). Thus, the reason for very slow transesterification could be mainly FFA adsorption on the catalyst active cites, blocking them, and causing the part of the catalyst not to be available for TG transesterification.

3. 2. Pretreatment of WCO

3. 2. 1. Adsorption using quicklime

Results of WCO methanolysis with a smaller amount of catalyst indicated the negative effect of FFA on the methanolysis process, suggesting that some pretreatment should be applied. The idea of using quicklime for the pretreatment was to reduce the amount of FFA present in WCO by simple adsorption. Detailed characterization of used material has been reported previously and only a short overview of these results is reported in the present paper. The XRD analysis indicated the peaks originated from the well-crystallized CaO phase, which is the main phase of raw quicklime, with only barely noticeable peaks of $Ca(OH)_2$ [31]. Raw quicklime has a low specific surface area of 4.6 m^2 g^{-1}, with the total pore volume of 85 mm^3 g^{-1}, and the basic strength in the range of 9.3–10.0 [31]. According to the results of the analysis of textural properties, quicklime used without calcination has a very low porosity and can be even classified as a nonporous material [31].

The efficiency of FFA removal was investigated with respect to the influence of quicklime calcination, amount, particle size, and pretreatment temperature (Table 2). The use of quicklime without calcination resulted in a slightly better decrease in the FFA content. It was higher at higher temperatures, however, at 60 °C formation of soaps was visually observed, not present at lower temperatures.

Table 2. Removal efficiency of FFA at different conditions (t = 1h in all experiments)

T / °C	Calcination temperature, °C	Particle size, mm	Quicklime content, wt.%	X_{FFA} / %
60	550	<0.2	1	88
60	/	<0.2	1	94
40	/	<0.2	1	58
30	/	<0.2	1	72
30	/	0.2<d<0.6	1	41
30	/	0.2<d<0.6	2	55
30	/	0.6<d<0.8	1	8
30	/	0.6<d<0.8	4	33

The reason for this finding could be desorption of the formed compound between CaO and FFA, which is an endothermal process and, thus, at lower temperatures adsorption of FFA at the surface of the particles is more pronounced. An increase in temperature causes desorption of the molecules from the surface [2], in this case soaps formed in the reaction of CaO with FFA, which became visible in the mixture. When smaller particle sizes were used (diameter < 0.2 mm), a higher FFA removal was achieved, caused by a higher surface area available for the adsorption. The amount

of Ca^{2+} present in the oil after the pretreatment at optimal conditions (uncalcined quicklime, 30 °C, *d* < 0.2 mm, 1 wt.%) was determined to be 12.64 mg kg^{-1}, showing that very small amount of calcium from CaO was dissolved in the treated WCO.

3. 2. 2. Adsorption kinetics

The removal of FFA on quicklime adsorbent as a function of contact time, under condition determined as optimal (uncalcined quicklime, 30 °C, *d* < 0.2 mm, 1 wt.%) was studied with the aim to determine the required time to reach the equilibrium conditions and results are presented in Fig. 3a.
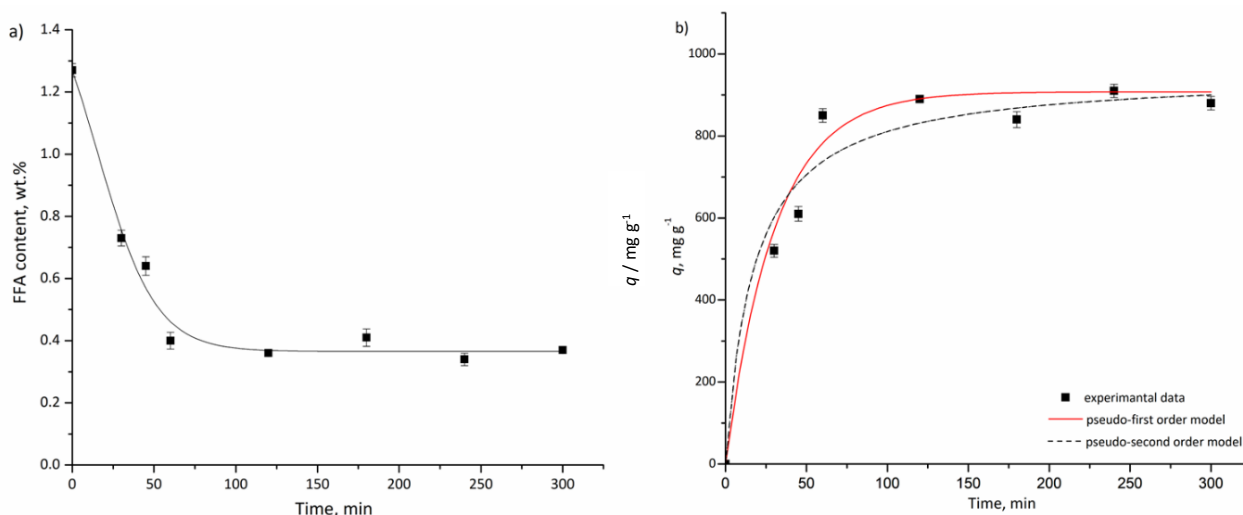
Figure 3. FFA adsorption at quicklime over time at optimal adsorption conditions (30 °C, d < 0.2 mm, 1 wt.%): a) FFA content reduction; b) adsorption capacity of quicklime determined experimentally and calculated by using kinetic models with kinetic parameters determined by least-squares fits

It can be seen that the concentration of FFA present in the oil (1.27 wt.% at the beginning) decreased over time and reached a constant value (0.44 wt.%), indicating the attainment of equilibrium at which further adsorption was not possible. The time necessary to reach equilibrium was about 60 min under the operating conditions used in this work. Similarly, it has been reported that 60 min was required to reach the equilibrium for adsorption of oleic acid added to sunflower oil (3 wt.%) on zeolite 13X at 30 °C, but with 10 wt.% of the adsorbent [17], while much longer contact time, 240–300 min was necessary for oleic acid adsorption from vegetable oils onto different anion exchange resins [15,16] as well as for FFA adsorption from crude palm oil on magnesium silicate derived from rice husk [23]. Additionally, Ilgen reported that adsorption of oleic acid from sunflower oil on Amberlyst A26 (OH) resin reached equilibrium after 360 min regardless of the temperature and adsorbent amount [14].

Analysis of the adsorption kinetics was performed by using the pseudo-first (Eq. 4) and pseudo-second order (Eq. 6) kinetic models. The pseudo-first model parameters q_e and k_1 were determined from the intercept and slope of plot log (q_e - q_t) versus time (Fig. D-1a, Supplementary material), while pseudo-second model parameters q_e and k_2 were determined from the intercept and slope of t/q_e versus time (Fig. D-1b), Supplementary material) and the obtained values are presented in Table 5. Comparison of the experimental data and calculated using kinetic models is presented in Fig. 3b. According to the obtained values of correlation coefficient R^2, the pseudo-second order model better describes the adsorption of FFA from WCO onto quicklime as adsorbent. In addition, in order to provide more relevant information on the models' adequacy, MRPD between the values of q_e determined experimentally and predicted by models was calculated. The MRPD of ± 6.2 and 8.0 % for the pseudo-first and the pseudo-second model, respectively, suggested that slightly better agreement was accomplished with pseudo-first order model. Due to the contradictory results of R^2 and MRPD, as well as the fact that 5 out of 7 measured data are already at equilibrium, no definite conclusion about the best kinetic model can be drawn. In the literature, both models were successfully used to describe adsorption kinetics. It was reported that adsorption of oleic acid from sunflower oil on Amberlist 26 (OH) resin [14], iron

oxide magnetic nanoparticles [21] and zeolite 13X at higher temperatures of 50 and 75 °C [17] followed the pseudo-second order kinetic model, while for adsorption onto the zeolite 13X at 30 °C and ion-exchange resin [15] followed the pseudo-first order kinetic model. It was also observed that both models describe the data well with correlation coefficients greater than 0.99 in adsorption process using two mixed bed ion-exchange [16].

Table 3. Kinetic model parameters

	Pseudo-first order			Pseudo-second order		
q_e (exp) / mg g^{-1}	k_1 / min^{-1}	q_e (calc) / mg g^{-1}	R^2	k_2 / g mg^{-1} min^{-1}	q_e (calc.) / mg g^{-1}	R^2
910	0.033	907.8	0.898	6.01·10^{-5}	952.4	0.992

The experimentally determined equilibrium adsorption capacity of quicklime was 910 mg g^{-1}. This value is higher than most of the removal capacities reported in literature for different adsorbent materials, which were in the range from 18 to 647 mg g^{-1} [10–12,14–17,20,23]. Only Pereira et al. obtained much higher values of adsorption capacity (2750–7000 mg g^{-1}) for Ca(OH)$_2$ nanoplates supported on activated carbon as adsorbents [18]. However, it is necessary to highlight the advantage of quicklime used in this study - it is a cheap, available, natural material and can be used without any heat treatment.

3.2.3 FTIR analysis

FTIR spectra of quicklime before and after different times of the adsorption process are shown in Fig. 4.
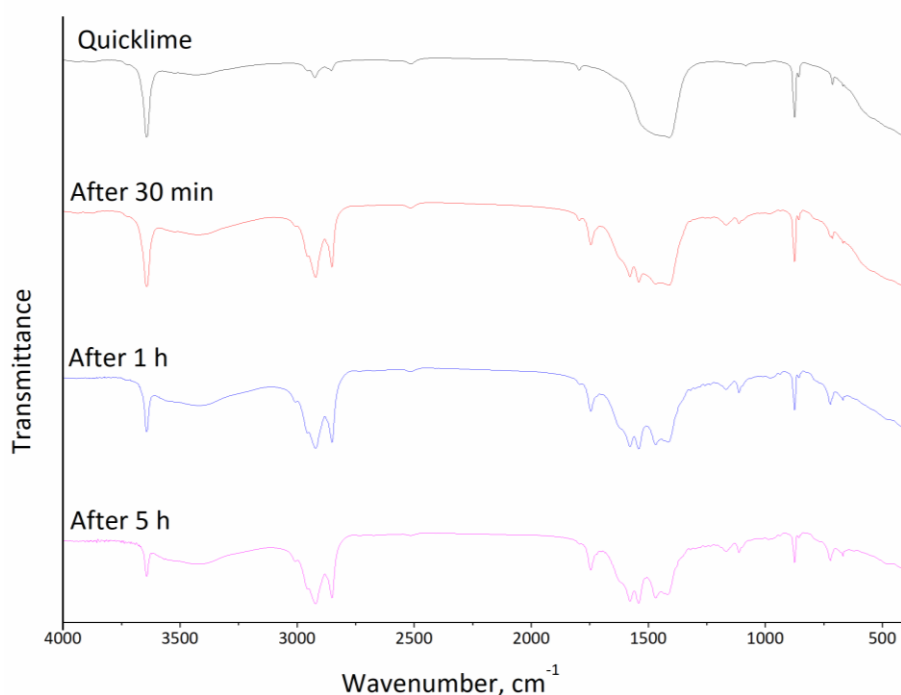
Figure 4. FTIR spectra of quicklime before and at different times of the adsorption process

The spectrum of quicklime indicates only the presence of calcium carbonate (the broad band centered at 1465 cm^{-1} and bands at 874 and 712 cm^{-1}) as well as OH groups of Ca(OH)$_2$ (the sharp band at 3643 cm^{-1}). Also, the regions at 3000–3500 cm^{-1} correspond to the possible contribution of water physisorbed on the surface of CaO, which is the result of very rapid carbonation and hydration of CaO in air [30]. After FFA adsorption, bands at 2932, 2882, and 2846 cm^{-1} appeared, associated with symmetrical and asymmetrical C–H stretching vibrations of –CH$_2$ and CH$_3$ groups of FFA. The carboxylate bands typically exist in pairs corresponding to the asymmetric and symmetric carboxylate vibrations at 1575–1530 and 1460–1400 cm^{-1}, respectively [36]. A doublet band of carboxylate groups associated with calcium ions at around 1540 and 1575 cm^{-1} appears at higher concentrations of adsorbed FFA [18,37]. According to Lu and Miller, it

is assigned to physically adsorbed FFA [37], while Cano et al. reported that the presence of vibration bands of coordinated carboxylate groups (1524 and 1408 cm^{-1}) indicates covalent binding of FFA [21]. The peak at 1453 cm^{-1} corresponds to CH bending, and the peak at 1436 cm^{-1} to symmetric COO− stretching [37], while absorption in the 1746 cm^{-1} region is characteristic of ester stretching of carbonyl group C=O and indicates possible oil contamination on quicklime [18]. The presence of carboxylate ion is clearly visible at all spectra of quicklime after the adsorption of FFA confirming the interaction of the carboxyl group in FFA with the active site of the adsorbent.

3.2.4. Esterification using quicklime

In the present work, the idea of adding a small amount of methanol (FFA to methanol molar ratio = 1:3) was explored with the intention to remove FFA in the reaction with methanol and not only by adsorption, where quicklime would act as a catalyst for esterification. At 30 °C almost the same efficiency in the FFA removal was achieved as without methanol (68 % compared to 72 %, Table 2), while at 60 °C it was much lower (57 % compared to 94 % removal, Table 2). It might be concluded that the use of methanol during pretreatment of WCO did not have a significant effect on the FFA removal and that methanol decreased the CaO capacity for FFA adsorption. The same conclusion was derived when methanol was added to an oleic acid/soybean oil system with the mixture of two mixed bed ion-exchange resins (Dowex Monosphere MR-450 UPW and Amberlite MB-150) [16].

According to the above results, the following conditions for pretreatment of WCO were proposed: 1 wt.% of quicklime based on the amount of oil; temperature of 30 °C, the particle size *d* < 0.2 mm and 1 h time in the batch process with mixing intensity of 1000 rpm.

3. 3. Methanolysis of pretreated WCO

After the pretreatment, quicklime was removed by filtration, and the oil with the decreased FFA content to 0.44 % was subjected to methanolysis with using CaO·ZnO as a catalyst at 60 °C. The results are compared to those obtained in the direct methanolysis of WCO under the same conditions (Fig. 5). As can be seen, the WCO pretreatment had a positive effect on the methanolysis process rate. The achieved FAME yield was over 96 % after 15 min, while the same FAME yield was detected only after 1 h of transesterification without the pretreatment.
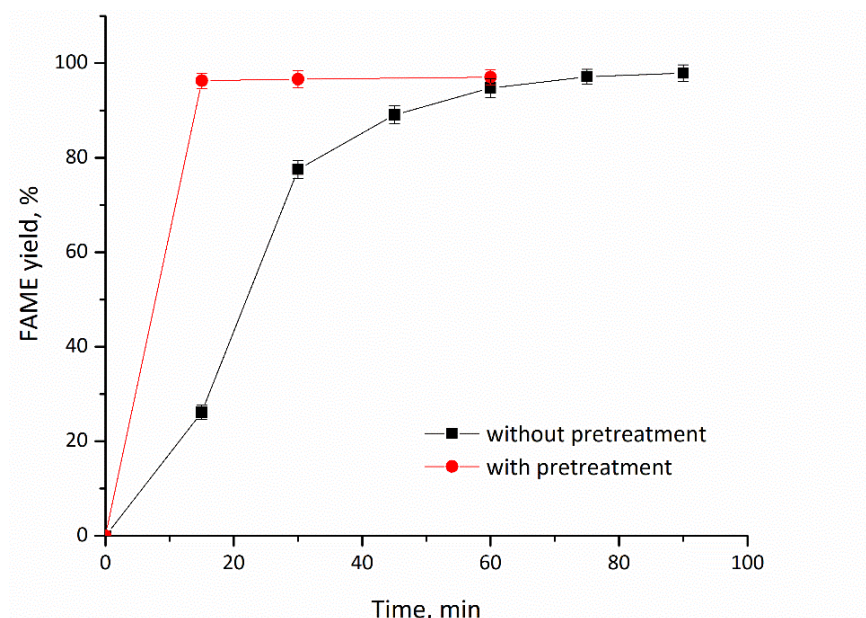
Figure 5. FAME yield in WCO methanolysis with the use of CaO·ZnO catalyst (reaction conditions: 60 °C, 1000 rpm, methanol to oil molar ratio of 10:1, 2 wt.% of catalyst)

Two-step processes were frequently reported in literature, however, studies in which the FFA content is decreased by adsorption in the first stage of the two-step process are few. Ilgen reported that after the oleic acid content was

decreased to 0.2 % via adsorption by using Amberlyst 26 (OH), transesterification with KOH enabled the biodiesel yield of 94 % [14]. Similarly, after the pretreatment of soybean oil mixed with oleic acid using Ca(OH)$_2$/activated carbon, transesterification with the use of NaOH as a homogeneous catalyst, resulted in FAME yields of 96-98 % [18]. Results from the present study are in line with the majority found in the literature reported for CaO or CaO-based catalysts [38]. Most of pure CaO catalysts or modified by doping with different compounds, supporting onto carriers, or mixing with other metal oxides are efficient in transesterification of virgin oils or feedstock with low free fatty acid contents, however, weaker catalytic activity in the presence of moisture and high FFA feedstock was observed [38]. Moreover, methanolysis of WCO using CaO derived from waste oyster shells gave a maximum biodiesel yield of 87.3 % after 3 h of reaction time under the optimized conditions (9:1 methanol to oil molar ratio, 6 wt.% of catalyst) [39]. Similarly, biodiesel yield of 93.4 % was obtained in a pilot-scale microreactor using WCO with the acid value of only 0.04 mg KOH g^{-1} oil and limescale as a catalyst [40]. The maximum FAME yield was 93.7 % in methanolysis of WCO with the FFA content of 1.1 wt.% catalyzed with zeolite supported CaO derived from chicken eggshell [41], while with Zn doped CaO nanocatalyst the yield of 96.7 % was attained under the reaction conditions of 20:1 methanol to oil molar ratio, 5 wt.% catalyst loading after 4 h with WCO containing 0.84 wt.% of FFA [42]. Magnetic CaO/ZnFe$_2$O$_4$ hollow microspheres showed high catalytic performance with 98 % biodiesel yield obtained under optimized conditions, including the molar ratio of methanol to oil of 12:1 and catalyst concentration of 6 wt.% at 65 °C for 3 h, but the acid value of WCO was only 0.73 mg KOH g^{-1} oil [43]. An algal biochar/CaO/K$_2$CO$_3$ catalyst enabled the yield of 98.8 % in transesterification of WCO, however, a two-step process was applied, and transesterification was performed after reducing the FFA content to < 1 % by esterification with HCl [44]. The two-step process proposed in the present study allowed obtaining a high FAME yield from WCO with the FFA content > 1 % in a shorter time compared to most of the results reported in literature, as well as compared to the one-step process with mixed oxides CaO·ZnO used as a catalyst.

Possibility to reuse the catalyst in methanolysis was also examined. After each run, the liquid product was separated from the solid catalyst that remained at the bottom of the flask. A new batch of oil and methanol were added to the flask and the subsequent cycle was carried out under the same reaction conditions. The solid catalyst was reused without any purification in several repeated FAME synthesis. In the case of WCO use without pretreatment, in the second repeated test, a substantial decrease in the catalyst activity and FAME yield of only 11.8 % were observed, Figure 6. Still, the reusability test with pretreated oil showed that the FAME yield in the second run, although higher than without pretreatment, was still unsatisfactory amounting to only 46.6 % (Figure 6).
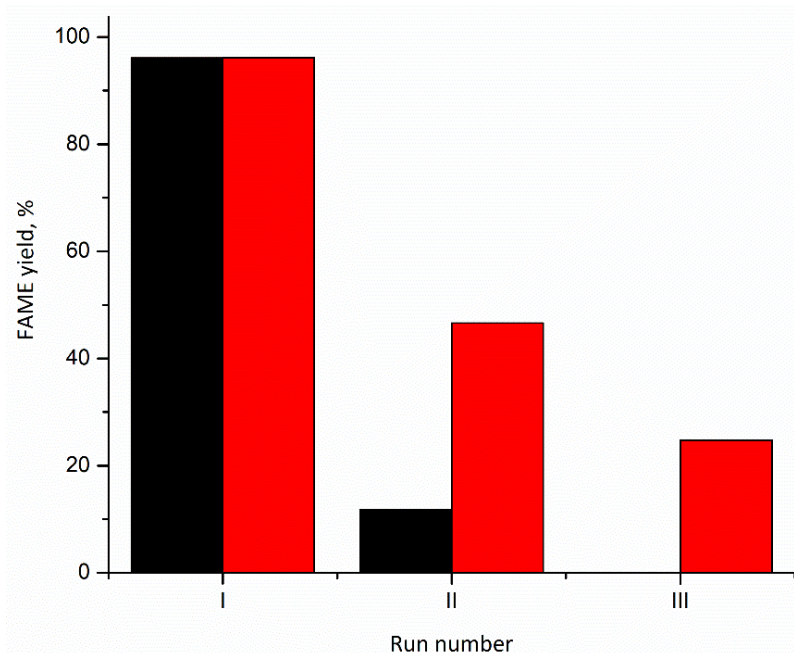
Figure 6. Reuse of the catalyst: FAME yields in 3 consecutive runs; ■—WCO without the pretreatment; ■—WCO after pretreatment with quicklime

Leaching of active species from the solid catalyst could be one of the reasons for the drop in activity. Solubility of the CaO·ZnO catalyst in methanol was negligible [29,30], however, López Granados et al. showed that the solubility of pure CaO is one order of magnitude higher in a biodiesel–glycerol–methanol mixture than in methanol [45]. Thus, the concentration of Ca^{2+} ions present in the FAME phase after methanolysis of the pretreated WCO and catalyst removal was analyzed, amounting to 229 mg kg^{-1}. This value is lower than some other reported for CaO-based catalysts. Namely, leaching from CaO from eggshell supported on a fly ash-based zeolitic material into sunflower oil yielded the concentration of 1170.4 mg kg^{-1} [46], while from the CaO-based catalyst derived from palm kernel shell biochar it was 722 mg kg^{-1} [47]. Besides, solubility of the neat CaO in the modeled biodiesel-methanol-glycerol mixture was reported to be 600 mg dm^{-3} (or 680 mg kg^{-1}) [45]. On the contrary, lower leaching was also reported, for example, for a CaO/ZnFe$_2$O$_4$ hollow magnetic microspheres catalyst yielding the concentration of 21.3 mg kg^{-1} [43] or CaO prepared with pectin as a modifier amounting to 0.7 mg kg^{-1} [48]. Nevertheless, the leached amount of calcium ions can be considered as low and not sufficient to reduce the catalytic activity of the CaO·ZnO catalyst [46].

Since the reason for a decrease in activity could be a change in the catalyst structure, or adsorption of products formed during the transesterification process, the catalyst after methanolysis of the pretreated WCO was characterized by using FTIR and XRD analyses (Figure 7).
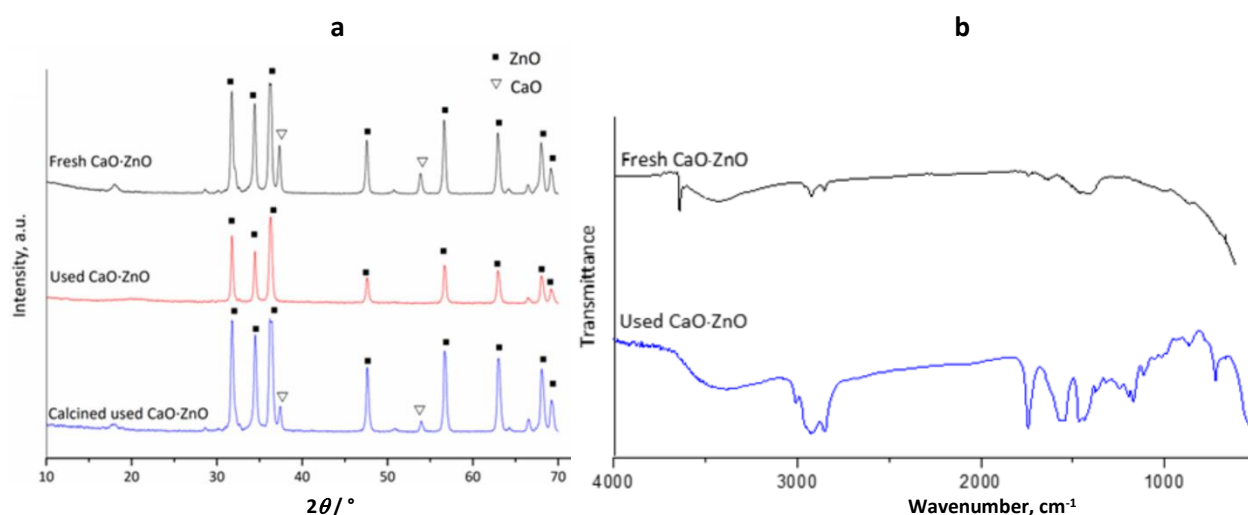
Figure 7. Analyses of the fresh CaO·ZnO catalyst and after methanolysis of the pretreated WCO: a) XRD patterns; b) FTIR spectra

Figure 7a shows diffractograms of the catalyst after the methanolysis reaction and after the reaction and calcination at 700 °C. The XRD pattern of the used catalyst revealed only peaks characteristic for ZnO, while peaks corresponding to CaO were not observed neither the peaks of other Ca compounds that could have been formed in the reaction of Ca with glycerol or the mixture of glycerol and methanol (*e.g.* Ca glyceroxide). This means that there could have been either a change in the structure of the catalyst or "poisoning" of the active sites, in this case CaO, by various compounds present in the reaction mixture. Therefore, after the used catalyst was calcined at 700 °C, peaks corresponding to CaO appeared in the XRD pattern, but of slightly lower intensity compared to the starting catalyst. This indicates that the active sites are probably blocked, and the FTIR spectra can provide more information about organic compounds that could have blocked the active centers of the catalyst.

The FTIR spectra of the used catalyst confirmed the presence of organic compounds on the catalyst surface (Fig. 7b). The intense band at 1744 cm^{-1} originates from the stretching vibration of the ester carbonyl functional group (C=O), and at 1171 cm^{-1} from the stretching vibration of the C–O bond [49]. Bands at around 1457 and 1568 cm^{-1} when appearing together in the spectrum are attributed to the symmetric and asymmetric vibrations of carboxylate groups and may indicate that chemisorption of FAME molecules has occurred [49]. More intense bands at 2922 and 2852 cm^{-1} in the FTIR spectrum of the catalyst after transesterification is assigned to the asymmetric and symmetric stretching vibrations of methylene groups of the alkyl chain of FAME [49].

4. CONCLUSION

High FAME yields could be achieved in methanolysis of WCO using CaO·ZnO catalyst under different reaction conditions. However, presence of FFA has a negative impact on the methanolysis rate so that the pretreatment of WCO using quicklime was proposed in the present work for the acid removal. The results showed that FFA from WCO could be successfully removed using quicklime as adsorbent at a lower temperature of 30 °C with the removal efficiency of 72 % and the equilibrium adsorption capacity of 910 mg g^{-1}. When the pretreated oil was used as feedstock for methanolysis with a CaO·ZnO catalyst, a higher rate of transesterification was observed compared to methanolysis of untreated WCO, with over 96 % of FAME yield achieved after 15 min of the process. Based on the obtained results, it can be concluded that quicklime has considerable potential for the FFA removal from WCO, being cheap, available, and efficient. Besides, both adsorption and heterogeneously catalyzed methanolysis are environmentally and economically acceptable processes.

REFERENCES

[1]   Enweremadu CC, Mbarawa MM, Technical aspects of production and analysis of biodiesel from used cooking oil—A review. *Renew Sust Energ Rev.* 2009; 13: 2205–2224. https://doi.org/10.1016/j.rser.2009.06.007

[2]   Maddikeri GL, Pandit AB, Gogate PR, Intensification Approaches for Biodiesel Synthesis from Waste Cooking Oil: A Review. *Ind Eng Chem Res.* 2012; 51: 14610–14628. https://doi.org/10.1021/ie301675j

[3]   Yaakob Z, Mohammad M, Alherbawi M, Alam Z, Sopian K, Overview of the production of biodiesel from waste cooking oil. *Renew Sust Energ Rev.* 2013; 18: 184–193. https://doi.org/10.1016/j.rser.2012.10.016

[4]   Refaat AA, Different techniques for the production of biodiesel from waste vegetable oil. *Int J Environ Sci Tech.* 2010; 7(1): 183–213. https://doi.org/10.1007/BF03326130

[5]   Çanakçi M, Van Gerpen J, A pilot plant to produce biodiesel from high free fatty acid feedstocks *Trans ASABE.* 2003; 46: 945–954. https://doi.org/10.13031/2013.13949

[6]   Corro G, Tellez N, Jimenez T, Tapia A, Banuelos F, Vazquez-Cuchillo O, Biodiesel from waste frying oil. Two step process using acidified SiO$_2$ for esterification step. *Catal Today* 2011; 166: 116–122. https://doi.org/10.1016/j.cattod.2010.09.011

[7]   Wang Y, Ou S, Liu P, Zhang Z, Preparation of biodiesel from waste cooking oil via two-step catalyzed process. *Energy Convers Manag.* 2007; 48: 184–188. https://doi.org/10.1016/j.enconman.2006.04.016

[8]   Cvengros J, Cvengrosova Z, Used Frying Oils and Fats and their Utilization in the Production of Methyl Esters of Higher Fatty Acids. *Biomass Bioenerg.* 2004; 27: 173–181. https://doi.org/10.1016/j.biombioe.2003.11.006

[9]   Díaz L, Brito A, FFA Adsorption from Waste Oils or Non-Edible Oils onto an Anion Exchange Resin as Alternative Method to Esterification Reaction Prior to Transesterification Reaction for Biodiesel Production. *J Adv Chem Eng.* 2014; 4: 105. http://dx.doi.org/10.4172/2090-4568.1000105

[10]   Demirbas A, Sari A, Isildak O, Adsorption thermodynamics of stearic acid onto bentonite. *J Hazard Mater.* 2006; 135: 226–231. https://doi.org/10.1016/j.jhazmat.2005.11.056

[11]   Sari A, Iþýldak Ö, Adsorption properties of stearic acid onto untreated kaolinite. *Bull Chem Soc Ethiop.* 2006; 20(2): 259–267. https://doi.org/10.1016/10.4314/bcse.v20i2.61410

[12]   Bayrak Y, Application of Langmuir isotherm to saturated fatty acid adsorption. *Microporous and Mesoporous Mater.* 2006; 87: 203–206. https://doi.org/10.1016/j.micromeso.2005.08.009

[13]   Sari A, Soylake M, Equilibrium and thermodynamic studies of stearic acid adsorption on Celtek clay. *J Serb Chem Soc.* 2007; 72(5): 485–494. https://doi.org/10.2298/JSC0705485S

[14]   Ilgen O, Adsorption of oleic acid from sunflower oil on Amberlyst A26 (OH). *Fuel Process Technol.* 2014; 118: 69–74. http://dx.doi.org/10.1016/j.fuproc.2013.08.012

[15]   Maddikeri GL, Pandit AB, Gogate PR, Adsorptive Removal of Saturated and Unsaturated Fatty Acids Using Ion-Exchange Resins. *Ind Eng Chem Res.* 2012; 51: 6869–6876. http://dx.doi.org/dx.doi.org/10.1021/ie3000562

[16]   Jamal Y, Boulanger BO, Separation of oleic acid from soybean oil using mixed-bed resins. *J Chem Eng Data* 2010; 55: 2405–2409. http://dx.doi.org/10.1021/je900829c

[17]   Ilgen O, Dulger HS, Removal of oleic acid from sunflower oil on zeolite 13X: Kinetics, equilibrium and thermodynamic studies. *Ind Crops Prod.* 2016; 81: 66–71. http://dx.doi.org/10.1016/j.indcrop.2015.11.050

[18]   Pereira MRDN, Salviano AB, de Medeiros TPV, Santos MRD, Cibaka TE, de Andrade MHC, de Oliveira Porto A, Lago RM. Ca(OH)$_2$ nanoplates supported on activated carbon for the neutralization/removal of free fatty acids during biodiesel production. *Fuel* 2018; 221: 469–475. http://dx.doi.org/10.1016/j.fuel.2018.01.123

[19] Nor Shafizah I, Irmawati R, Omar H, Yahaya M, Alia Aina A, Removal of free fatty acid (FFA) in crude palm oil (CPO) using potassium oxide/dolomite as an adsorbent: Optimization by Taguchi method. *Food Chem.* 2022; 373: 131668. https://doi.org/10.1016/j.foodchem.2021.131668

[20] Díaz L, Mertes L, Brito A, Rodríguez KE, Valorization of energy crop shells as potential green adsorbents for free fatty acid removal from oils for biodiesel production. Biomass Convers Bioref. 2022; 12: 655–668. https://doi.org/10.1007/s13399-020-01089-y

[21] Cano M., Sbargoud K., Allard E., Larpent C, Magnetic separation of fatty acids with iron oxide nanoparticles and application to extractive deacidification of vegetable oils. *Green Chem.* 2012; 14: 1786–1795. https://doi.org/10.1039/c2gc35270b

[22] Kalapathy U, Proctor A, New Method for Free Fatty Acid Reduction in Frying Oil Using Silicate Films Produced from Rice Hull Ash. *JAOCS.* 2000; 77(6): 593–598. https://doi.org/10.1007/s11746-000-0095-4

[23] Clowutimon W, Kitchaiya P, Assawasaengrat P, Adsorption of Free Fatty Acid from Crude Palm Oil on Magnesium Silicate Derived From Rice Husk. *Eng J.* 15 2011; 15(3):15–25. https://doi.org/10.4186/ej.2011.15.3.15

[24] Kim M, Yoon SH, Choi E, Gil B, Comparison of the adsorbent performance between rice hull ash and rice hull silica gel according to their structural differences. *LWT-Food Sci Technol.* 2008; 41: 701–706. https://doi.org/10.1016/j.lwt.2007.04.006

[25] Topallar H, Bayrak Y, Investigation of Adsorption Isotherms of Myristic, Palmitic and Stearic Acids on Rice Hull Ash. *Turk J Chem.* 1999; 23: 193–198.

[26] Adam F, Chua JH, The adsorption of palmitic acid on rice husk ash chemically modified with Al(III) ion using the sol–gel technique. *J Colloid Interface Sci.* 2004; 280: 55–61. https://doi.org/10.1016/j.jcis.2004.07.006

[27] Bao Y, Zhou Q, Zhang M, Zhang H, Luan Q, Zhou W, Tang H, Huang F, Wet-spun nanoTiO$_2$/chitosan nanocomposite fibers as efficient and retrievable absorbent for the removal of free fatty acids from edible oil. *Carbohydr Polym* 2019; 210: 119–126. https://doi.org/10.1016/j.carbpol.2019.01.035

[28] Adewuyi A, Ogagbolo AI, Lau WJ, Oderinde RA, Synthesis of spinel ferrite and its role in the removal of free fatty acids from deteriorated vegetable oil. Chinese Journal of Chemical Engineering 2021; 40: 78–87. https://doi.org/10.1016/j.cjche.2020.08.054

[29] Lukić I, Kesić Ž, Maksimović S, Zdujić M, Liu H, Krstić J, Skala D, Kinetics of sunflower and used vegetable oil methanolysis catalyzed by CaO·ZnO. *Fuel* 2013; 113: 367–78. https://doi.org/10.1016/j.fuel.2013.05.093

[30] Kesić Ž, Lukić I, Brkić D, Rogan J, Zdujić M, Liu H, Skala D, Mechanochemical preparation and characterization of CaO·ZnO used as catalyst for biodiesel synthesis. *Appl Catal A* 2012; 427–428: 58–65. https://doi.org/10.1016/j.apcata.2012.03.032

[31] Miladinović MR, Krstić JB, Tasić MB, Stamenković OS, Veljković VB, A kinetic study of quicklime-catalyzed sunflower oil methanolysis. *Chem Eng Res Des.* 2014; 92(9) 1740–1752. https://doi.org/10.1016/j.cherd.2013.11.023

[32] Lukić I, Kesić Ž, Maksimović S, Zdujić M, Krstić J, Skala D. Kinetics of heterogeneous methanolysis of sunflower oil with CaO·ZnO catalyst: Influence of different hydrodynamic conditions. *Chem. Ind. Chem. Eng. Q.* 2014; 20: 425–439. https://doi.org/10.2298/CICEQ130514025L

[33] Qiu H, Lv L, Pan B, Zhang Q, Zhang W, Zhang Q, Critical review in adsorption kinetic models. *J Zhejiang Univ Sci A* 2009; 10(5)716–724. https://doi.org/10.1631/jzus.A0820524

[34] Song G, Zhu X, Chen R, Liao Q, Ding Y, Chen L, An investigation of CO$_2$ adsorption kinetics on porous magnesium oxide. *Chem Eng J.* 2016; 283: 175–183.

[35] Ho YS, McKay G, Pseudo-second order model for sorption processes. *Process Biochem.* 1999: 34(5): 451–465. https://doi.org/10.1016/S0032-9592(98)00112-5

[36] Filopoulou A, Vlachou S, Boyatzis SC, Fatty Acids and Their Metal Salts: A Review of Their Infrared Spectra in Light of Their Presence in Cultural Heritage. *Molecules* 2021; *26*(19): 6005. https://doi.org/10.3390/molecules26196005

[37] Lu Y, Miller JD, Carboxyl Stretching Vibrations of Spontaneously Adsorbed and LB-Transferred Calcium Carboxylates as Determined by FTIR Internal Reflection Spectroscopy. *J Colloid Interface Sci.* 2002; 256: 41–52. https://doi.org/doi:10.1006/jcis.2001.8112

[38] Zul NA, Ganesan S, Hamidon TS, Oh W-D, Hussin MH, A review on the utilization of calcium oxide as a base catalyst in biodiesel production. *J Environ Chem Eng* 2021: 9(4): https://doi.org/10.1016/j.jece.2021.105741

[39] Lin Y-C, Amesho KTT, Chen C-E, Cheng P-C, Chou F-C, A cleaner process for green biodiesel synthesis from waste cooking oil using recycled waste oyster shells as a sustainable base heterogeneous catalyst under the microwave heating system. *Sustain Chem Pharm* 2020; 17: 100310 https://doi.org/10.1016/j.scp.2020.100310

[40] Aghel B, Mohadesi M, Ansari A, Maleki M, Pilot-scale production of biodiesel from waste cooking oil using kettle limescale as a heterogeneous catalyst. *Renew Energy* 2019; 142: 207–214. https://doi.org/10.1016/j.renene.2019.04.100

[41] Yusuff AS, Gbadamosi AI, Atray N, Development of a zeolite supported CaO derived from chicken eggshell as active base catalyst for used cooking oil biodiesel production. *Renew Energy* 2022; 197: 1151–1162. https://doi.org/10.1016/j.renene.2022.08.032

[42] Borah MJ, Das A, Das V, Bhuyan N, Deka D, Transesterification of waste cooking oil for biodiesel production catalyzed by Zn substituted waste egg shell derived CaO nanocatalyst. *Fuel* 2019; 242: 345–354. https://doi.org/10.1016/j.fuel.2019.01.060.

[43] Torkzaban S, Feyzi M, Norouzi L, A novel robust CaO/ZnFe$_2$O$_4$ hollow magnetic microspheres heterogenous catalyst for synthesis biodiesel from waste frying sunflower oil, *Renew Energy* 2022; 200: 996–1007. https://doi.org/10.1016/j.renene.2022.09.077.

[44] Foroutan R, Mohammadi R, Razeghi J, Ramavandi B, Biodiesel production from edible oils using algal biochar/CaO/K$_2$CO$_3$ as a heterogeneous and recyclable catalyst. *Renew Energy* 2021; 168: 1207–1216. https://doi.org/10.1016/j.renene.2020.12.094

[45] López Granados M, Martín Alonso D, Sádaba I, Mariscal R, Ocón P, Leaching and homogeneous contribution in liquid phase reaction catalysed by solids: the case of triglycerides methanolysis using CaO. *Appl Catal B* 2009; 89: 265–272. https://doi.org/10.1016/j.apcatb.2009.02.014

[46] Pavlović SM, Marinković DM, Kostić MD, Janković-Častvan IM, Mojović LjV, Stanković MV, Veljković VB, A CaO/zeolite-based catalyst obtained from waste chicken eggshell and coal fly ash for biodiesel production. *Fuel* 2020; 267: 117171. https://doi.org/10.1016/j.fuel.2020.117171.

[47] Kostić MD, Bazargan A, Stamenković OS, Veljković VB, McKay G, Optimization and kinetics of sunflower oil methanolysis catalyzed by calcium oxide-based catalyst derived from palm kernel shell biochar. *Fuel* 2016; 163: 304–313. 10.1016/j.fuel.2015.09.042.

[48] Acosta PI, Campedelli RR, Correa EL, Bazani HAG, Nishida EN, Souza BS, Mora JR, Efficient production of biodiesel by using a highly active calcium oxide prepared in presence of pectin as heterogeneous catalyst. *Fuel* 2020; 271: 117651. https://doi.org/10.1016/j.fuel.2020.117651.

[49] López Granados M, Martín Alonso D, Sádaba I, Mariscal R, Ocón P, Surface chemical promotion of Ca oxide catalysts in biodiesel production reaction by the addition of monoglycerides, diglycerides and glycerol. *J Catal* 2010; 276: 229–236. https://doi.org/10.1016/j.jcat.2010.09.016

Adsorpcioni predtretman otpadnog jestivog ulja primenom kreča za sintezu metil estara masnih kiselina

Ivana Lukić¹, Željka Kesić¹, Miodrag Zdujić² and Dejan Skala¹

²Univerzitet u Beogradu, Tehnološko-metalurški fakultet, Karnegijeva 4, 11000 Beograd, Srbija
²Institut tehničkih nauka SANU, Knez Mihailova 35, 11000 Beograd, Srbija

(NAUČNI RAD)

Izvod

Sinteza biodizela iz različitih biljnih ulja ostvaruje se transesterifikacijom triglicerida sa metanolom ili reakcijom koja se obično definiše kao metanoliza. Korišćenje ulja lošijeg kvaliteta, kao što je otpadno jestivo ulje (engl. *waste cooking oil*, WCO), prate neželjene sporedne reakcije kao posledica povećanog sadrđžaja slobodnih masnih kiselina (engl. *free fatty acids*, FFA) i vode. Prisustvo FFA u tim uljima obično zahteva fazu prethodne obrade pre nego što se ulje podvrgne procesu transesterifikacije. U ovom radu istražena je heterogeno kanalizovana metanoliza WCO sa i bez predtretmana. Uklanjanje FFA iz WCO obavljeno je korišćenjem samo kreča ili uz dodatak male količine metanola (molarni odnos FFA prema metanolu = 1:3). Dobijeni rezultati su pokazali da se u predtretmanu WCO krečom na 30 °C nakon 1 h može smanjiti sadržaj FFA za 72%, dok je određeno da je ravnotežni kapacitet adsorpcije 910 mg g⁻¹. Predtretman adsorpcijom, kao jednostavnom operacijom, korišćenjem jeftinog kreča pod blagim uslovima, pozitivno je uticao na brzinu reakcije transesterifikacije s CaO·ZnO kao katalizatorom, omogućujući postizanje preko 96 % prinosa biodizela za samo 15 min, u poređenju sa potrebnim vremenskim periodom od 1 h za postizanje istog prinosa iz ulja bez predtretmana. Nadalje, prethodno tretirano WCO omogućuje povećan broj ciklusa ponovne upotrebe katalizatora i ukupnu uštedu potrebne količine katalizatora. Ova studija je pokazala da je kreč ekonomičan, ekološki prihvatljiv i održiv materijal za uklanjanje FFA iz WCO.

Stability evaluation of biodiesel supplemented with synthetic and bio-based antioxidants by a pressurized accelerated oxidation method

Nataša Đurišić-Mladenović[1], Milan Tomić[2], Biljana Pajin[1], Maja Buljovčić[1], Ivana Lončarević[1] and Milica Rankov Šicar[1,3]

[1]University of Novi Sad, Faculty of Technology Novi Sad, Novi Sad, Serbia
[2]University of Novi Sad, Faculty of Agriculture, Novi Sad, Serbia
[3]SP Laboratorija a.d., Bečej, Serbia

Abstract

This work examines pressurized accelerated oxidation by a RapidOxy tester as an alternative method for determination of biodiesel oxidation stability. Sunflower oil-based biodiesel was synthesized and treated with antioxidants: tert-butylhydroquinone (TBHQ) - a synthetic antioxidant known for its powerful protective effect, and a mixture of bio-based antioxidant compounds extracted from vinery waste, VWE$_{eth}$. The antioxidant potency of TBHQ was evaluated at varying temperatures (110 - 140 °C) and concentrations (250 - 2,000 mg dm^{-3}) by the RapidOxy method; assessment of selected results was performed by comparison with relevant data obtained by the standard Rancimat method. VWE$_{eth}$ was added in two high dosages to biodiesel (87,500 and 150,000 mg dm^{-3}) and analyzed at 140 °C by the RapidOxy method. Both antioxidants at all applied dosages showed beneficial effects on improving the oxidative stability of biodiesel, but not all of the achieved improvements reached the stability minimum identified by the EN14214 standard. The lowest addition of TBHQ seemed to have a similar effect as the tested dosages of VWE$_{eth}$ but these additions did not increase the induction period above the limit of 8 h; two-fold higher quantity of TBHQ was successful in this respect, increasing the initial oxidation stability by a factor of about 2, which was determined by both methods. The RapidOxy method proved to be a very fast method suitable for testing a large number of samples, which is particularly important for efficient testing of different types and doses of antioxidants.

Keywords: induction period; Rancimat; RapidOxy; *tert*-butylhydroquinone TBHQ; vinery waste ethanolic extract.

Available on-line at the Journal web address: http://www.ache.org.rs/HI/

1. INTRODUCTION

Currently, biodiesel represents the most widely used renewable substituent for conventional fuel for diesel engines. It is a biofuel consisting of fatty acid alkyl esters (FAAEs) that can be derived from different oleo feedstocks such as vegetable oils (edible and non-edible), waste cooking oils, animal fats, and algal or microbial oils. However, its usage is linked with some disadvantages over conventional fuel for a diesel engine as a consequence of distinct chemical composition that differs from the hydrocarbon (HC) nature of the fossil diesel. One of the most prominent lacks of biodieselis its low oxidation stability. Oxidation stability indicates the potency of a fuel to resist oxidative degradation. This property of biodiesel is linked to the presence of unsaturated fatty acid chains inherent in the oily feedstock composition. Fatty acid chains that exist in molecules of feedstock's triglycerides (or free fatty acids) are introduced into the molecules of FAAEs by the reaction of transesterification (or esterification) during the synthesis of biodiesel. By transesterification with, for instance, methanol, triglycerides are converted to fatty acid methyl esters (FAMEs) and glycerol. Double bonds in FAAEs represent the weakest points of biodiesel under the attack of aggressive oxidative species. In brief, deterioration of biodiesel composition by the oxidative degradation starts with the removal of hydrogen in (bis)allylic position relative to the double bond in (poly)unsaturated fatty acid chains in the presence of free

radicals, further creating reactive species through a multi-step reaction process [1-3]. Peroxides and hydroperoxides are primary oxidation products, but being unstable they further react forming various secondary products, including shorter-chain compounds such as aldehydes, alcohols, and low volatile acids, as well as polymers [3-5]. The composition change induced by the oxidation of unsaturated fatty acid chains of FAAEs deteriorates standardized fuel properties, primarily the acid value, viscosity, and sediment content. For biodiesel fuel applications, oxidative degradation can occur during storage or use in the vehicle's engine, causing the formation of deposits or mechanical component failure, involving injector blockage, filter plugging, and pump wear [1,4].

The use of antioxidant additives is the most usual way to improve the biodiesel oxidation stability towards reaching or maintaining the standardized quality. Concerning the origin, antioxidants can be synthetic or natural. Despite the efficiency, synthetic antioxidants exhibit significant drawbacks including toxicity, low biodegradability, and the high price that increases the already high cost of biodiesel. Thus, natural antioxidants attract increasing attention as an alternative for controlling oxidation in biodiesel with some of the studies reporting significant efficiencies of such additives [6-10]. Considering the type of stabilizing mechanism, antioxidants can be regarded as primary and secondary: primary antioxidants interrupt the oxidation chain reaction, while the secondary ones act indirectly, *e.g.* by complexing a metal acting as a catalyst for oxidation reaction, decomposing the existing hydroperoxides to a non-radical species, or by absorbing radiation in the initiation stage of oxidative processes [11]. Chemically, there are amine-based substances with antioxidant effects (*e.g.* N,N'-di-*sec*-butyl-*p*-phenylenediamine) [12], but phenolic antioxidants such as butylated hydroxytoluene (BHT), butylated hydroxyanisole (BHA), *tert*-butylhydroquinone (TBHQ), pyrogallol (PY), propyl gallate (PG), have been applied more frequently [13].

Several methods exist to determine the oxidation stability of biodiesel, with the most applicable being a method of accelerated degradation in a Rancimat instrument. A sample is placed in the heating block and intensively oxidized by air flow, resulting in the formation of volatile secondary oxidation products (mainly formic and acetic acids) that are transferred into a measuring flask with distilled water; after some time of analysis, large quantities of the oxidation products introduced into the water induce a sudden increase in the water conductivity. The time that corresponds to the inflection point in the oxidation curve (conductivity *vs.* time) is the so-called induction period [14]. The induction period determined by the Rancimat method under the standardized conditions (EN14112) is directly comparable with a limit of 8 h defined as the minimum oxidation stability by the European standard on biodiesel quality EN14214. However, this method is time-consuming particularly when testing or formulating different antioxidant additives. It also provides an incomplete analysis of the sample oxidation stability because the results are based only on detected highly volatile oxidation products [15]. An alternative method reported by Neumann *et al.* [16] is more rapid and it is based on the induction period determination as a consequence of the pressure loss in the oxygen atmosphere above the sample in a sealed reaction chamber due to oxygen consumption by all sample compounds (volatile and non-volatile) susceptible to oxidation [15]. This so-called PetroOXY method is standardized in the USA (ASTM D7545-14). In the EU it is included in a draft standard prEN16091:2021, which specifies the determination of the oxidation stability of middle distillate fuels, FAMEs, and their blends. The PetroOXY method provides the induction period as a time of accelerated oxidative degradation of the sample by heat (140 °C) in the atmosphere of oxygen (initial pressure of 700 kPa) till the moment when a pressure drop of 10% is detected in relation to the maximum pressure recorded. It has been determined that the time needed to achieve a fixed pressure drop is directly related to the fuel oxidation stability [16]. In both methods, Rancimat and PetroOXY, longer induction periods indicate better oxidation stability. However, none of the standards on biodiesel fuel quality define the oxidation stability limit towards the induction period determined by a pressurized accelerated method such as the PetroOXY. This is why several studies compared Rancimat and PetroOXY methods with the aim to establish a correlation between the results for biodiesel [15-17]: a linear dependence between the results of these two methods was confirmed, and it has been concluded that the regression models largely depends on the origin of biodiesel and the presence of antioxidant additives.

The aim of the present study was to evaluate the effect of antioxidant additions to biodiesel by the RapidOxy stability tester, which determines the induction period on the same principle as the pressurized PetroOXY method. The antioxidant potency of TBHQ as a synthetic antioxidant was evaluated at different temperatures and concentrations. Additionally, a

vinery waste ethanolic extract (VWE$_{eth}$) was prepared and preliminarily tested as an alternative bio-additive for the enhancement of biodiesel oxidation stability. The RapidOxy data were compared with selected values obtained by the Rancimat method at 110 ^{o}C. The study contributes to previous efforts to collect new data on the pressurized accelerated method for determination of biodiesel oxidation stability, and it also explores local biowaste as a source of valuable antioxidant additives.

2. MATERIALS AND METHODS

2. 1. Biodiesel synthesis

Biodiesel was synthesized from commercial refined sunflower oil (Serbia). The fatty acid composition is determined by the gas chromatographic (GC) method and presented in Table S-1 in the Supplementary Material. Oil was transesterified with methanol (p.a., Lachner, Czech Republic) in the presence of KOH (p.a., Alkaloid Skopje, North Macedonia) as a catalyst in a 2 dm^3 stainless steel reactor (methanol to oil mole ratio 5:1; 1 mas.% KOH catalyst in oil) at a temperature ~64 °C for 1 h. After the reaction, the product mixture was allowed to settle: the upper layer of biodiesel was collected, while the lower glycerol layer was discarded. Methanol was removed from biodiesel by rotary vacuum evaporation. Biodiesel was purified with warm distilled water and finally dried with silica gel. Characterization of biodiesel was performed in accordance with selected requirements of the EN 14214 standard.

2. 2. Preparation of vinery waste extract as an antioxidant bio-additive

Waste after the production of red wine in a local vinery (Vojvodina Province, Serbia) was collected in early autumn 2019 and dried at about 50 °C till constant mass. VWE$_{eth}$ was prepared as follows: a sample of dried vinery waste (10.0 g) was grounded by a laboratory mixer and added to 50 cm^3 of absolute ethyl alcohol (*p.a.*, Zorka Pharma, Serbia). This mixture was shaken by a laboratory shaker (Promax 2020, Heidolph, Germany) at 140 rpm for 48 h and then filtered into a 50-cm^3 volumetric flask followed by addition of ethanol to bring the volume to the mark. Multiple extracts were prepared in order to test repeatedly the addition of two extract's dosages to the synthesized biodiesel: 25 and 50 cm^3. After evaporation of the selected VWE$_{eth}$ dosage till dryness by a rotary vacuum evaporator (Laborota 4000, Heidolph, Germany), a known volume of biodiesel was added into the same evaporator rotating flask that kept rotating for about 20 min before analyzing the oxidation stability. Before the addition of biodiesel, the extract's dry matter was weighed in order to calculate the VWE$_{eth}$ dosages relative to the biodiesel volume. In this way, the tested dosages of VWE$_{eth}$ were 87,500 mg dm^{-3} (VWE$_{eth1}$) and 150,000 mg dm^{-3} (VWE$_{eth2}$). Finally, the oxidation stability of biodiesel samples blended with the extract's dry matter was analyzed using the RapidOxy instrument.

2. 3. Determination of biodiesel oxidative stability

A sample of synthesized biodiesel (before the treatment with antioxidant, *i.e*. untreated) was analyzed for oxidation stability by both Rancimat and RapidOxy methods.

Equipment for determination of oxidation stability in accordance with the Rancimat method was tailored as described in the EN 14112 standard (Figure D1, Supplementary Material). A portion of biodiesel (3 cm^3) was simultaneously subjected to heating at 110 ^{o}C and airflow of 10 dm^3 h^{-1} following the requirements of the EN 14112 standard. Electrical conductivity was measured by a conductometer (HQ440d multi, Hach, USA) with a probe inserted into a measuring flask containing 50 cm^{-3} of distilled water [14]. Pairs of conductivity values and time were recorded to obtain the oxidation curve (conductivity *vs* time). The inflection points of the curve represented the Rancimat induction period (in h). The Rancimat induction period is directly comparable with the limit on oxidation stability defined by the EN 14214 standard. The Rancimat method was used for testing the oxidation stability of untreated biodiesel and also of biodiesel treated with different dosages of the synthetic additive TBHQ, known for its potent antioxidant activity in fuels.

Induction period determined by the oxidation stability tester RapidOxy 100 (Anton Paar, Germany, Figure D2) represents the time (in min) that elapsed between the start of the test (*i.e.* when the oxygen pressure is stabilized at 700 kPa in the sealed instrument test chamber with the sample portion of 4 cm^{-3} before heating to the specified temperature)

to the pressure drop of 10 % with respect to the maximum pressure recorded at the specified temperature. The analytical run consists of the following steps: purging of the instrument test chamber containing the sample portion with oxygen, pressurizing the chamber with oxygen to 700 kPa, heating to the selected temperature, measuring of the pressure drop (till the specified value of the drop), cooling (to 20°C), discharging, and final purging with air. The RapidOxy measurement of untreated biodiesel and the TBHQ-treated biodiesel were performed at different temperatures, *i.e.* at 110, 120, 130, and 140 °C. The effect of different concentrations of TBHQ (250, 500, 1,000, and 2,000 mg dm^{-3}) was also tested by the RapidOxy method but only at 140 °C. The induction period of biodiesel with VWE$_{eth}$ was determined at 140 °C by the RapidOxy method, too. In this way, TBHQ was used as a proved, well known potent antioxidant for comparison of the RapidOxy *vs.* standard Rancimat method, as well as to evaluate preliminary VWE$_{eth}$ as an alternative natural additive. Efficiency of the added antioxidant, *i.e.* its antioxidative potency was expressed as a stabilization factor, calculated by dividing the induction period obtained for biodiesel after the antioxidant addition (treated biodiesel) with the induction period of the untreated biodiesel at the same test temperature. All experiments were performed in duplicates.

3. RESULTS AND DISCUSSION

3.1. Oxidation stability of untreated and TBHQ treated biodiesel

The results of biodiesel characterization are presented in Table 1 with the test methods used. Based on the average induction period of 3.76 h determined at 110 °C by the Rancimat method (Table 1), biodiesel failed to satisfy the limit set by the standard EN 14214. This was not surprising, knowing that the iodine value (*i.e.* the total unsaturation level) of sunflower oil is usually higher than the value for rapeseed oil (usual feedstock for biodiesel in the EU) because of higher contents of linoleic acid: the inherited fatty acid composition of the sunflower oil-based biodiesel results often in non-compliance with the EN standard requirements for iodine value and oxidation stability [18].

Induction periods of freshly synthesized biodiesel determined at different temperatures by the RapidOxy tester are given in Table 2 and Figure D3 (Supplementary Material). It can be easily seen how this method is fast if compared to the Rancimat: 12 times shorter induction period at 110 °C was obtained for untreated biodiesel. Results in Table 2 also proved repeatability of measurements by the RapidOxy instrument: the range of the relative standard deviations was 2.24-5.13 %, with higher RSDs obtained at two higher test temperatures (130 and 140 °C) at which the induction periods were 1.6- and 1.8-fold shorter than the period at 110 °C (Table 2). This high precision coincided with the results of Neumann *et al.*, who reported repeatability and reproducibility for biodiesel induction periods determination by the PetroOXY method to be <5 % and <8 %, respectively [16]. The EN14112 standard (Annex A of EN14214) defines the precision (in h) of the oxidation stability measurement by the equation:

Precision = 0.26X + 0.23   (1)

where X is the mean value of two results on induction period that are compared.

According to the eq. (1) acceptable deviation for the Rancimat induction period of biodiesel synthesized in this study is 1.21 h, accounting for ~32 % of the measured value (3.76 h). The EN14214 standard defines reproducibility of 2.3 h at the oxidation stability limit, accounting for 28.7 % of the 8 h-minimum specified by this standard. Neumann *et al.* [16] concluded that the significantly enhanced reproducibility by the pressurized method over the Rancimat method improves the consistency of test results, and that testing of antioxidant dosages can be more precise, *i.e.* much closer to the actual required level.

Table 1. Selected properties of biodiesel synthesized in this study and compared with the limits set by the EN 14214 standard

Property	EN 14214 limit	Average value (SD*)	Method
Ester content, wt.%	> 96.5	98.9 (0.6)	EN 14103
Density at 20°C, kg m^{-3}	860-900	861 (1.4)	EN ISO 3675
Kinematic viscosity at 40 °C, mm^2 s^{-1}	3.5-5.0	4.6 (0.1)	EN ISO 3104
Water content, mg kg^{-1}	< 500	250 (7.1)	EN ISO 12937
Acid value, mg KOH g^{-1}	< 0.5	0.47 (0.01)	EN 14104
Methyl ester of linolenic acid, mas.%	< 12	0.97 (0.04)	EN 14103
Oxidation stability at 110 °C, h	> 8	3.76 (0,37)	EN 14112

*SD-standard deviation

Table 2. Induction periods of synthesized biodiesel determined at different temperatures by the RapidOxy tester

t / °C	Number of analyzed sample aliquots	Average induction period, min	RSD[a], %
110	5	19.25	2.25
120	5	14.60	3.63
130	6	11.95	5.13
140	6	10.51	4.80

[a]Relative standard deviation (RSD) is determined as the standard deviation of measured values for the given temperature relative to the corresponding average value multiplied by 100 to obtain the percentage

Stabilization factors reflecting the antioxidant potency of TBHQ in biodiesel at different temperatures are given in Table 3. Comparison of the induction periods obtained at 140 °C for varying additions of TBHQ is presented in Table 4.

Stabilization factors proved the beneficial effects of TBHQ on retarding oxidative degradation of biodiesel under the testing conditions. Within the range of applied temperatures, the initial induction period was increased for about 3 to 7 times, with the highest increase observed at the highest TBHQ dosage and the lowest testing temperature (Table 3).

As expected, the induction period was reduced with the increase in the test temperature; an exponential trend described the dependence of the average induction period, IP / min, of untreated biodiesel (neat) on temperature, t / °C, which can be presented with the equation (2):

$$\ln IP_{neat} = 3.1078 - 0.193t \tag{2}$$

The coefficient of determination was $R^2 = 0.9599$. Induction periods of the biodiesel samples treated with two dosages of TBHQ similarly depended on the testing temperature described with equations (3) and (4):

$$\ln IP_{TBHQ1} = 5.1704 - 0.466t \tag{3}$$
$$\ln IP_{TBHQ2} = 5.2720 - 0.446t \tag{4}$$

where eq. (3) describes experimental results obtained for TBHQ dosage of 1,000 mg dm^{-3} (TBHQ1) with the coefficient of determination of $R^2 = 0.9845$, while eq. (4) describes experimental results obtained for TBHQ dosage of 2,000 mg dm^{-3} (TBHQ2) with the coefficient of determination of $R^2 = 0.9912$.

Table 3. Stabilization factors as indicators of antioxidant potency of TBHQ added to biodiesel at two levels (TBHQ1: 1,000 mg cm^{-3} and TBHQ2: 2,000 mg cm^{-3}) determined at different temperatures by the RapidOxy tester

Temperature, °C	Stabilization factor[a]	
	TBHQ1	TBHQ2
110	6.14	6.68
120	4.40	5.41
130	3.44	3.98
140	2.68	3.18

[a]Stabilization factor is calculated as a ratio of the induction period obtained for biodiesel after the addition and the induction period of biodiesel prior the addition at the same test temperature.

Table 4. Induction periods of biodiesel treated with varying concentrations of TBHQ determined at 140 °C by the RapidOxy oxidation stability tester and the corresponding stabilization factors

TBHQ dosage, mg dm^{-3}	IP, min	Stabilization factor	Stabilization factor per dosage, dm^3 mg^{-1}
250	13.30	1.23	0.0048
500	22.20	2.05	0.0042
1000	28.98	2.68	0.0027
2000	34.38	3.18	0.0016

Hence, a negative effect of temperature on the oxidation stability was observed regardless of the treatment, while the reduction in stability (*i.e.* induction periods) followed different trends depending on the TBHQ absence/presence. The similarity of respective coefficients in equations (3) and (4) suggested similar degradation mechanisms in the TBHQ-treated biodiesel under applied conditions of accelerated oxidation regardless of the TBHQ dosage. On the other hand, coefficients in eq. (2) differed from the corresponding ones in eqs. (3) and (4), implying different mechanisms of the induction period disturbance with increasing temperature in the untreated biodiesel. It was indicated in a study of changes of selected biodiesel fuel parameters during accelerated oxidation at different temperatures that at

temperatures above 75 °C thermal degradation of original biodiesel composition occurs along with the oxidative decomposition [19]. Accordingly, it might be expected that thermal degradation is more pronounced at higher temperatures. This could be the explanation for the obtained exponential dependence of induction periods on temperature. Differences between the equations for untreated (eq. 2) and treated (eqs. 3 and 4) biodiesel might be ascribed to the presence of TBHQ and its active antioxidant action superimposed over the oxidation and thermal degradation of unsaturated fatty acid methyl esters. Besides the consumption of TBHQ during its protective antioxidative action, its thermal degradation might be also presumed to occur; the formed degradation products may affect the induction periods [22], as is explained hereafter.

High antioxidant potency of TBHQ is well known and explained by its unique molecular structure. It consists of two -OH groups linked to aromatic ring in *para*(1,4-) position and one *tert*-butyl group in *ortho*(2-) position. Such dihydroxyl aromatic structure interrupts more easily the propagation step of the free radical chain reaction than phenolic antioxidants with only one -OH group in molecules [14,20,21]. The presence of alkyl groups is also important for efficient protection from oxidation. In this way, the electron density on the -OH groups is increased, which facilitates the release of a hydrogen radical, enabling more efficient stabilization of ester radicals formed during the oxidation stress [21]. Apart from the favorable structure, high efficiency of TBHQ is additionally related to the products known to be formed during its antioxidative activity that may also exhibit antioxidant properties, synergistically retarding the oxidation [14,22].

Dependence of RapidOxy induction periods, IP_i / min, on different dosages of TBHQ, i / mg dm^{-3}, also did not follow a linear trend (Table 4):

$$IP_i^{RapidOxy} = 10.102 \ln i - 41.564 \text{ with } R^2 = 0.9876 \tag{5}$$

The shape of the curve (Figure D4) suggested changes in rates of stability enhancement in the range of tested dosages: faster increase at lower and slower at higher dosages of TBHQ. This might be also illustrated by stabilization factors at different TBHQ dosages (Table 4).

Induction periods for the biodiesel supplemented with different TBHQ dosages determined at 110 °C by the Rancimat method and the corresponding stabilization factors are presented in Table 5. The difference between the RapidOxy and Rancimat results should be ascribed to different phenomena behind these two methods and their repeatability as explained previously. Still, both methods showed a 2-fold increase in the induction period with the TBHQ dosage of 500 mg dm^{-3}, and according to the Rancimat results it was sufficient for achieving the oxidation stability above the EN14214 standard limit. A preliminary exponential model correlating the respective results obtained by the Rancimat (at 110 °C) and PetroOxy (at 140 °C) methods is presented in Figure D5 (Supplementary Material); however, further study is needed to confirm the applicability of the model.

Table 5. Induction periods of biodiesel treated with varying concentrations of TBHQ determined at 110 °C by the Rancimat method and the corresponding stabilization factors

TBHQ dosage, mg dm^{-3}	IP, h	Stabilization factor
250	4.9	1.3
500	9.2	2.4
1000	15.7	4.2

3.2. Oxidation stability of biodiesel treated with VWE$_{eth}$

As mentioned previously, the high price, nonrenewable origin, and toxicity of conventional synthetic fuel additives have triggered the search and development of alternative, cheaper, non-toxic, and renewable additives for biodiesel, which efficiently address known disadvantages in the fuel properties. Substantial achievements have been recorded in recent years and they are reviewed in the work of Lawan *et al.* [6]. The majority of studies dealing with bio-based additives explored extracts of varying plants such as rosemary [22], ginger [23], oregano [22], basil [22], *Moringa oleifera* [8], etc. However, it is worth mentioning that the use of plants known for their therapeutic and/or nutritional values in the fuel industry additionally contributes to the already raised controversy of biodiesel regarding food *vs.* fuel dilemma. Thus, a more sustainable option is to obtain alternative bio-based antioxidants from non-edible feedstock, especially from food and agro-industry waste. Utilizing biowaste as feedstock for bio-based additives could reduce the biofuel cost providing

also a good waste management strategy [10]. Some of biowaste examined as sources of antioxidants for biodiesel were barley waste [8], potato peel [9], and spent coffee grounds waste [10]; regardless of the applied extraction procedures, addition of the obtained extracts to biodiesel of various origins proved to be beneficial for the fuel oxidation stability. For instance, extract of 10 g of dried potato peels by 100 cm^{-3} of absolute ethanol for 3 h was added as dry matter at different dosages (100 - 250 ppm) to biodiesel synthesized from Nahor oil (*Mesua ferrea*) [9]. Rancimat induction periods of the treated biodiesel were in the range of 5.95 h for 100 ppm extract to 7.02 h for 250 ppm extract, whereas the initial induction period of the untreated biodiesel was 5.63 h [9]. Thus, stabilization factors were in the range 1.06 to 1.25.

Natural antioxidants obtained in the present study from vinery waste also proved protective capacity as induction periods of the VWE$_{eth}$-treated biodiesel samples were improved for a factor of about 1.3 (Table 6). The slightly higher stabilization factors achieved here in comparison to those obtained for the previously mentioned potato peel extract might be the consequence of the higher quantity of dried feedstock extracted (0.2 g vinery waste per cm^{-3} of solvent *vs*. 0.1 g potato peel per cm^{-3} of solvent), longer extraction periods, and/or different antioxidant compounds present in the extracts. The exponential equation describing the relationship between the Rancimat and RapidOxy induction periods (Figure D5, Supplementary Material) was applied to the VWE$_{eth}$-related values measured by the RapidOXY method resulting in the corresponding Rancimat periods of 4.8 and 5.0 h. This result implies that the tested additions of VWE$_{eth}$ were not sufficient to enhance the biodiesel oxidation stability above the EN14214 standard limit. Comparison of the RapidOxy induction periods obtained for additions of natural VWE$_{eth}$ and synthetic TBHQ implies that the tested dosages of the former additive had protective power similar as the TBHQ dosage of 250 mg dm^{-3}. If eq. (5) is applied for the VWE$_{eth}$-induction periods presented in Table 6, the equivalent TBHQ concentrations of 231 and 248 mg dm^{-3} are obtained. Knowing that the TBHQ addition of 250 mg dm^{-3} led to the Rancimat induction period of 4.9 h (Table 5), this equivalency also showed that the applied VWEs dosages were not sufficient to improve the biodiesel oxidation stability above the EN14214 standard limit.

It is interesting to note that the linear regression model of Botella *et al.* [15], correlating the Rancimat and PetroOXY induction periods (in min) for biodiesel with additives, applied on the RapidOxy periods for VWE$_{eth}$ additives, predicted similar values for the Rancimat periods: *i.e*. 4.3 h and 4.4 h. The comparison proved that the obtained model may be used as a quick means for converting the RapidOxy measurements into the Rancimat values for the tested biodiesel with VWEs additives, and that such value may indicate if the oxidation stability reached the standard limit. Nevertheless, more data are needed to obtain a more accurate and general correlation.

Rather similar factors of stability enhancement obtained for two dosages of VWE$_{eth}$ could be explained by possible aliquot (in)homogeneity during the transfer to a flask for blending with biodiesel. Markedly lower stabilization factor per dosage calculated for VWE$_{eth}$ (Table 6) in comparison to TBHQ (Table 4) suggested that only a certain part of the VWE$_{eth}$ could be related to antioxidants with protective power for biodiesel and/or the presence of less potent antioxidant compounds. Higher quantities of vinery waste (>0.2 g cm^{-3}) are necessary to be tested as potential means for increasing the antioxidant potency.

Table 6. Induction periods determined at 140°C by the RapidOxy method and the corresponding stabilization factors after addition of vinery waste ethanolic extracts (VWE$_{eth}$) as bio-based antioxidants

VWE$_{eth}$ dosage, mg dm^{-3}	IP, min	Stabilization factor	Stabilization factor per dosage, dm^3 mg^{-1}
87,500	13.41	1.28	0.0000153
150,000	14.12	1.34	0.0000085

4. CONCLUSION

The results suggested the RapidOxy method as a high-throughput analytical technique with high repeatability. Dependence of RapidOxy induction periods on test temperatures was described by an exponential equation, capturing the effects of oxidative stress and thermal degradation in the applied range of temperatures; different equations obtained for untreated and TBHQ-treated biodiesel, reflected the additional antioxidation action of TBHQ. The addition of TBHQ to sunflower oil-based biodiesel in a dosage of 500 mg dm^{-3} enabled compliance with the EN14214 standard.

The VWE$_{eth}$ extract showed protective potency as an antioxidant additive for biodiesel, but the tested dosages were not sufficient to achieve the EN14214 standard limit.

Further studies are needed to characterize VWEs since by knowing the VWEs composition, particularly compounds exhibiting antioxidant properties, the mechanism of its interaction with biodiesel may be proposed. Continuation of the present study should aim at determination of VWEs dosages, applied either individually or in combination with a powerful synthetic antioxidant such as TBHQ, sufficient to reach the relevant limit without impairment of the other fuel properties. Investigation of different extraction methods/conditions would reveal if a more powerful antioxidant action of VWE$_{eth}$ might be achieved. Techno-economic analysis and life cycle assessment would confirm the sustainability of the final results.

REFERENCES

[1] Tomić M, Đurišić-Mladenović N, Mićić R, Simikić M, Savin L. Effects of accelerated oxidation on the selected fuel properties and composition of biodiesel. *Fuel.* 2019; 235: 269-276 https://doi.org/10.1016/j.fuel.2018.07.123

[2] Alves-Fortunato M, Ayoub E, Bacha K, Mouret A, Dalmazzone C. Fatty Acids Methyl Esters (FAME) autoxidation: New insights on insoluble deposit formation process in biofuels. *Fuel.* 2020; 268: 117074 https://doi.org/10.1016/j.fuel.2020.117074

[3] Sia CB, Kansedo J, Tan YH, Lee KT. Evaluation on biodiesel cold flow properties, oxidative stability and enhancement strategies: A review. *Biocatal Agric Biotechnol* 2020; 24: 101514. https://doi.org/10.1016/j.bcab.2020.101514

[4] Bacha K, Ben-Amara A, Vannier A, Alves-Fortunato M, Nardin M. Oxidation stability of diesel/biodiesel fuels measured by a PetroOxy device and characterization of oxidation products. *Energy Fuels.* 2015; 29: 4345-4355 https://doi.org/10.1021/acs.energyfuels.5b00450

[5] Yaakob Z, Narayanan BN, Padikkaparambil S, Surya Unni K, Akbar MP. A review on the oxidation stability of biodiesel. *Renew Sustain Energy Rev* 2014; 35: 136-153 https://doi.org/10.1016/j.rser.2014.03.055

[6] Lawan I, Zhou W, Garba ZN, Zhang M, Yuan Z, Chen L. Critical insights into the effects of bio-based additives on biodiesels properties. *Renew Sustain Energy Rev.* 2019; 102: 83-95 https://doi.org/10.1016/j.rser.2018.12.008

[7] Kumar D, Singh B. Tinospora cordifolia stem extract as an antioxidant additive for enhanced stability of Karanja biodiesel. *Ind Crops Prod.* 2018; 123: 10-16 https://doi.org/10.1016/j.indcrop.2018.06.049

[8] Valenga MGP, Boschen NL, Rodrigues PRP, Maia GAR. Agro-industrial waste and Moringa oleifera leaves as antioxidants for biodiesel. *Ind Crops Prod* 2019; 128: 331-337 https://doi.org/10.1016/j.indcrop.2018.11.031

[9] Devi A, Das VK, Deka D. Evaluation of the effectiveness of potato peel extract as a natural antioxidant on biodiesel oxidation stability. *Ind Crops Prod* 2018; 123: 454-460 https://doi.org/10.1016/j.indcrop.2018.07.022

[10] Tongcumpou C, Usapein P, Tuntiwiwattanapun N. Complete utilization of wet spent coffee grounds waste as a novel feedstock for antioxidant, biodiesel, and bio-char production. *Ind Crops Prod* 2019; 138: 111484 https://doi.org/10.1016/j.indcrop.2019.111484

[11] Roveda AC, de Oliveira IP, Caires ARL, Rinaldo D, Ferreira VS, Trindade MAG. Improving butylhydroxytoluene activity with alternative secondary antioxidants: High synergistic effect in stabilizing biodiesel/diesel fuel blends in the presence of pro-oxidative metal. *Ind Crops Prod* 2022; 178: 114558 https://doi.org/10.1016/j.indcrop.2022.114558

[12] Alberici RM, Simas RC, Abdelnur P V, *et al.* A highly effective antioxidant and artificial marker for biodiesel. *Energy Fuel.* 2010; 24(11): 6522-6526 https://doi.org/10.1021/ef100968b

[13] van der Westhuizen I, Focke WW. Stabilizing sunflower biodiesel with synthetic antioxidant blends. *Fuel.* 2018; 219: 126-131 https://doi.org/10.1016/j.fuel.2018.01.086

[14] Rankov Šicar M, Mićić R, Tomić M, Đurišić-Mladenović N. Efficiency of different additives in improvement of oxidation stability of fatty acid methyl esters with different properties. *J Serb Chem Soc.* 2021; 86: 739-752 https://doi.org/10.2298/JSC210209029R

[15] Botella L, Bimbela F, Martín L, Arauzo J, Sánchez JL. Oxidation stability of biodiesel fuels and blends using the Rancimat and PetroOXY methods. Effect of 4-allyl-2,6-dimethoxyphenol and catechol as biodiesel additives on oxidation stability. *Front Chem.* 2014; 2: 43 https://doi.org/10.3389/fchem.2014.00043

[16] Neumann A, Jebens T, Wierzbicki V. A method for determining oxidation stability of petrodiesel, biodiesel, and blended fuels. *Am Lab.* 2008; 40: 22-26 https://www.americanlaboratory.com/914-Application-Notes/34716-A-Method-for-Determining-Oxidation-Stability-of-Petrodiesel-Biodiesel-and-Blended-Fuels/

[17] Araújo S V, Luna FMT, Rola Jr EM, Azevedo DCS, Cavalcante Jr CL. A rapid method for evaluation of the oxidation stability of castor oil FAME: influence of antioxidant type and concentration. *Fuel Process Technol.* 2009; 90(10): 1272-1277 https://doi.org/10.1016/j.fuproc.2009.06.009

[18] Đurišić-Mladenović N, Kiss F, Škrbić B, Tomić M, Mićić R, Predojević Z. Current state of the biodiesel production and the indigenous feedstock potential in Serbia. *Renew Sustain Energy Rev* 2018; 81: 280-291 https://doi.org/10.1016/j.rser.2017.07.059

[19] Dunn RO. Effect of oxidation under accelerated conditions on fuel properties of methyl soyate (biodiesel). *J Am Oil Chem Soc* 2002; 79(9): 915-920 https://doi.org/10.1007/s11746-002-0579-2

[20] Agarwal S, Singhal S, Singh M, Arora S, Tanwer M. Role of Antioxidants in Enhancing Oxidation Stability of Biodiesels. *ACS Sustain Chem Eng* 2018; 6(8): 11036-11049 https://doi.org/10.1021/acssuschemeng.8b02523

[21] Zhou J, Xiong Y, Shi Y. Antioxidant Consumption Kinetics and Shelf-Life Prediction for Biodiesel Stabilized with Antioxidants Using the Rancimat Method. *Energy Fuels.* 2016; 30(12): 10534-10542. https://doi.org/10.1021/acs.energyfuels.6b02199

[22] Spacino KR, Silva ET da, Angilelli KG, Moreira I, Galão OF, Borsato D. Relative protection factor optimisation of natural antioxidants in biodiesel B100. *Ind Crops Prod* 2016; 80: 109-114. https://doi.org/10.1016/j.indcrop.2015.11.034

[23] Devi A, Das VK, Deka D. Ginger extract as a nature based robust additive and its influence on the oxidation stability of biodiesel synthesized from non-edible oil. *Fuel.* 2017; 187: 306-314 https://doi.org/10.1016/j.fuel.2016.09.063

Procena stabilnosti biodizela sa sintetičkim i bio-antioksidansima primenom ubrzane metode pod pritiskom

Nataša Đurišić-Mladenović[1]*, Milan Tomić[2], Biljana Pajin[1], Maja Buljovčić[1], Ivana Lončarević[1] i Milica Rankov Šicar[1,3]

[1]Univerzitet u Novom Sadu, Tehnološki fakultet Novi Sad, Novi Sad, Srbija
[2]Univerzitet u Novom Sadu, Poljoprivredni fakultet, Novi Sad, Srbija
[3]SP Labortorija a.d., Bečej, Srbija

(Naučni rad)

Izvod

U radu je ispitana metoda ubrzane oksidacije pod pritiskom pomoću RapidOxy uređaja kao alternative za određivanje oksidacione stabilnosti biodizela. Pripremljen je biodizel od suncokretovog ulja i tretiran je antioksidansima: sintetičkim antioksidansom terc-butil hidrohinonom (engl. *tert*-butylhydroquinone, TBHQ), koji je poznat po svom snažnom zaštitnom dejstvu, i smeša jedinjenja sa antioksidativnim dejstvom ekstrahovana etanolom iz otpada vinarije, (engl. vinary waste ethanolic extract, VWEeth). Antioksidaciona moć aditiva TBHQ je ispitana pri različitim temperaturama (110 do 140 °C) i koncentracijama (250 do 2000 mg dm^{-3}) primenom RapidOxy metode; procena odabranih rezultata je izvršena njihovim poređenjem sa relevantnim podacima dobijenim pomoću standardne Rancimat metode. Oba antioksidansa u svim testiranim dozama su pozitivno uticali na poboljšanje oksidacione stabilnosti biodizela, ali nisu sve doze dovele do postizanja minimalne stabilnosti definisane standardom EN14214. Najmanja doza aditiva TBHQ je pokazala dejstvo slično testiranim dozama ekstrakta VWEeth, ali ove doze nisu povećale indukcioni period iznad granične vrednosti od 8 h; dvostruko veća doza aditiva TBHQ je bila uspešna, povećavajući početnu oksidacionu stabilnost za faktor 2, što je utvrđeno pomoću obe korišćene metode. RapidOxy metoda se pokazala kao veoma brza metoda pogodna za ispitivanje velikog broja uzoraka, što je naročito važno za efikasno ispitivanje dejstva različitih vrsta i doza antioksidanasa.

DOKTORSKE DISERTACIJE HEMIJSKO–TEHNOLOŠKE STRUKE ODBRANJENE NA UNIVERZITETIMA U SRBIJI U 2022. GODINI

TEHNOLOŠKO-METALURŠKI FAKULTET, UNIVERZITET U BEOGRADU

	Ime i prezime	Naslov	Mentor/i
1.	**Marija Riđošić**	Elektrohemijsko taloženje i karakterizacija Zn-Co-CeO$_2$ nanokompozita	Dr Bajat Jelena
2.	**Egerić Marija**	Separacija /stabilizacija odabranih teških metala iz vode i zemljišta primenom otpadnih ljuštura školjki	Dr Perić-Grujić Aleksandra Dr Smičiklas Ivana
3.	**Mijatović Nevenka**	Hemometrijski pristup ispitivanju uticaja hemijskih svojstava elektrofilterskog pepela , zeolita i bentonita na svojstva ekološki prihvatljivih građevinskih materijala	Dr Živojinović Dragana
4.	**Ayoub Giuma**	Procesiranje , svojstva i primena dentalnih inserata na bazi kalcijum-fosfata i cirkonijum(IV)-oksida	Dr Janaćković Đorđe
5.	**Simović Bojana**	Sinteza i karakterizacija nanostrukturnih materijala na bazi cink-oksida, titan-dioksida i cerijum-dioksida za primenu u fotokatalizi	Dr Dapčević Aleksandra
6.	**Zečević Bojana**	Uticaj radne temperature na otpornost na nastanak i rast prslina niskougljeničnog mikrolegiranog čelika za termoenergetska postrojenja	Dr Milović Ljubica
7.	**Svetozarević Milica**	Biorazgradnja antrahinonske boje peroksidazom izolovanom iz otpadnog materijala u šaržnom i kontinualnom sistemu	Dr Mijin Dušan Dr Šekuljica Nataša
8.	**Jelić Aleksandra**	Mehanička i termička svojstva sintetisanih nanokompozitnih materijala na bazi halojzita i kalcijum-silikata	Dr Putić Slaviša
9.	**Kazuz Abdul**	Bioaktivni materijali na bazi α-trikalcijum-fosfatnih cementa i fluoroapatita: sinteza, svojstva i primena u stomatologiji	Dr Janaćković Đorđe
10.	**Assaleh Mohamed**	Imino derivati tiouglene i amida cimetnih kiselina: korelacije strukture i aktivnosti	Dr Marinković Aleksandar Dr Bjelogrlić Snežana
11.	**Milošević Dragana**	Modifikacija , karakterizacija i primena adsorbenata na bazi gljive Handkea utriformis za uklanjanje jona metala iz vode	Dr Petrović Rada
12.	**Prokić Vidojević Dragana**	Sinteza , karakterizacija i ispitivanje renijum/paladijum aerogel i kserogel katalizatora za reakcije desulfurizacije dibenzotiofena i supstituisanog 4,6-dimetil dibenzotiofena u prisustvu vodonika	Dr Glišić Sandra
13.	**Radisavljević Anđela**	Procesiranje i karakterizacija polimernih nanovlakana sa antimikrobnim efektom za prevenciju infekcija izazvanih kateterizacijom urinarnog trakta	Dr Petar Uskoković Dr Rajilić-Stojanović Mirjana
14.	**Mašulović Aleksandra**	Multifunkcionalni derivati 2-piridona dipolarne strukture i njihova potencijalna primena	Dr Mijin Dušan
15.	**Kojić Marija**	Optimizacija kvaliteta materijala dobijenog hidrotermalnom karbonizacijom i njegova primena u adsorpciji teških metala iz vodenih rastvora	Dr Onjia Antonije Dr Ercegović Marija
16.	**Matović Luka**	Sinteza i svojstva novih boja sa azo i vinil-grupom za primenu u solarnim ćelijama aktiviranim bojom	Dr Mijin Dušan
17.	**Jovanović Jelena**	Inkapsulacija aktivnih komponenti u pektin i hitozan za primenu u aktivnom pakovanju i biopesticidima	Dr Vukašinović-Sekulić Maja Dr Ćirković Jovana

TEHNOLOŠKI FAKULTET, UNIVERZITET U NOVOM SADU

	Ime I Prezime	Naslov	Mentor/i
1.	Mirna Drašković Berger	Uticaj soli, temperature i starter kulture na fizičko-hemijske i mikrobiološke promene u toku fermentacije kupusa u glavicama	Dr Aleksandra Tepić Horecki
2.	Jelena Perović	Razvoj novog bezglutenskog funkcionalnog flips proizvoda oplemenjenog korenom cikorije (*Cichorium intybus* L.)	Dr Vesna Tumbas Šaponjac
3.	Ana Varga	Uticaj etarskih ulja na biofilmove odabranih sojeva enterobakterija formiranih na lisnoj površini povrća	Dr Sunčica Kocić-Tanackov
4.	Maja Buljovčić	Teški elementi i novootkrivena organska zagađujuća jedinjenja u izabranim matriksima životne sredine i procena rizika	Dr Biljana Škrbić
5.	Tea Sedlar	Nusproizvod agroindustrije - zeleno lišće: novi izvor proteina i bioaktivnih jedinjenja	Dr Ljiljana Popović
6.	Danka Dragojlović	Potencijal brašna od različitih vrsta insekata kao alternativnih izvora proteina u ishrani životinja	Dr Ljiljana Popović Dr Olivera Đuragić
7.	Stefan Vukmanović	Valorizacija proizvoda fermentacije kombuhe na otpadnom toku iz proizvodnje vina	Dr Jasmina Vitas
8.	Maja Stojković	Optimizacija procesa proizvodnje medovine uz dodatak voćnog soka od aronije kao proizvoda poboljšanih funkcionalnih svojstava	Dr Dragoljub Cvetković

TEHNOLOŠKI FAKULTET U LESKOVCU, UNIVERZITET U NIŠU

	Ime i prezime	Naslov	Mentor/i
1.	Biljana Đorđević	Ekstrakcija masnog ulja i fenola iz semena slačice (*Brassica nigra* L.) eutektičkim rastvaračima i etanoliza masnog ulja u prisustvu kalcijum - oksida	Dr Zoran Todorović

TEHNIČKI FAKULTET U BORU, UNIVERZITET U BEOGRADU

	Ime i prezime	Naslov	Mentor/i
1.	Jelena Ivaz	Modeliranje uticajnih faktora i predikcija pojave povreda na radu u rudarstvu	Dr Dejan Petrović
2.	Jasmina Petrović	Strukturne , mehaničke i fizičko-hemijske karakteristike hibridnog kompozita sa EN AW 6061 metalnom matricom dobijenog postupkom vrtoložnog livenja	Dr Srba Mladenović
3.	Slavoljub Toskić*	Zagađenje vazduha u Boru u periodu od 2010. do 2020. godine	Dr Snežana Šerbula

**Magistarska teza*

Spisak recenzenata radova čije je procesiranje završeno tokom 2022. godine

List of reviewers of papers whose processing has been completed during 2022

1. **Jelena Bajat**, *Tehnološko-metalurški fakultet, Univerzitet u Beogradu, Srbija*
2. **Ivana Banković Ilić**, *Tehnološki fakultet u Leskovcu, Univerzitet u Nišu, Srbija*
3. **Nemanja Barać,** *Inovacioni centar Tehnološko-metalurškog fakulteta, Beograd, Srbija*
4. **Mamta Baunthiyal,** *Department of Biotechnology, Govind Ballabh Pant Engineering College, Uttarakhand, India*
5. **Edin Berberović**, *Mašinski fakultet, Univerzitet u Zenici, Bosna i Hercegovina*
6. **Dejan Bezbradica**, *Tehnološko-metalurški fakultet, Univerzitet u Beogradu, Srbija*
7. **Konrad Boettcher**, *Technische Universität Dortmund, Dortmund, Germany*
8. **Nevenka Bošković Vragolović,** *Tehnološko-metalurški fakultet, Univerzitet u Beogradu, Srbija*
9. **Jonathan Castillo**, *University of Atacama, Chile*
10. **Aleksandar Dekanski,** *Institut za hemiju tehnologiju i metalurgiju, Univerzitet u Beogradu, Srbija*
11. **Snežana Dimitrijević,** *Odsek za poljoprivredna istraživanja i razvoj, Institut Josif Pančić, Beograd, Srbija*
12. **Ivana Drvenica**, *Institut za medicinska istraživanja, Univerzitet u Beogradu, Srbija*
13. **Veljko Đokić**, *Inovacioni centar Tehnološko-metalurškog fakulteta, Beograd, Srbija*
14. **Maja Đolić**, *Tehnološko-metalurški fakultet, Univerzitet u Beogradu, Srbija*
15. **Nataša Đurišić Mladenović,** *Tehnološki fakultet, Univerzitet u Novom Sadu*
16. **Enis Džunuzović**, *Tehnološko-metalurški fakultet, Univerzitet u Beogradu, Srbija*
17. **Jelena Gulicovski**, *Institut za nuklearne nauke "Vinča", Univerzitet u Beogradu, Srbija*
18. **Miće Jakić**, *Faculty of Chemistry and Technology, University of Split, Split, Croatia*
19. **Dijana Jelić**, *Prirodno-matematički fakultet, Univerzitet u Banjoj Luci, Bosna i Hercegovina*
20. **Yasuharu Kanda,** *College of Environmental Technology, Muroran Institute of Technology, Japan*
21. **Zvonimir Katančić,** *Fakultet kemijskog inzenjerstva i tehnologije, Sveučilište u Zagrebu, Hrvatska*
22. **Borut Kosec**, *Naravoslovnotehniška fakulteta, Univerza v Ljubljani, Slovenija*
23. **Stjepan Kožuh**, *Sveučilište u Zagrebu, Metalurški fakultet, Sisak, Hrvatska*
24. **Divna Majstorović**, *Tehnološko-metalurški fakultet, Univerzitet u Beogradu, Srbija*
25. **Dragan Manojlović**, *Hemijski fakultet, Univerzitet u Beograd, Srbija*
26. **Vaso Manojlović,** *Tehnološko-metalurški fakultet, Univerzitet u Beogradu, Srbija*
27. **Dušan Mijin**, *Tehnološko-metalurški fakultet, Univerzitet u Beogradu, Srbija*
28. **Marija Nikolić,** *Tehnološko-metalurški fakultet, Univerzitet u Beogradu, Srbija*
29. **Bojana Obradović**, *Tehnološko-metalurški fakultet, Univerzitet u Beogradu, Srbija*
30. **Vladimir Pavićević,** *Tehnološko-metalurški fakultet, Univerzitet u Beogradu, Srbija*
31. **Marija Pergal,** *Institut za hemiju, tehnologiju i metalurgiju, Univerzitet u Beogradu, Serbia*
32. **Aleksandra Perić-Grujić**, *Tehnološko-metalurški fakultet, Univerzitet u Beogradu, Srbija*
33. **Rada Petrović,** *Tehnološko-metalurški fakultet, Univerzitet u Beogradu, Srbija*
34. **Rada Pjanović,** *Tehnološko-metalurški fakultet, Univerzitet u Beogradu, Srbija*
35. **Dragan Povrenović**, *Tehnološko-metalurški fakultet, Univerzitet u Beogradu, Srbija*
36. **Mateja Primožič,** *Fakulteta za kemijo in kemijsko tehnologijo, Univerza v Mariboru, Slomškov trg 15, 2000 Maribor, Slovenia*
37. **Nenad Radić,** *Institut za hemiju tehnologiju i metalurgiju, Univerzitet u Beogradu, Srbija*
38. **Vesna Radojević,** *Tehnološko-metalurški fakultet, Univerzitet u Beogradu, Srbija*
39. **Bojana Radojković**, *Institut za hemiju tehnologiju i metalurgiju, Univerzitet u Beogradu, Srbija*
40. **Dragana Radovanović,** *Inovacioni centar Tehnološko-metalurškog fakulteta, Beograd*

41. **Mirjana Ristić,** *Tehnološko-metalurški fakultet, Univerzitet u Beogradu, Srbija*
42. **Kamila Salasinska***, Warsaw University of Technology, Poland*
43. **Aman Santoso***, Department of Chemistry, Faculty of Mathematics and Natural Sciences, Universitas Negeri Malang, Indonesia*
44. **Gordana Stojanović***, Prirodno-matematički fakultet, Univerzitet u Nišu, Srbija*
45. **Monika Šabić Runjavec,** *Fakultet kemijskog inženjerstva i tehnologije, Sveučilište u Zagrebu, Hrvatska*
46. **Ivan Švancara***, Department of Analytical Chemistry, Faculty of Chemical Technology, University of Pardubice, CZ-532 10 Pardubice, Czech Republic*
47. **Milica Vasić, Institut** *IMS, Beograd, Srbija*
48. **Đenđi Vaštag***, Prirodno-matematički fakultet, Univerzitet u Novom Sadu, Srbija*
49. **Đorđe Veljović***, Tehnološko-metalurški fakultet, Univerzitet u Beogradu, Srbija*
50. **Tatjana Volkov Husović,** *Tehnološko-metalurški fakultet, Univerzitet u Beogradu, Srbija*
51. **Emila Živković***, Tehnološko-metalurški fakultet, Univerzitet u Beogradu, Srbija*
52. **Nikola Živković,** *Institut za nuklearne nauke "Vinča", Univerzitet u Beogradu, Srbija*